Selective Wettability Membranes and Surfaces for the Separation of Oil–Water Mixtures, Extractions, and Fouling Prevention

by

Ethan R. Post

A dissertation submitted in partial fulfillment
of the requirements for the degree of
Doctor of Philosophy
(Macromolecular Science and Engineering)
in The University of Michigan
2018

Doctoral Committee:

    Associate Professor Anish Tuteja, Chair
    Professor Jinsang Kim
    Assistant Professor Geeta Mehta
    Associate Professor Pramod Sangi Reddy

Ethan R. Post

erpost@umich.edu

ORCID iD: 0000-0001-5206-3546

DEDICATION

I would like to dedicate this thesis and my doctoral work to my family members, who have always been there to support and encourage me. Thank you to my parents and grandparents who raised me in an environment where I learned the value of hard work, discipline, selflessness, and humility. They gave me every opportunity to succeed and I could never have accomplished this without them. Also, thank you to my beloved wife, Elisa. Your love has made the years of graduate school more bearable, rewarding, and exciting. Meeting and marrying you were the greatest blessings during my time at the University of Michigan.

ACKNOWLEDGMENTS

TABLE OF CONTENTS

LIST OF FIGURES

LIST OF TABLES

LIST OF APPENDICES

ABSTRACT

The separation of miscible and immiscible liquid mixtures is one of the most widely utilized unit operations in the world. The energy-efficient separation of immiscible oil-water mixtures is critical for a wide variety industries including: petroleum drilling and refining, hydraulic fracturing, wastewater treatment, mining, metal fabrication and machining, textile and leather processing, and rendering. Membrane-based methods have become increasingly attractive for the separation of oil-water mixtures because they are relatively energy-efficient, can be readily used to separate a variety of industrial feed streams, and provide consistent permeate quality. In this dissertation, I discuss the design strategies for membranes with selective wettability, i.e., membranes that either selectively wet, or prevent wetting, by the non-polar or polar phase. The design strategies include the parameterization of two important physical characteristics: the surface porosity/geometry and the breakthrough pressure.

On the basis of this understanding, I explore principles that allow for the systematic design of membranes with selective wettability that enable high-efficiency separation of a range of oil-water mixtures. Furthermore, I investigate and shed light on solving one of membrane technology's greatest challenges: organic fouling. A highly versatile silanization methodology was developed, which allows water to permeate through the membranes, while repelling oil (hydrophilic and oleophobic) in air and underwater. This approach is valid for a variety of membrane pore sizes, including 5 nm

diameters, and several substrate classes including: polymers, ceramics, and metals. Due to our selective wetting membranes, I accomplished complete separation of difficult-to-separate, surfactant-stabilized oil-in-water emulsions with enhanced performance due to anti-fouling surface modification, in both batch and cross-flow modes of operation. The anti-fouling ability doubled the untreated membrane's permeation rate after >500 h of operation.

The developed membranes also enable the energy-efficient separation of miscible liquids. By combining the developed membranes with liquid-liquid extraction (LLE), we engineered a new separation methodology termed CLEANS (Continuous Liquid-Liquid Extraction and *In-situ* Membrane Separation). CLEANS achieves >250% increases in extraction factors and avoids energy-intensive distillation, solely by addition of a common surfactant to the extractant. This is the first time anyone has intentionally created emulsions, to benefit from increased mass transfer surface area, in LLE. This was only possible due to our membrane's unique capability to break up a variety of emulsions on contact.

Additionally, I applied my knowledge of surface wetting and anti-fouling chemistry to develop a highly effective and dually functional easy-clean and anti-fog coating. The hydrophilicity of the substrate polymer prevents water droplets from condensing into light scattering features, while the post-modification imbues the surface with oil shedding ability. The coating is designed to be scalable in application by spray coating and is well bonded directly to polycarbonate substrates.

Finally, by understanding liquid breakthrough pressure on chemically modified membranes, I developed a method of freeze concentration where the crystallizer and

separator unit operations were combined into one. This is made possible by the membrane breakthrough pressure being high enough to hold the feed liquid in the freeze concentrator, but low enough that it can be actuated by partial vacuum to collect the concentrate. Proof of concept was provided for the freeze concentration of apple juice, ethanol solution, and dyed water. In summary, my dissertation projects resulted in several new prototype membrane-based purification systems and new anti-fog windows and glasses.

CHAPTER 1

Introduction

This chapter contains sections adapted from a first author review article published in and reprinted with permission from *MRS Communications.*[1]

1.1 Introductory Remarks

Humans have been studying how liquids wet solid surfaces and innovating solutions to everyday problems for thousands of years. Materials such as pitch, tar, and beeswax were used to keep ships afloat and preserved, houses dry, and food protected.[2] The study of highly liquid repellent surfaces has continued today at an increasing rate. By analyzing publication data with Web of Science, papers focused on terms such as "superhydrophobic" and "oleophobic" have increased in number from 5 and 10, respectively, in 2000 to 1,620 and 73 in 2017. The field of surface science has been highly inspired by liquid repellent surfaces found in nature including: lotus leaves, fish scales, butterfly wings, rice leaves, rose petals, Namib desert beetle shells, and the springtail.[3] These surfaces serve to self-clean, protect, and help these living things survive. We have learned that precisely controlling the surface chemistry and roughness/geometry enables unique wetting properties, and this knowledge has been used to develop solutions to a plethora of engineering problems such as liquid purification, fouling prevention, and fog prevention, which are all discussed in this dissertation.

1.2 Selective Wetting's Impact on Oil & Water Separation

1.2.1 Challenges to Address

The separation of oil-water mixtures is a widely utilized unit operation, used for handling a wide variety of mixtures from industry including: petroleum drilling and refining, hydraulic fracturing, waste-water treatment, mining, metal fabrication and machining, textile and leather processing, and rendering.[4] The limitations on oil and grease content set by the U.S. Environmental Protection Agency have become increasingly stringent over the years. The best available technology (BAT) limit on oil and grease discharge in produced water is now 42 mg/L for any one day, with a 29 mg/L thirty, consecutive-day average.[5] Depending on the industry, the oil and grease concentration in the untreated effluent can typically range from a few hundred to 200,000 mg/L.[6] The mixtures, produced from various industries, range from free oil and water to surfactant-stabilized oil-water emulsions. Emulsions can be particularly difficult, energy intensive, and expensive to separate. The large volumes of contaminated mixtures, including from accidents such as the Deepwater Horizon spill, necessitate the development of durable, cost-effective means of selectively separating oil and water mixtures with a high volume throughput.

The difficulties associated with separating oil-water mixtures depend primarily on the dispersed phase size and its stability in the mixture. Mixtures of oil and water are classified, in terms of the diameter (d) of the dispersed phase, as free oil and water if $d >$ 150 μm, a dispersion if 20 μm $\leq d \leq$ 150 μm, or an emulsion if $d <$ 20 μm.[4] The stability of oil-water emulsions is greatly enhanced by the addition of surfactants, which decreases

the interfacial tension between the oil and water phases, and hinders the coalescence of droplets.[7]

1.2.2 Current Separation Techniques Versus Membrane Technology

Numerous methods, including gravity separation, flotation, oil-absorbing materials, electrocoagulation, and flocculation, have traditionally been used to separate oil-water mixtures.[4, 8-12] Gravity separation or skimming is effective for separating free oil and water, however, it is unsuitable for the separation of smaller oil droplets or oil-water emulsions.[9] Flotation uses streams of air bubbles to enhance coalescence of smaller oil droplets, and it is typically followed by demulsification (i.e., conversion of an oil-water emulsion to a free oil and water) with chemicals and/or heat.[11, 13] Porous materials have also been widely used to absorb oil from water in case of oil-spills in the ocean. However, these materials absorb not only oil, but also water, due to a lack of selectivity, resulting in low separation efficiency.[14-15] Electric-field-driven coalescence or chemical addition can be effective for demulsifying emulsions, but these methods typically lead to significant energy consumption and secondary pollution.[12, 16]

Membrane-based methods have become increasingly attractive for the separation of oil-water mixtures because they are relatively energy-efficient, can be readily used to separate a variety of industrial feed streams and provide consistent permeate quality.[4, 9] Major steps in membrane technology began in the 1950s and 1960s[17] and they have been studied for decades, yet there are still some disadvantages associated with membrane-based oil-water separation; the biggest drawback is membrane fouling due to surfactant adsorption or pore plugging by oil droplets, resulting in diminished permeate flux.[18-19]

Research on membranes with selective wettability promises to improve the separation efficiency, as well as, imbue anti-fouling properties to oil-water separating membranes.[4] If a membrane demonstrates a different wettability with water versus oil, it may be useful for the extremely efficient separation of oil-water mixtures.[20] This idea has led to a large number of membranes with selective wettability being developed and applied for separating a range of different oil-water mixtures.

1.2.3 Fundamentals of Wetting

A surface's wettability is commonly characterized by a contact angle.[21] On a non-textured (or smooth) surface, the equilibrium contact angle θ is given by Young's relation:[22]

$$\cos\theta = \frac{\gamma_{SV} - \gamma_{SL}}{\gamma_{LV}} \qquad (1.1)$$

Here, γ is the interfacial tension between two phases and S, L, and V refer to the solid, liquid, and vapor phases, respectively. Thus, γ_{SV} is the interfacial tension between the solid and vapor phases, and it is commonly called the solid surface energy. γ_{LV} is typically referred to as the liquid surface tension. Based on previous literature,[23-25] the wettability of the solid surface can be classified into four regimes using contact angles for water: superhydrophobic ($\theta_{water} > 150°$), hydrophobic ($\theta_{water} > 90°$), hydrophilic ($\theta_{water} < 90°$) and superhydrophilic ($\theta_{water} \sim 0°$). Similarly, based on contact angles for a low surface tension liquid such as an oil or alcohol, surfaces are considered superoleophobic ($\theta_{oil} > 150°$), oleophobic ($\theta_{oil} > 90°$), oleophilic ($\theta_{oil} < 90°$) and superoleophilic ($\theta_{oil} \sim 0°$). Typically superhydrophobic or superoleophobic surfaces are referred to as super-repellent surfaces.

4

When a liquid droplet is placed on a textured (or rough) surface, the apparent contact angle (θ^*) on the surface can be significantly different from the Young's contact angle θ. The addition of a liquid droplet to a textured surface may lead to either the 'fully-wetted' Wenzel[26] or the Cassie-Baxter[27] state, forming a composite solid-liquid-air interface. The Wenzel state exists when the liquid fully permeates and wets the textured
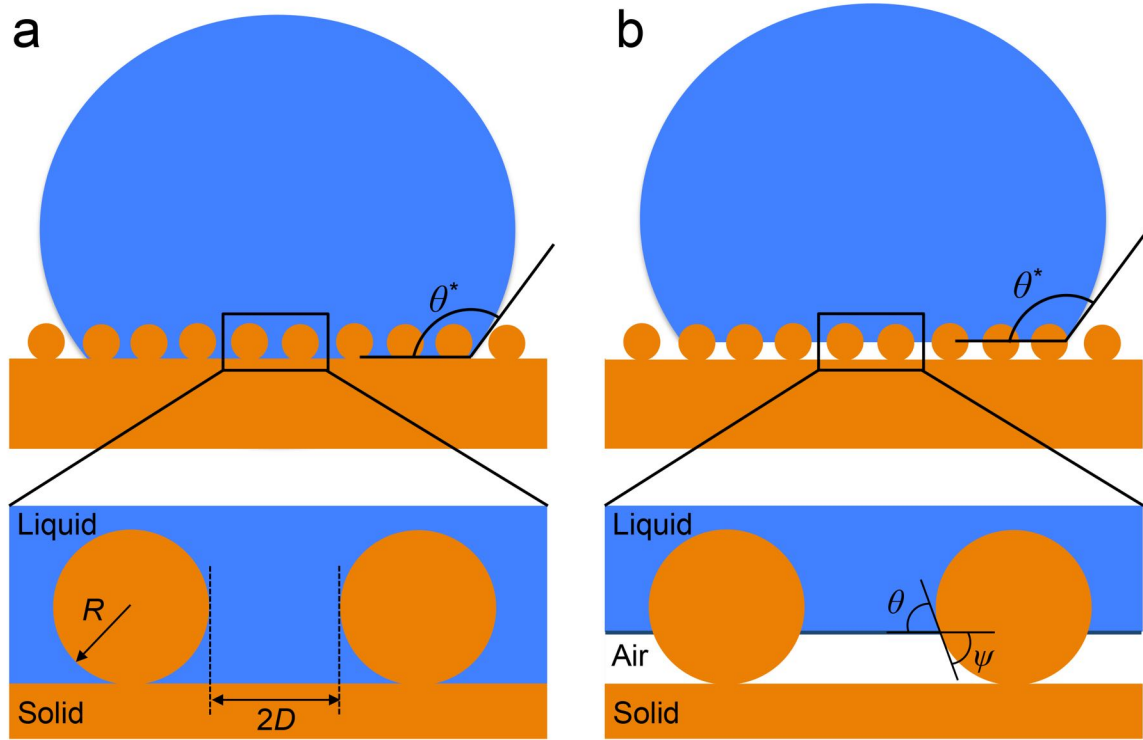
Figure. 1.1: Liquid droplets on textured surfaces. The (a) Wenzel and (b) Cassie-Baxter states are shown. In the diagrams, R is the feature radius, $2D$ is the inter-feature spacing, θ is the equilibrium contact angle, θ^* is the apparent contact angle, and ψ is the texture angle. Adapted from Kota *et al.*[25] © 2014 with permission from Nature Publishing Group.

surface, as seen in Figure 1.1a. In this state, the overall free energy reaches its minimum when the apparent contact angle becomes θ^*, given by the Wenzel relation as:[26]

$$\cos\theta^* = r\cos\theta .$$

$$(1.2)$$

Here r is the surface roughness defined as the ratio of the actual surface area to the

projected surface area. Per its definition, $r \geq 1$. Consequently, roughness yields a lower apparent contact angle for a liquid with $\theta < 90°$. On the other hand, a higher apparent contact angle can be achieved for a liquid with $\theta > 90°$.

The Cassie-Baxter state exists when air is trapped underneath the liquid droplet, forming a composite solid-liquid-air interface, as seen in Figure 1.1b. The apparent contact angles in this state can be calculated using the Cassie-Baxter relation,[27] given as:

$$\cos\theta^* = f_{SL}\cos\theta + f_{LV}\cos\pi = f_{SL}\cos\theta - f_{LV} \ . \qquad (1.3)$$

This relation describes how the apparent contact angle varies with the local areal fractions of the solid-liquid (f_{SL}) and the liquid-air (f_{LV}) interfaces in the vicinity of the triple-phase (solid-liquid-air) contact line.[28] For most surfaces, the local and global areal fractions are equivalent.

Both the Wenzel and the Cassie-Baxter relations provide correlations between the apparent contact angle θ^* and the Young's contact angle, θ, based on free energy analysis. It is evident from Equations 1.2 and 1.3 that higher apparent contact angles can be encouraged in either the Wenzel state, if $\theta > 90°$ and $r \gg 1$, or in the Cassie-Baxter state, if $f_{SL} \ll 1$. However, contact angle hysteresis (i.e., the difference between the advancing and receding contact angles) for the two states can be significantly different. The difference between the advancing (the maximum contact angle on a given surface) and receding (the minimum contact angle on a given surface) contact angles arises due to the presence of multiple metastable energy states on real, heterogeneous surfaces.[29] Typically, the contact angle hysteresis in the Wenzel state is larger than in the Cassie-Baxter state. This is because the solid-liquid interface is pinned on the textured surface.[30] By contrast, a composite solid-liquid-air interface in the Cassie-Baxter state leads to

lower contact angle hysteresis and higher apparent contact angles when the contact area between the solid and the liquid is small.[30-31] Consequently, the development of composite interfaces is essential for fabricating super-repellent surfaces.

1.2.4 Robust Composite Interfaces

Although the development of composite interfaces is necessary in engineering super-repellent surfaces, the details of the surface texture can significantly affect the stability of such an interface. Previous literature[32-35] revealed that the formation of the stable Cassie-Baxter state is possible only if the Young's contact angle θ is greater than
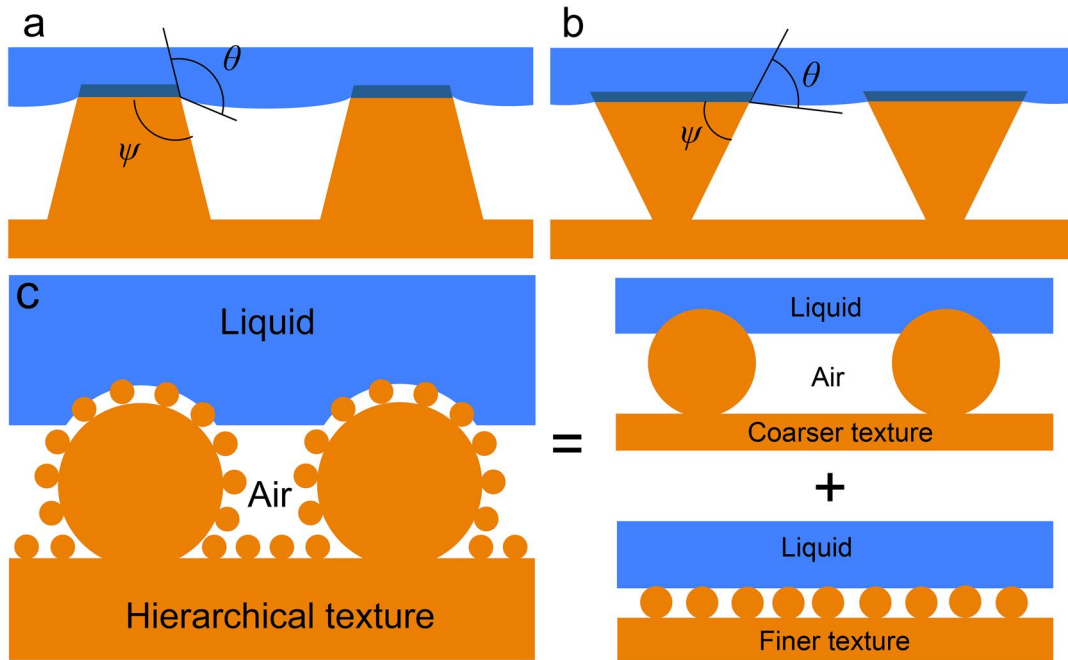
Figure. 1.2: Composite interfaces and hierarchical texture. (a) A Cassie-Baxter state on a concave texture with $\psi > 90°$ and $\theta > 90°$. (b) A similar state exists with a lower surface tension liquid ($\theta < 90°$) on convex, re-entrant texture ($\psi < 90°$). (c) A hierarchical texture combines coarser and finer textures to maximize the solid-air interface. Adapted from Kota *et al.*[25] © 2014 with permission from Nature Publishing Group.

the local texture angle ψ. To illustrate this, two types of surface texture are considered here (Figures 1.2a and 1.2b). The surface texture shown in Figure 1.2a (texture angle ψ

> 90°) can lead to the formation of a composite interface when $\theta \geq \psi$. If $\theta < 90°$, which is common for low surface tension liquids such as different oils on most surfaces, the surface texture cannot maintain a stable composite interface, regardless of its surface energy or composition. However, for the same low surface tension liquid with $\theta < 90°$, it is possible to support a composite interface as long as $\theta \geq \psi$. Such surface geometry with $\psi < 90°$ is known as re-entrant texture. Re-entrant texture allows for the formation of a composite interface with low surface tension liquids, which may lead to oleophobic or superoleophobic properties. Further design strategies for increasing the robustness (repellency with high breakthrough pressure) of a composite interface are described in the following section.

1.2.5 Design Strategies for Membranes with Selective Wettability

Systematic design of membranes for oil-water separation requires the parameterization of two important physical characteristics.[36] One is surface porosity, which affects the rate of liquid permeation through the membrane. It is evident from the Hagen-Poiseuille relation[37] that the volumetric flow rate $Q \propto r^4$ (r is the pore radius), when all other parameters are held constant. As the pore diameter decreases, viscous resistance to fluid flow through the membrane pores increases and consequently, the flux decreases. Although the Hagen-Poiseuille relation provides a correlation between the flow rate and the pore size, it does not account for the spacing between the pores, which also impacts flux. Previous work[23, 34, 38-39] discussed the spacing ratio, D^*, which provides a dimensionless measure of surface porosity by considering both the pore size and spacing. For membranes possessing a predominantly cylindrical texture, such as

interwoven meshes or fabrics, $D^*_{cylinder} = (R+D)/R$. Here R is the radius of a cylinder and $2D$ is the inter-cylinder spacing. Surface porosity increases with increasing D^*. Thus, membranes with higher values of D^* will show a higher permeation rate for a given contacting liquid.

The other critical physical characteristic is the breakthrough pressure ($P_{breakthrough}$), defined as the maximum pressure differential across the membrane up until which the membrane prevents the permeation of a given liquid. In order to parameterize $P_{breakthrough}$ for a known surface texture and chemistry, previous work[34, 38-40] discussed the robustness factor A^*. This dimensionless value is obtained by scaling $P_{breakthrough}$ with respect to a reference pressure $P_{ref} = 2\gamma_{LV}/l_{cap}$. Here, $l_{cap} = \sqrt{\gamma_{LV}/\rho g}$ is the capillary length of a liquid, ρ is the liquid density and g is the acceleration due to gravity. P_{ref} is close to the minimum possible pressure differential across a millimeter-sized liquid droplet or a puddle.[34] Consequently, large values of A^* ($A^* \gg 1$) indicate the formation of a robust composite interface with a high $P_{breakthrough}$. On the other hand, membranes with robustness factor $A^* \leq 1$, for a given contacting liquid, cannot support a composite interface, allowing the contacting liquid to penetrate into the pores and be fully imbibed. The robustness factor, for a surface possessing predominantly cylindrical texture, is given as:[38, 40]

$$A^*_{cylinder} = \frac{P_{breakthrough}}{P_{ref}} = \frac{l_{cap}}{R(D^*_{cylinder}-1)}\frac{(1-\cos\theta)}{(D^*_{cylinder}-1+2\sin\theta)} \qquad (1.4)$$

For the effective separation of oil and water, membranes must be designed for a high permeation rate of one phase (e.g., water) and simultaneously, a high breakthrough pressure for the other phase (e.g., oil). This can be achieved by maximizing the two

design parameters D^* and A^*.

However, D^* and A^* are strongly coupled for membranes with a periodic, cylindrical geometry,[34, 38, 40] as is evident from Equation 1.4. The value of D^* can be increased by either increasing D or reducing R, both of which lead to a decrease in A^*. As discussed above, it is crucial to increase A^* without affecting D^* in order for the membranes to maintain a high rate of permeation for one phase (e.g., water), and a high breakthrough pressure for the other (e.g., oil) simultaneously. Such an enhancement can be achieved by introducing low surface energy materials on the solid surface, which leads to an increase in the values of Young's contact angle θ. Using this approach, the values of A^* and the breakthrough pressure can be increased without changing the membrane geometry. However, lowering the surface energy of the solid may result in omniphobic surfaces, which repel both water and oil.[34, 41-42] Consequently, membranes with such surfaces may not allow selective permeation of one phase over the other phase. As described by Kota et $al.,$[25] there are other design methods for increasing A^* without affecting D^* and vice-versa. Utilizing a finer length scale texture, which decreases both R and D in such a way that the spacing ratio, D^*, remains constant, will increase A^* according to Equation 1.4. On the other hand, D^* can be increased, while A^* remains constant, by adding hierarchical scales of texture. This is due to composite interfaces being the least stable on the largest scale of texture. Therefore, $A^*_{hierarchical} \approx A^*_{micro}$, if both micro and nanostructures are present, while $D^*_{hierarchical} >> D^*_{micro}$ due to the extra air captured within the multiple texture scales. Both A^* and D^* can be maximized in this way for fabricating a robust membrane with a high permeation rate.

Membranes possessing high A^* values for one phase ($A^*_{liquid1} >> 1$), as well as

small A^* values for the other phase ($A^*_{liquid2} \leq 1$), allow for selective permeation of one liquid over the other. Such membranes can be achieved by developing surfaces that display significant differences between θ_{water} and θ_{oil}. In general, membranes can be categorized into four groups based on their contact angles with oil and water (Figure 1.3): 1. Hydrophobic and Oleophilic, 2. Hydrophilic and Oleophilic, 3. Hydrophilic and Oleophobic and 4. Hydrophobic and Oleophobic. In the following sections, we discuss recent developments and progress on membranes used for the separation of oil and water and where they fall on the diagram shown in Figure 1.3.
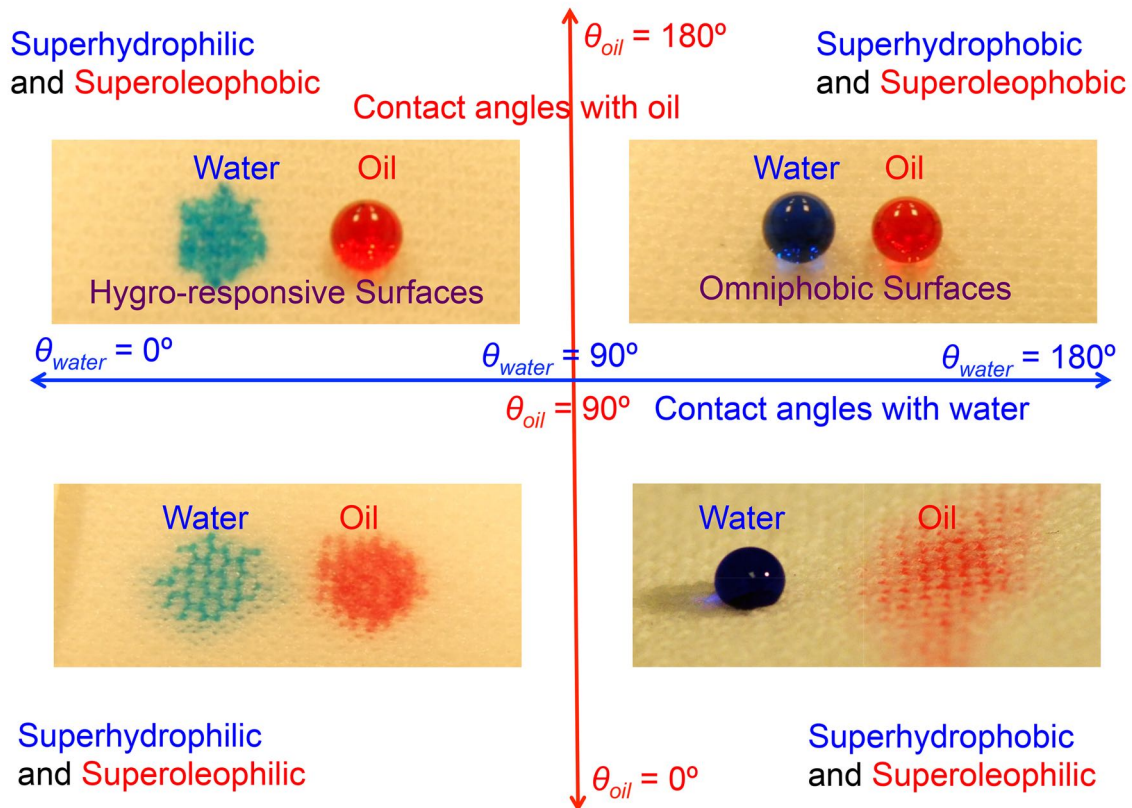
Figure 1.3: Membrane classification based on selective wettability for oil and water.
A membrane is Hydrophobic and Oleophilic when $\theta^*_{water} > 90°$ and $\theta^*_{oil} < 90°$, Hydrophilic and Oleophilic when $\theta^*_{water} < 90°$ and $\theta^*_{oil} < 90°$, Hydrophilic and Oleophobic when $\theta^*_{water} < 90°$ and $\theta^*_{oil} > 90°$, and Hydrophobic and Oleophobic when $\theta^*_{water} > 90°$ and $\theta^*_{oil} > 90°$.

1.3 Membranes with Selective Wettability

1.3.1 Hydrophobic and Oleophilic Membranes (HP/OL)

One variation of surfaces with selective wettability is a substrate that is both hydrophobic and oleophilic. There are a few examples of this in nature, such as the lotus leaf and duck feathers. Many groups have been using this form of wettability to selectively separate oil and water mixtures by creating membranes that allow various oils to permeate while repelling water. Typically, such membranes are developed by coating a material with selective wettability onto porous substrates. A range of flexible and rigid substrates have been used for this purpose including: stainless steel and copper meshes, polymers, textiles, and filter papers. It should be noted that a number of previous publications fail to explicitly discuss if the measured contacts angles are advancing, receding, or static. In this chapter, we have provided the contact angles (advancing, receding, or static) exactly as described in the original publication.

Feng et $al.$[43] spray coated an aqueous 30 wt% polytetrafluoroethylene (PTFE) emulsion, also containing an adhesive, a dispersant, and a surfactant, onto a stainless-steel mesh. After half an hour in a 350°C oven, the solvent evaporated. The other organic, non-Teflon components were decomposed at this temperature, leaving behind a rough PTFE surface (Figures 1.4a and 1.4b). The surface contained micro and nanoscale roughness yielding a static $\theta^*_{water} = 156.2 \pm 2.8°$ and $\theta^*_{diesel\ oil} = 0 \pm 1.3°$ (Figures 1.4c and 1.4d). A free diesel oil and water mixture was poured over the developed membrane, which was mounted at approximately 45° in a glass tube to allow the lower density diesel oil to contact the membrane. It allowed for the separation of the diesel oil and water under gravity with > 95% separation efficiency. PTFE was also used in conjunction with
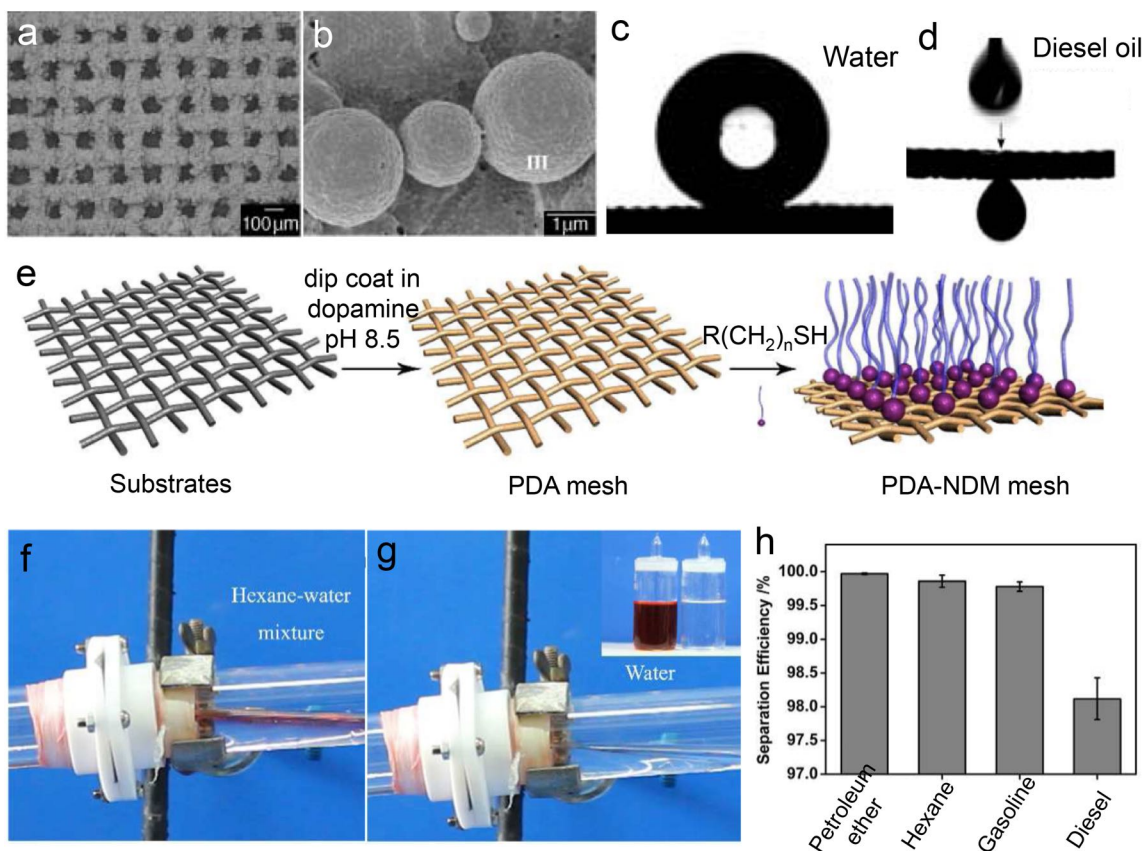
Figure 1.4: Coated stainless steel meshes with selective wettability. (a-b) Textured Teflon coating on stainless steel mesh. (c-d) The superhydrophobic and superoleophilic nature of the mesh. Reproduced from Feng *et al.*[44] © 2004 WILEY-VCH Verlag GmbH & Co. KGaA, Weinheim with permission from John Wiley & Sons, Inc. (e) The fabrication of a *n*-dodecyl mercaptan treated mesh. (f-g) The separation of a hexane-water mixture with the apparatus at a 15° tilt angle. (h) Efficiencies for the separation of a variety of oils and water with the PDA-NDM mesh. Adapted with permission from Cao *et al.*[45] Copyright 2013 American Chemical Society.

ZnO on a stainless-steel mesh by Wu *et al.*[46] A 0.2 M zinc acetate solution was spray coated onto a cleaned mesh at 180°C to form ZnO seeds. Following spray coating, the ZnO crystals on the mesh were grown further in a basic 0.1 M zinc acetate solution. Finally, the rough ZnO surface was spin coated with PTFE to create a low surface energy, hierarchically textured surface. This led to the formation of 1–2 μm sized flowers and nanorods. On the fabricated surface, static $\theta^*_{water} = 157°$ (sliding angle of $< 5°$) and static $\theta^*_{diesel\ oil}$ was nearly 0°. To demonstrate the separation ability of the surface with

diesel oil and water, droplets of each were simultaneously poured on the membrane. The water rolled off the surface, while the oil passed through the mesh. Tuteja *et al.*[23] achieved a superhydrophobic and superoleophilic surface by electrospinning fluorodecyl POSS-PMMA fibers onto a steel mesh. A fibrous mat with multiple scales of texture was achieved, with the f-POSS bringing additional roughness to the "beads on a string" fibers. $\theta^*_{water} = 161 \pm 2°$ and $\theta^*_{alkane} = 0°$ for a membrane created by electrospinning a 9.1 wt% f-POSS in PMMA mixture. With the membrane suspended above a glass jar, a free octane and water mixture was cleanly separated.

Other groups have worked to chemically modify the underlying porous substrate. Wang *et al.*[47] used a stainless steel mesh modified with 1H, 1H, 2H, 2H-Perfluoroalkyltriethoxysilane (PFAS). The surface displayed $\theta^*_{water} = 148.2°$ and $\theta^*_{diesel} = 0°$. The developed membrane was used to separate two different oil and water mixtures: xylene/water (94.0 wt% water) and diesel/water (95.1 wt% water). The membrane allowed the oils to permeate through, while the water was retained. For the xylene/water system, the permeate contained 0.081 wt% water, while for the diesel/water system, 0.028 wt% water was measured in the permeate. Cao *et al.*[45] coated a stainless steel mesh with a polydopamine film to act as an adhesive layer for the subsequent addition of *n*-dodecyl mercaptan (NDM) by a Michael's addition reaction (Figure 1.4e). The surface was covered with nano-papillae, which along with the NDM, yielded a hydrophobic surface. They found $\theta^*_{water} = 143.8 \pm 1.0°$ and $\theta^*_{diesel\ oil}$ close to 0°. To test the oil-water separation ability, the membrane was placed inside a glass tube and the tube was tilted at a 15° angle to allow the oil to contact the mesh, despite the density difference between the oil and water (Figures 1.4f and 1.4g). Diesel/water, petroleum ether/water, and

gasoline/water mixtures were separated with $\eta = 98.1\%$ efficiency for diesel/water and $\eta > 99.7\%$ for the other two separations (Figure 1.4h).
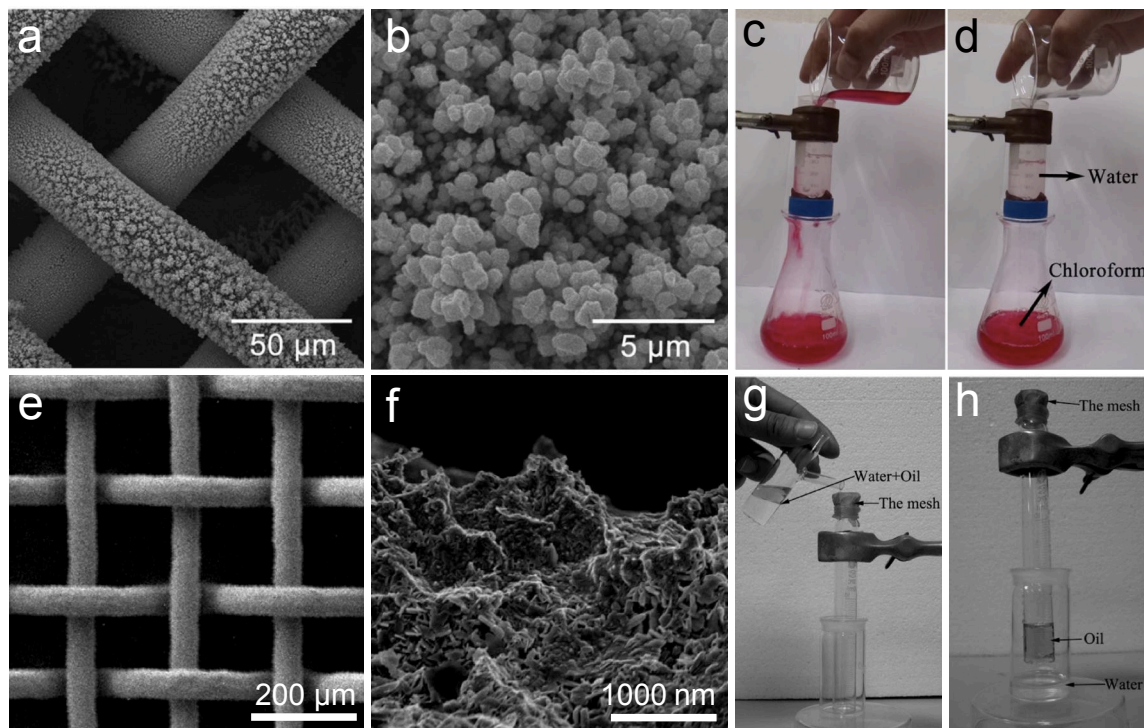
Figure 1.5: Copper mesh modification and separation ability. (a-b) SEM images of a copper mesh coated with Cu nanoparticles. (c-d) The separation of chloroform and water with the as-prepared copper mesh. Reprinted with permission from Wang and Guo.[48] © 2013 AIP Publishing LLC. (e-f) Etched and 1-hexadecanethiol treated copper mesh with 135 μm pore size and "nano-hills." (g-h) Removal of diesel oil from water as the oil permeates and the water rolls off the mesh into the surrounding vial. Adapted with permission from Wang *et al.*[49] Copyright 2009 American Chemical Society.

Several groups have also used a modified copper mesh substrate for the separation. Wang *et al.*[50] achieved hierarchical copper surfaces by cathodic electrodeposition on copper meshes. Copper microclusters with 30–50 nm nanoparticles were developed on the mesh surface, and the textured copper meshes were soaked in a solution of *n*-dodecanoic acid for 12 hours to yield $\theta^{*}_{water} = 158 \pm 2°$ (and a 2° sliding angle), while $\theta^{*}_{diesel\ oil}$ was $\approx 0°$. The superhydrophobic and superoleophilic membrane was found to be an effective diesel oil and water separator. Wang and Guo[48] used a

similar electrochemical approach and deposited a ~2 μm thick coating of copper nanoparticles on top of a copper mesh followed by n-octadecyl thiol grafting (Figures 1.5a and 1.5b). $\theta^*_{water} = 154.1°$ and $\theta^*_{chloroform} = 0°$ were achieved, and a mixture of chloroform and water was separated by the prepared mesh mounted inside a tube (Figures 1.5c and 1.5d). Wang et al.[49] utilized the nitric acid etching of a copper mesh, followed by chemically modifying the surface with hexadecanethiol (Figures 1.5e and 1.5f). The mesh showed $\theta^*_{water} = 153 \pm 1°$ (< 5° sliding angle), while diesel oil permeated through the mesh ($\theta^*_{diesel} = 0°$). Diesel oil and water separation was demonstrated by pouring a mixture onto a mesh at the opening of a test tube. The diesel permeated through, while the water rolled off into a secondary beaker (Figures 1.5g and 1.5h).

Liu et al.[51] fabricated a textured copper mesh with hydrophobic and oleophilic wetting properties, which could be reversibly switched to hydrophilic and underwater oleophobic (Figures 1.6a and 1.6b). A copper mesh was textured with $Cu(OH)_2$ nanoneedles by oxidation with 0.05 M $K_2S_2O_8$ and 1.0 M NaOH (Figures 1.6c–e). The as-prepared membrane was found to be superhydrophilic. After surface modification using a self-assembling monolayer of stearic acid, formed by dipping the membrane in a 0.05 M solution for 5 minutes, the membrane became superhydrophobic and superoleophilic with $\theta^*_{water} = 155.4 \pm 1.3°$ and $\theta^*_{diesel} = 0°$. This mesh could separate diesel oil and water mixtures by allowing oil to permeate through, while retaining water (Figures 1.6f and 1.6g). Interestingly, the surface wettability was altered to superhydrophilic and underwater superoleophobic by immersion in tetrahydrofuran (THF) for 5 minutes due to the desorption of stearic acid. Such wettability reversal allowed water to permeate through while retaining diesel oil, leading to switchable oil-

16

water separation (Figures 1.6h and 1.6i).
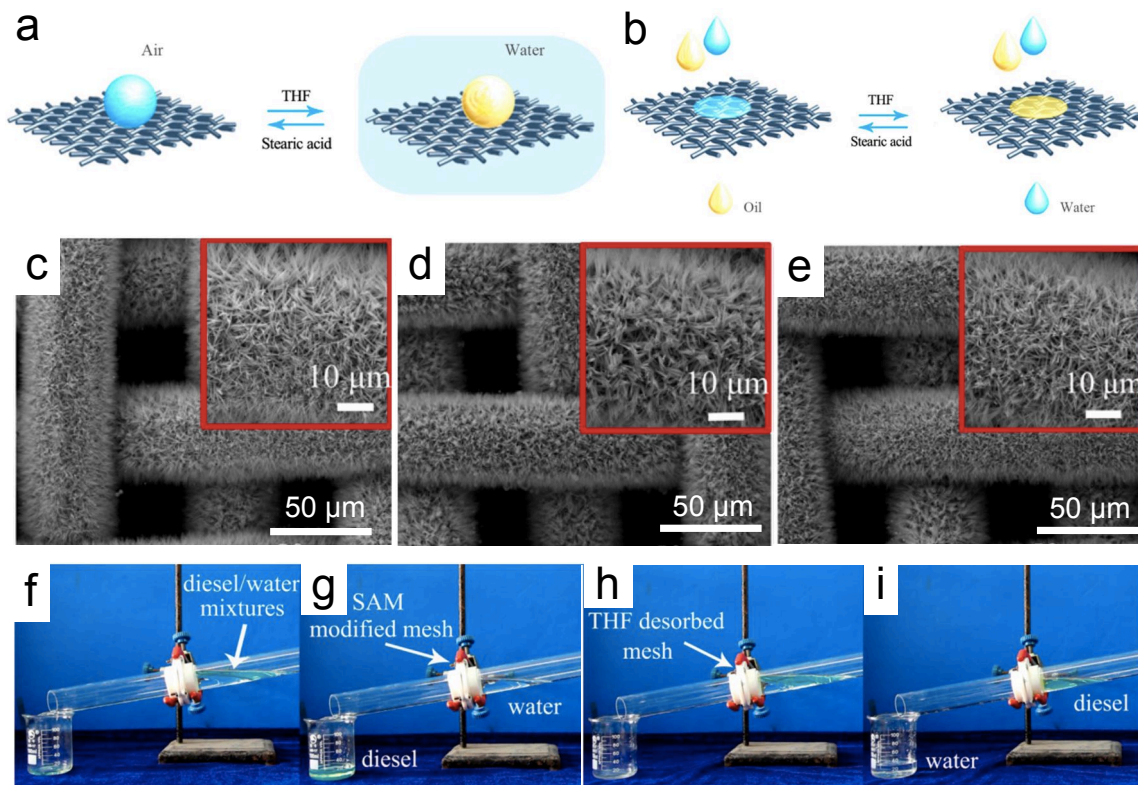
Figure 1.6: The switchable wetting of stearic acid modified Cu(OH)$_2$ nanoneedles on a copper mesh. (a-b) Schematics illustrating the switchable wettability for the mesh. Stearic acid self-assembled monolayer (SAM) provides superhydrophobicity, while THF desorbs this layer to provide a superhydrophilic and underwater superoleophobic mesh. SEM images are provided, with higher magnification insets, of (c) a mesh with Cu(OH)$_2$ nanoneedles, (d) a SAM modified mesh, and (e) a THF desorbed mesh. (f) A diesel-water mixture was tested on the membrane showing that the SAM modified mesh allowed diesel permeation (g), while the THF desorbed mesh permeated water (h-i). Adapted with permission from Liu *et al.*[51] Copyright 2014 American Chemical Society.

Copper meshes have also been coated with polymers to achieve hydrophobic and oleophilic properties. Crick *et al.*[52] deposited Sylgard 184 silicone elastomer (PDMS) on copper meshes using aerosol assisted chemical vapor deposition (AACVD). The PDMS-based elastomer was dissolved in chloroform and used in the AACVD process to develop 3–5 μm tall micropillars on the mesh surface, which became superhydrophobic with θ^*_{water} = 152°–167° for various mesh sizes. The toluene, petroleum ether, and hexane

contact angles on the fabricated mesh were $\theta^*_{oil} = 0°$. The membrane was used to separate mixtures of water/toluene, water/petroleum ether, and water/hexane. Almost no water permeated through the mesh, and greater than 99% of the oil phase could be removed from the water.

Not all membranes have used metal meshes as the substrate; polymeric substrates have also been found to work well. The porous polymer substrates with desired wetting properties may be formed directly, or they may be modified through additional texture and chemical treatments, as necessary. Shang *et al.*[53] formed a nanofiber membrane substrate from electrospun cellulose acetate. Thermosetting 2,2-bis(3-*m*-trifluoromethylphenyl-l-3,4-dihydro-2*H*-1,3-benzoxazinyl)propane (BAF-tfa) monomer and SiO_2 nanoparticles (7–40 nm) were added on top by dip coating, followed by polymerization at 190°C. The hydrophobic polymer is referred to as fluorinated polybenzoxazine (F-PBZ) and binds the nanoparticles to the cellulose acetate fibers. The particles add hierarchical roughness, while the F-PBZ provides a low surface energy. The fiber diameter and roughness were controlled by varying the wt% of BAF-tfa and SiO_2 nanoparticles in the dip coating solutions (Figure 1.7a). A static contact angle of up to $\theta^*_{water} = 161°$ was measured, along with a $\theta^*_{dichloromethane} = 3°$. This membrane was shown to quickly separate a dichloromethane and water (50% v/v) mixture (Figure 1.7b). Tang *et al.*[54] continued this work, with a F-PBZ coating on an electrospun substrate, to improve the physical properties of the membrane. Their synthesis procedure was very similar, but the materials were slightly different. The cellulose acetate was exchanged for poly(*m*-phenylene isophthalamide) (PMIA) with added multi-walled carbon nanotubes (MWCNTs). Also, a new version of F-PBZ was utilized; the new monomer was 2,2-
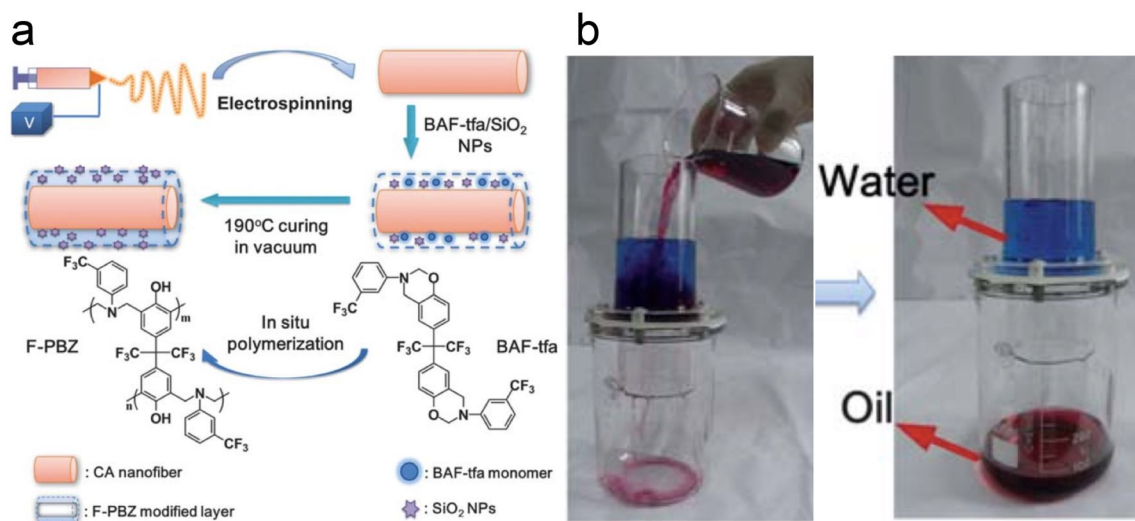
Figure 1.7: F-PBZ/SiO₂ nanoparticle-modified, electrospun cellulose acetate membranes. (a) The fabrication strategy for a nanofibrous membrane produced using electrospinning and (b) the separation ability of the fabricated membrane tested with a 50% v/v mixture of dichloromethane and water. Adapted from Shang *et al.*[53] © 2012 with permission from The Royal Society of Chemistry.

bis(3-octadecyl-3,4-dihydro-2*H*-1,3-benzoxazinyl)hexafluoro propane (BAF-oda). The coating allowed the membrane to achieve θ^*_{water} = 161° and $\theta^*_{dichloromethane}$ = 0° and to cleanly separate a mixture of dichloromethane and water (50% v/v). By adjusting the polymers used in this work, this new membrane was stable up to 350°C, resistant to hot water at 80°C, and showed a mechanical strength of 40.8 MPa.

Huang *et al.*[55] developed another method for achieving hydrophobic and oleophilic membranes with fluorinated benzoxazine using silica nanofibers, alumina (Al₂O₃) nanoparticles, and 3-(3-(trifluoromethyl)phenyl)-2*H*-benzoxazine-6-carbaldehyde (BAF-CHO) monomer (Figure 1.8a). θ^*_{water} = 161° and $\theta^*_{rapeseed\ oil}$ = 0°, and the membrane could gravity separate a surfactant-stabilized water-in-petroleum ether, micron-scale emulsion (Figures 1.8b and 8c). The petroleum ether phase was shown to pass through the membrane under gravity, while retaining the water (Figure 1.8b). The

filtrate showed no water droplets, indicating almost complete separation (Figure 1.8c).
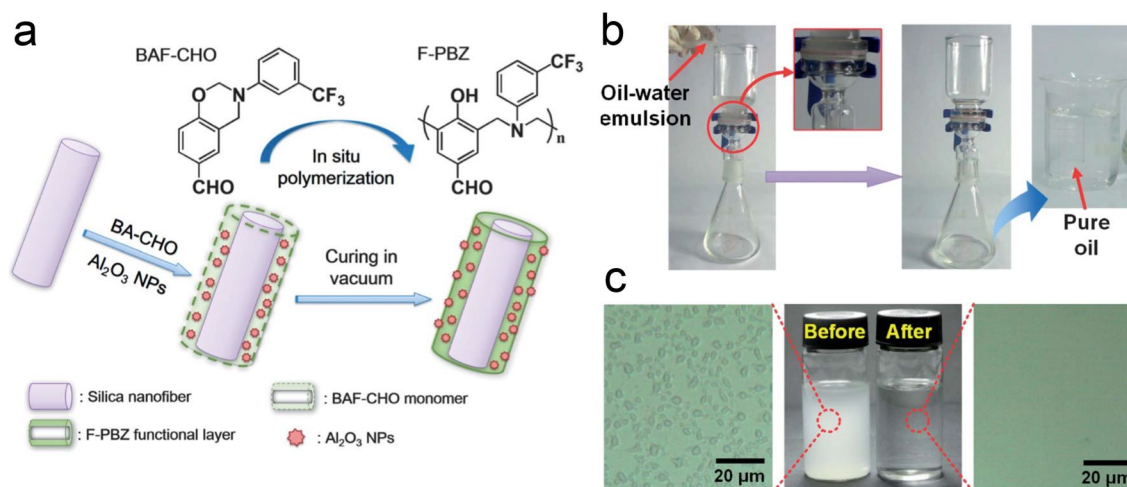
Figure 1.8: F-PBZ/Al₂O₃ nanoparticle-modified, electrospun silica nanofibrous (SNF) membranes. (a) Procedure for the synthesis of relatively durable nanofibrous membranes (b) The gravity-driven separation of a Span 80-stabilized water-in-petroleum ether nanoemulsion. (c) The optical clarity of the oil after separation is apparent in the photograph and optical micrographs. Adapted from Huang *et al.*[55] © 2013 with permission from The Royal Society of Chemistry.

Zhang *et al.*[56] utilized a phase-inversion process to form a hierarchical poly(vinylidene fluoride) (PVDF) membrane for separating surfactant-stabilized emulsions. The PVDF solution was first prepared in N-methylpyrrolidone followed by drop casting onto a PTFE substrate. This was subsequently dipped in water for phase inversion, and the resulting PVDF membrane was peeled off the PTFE substrate. The prepared PVDF membrane showed microparticles, with surface nanostructure, interconnected by fibers. The membrane showed $\theta^*_{water} = 158°$ and $\theta^*_{dichloromethane} < 1°$, and the separation capability was tested with water-in-oil emulsions (5 – 20 μm droplets), with and without surfactant. The oils used included: petroleum ether, toluene, isooctane, and dichloromethane. The membranes could separate the various water-in-oil emulsions under gravity with $\eta > 99.95\%$ separation efficiency.

Multiple groups have been successful in modifying commercially available filter papers to impart them with hydrophobic and oleophilic properties. Wang *et al.*[57] fabricated hydrophobic and oleophilic membranes by dip coating a cellulose filter paper in a solution containing polystyrene and PDMS-modified, hydrophobic silica nanoparticles. The polystyrene and silica nanoparticles were used in a 1:1 mass ratio for optimum results. A static $\theta^*_{water} = 157 \pm 2°$ was measured, while diesel oil spread and permeated through the surface ($\theta^*_{diesel\,oil} = 0°$). Using this membrane, mixtures of diesel oil and water, with volume ratios ranging from 1:15 to 1:1 (oil:water), demonstrated a separation efficiency $\eta > 96\%$ upon pouring over the membrane. Du *et al.*[58] fabricated a polystyrene film, with embedded PTFE nanoparticles (200 nm), on top of filter paper (15-20 μm pore size) to achieve superhydrophobic and superoleophilic membranes. PTFE and polystyrene nanoparticle colloidal solutions, 6 wt% and 1 wt% respectively, were mixed in a 3:2 ratio. The filter paper was dipped in the solution for 30 minutes and then heated at 220°C for 20 minutes to melt only the polystyrene nanoparticles, while retaining roughness from the PTFE nanoparticles. The $\theta^*_{water} = 155 \pm 2°$ and $\theta^*_{hexane} = 0°$ on the developed membranes. To test the separation ability, a hexane and water mixture was poured over the membrane inside a funnel. The membrane allowed only the hexane to permeate through, yielding a $\eta > 99\%$ separation efficiency.

Carbon is also useful, when used in conjunction with polymers and filter papers, for forming composite membranes that are hydrophobic and oleophilic, as well as electrically conductive. Asthana *et al.*[59] utilized combinations of carbon black (CB), graphene nanoplatelets (GNP) and carbon nanotubes (CNT) with Capstone ST-100 fluoroacrylic polymer to achieve conducting, hydrophobic and oleophilic membranes. A

2 wt% solution of the fluoropolymer and a separate 2 wt% solution of the various carbon fillers were made. The two solutions were mixed to achieve the desired carbon filler to polymer ratio. Different ratios of carbon fillers and fillers-to-polymer were tested until the best overall mixture for water-impalement resistance and conductivity was found to be a 1:1:2 CB:GNP:Polymer mass ratio. The prepared solution mixture was drop cast onto cellulose filter paper and cured at 160°C to melt the polymer. The rough hierarchical surface showed superhydrophobicity with $\theta^*_{water} > 150°$ and oleophilicity with $\theta^*_{mineral\ oil} = 0°$. A mineral oil ($\rho_{oil} = 0.838$ g/mL) and water (1:1 v/v) mixture was completely gravity separated with the CB/GNP membrane inside a funnel. The funnel geometry allowed the lower density oil to contact the membrane.

Shi et al.[60] fabricated films composed of purely single-walled carbon nanotubes (SWCNTs). This film met the need for achieving the thinnest membrane possible, while maintaining a useful pore size for maximum permeation rates. A SWCNT suspension was filtered through a mixed cellulose ester (MCE) membrane to form the film. Immersion in acetone dissolved the MCE membrane and the SWCNT film floated to the surface (Figure 1.9a). Membranes with thicknesses of 30-120 nm and corresponding pore sizes of 200-20 nm were fabricated. For static droplets on the 70 nm thick membrane, $\theta^*_{water} = 94°$ and $\theta^*_{dichloromethane} = 0°$. The film was placed on a ceramic support for liquid separation testing, and several different emulsions, both surfactant-free and surfactant-stabilized water-in-oil emulsions, were separated, including water-in-petroleum ether and span80-stabilized water-in-toluene emulsions (Figure 1.9c). All separations showed no water droplets in the oil permeate, and the oil was tested to be > 99.95 wt% pure, while maintaining very high permeation rates up to 107,140 L m^{-2} h^{-1} bar^{-1} for the 30 nm thick

film (obtained using surfactant-free water-in-petroleum ether emulsion).
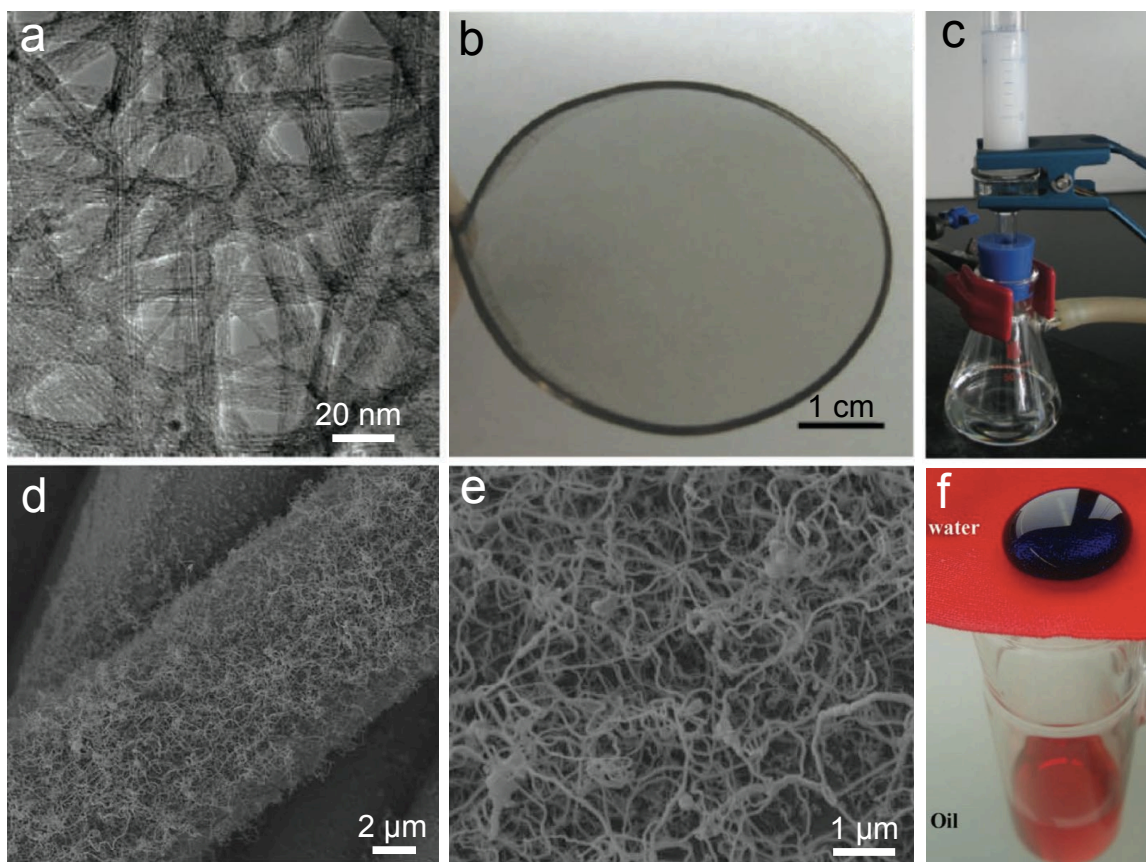
Figure 1.9: SWCNTs and silicone nanofilament membranes. (a) A TEM image of a 70 nm thick SWCNT film showing its interlaced structure. (b) The SWCNT film supported by a steel hoop and (c) the selective permeation of oil from an emulsion using this film. Reproduced from Shi *et al.*[60] © 2013 WILEY-VCH Verlag GmbH & Co. KGaA, Weinheim with permission from John Wiley & Sons, Inc. (d-e) Silicone nanofilaments grown on a polyester textile. (f) The simple separation of an octane and water mixture. Reproduced from Zhang *et al.*[61] © 2011 WILEY-VCH Verlag GmbH & Co. KGaA, Weinheim with permission from John Wiley & Sons, Inc.

Zhang and Seeger[61] modified polyester textiles to achieve superhydrophobic and superoleophilic membranes through the chemical vapor deposition of trichloromethylsilane, which grew silicone nanofilaments on the textile (Figures 1.9d and 1.9e). The rough, fibrous surface helped achieve superhydrophobicity ($\theta^*_{water} > 150°$),

with a water roll-off angle of $\omega = 3°$ and $\theta^*_{octane} = 0°$. A mixture of octane and water was separated by pouring it over the membrane (Figure 1.9f).

Li *et al.*[62] achieved superhydrophobic coatings by adding family VIII and IB metal oxide nanocrystals and octadecyl thiol to textiles (65% polyester and 35% cotton). Nanocrystal suspensions were formed and the textiles were dipped in them for 5 minutes. After washing and drying the textiles, they were dipped in 20 mM octadecyl thiol for 24 hours to become superhydrophobic and superoleophilic. They obtained $\theta^*_{water} > 150°$ and $\theta^*_{hexane} = 0°$. A mixture of hexane and water was poured on the membrane mounted in a tube, and the hexane permeated quickly while retaining the water. No water was found in the hexane permeate.

Kavalenka *et al.*[63] turned to a biodegradable and non-toxic alternative for achieving a superhydrophobic and superoleophilic surface. They processed lignin and wood fibers to create a microhaired membrane by hot pulling their "liquid wood" polymer, Arbofill® spruce. The surface fibers were about 5 μm in diameter and > 200 μm long. A static $\theta^*_{water} = 153.8 \pm 2.1°$ and an oil contact angle $\theta^*_{Total\ Azolla\ ZS\ 10} = 0°$ were measured. The oil and water separation ability was demonstrated by placing drops of Total Azolla ZS 10 (hydraulic oil) and water mixture onto the surface; the oil permeated, while the water was retained.

Although many different methods have now been developed for separating oil and water mixtures with a hydrophobic/oleophilic membrane, there are inherent difficulties with this type of wettability. First, gravity separation is prevented if water contacts the membrane before oil, due to its higher density and the hydrophobicity of the membrane. Secondly, these membranes encounter fouling, as oils adsorb to the membrane surface,

24

which decreases the desired oil flux.[64-65] This can add significant downtime, cleaning, and membrane replacement costs when using these types of membranes. To overcome these disadvantages, membranes with other selective wettabilities have also been explored.

1.3.2 Hydrophilic and Oleophilic Membranes (HL/OL)

Recently, a new concept of underwater superoleophobic surfaces has been proposed, which was inspired by the non-wetting behavior of oil droplets on fish scales underwater.[66] From Young's relation, Equation 1.1, it is clear that hydrophilic surfaces in air can become oleophobic when underwater.[66-67] In the presence of hydrophilic rough structures, water readily wets and fills all the cavities present on the surface, leading to a composite solid-oil-water interface. Similar to the composite solid-oil-air interface formed on superoleophobic surfaces in air, this new composite interface prevents the permeation of oil droplets, yielding underwater superoleophobicity. Such superhydrophilic and underwater superoleophobic surfaces exhibit excellent oil fouling resistance, which is attributed to the low affinity for oil droplets when submerged in water.[66] However, these types of membranes may not be effective in stop-and-go operations where the loss of water would allow oil contamination to occur. A number of membranes that display superhydrophilicity in air and underwater superoleophobicity have been fabricated.

One of the first reports on superhydrophilic and underwater superoleophobic membranes was from Xue *et al.*[68] in 2011. They fabricated polyacrylamide (PAM) hydrogel-coated membranes, which consisted of rough hydrogel coatings on top of porous, stainless steel substrates (Figure 1.10a). The PAM hydrogel-coated mesh showed

underwater superoleophobicity with a $\theta^*_{1,2\text{-}dichloroethane}$ = 155.3 ± 1.8°. They also demonstrated that the hydrogel coating reduced the affinity for oil droplets, which could foul typical membranes, through a reduction in the adhesion force of an oil droplet from 46.5 ± 2.3 µN, on the uncoated stainless steel mesh, to 0.8 ± 0.3 µN for the underwater, hydrogel-coated mesh. Utilizing this underwater, superoleophobic membrane, they achieved separations of various free oil-water mixtures including: crude oil, gasoline, and diesel with η > 99% (Figures 1.10b and 1.10c). Recently, Teng et al.[69] developed superhydrophilic in air and underwater superoleophobic hydrogel-coated membranes that exhibit stability under harsh environmental conditions. Poly (3,4-ethylenedioxythiophene)-poly(styrenesulfonate) (PEDOT-PSS) hydrogel meshes with hierarchical structures were fabricated by in-situ polymerization on a titanium (Ti) mesh substrate (Figure 1.10d). The membrane displayed θ^*_{water} = 0° in air and $\theta^*_{1,2\text{-}dichloroethane}$ = 156° contact angle underwater. They demonstrated that the membranes would separate a series of oil-water mixtures containing acidic, basic, and aqueous salt solutions, with η > 99.9% (Figures 1.10e and 1.10f). Furthermore, the membranes achieved η = 99.5% even after 50 separation operations, demonstrating their durability. Zhang et al.[70] fabricated chitosan-coated membranes inspired by the anti-oil-fouling behavior of shrimp shells. A coating of chitosan on a rough copper mesh (Figure 1.10g) maintained underwater superoleophobicity with low oil adhesion in pure and hyper-saline aqueous solutions. Similar to shrimp shells, the chitosan-coated mesh was hydrophilic (θ^*_{water} = 7.1 ± 3.0°) and oleophilic ($\theta^*_{1,2\text{-}dichloroethane}$ = 11.8 ± 2.0°) in air, whereas it possessed underwater superoleophobicity ($\theta^*_{1,2\text{-}dichloroethane}$ = 155.9 ± 1.0° in deionized water; $\theta^*_{1,2\text{-}dichloroethane}$ = 153.0 ± 1.4° in seawater). The prepared membranes separated free oil-water mixture
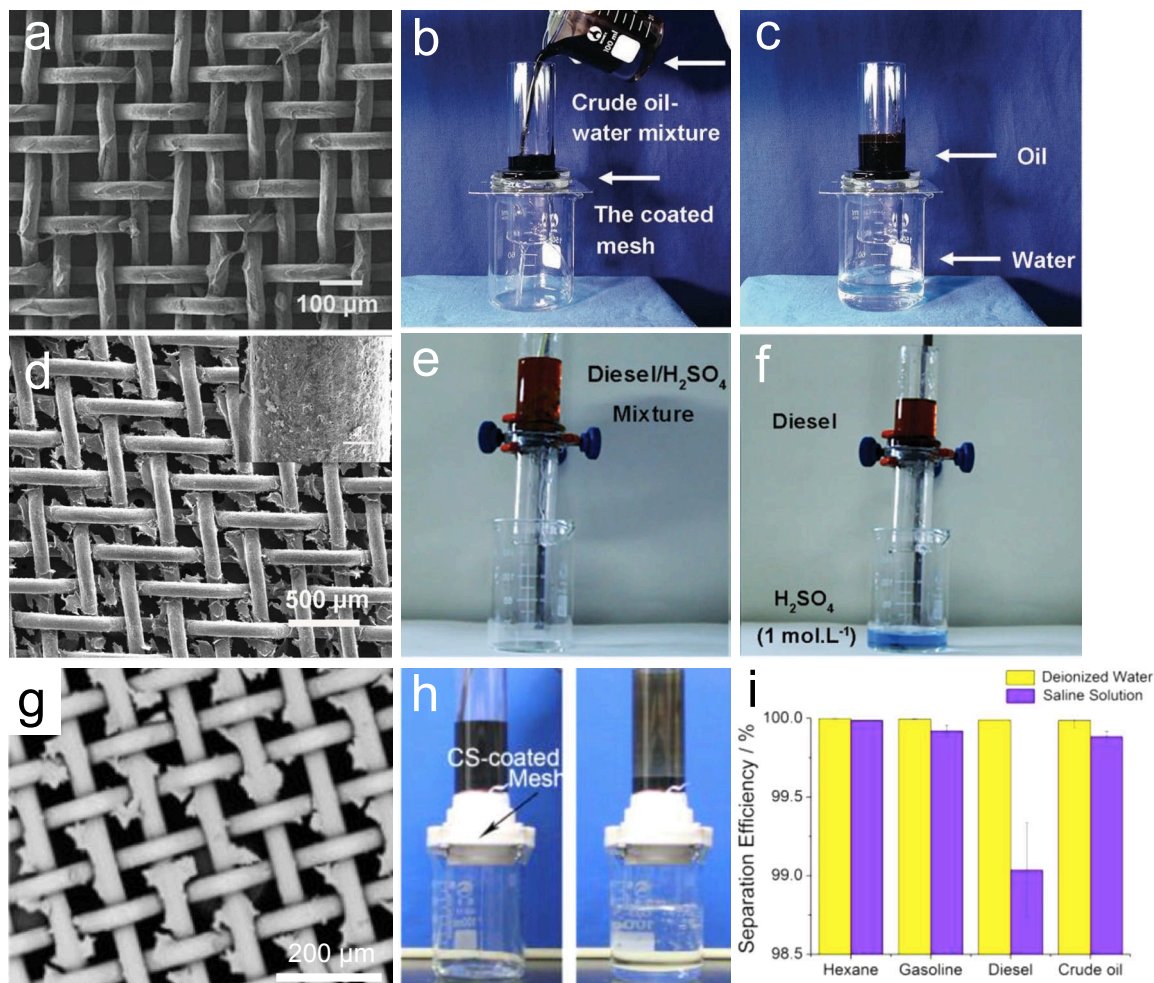
Figure 1.10: Hydrogel and chitosan coated meshes for oil and water separations. (a) 50 μm, stainless steel mesh coated with a PAM hydrogel. (b-c) Water, from a crude oil-water mixture, selectively permeated through the membrane. Reproduced from Xue *et al.*[68] © 2011 WILEY-VCH Verlag GmbH & Co. KGaA, Weinheim with permission from John Wiley & Sons, Inc. (d) SEM image of a PEDOT-PSS hydrogel coated Ti mesh. (e-f) The mesh was used to separate a diesel and 1 M sulfuric acid mixture without any degradation. Reproduced from Teng *et al.*[69] © 2014 WILEY-VCH Verlag GmbH & Co. KGaA, Weinheim with permission from John Wiley & Sons, Inc. (g) Chitosan coated on a rough Cu mesh with nano papillae. (h) The water permeated out of a crude oil and water mixture and (i) a high separation efficiency was seen for several oils, even in saline conditions. Adapted with permission from Zhang *et al.*[70] Copyright 2013 American Chemical Society.

containing various oils including: hexane, gasoline, diesel, and crude oil, as well as, saline (2 M NaCl) mixtures with these oils, with $\eta > 99\%$ (Figures 1.10h and 1.10i). Further, they demonstrated that the membranes could separate a range of oil-water

mixtures in hyper-saline and broad pH conditions after fully cross-linking chitosan. Lu *et al.*[71] fabricated cellulose hydrogel-coated nylon membranes. The as-prepared membrane showed superhydrophilicity in air with $\theta^*_{water} = 0°$ and underwater superoleophobicity with a $\theta^*_{1,2\text{-}dichloroethane} > 150°$. They demonstrated that the membrane was effective in the separation of multiple free oil-water mixtures including: *n*-hexane, petro-ether, gasoline, and diesel.

Although hydrogel coated meshes have been successfully fabricated and have demonstrated their utility in separating oil-water mixtures, the binding of hydrogel to the underlying porous substrate is often very weak, leading to low membrane durability. Jing *et al.*[72] demonstrated that poly(glycidyl methacrylate) (PGMA) could be grafted onto stainless steel mesh by thermal treatment. Subsequently, polyacrylamide-co-poly(acrylic acid) (PAM-co-PAA) hydrogel particles were grafted onto the PGMA-modified stainless steel mesh. This led to static $\theta^*_{water} = 4.4 \pm 0.4°$ in air, and a static underwater $\theta^*_{dodecane} = 157.1 \pm 2.6°$. The PAM-co-PAA coated membranes were used to separate different free oil-water mixtures, including water-dodecane and water-rapeseed oil mixtures.

In addition to hydrogels, various other hydrophilic materials have also been utilized for coating porous meshes to engender superhydrophilicity and underwater superoleophobicity. Dong *et al.*[73] fabricated hydrophilic graphene oxide (GO) nanosheet coated membranes using a stainless steel mesh substrate (Figure 1.11a). Due to the hydrophilic GO coating, and the mesh morphology, a static $\theta^*_{water} < 10°$ in air, while the static underwater $\theta^*_{oil} > 150°$ for various oils. As-prepared GO-coated membranes were used to separate a number of free oil-water mixtures, including: *n*-hexane, gasoline, diesel, toluene etc., with $\eta > 90\%$ separation efficiencies (Figures 1.11b and 1.11c).
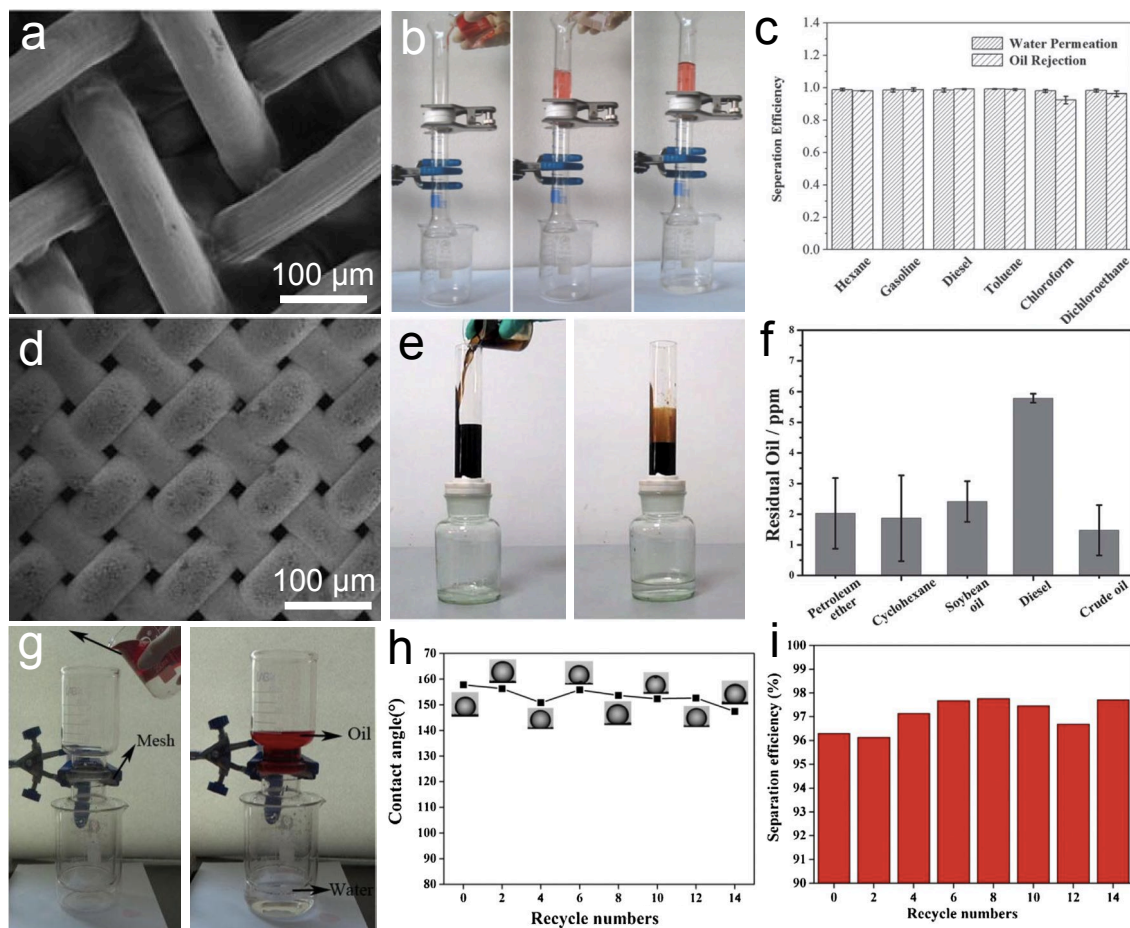
Figure 1.11: Graphene oxide and zeolite coated mesh membranes. (a) Graphene oxide (GO) coated on 38 μm pore size stainless steel mesh. (b) The separation apparatus showing the permeation of water and rejection of hexane (dyed red) by the GO coated mesh. (c) High separation efficiency was seen for a variety of oils. Adapted from Dong *et al.*[73] © 2014 with permission from The Royal Society of Chemistry. (d) An SEM image of the zeolite-coated mesh film (ZCMF-12) and (e) a demonstration of its ability to selectively remove water from crude oil. (f) The residual oil content in water for different oils after the separation. Adapted from Wen *et al.*[74] © 2013 with permission from The Royal Society of Chemistry. (g-i) A zeolite membrane on top of stainless steel mesh separated chloroform (dyed red) and water mixtures efficiently while maintaining high dichloromethane contact angles over fourteen separations. Reprinted from Zeng *et al.*[75], Copyright 2014, with permission from Elsevier.

Due to their hydrophilicity, and chemical stability, zeolites have also attracted research interest in the field of oil-water separation. Wen *et al.*[74] developed zeolite-coated membranes for gravity-driven oil-water separation. Such membranes were fabricated by growing pure-silica zeolite, silicalite-1, crystals on a stainless steel mesh (Figure 1.11d).

The as-prepared membrane exhibited $\theta^*_{water} < 10°$ in air, whereas all contact angles for various oils underwater, including petroleum ether, soybean oil, diesel, and crude oil, were $\theta^*_{oil} > 150°$. High separation efficiency of various oils, including crude oil, diesel, and soybean oil, was achieved due to the superhydrophilicity and underwater superoleophobicity of the zeolite-coated membrane surface (Figures 1.11e and 1.11f). Zeng and Guo[75] demonstrated, in another report, that the zeolite-coated membranes possessed good reusability (Figures 1.11g and 1.11h) without a decline in separation efficiency (Figure 1.11i). Liu et al.[76] proposed a much simpler approach to fabricate superhydrophilic in air, and underwater superoleophobic, membranes. Chemical oxidation of a copper mesh leads to the formation of $Cu(OH)_2$ micro- and nanoscale hierarchical structure on the mesh surface (Figure 1.12a). This prepared mesh exhibited superhydrophilicity with $\theta^*_{water} = 0°$ in air, and underwater superoleophobicity with $\theta^*_{1,2\text{-}dichloroethane} = 166.2 ± 1.3°$. The membranes could separate various mixtures of organic solvents or oil and water with $\eta > 99.99\%$ (Figures 1.12b-d). They also demonstrated the reusability and stability of the membranes with no degradation after 60 separations (Figure 1.12e).

In addition to metal meshes, there have also been reports of superhydrophilic in air, and underwater superoleophobic, polymer membranes. Zhu et al.[77] fabricated zwitterionic polyelectrolyte brush (poly(3-(N-2-methacryloxyethyl-N,N-dimethyl) ammonatopropanesultone) or PMAPS)-grafted poly(vinylidene fluoride) (PVDF) membranes. After PMAPS grafting, the PVDF membrane displayed a static $\theta^*_{water} = 11°$ in air, while all static underwater contact angles for oil, including petroleum ether, soybean oil and hexane, were $\theta^*_{oil} > 150°$. Utilizing this membrane, they demonstrated
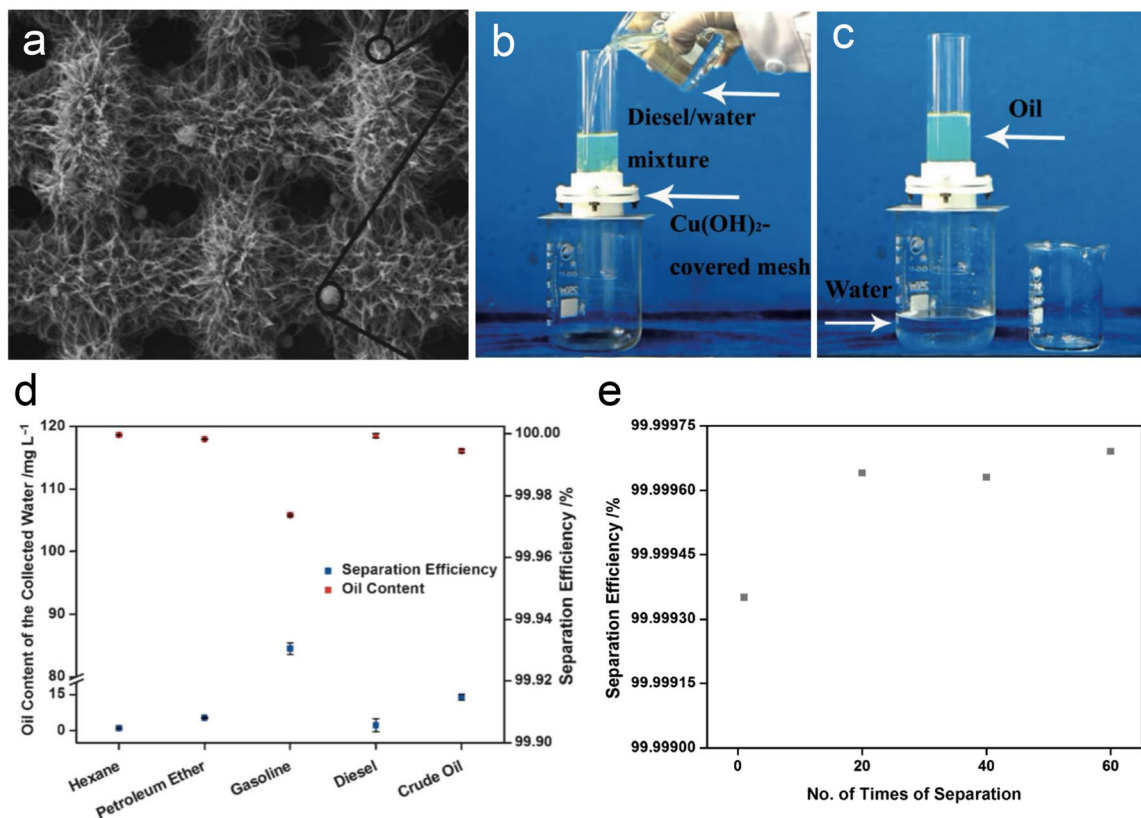
Figure 1.12: Hierarchically structured copper (II) hydroxide on copper mesh. (a) An SEM image of $Cu(OH)_2$ nanoneedles and microscale spherical crystals on top of a copper mesh. (b-c) Selective permeation of water and retention of diesel were achieved. (d) The oil content in the collected water, and the separation efficiency for a variety of oils. (e) Separation efficiency over extended numbers of separations. Reproduced from Liu *et al.*[76] © 2013 WILEY-VCH Verlag GmbH & Co. KGaA, Weinheim with permission from John Wiley & Sons, Inc.

the separation of a series of dispersed oil-water mixtures including: isooctane, hexane, diesel, and soybean oil. After the separations, the oil content in the water-rich permeates was less than 10 ppm for all systems. Chen *et al.*[78] developed hybrid polypropylene microfiltration membranes, which were optimized by grafting on poly(acrylic acid) (PAA) and depositing hydrophilic, nano-sized $CaCO_3$ minerals. In conjunction with the hydrophilic PAA layer, the $CaCO_3$ coating traps water, in an aqueous environment, to form a hydrated layer on the membrane pore surface. This leads to underwater superoleophobicity with $\theta^*_{1,2\text{-}dichloroethane} > 150°$. The membrane could separate free oil-

31

water, as well as, surfactant-stabilized oil-in-water emulsions (140 nm to 5.56 μm), with $\eta > 99\%$ separation efficiency. Yang *et al.*[79] developed a one-pot approach to modify
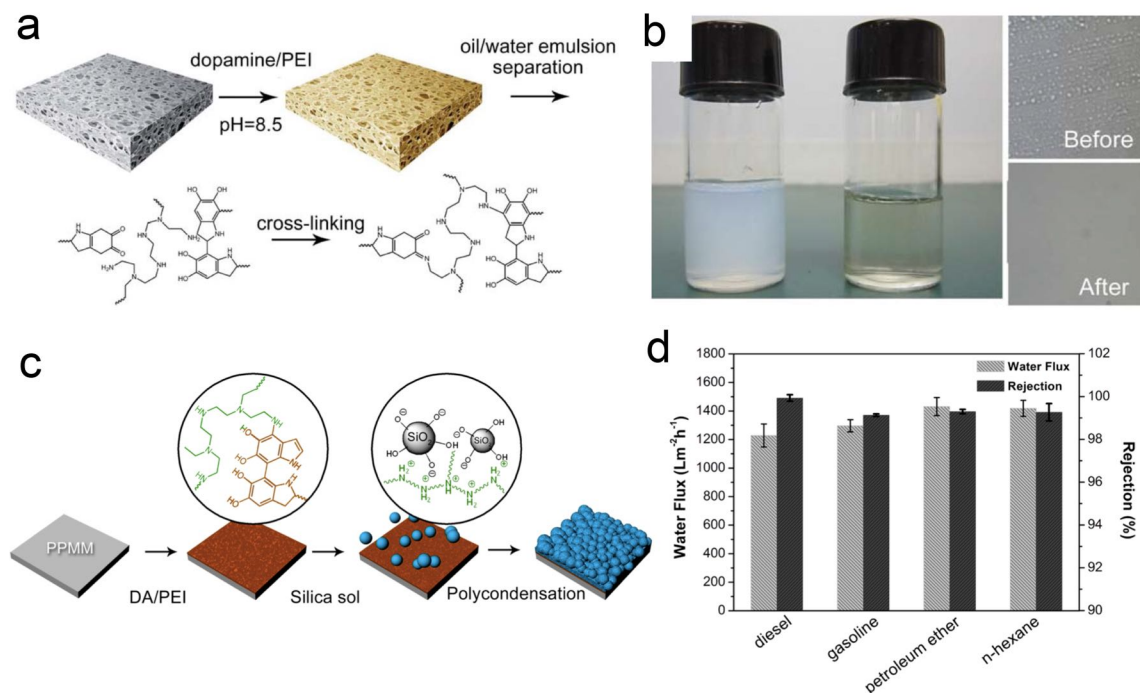
Figure 1.13: Modified polypropylene membranes for oil-water separation. (a) A schematic illustrating the treatment of a polypropylene membrane with dopamine and PEI, and (b) its use for separating a dichloroethane in water emulsion. Adapted from Yang *et al.*[79] © 2014 with permission from The Royal Society of Chemistry. (c) Method for producing silica and PDA/PEI decorated polypropylene membranes that (d) show high water permeation, while rejecting several oils. Adapted with permission from Yang *et al.*[80] Copyright 2014 American Chemical Society.

polypropylene membranes through the co-deposition of polydopamine (PDA) and polyethyleneimine (PEI) (Figure 1.13a). The PDA/PEI-coated membranes showed better stability in an alkaline environment due to the covalent cross-linking between PDA and PEI. They demonstrated that the membranes could separate a 1,2-dichloroethane-in-water emulsion with $\eta > 98\%$ separation efficiency (Figure 1.13b). In their recent work,[80] nano-silica particles were added to the PDA/PEI-coated polypropylene membranes (Figure 1.13c). The membranes could be used for the separation of a variety of surfactant

stabilized oil-in-water emulsions (polydisperse: 150 nm to > 10 μm) with η > 99%

separation efficiency (Figure 1.13d).

In other reports, the polymer membrane was directly fabricated by electrospinning.

Ahmed *et al.*[81] fabricated poly(vinylidene fluoride)-co-hexafluoropropylene (PVDF-

HFP), non-woven, nanofiber membranes by electrospinning a PVDF-HFP solution.

Immersing the membrane in an ionic liquid and cellulose solution, followed by ionic

liquid removal, yielded a cellulose/PVDF-HFP composite, resulting in enhanced

mechanical properties and wettability (Figure 1.14a). Cellulose-coated membranes

displayed θ^*_{water} = 0° in air, whereas $\theta^*_{dichloromethane}$ = 169 ± 3° underwater. They

demonstrated separations of oil-in-water emulsions (unstated size), using corn oil,

gasoline, and crude oil, with η > 99.98% separation efficiency (Figures 1.14b-e). Raza *et*

al.[82] developed multi-layered, nanofibrous membranes with a polyacrylonitrile

(PAN)/polyethylene glycol (PEG) base, and an additional in-situ cross-linked,

polyethylene glycol diacrylate (PEGDA) nanofiber layer spun on top (Figure 1.14f).

These membranes separated free oil-water mixtures, as well as, surfactant stabilized

soybean oil-in-water emulsions, between 5 and 40 μm in size (Figure 1.14g).

In addition to polymer membranes, inorganic fiber filters have also been utilized

for oil-water separation. Liu *et al.*[83] fabricated zwitterionic poly(sulfobetaine

methacrylate)-grafted (pSBMA) glass fiber filters using surface-initiated atom transfer

radical polymerization. pSBMA is a superhydrophilic polymer due to its strong

electrostatic interaction with water. Thus, in air, the water contact angle of pSBMA-

treated glass was θ^*_{water} = 8-15°, while underwater $\theta^*_{hexadecane}$ = 162-169°. The prepared

membranes demonstrated complete separation of free hexadecane-water mixtures. Chen

33
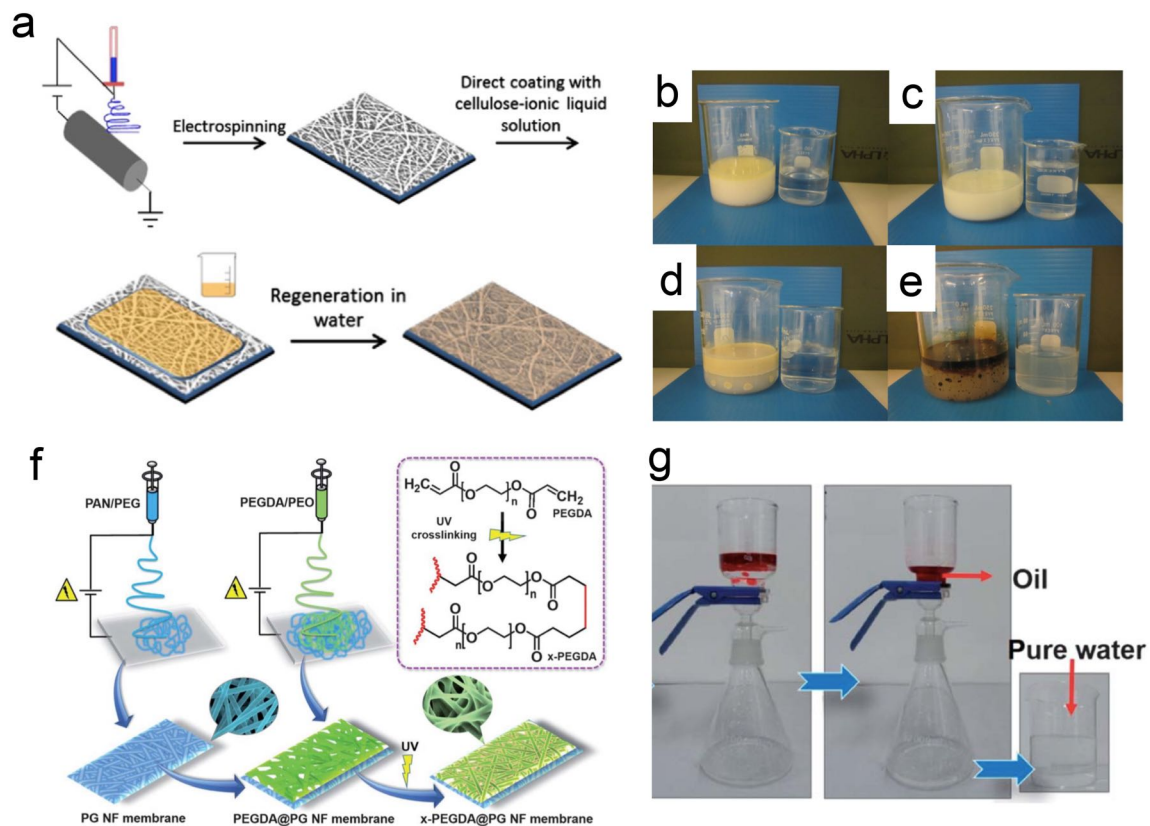
Figure 1.14: Electrospun composite polymer membranes for water purification. (a) Process for the fabrication of cellulose/PVDF-HFP composite membranes. 10 wt% oil-in-water emulsions were made with (b) corn oil, (c) gasoline, (d) motor oil, and (e) crude oil. In each window (b-e), the emulsion is on the left and the aqueous permeate is on the right. Reprinted from Ahmed *et al.*[81], Copyright 2014, with permission from Elsevier. (f) Fabrication procedure for cross-linked polyethylene glycol diacrylate nanofibers supported on polyacrylonitrile/polyethylene glycol nanofibrous (x-PEGDA@PG NF) membranes. (g) Soybean oil (dyed red) and water were separated using the x-PEGDA@PG NF membrane. Adapted from Raza *et al.*[82] © 2014 with permission from The Royal Society of Chemistry.

et al.[84] fabricated superhydrophilic, and underwater superoleophobic, membranes by combining a quartz fiber mesh with silica gel, which was further enhanced by adding 1,2-bis(triethoxysilyl)ethane (BTSE) and polyacrylamide (PAM). Because the silica gel is stable in acidic and saline environments, the membrane demonstrated the ability to separate free crude oil-water mixtures without being deteriorated by such harsh conditions.

Practical applications of hydrophilic or superhydrophilic membranes in oil-water separations are limited by contamination from low surface energy oil.[85-86] Once the membrane is fouled by oil, it is difficult to remove the adsorbed oil. This leads to decreased separation performance, and necessitates periodic washing of the membranes, resulting in higher operating costs. To overcome this limitation, self-cleaning membranes have also been studied. Zhang et $al.$[87] fabricated self-cleaning membranes using layer-by-layer (LBL) assembly of sodium silicate and TiO_2 nanoparticles on stainless steel mesh. The integration of self-cleaning ability using TiO_2 enables the convenient removal of contaminants by ultraviolet (UV) light. The developed membranes could separate free gasoline-water mixtures under gravity (Figures 1.15a and 1.15b). Furthermore, they evaluated the membrane's self-cleaning capability by measuring water contact angles on the membranes after five cycles of oleic acid contamination and UV illumination-based recovery (Figure 1.15c). This showed that the cleaned membranes still exhibited hydrophilicity similar to the uncontaminated membranes. Gao et $al.$[88] fabricated sulfonated graphene oxide (SGO) membranes with hierarchically nanostructured TiO_2 spheres. The TiO_2 spheres, bound by the hydrophilic SGO nanosheets, endowed this composite membrane with excellent mechanical and chemical durability. They demonstrated that the membrane could separate various surfactant-stabilized oil-in-water emulsions (200 nm) including: toluene, crude oil, vegetable oil, and diesel, at various temperatures and ionic concentrations (Figures 1.15d-f). The membrane was also found to recover its superhydrophilicity upon UV light illumination. Sawai et $al.$[89] fabricated titanium (Ti) membranes with a TiO_2 surface through the calcination of a Ti mesh at 500°C for 4 hours. They observed that the water contact angle on a membrane reduced
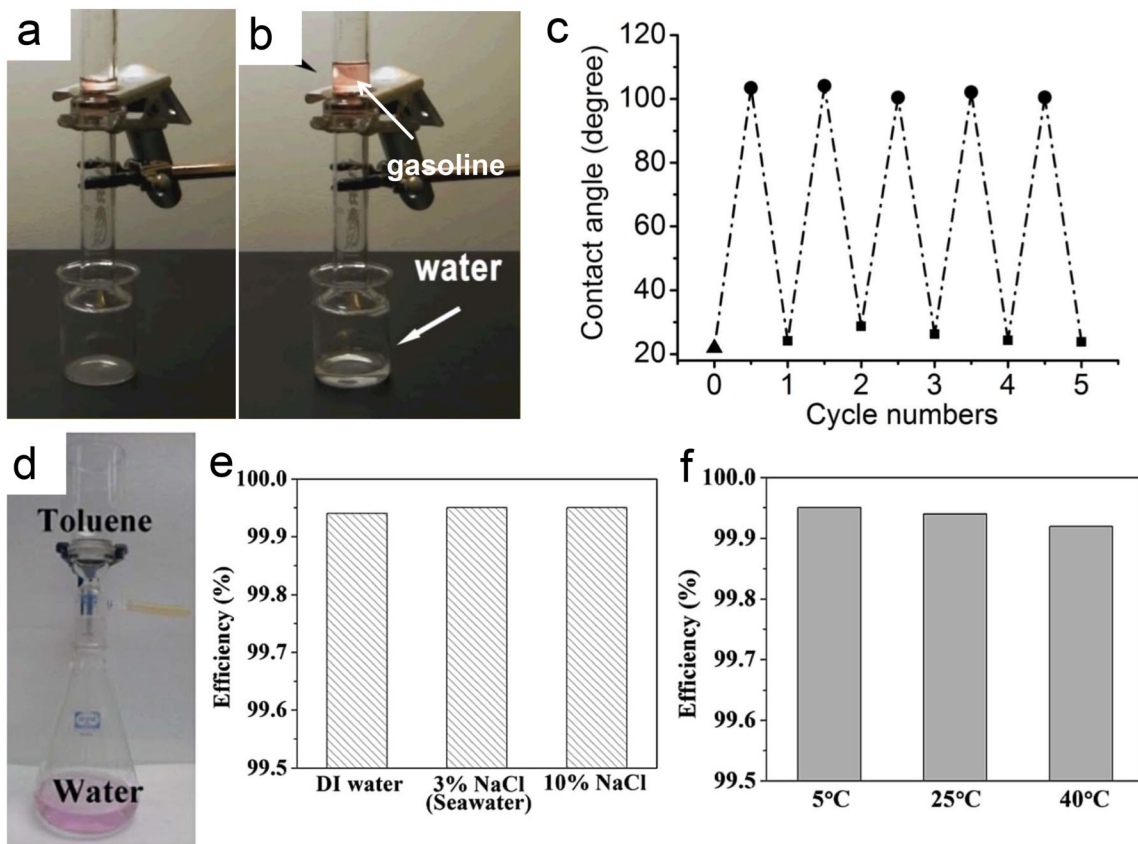
Figure 1.15: TiO₂ composite membranes. (a-b) Sodium silicate and TiO_2 nanoparticles on top of a stainless steel mesh selectively removed water from gasoline (c) Anti-fouling properties shown by water contact angle changes on the silicate/TiO_2 coated mesh in five cycles of oleic acid contamination and UV illumination-based recovery. Adapted from Zhang *et al.*[87] under Creative Commons License CC-BY 3.0 (d) A graphene-TiO_2 membrane could separate a surfactant stabilized toluene-in-water emulsion. (e-f) Water, with varying concentrations of salt, was also removed from crude oil at different temperatures. Adapted from Gao *et al.*[88] © 2014 with permission from The Royal Society of Chemistry.

from $\theta^*_{water} = 48.8 \pm 3.9°$ to less than 5° upon UV irradiation. Conversely, underwater contact angles for oils (heptane, dodecane and hexadecane) increased to static $\theta^*_{oil} > 160°$. This indicates that UV irradiated-TiO_2 exhibits extremely high oil repellency in water. Utilizing this membrane, they demonstrated the separation of free hexadecane-water mixtures.

Although membranes with superhydrophilic and underwater superoleophobic

properties can be successfully used for gravity-driven separation of oil-water mixtures, and are more resistant to fouling, they are unsuitable for the separation of free water-in-oil or water-in-oil emulsions. This is because both oil and water easily permeate through them, unless every pore within the membrane is pre-wet by water. Consequently, oil permeates through the membrane if water dries out from even a single pore within the superhydrophilic membrane, which can typically happen in a matter of minutes.[36]

1.3.3 Hydrophilic and Oleophobic Membranes (HL/OP)

As discussed in previous chapters, hydrophobic and oleophilic membranes are unsuitable for most gravity-driven separations. Although hydrophilic and oleophilic membranes are applicable for the gravity-driven separation of oil-in-water emulsions, they do not work for free oil-water or water-in-oil emulsions, unless they are repeatedly pre-wet by water. Hydrophilic and oleophobic membranes are expected to overcome these limitations. However, it has been considered challenging to fabricate such membranes due to the surface tension of water (γ_{LV} = 72.1 mN/m) being significantly higher than that of oils (γ_{LV} = 20-30 mN/m).

In our recent work,[36] we successfully fabricated hygro-responsive membranes that are both superhydrophilic and superoleophobic in air and underwater. We utilized a polymer blend consisting of 20 wt% 1H, 1H, 2H, 2H-heptadecafluorodecyl polyhedral oligomeric silsesquioxane (fluorodecyl POSS) and cross-linked polyethylene glycol diacrylate (x-PEGDA) as the coating material. With a porous substrate, such as stainless steel mesh or polyester fabric, water readily wet the coated surface (i.e., θ^*_{water} = 0°), while $\theta^*_{rapeseed\ oil,\ adv}$ = 152° (Figure 1.16a). We showed that such selective wettability of water over oil is attributed to the surface reconfiguration of the fluorodecyl POSS + x-

PEGDA coating (Figures 1.16b and 1.16c). It was demonstrated that the membrane could

separate surfactant-stabilized oil-in-water and water-in-oil emulsions (emulsion diameter:

10-20 μm) under gravity. We also demonstrated that the membrane could separate
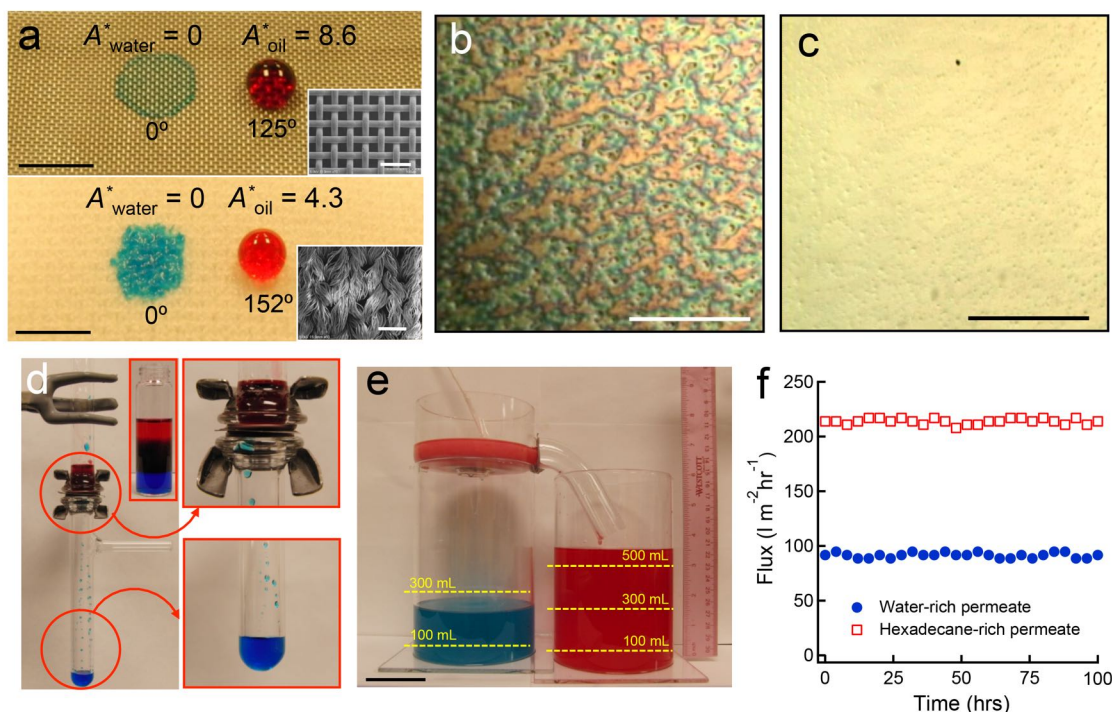
Figure 1.16: Hygro-responsive membranes for oil-water separation. (a) Water (blue) and rapeseed oil (red) contact angles on a stainless steel mesh (top) and a polyester fabric (bottom) dip coated in 20 wt% fluorodecyl POSS + x-PEGDA blend. (b) Optical microscopy image of a 20 wt% fluorodecyl POSS + x-PEGDA blend surface in air and (c) underwater showing the surface reconfiguration. (d) A four component mixture of water, hexadecane, 30:70 v:v water-in-hexadecane emulsion, and a 50:50 v:v hexadecane-in-water emulsion was separated with a 400 mesh stainless steel membrane coated with 20 wt% fluorodecyl POSS + x-PEGDA blend. (e) A continuous separation apparatus separated 30:70 v:v water-in-hexadecane emulsions stabilized by Polysorbate 80. It used a 20 wt% fluorodecyl POSS + x-PEGDA blend membrane (superhydrophilic and oleophobic) on the bottom, and a Desmopan 9370 coated sidewall membrane (hydrophobic and oleophilic). (f) The hexadecane and water fluxes for the continuous apparatus over a period of 100 hours. Reprinted from Kota *et al.*[36] © 2012 with permission from Nature Publishing Group.

virtually all types of oil-water mixtures, solely under gravity, with $\eta > 99\%$ separation

efficiency (Figure 1.16d). A continuous separation apparatus was engineered utilizing a

hygro-responsive membrane and a conventional hydrophobic and oleophilic membrane

operating in tandem (Figure 1.16e). During the continuous separation of oil-water emulsions, the fluxes for both water and oil did not decline over a period of 100 hours (Figure 1.16f).

In addition to polymer blends, synthesis of polymers possessing hydrophilic (HL) and oleophobic (OP) constituents has also been proposed for fabricating HL/OP coating materials. Yang *et al.*[85] developed a superhydrophilic and superoleophobic nanocomposite coating. They first synthesized a polymer with hydrophilic and oleophobic constituents through the reaction of poly(diallyldimethylammonium chloride) (PDDA) with sodium perfluorooctanoate (PFO). Superhydrophilic and superoleophobic surfaces were fabricated by spray casting PDDA-PFO/silica nanoparticles onto glass, stainless steel mesh, or paper. On the coated glass surface, the water contact angle in air was found to be $\theta^*_{water} = 0°$, while $\theta^*_{hexadecane} = 155 \pm 1°$. Separation membranes were fabricated by spray casting polymer-silica nanoparticles onto stainless steel mesh, and they demonstrated separation of free hexadecane-water mixtures under gravity. In another report,[90] PDDA was substituted with chitosan (CTS) for the hydrophilic constituent. CTS-PFO polymer and silica nanoparticles were sprayed onto stainless steel mesh, developing membranes with $\theta^*_{water} = 0°$ and $\theta^*_{hexadecane} = 157 \pm 1°$, which separated a free hexadecane-water mixture under gravity. Zhu *et al.*[91] fabricated membranes using PVDF, as the base matrix polymer, blended with additive polymers containing perfluoroalkyl polyethylene glycol surfactant chains. The developed membranes exhibited anti-organic and anti-biofouling properties. In another report,[92] they demonstrated that the membrane could separate crude oil or hexadecane-in-water emulsions (1-50 μm) with $\eta > 98\%$ separation efficiency.

Howarter and Youngblood[93] modified glass fiber membranes by bonding Zonyl®

FSN-100, a perfluorinated polyethylene glycol (f-PEG), to them using 3-isocyanatopropyldimethylchlorosilane as a linker. The f-PEG oligomer, containing both a low surface energy segment and a polar one, led to hydrophilic and oleophobic surfaces on various membranes, with pore sizes ranging from 10-20 μm to 145-174 μm. The best static contact angles were achieved on the 10-20 μm pore-sized membrane, $\theta^*_{water} = 30°$ and $\theta^*_{hexadecane} = 105°$, in air, and it maintained $\theta^*_{hexadecane} > 140°$ underwater. For testing oil rejection capability, a 12:1 volume ratio of water to hexadecane was mechanically dispersed to form an, approximately, 10 μm diameter oil-in-water emulsion. This was gravity fed through the modified 10-20 μm pore-sized membrane and only 2.6 ± 1.2 wt% of the hexadecane permeated through the membrane with the water. The larger pore-sized membranes permitted < 6 wt% of hexadecane to permeate through, while maintaining several times greater flow rates, as expected. The f-PEG layer was ≤ 5nm thick and should not have significantly altered the initial membrane pore size. Larger pore-sized membranes have greater flow rates, but may allow smaller oil droplets to permeate through.

Yoon et al.[94] developed superhydrophilic and oleophobic stainless steel meshes (initially 42-60 μm pore size) using a mixture of poly(diallyldimethylammonium chloride) (PDDA), sodium perfluorooctanoate (PFO), and 10-25 nm diameter silica particles. This provided a dense composite coating with a thickness of approximately 2.8 μm. The PDDA and silica provided hydrophilic components to the coating, and the PFO provided low energy, mobile fluorinated chains. The static $\theta^*_{water} = 0°$ and $\theta^*_{hexadecane} = 95°$. The separation ability was tested by mounting the prepared mesh in glassware and

pouring 50 mL of hexadecane on it, followed by 100 mL of water. The water displaced the oil and passed through in 12 minutes, while retaining the oil. It remained oleophobic for 2 weeks with 97% water recovery. Repeating the separation 30 times, with aqueous cleaning, and drying, performed between each trial, tested the mesh reusability. In addition, a graphene plug was added after the mesh to show that organics such as methylene blue could be removed from the water after the separation. The 2 cm thick plug decreased the permeation rate from 800,000 L m^{-2} h^{-1} bar^{-1} to 6,000 L m^{-2} h^{-1} bar^{-1}.

1.3.4 Hydrophobic and Oleophobic Membranes (HP/OP)

In contrast to membranes with selective wettability of water over oil or vice-versa, hydrophobic and oleophobic membranes prevent permeation of both oil and water. In order to utilize hydrophobic and oleophobic membranes (omniphobic) for the separation of oil-water mixtures, pressure must be selectively exerted on either the water or oil phase, leading to $P_{breakthrough,\ water} < P_{applied} < P_{breakthrough,\ oil}$ or vice-versa.

An electric field provides a facile route for tuning the wettability of polar (or conducting) liquids. The decrease in the macroscopic contact angle for a polar liquid droplet on a dielectric, in response to an external electric field, is known as electrowetting on a dielectric (EWOD) (Figures 1.17a-d). It is described by the Young-Lippmann equation:[95]

$$\cos\theta^{ew} = \cos\theta + \frac{\varepsilon_0 \varepsilon_d}{2\gamma_{12}d}V^2 \tag{1.5}$$

θ^{ew} is the macroscopic electrowetting contact angle, θ is Young's contact angle, ε_0 is the vacuum permittivity, ε_d is the dielectric permittivity, γ_{12} is the interfacial tension between
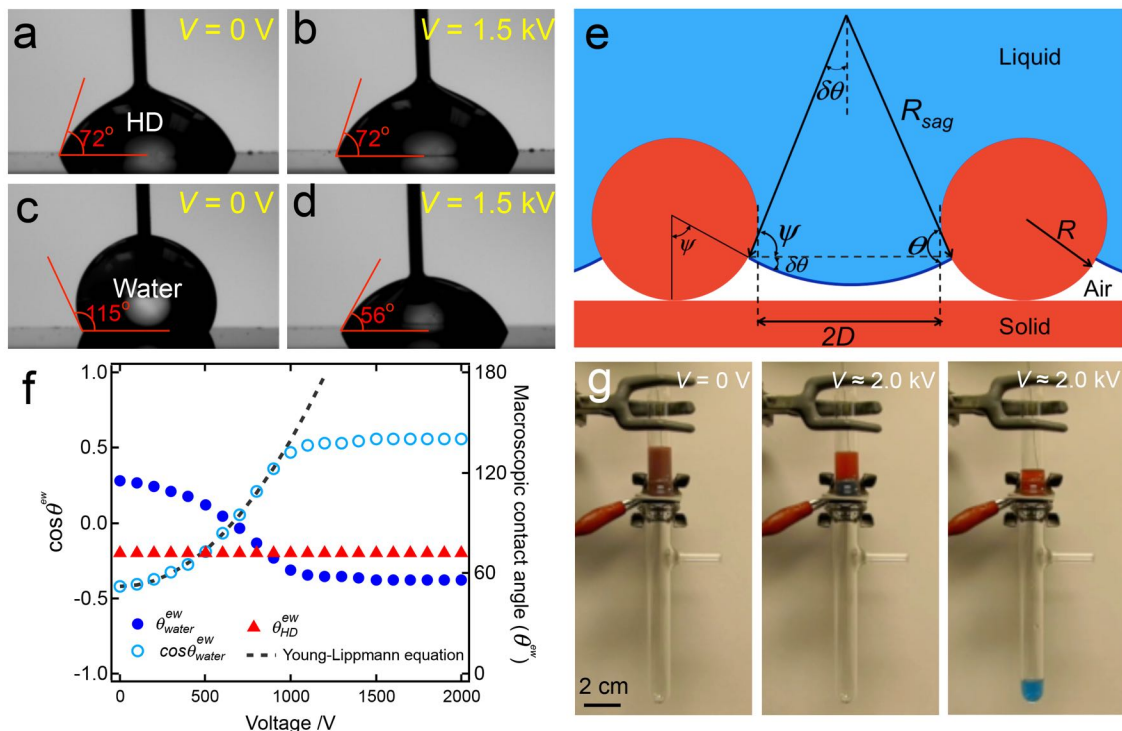
Figure 1.17: Electrowetting of an omniphobic surface. (a-b) Hexadecane's contact angle on a non-textured 50 wt% fluorodecyl POSS + x-PDMS substrate was unchanged by the application of a 1.5 kV potential, while (c-d) water's contact angle decreased significantly. (e) The macroscopic contact angles for water and hexadecane on the non-textured surface as a function of applied voltage. (f) A diagram illustrating the pressure-induced liquid-air interface sagging. (g) The EWOD effect was used to separate hexadecane (red) and water (blue) on-demand. Adapted from Kwon *et al.*[96] © 2012 WILEY-VCH Verlag GmbH & Co. KGaA, Weinheim with permission from John Wiley & Sons, Inc.

the liquid and surrounding medium, d is the dielectric thickness, and V is the voltage applied. Utilizing the EWOD phenomenon, we[96] recently developed an on-demand oil-water separation technology, where the separation is triggered upon the application of an electric field. For effective on-demand separation of oil-water mixtures, both oil and water must be retained above the membrane initially. Thus, we first developed an omniphobic membrane by dip coating nylon mesh with a blend of 50 wt% fluorodecyl POSS and cross-linked polydimethylsiloxane (x-PDMS). The membrane retained both water and oil before the application of an electric field. When an external electric field

was applied across the conducting liquid (e.g., water) and the electrode at the membrane, the conducting liquid, initially in the Cassie-Baxter state on the porous membrane, transitioned to the Wenzel state. This is because the Maxwell stress exerted on the conducting liquid surface pulls it outward along the surface normal. By contrast, a non-conducting liquid (e.g., oil) does not undergo such a transition (see Figure 1.17f). When transitioning to the Wenzel state, increasing the applied pressure, $P_{applied}$, sags the liquid-air interface (Figure 1.17e) until it reaches a critical texture angle, ψ_{cr}. This angle is where the surface can withstand the greatest pressure $P_{critical}$ before entering the Wenzel state. For cylindrical surface geometry, such as with our membranes, $P_{critical}$ is given by:[96]

$$P_{critical} = \frac{\gamma_{12}\sin(\theta - \psi_{cr})}{D + R - R\sin\psi_{cr}} \,, \tag{1.6}$$

$$\text{where } \psi_{cr} = \theta - \cos^{-1}\left(\frac{R\sin\theta}{R+D}\right). \tag{1.7}$$

As in Figure 1.17f, R is the cylinder radius and D is half of the cylinder spacing. Consequently, upon applying a sufficient electric field, a conducting liquid transitions to the Wenzel state and permeates through the membrane, while a non-conducting liquid is retained above the membrane. Utilizing this preferential transition, we demonstrated the on-demand separation of free oil and water, oil-in-water emulsions, and water-in-oil emulsions, with $\eta > 99.9\%$ separation efficiency (Figure 1.17g). Such on-demand separation could be useful for the remote operation of oil-water separation units, microfluidic valves, and lab-on-a-chip devices.

1.4 Overview of Research

The development of membranes with selective wettability is an ongoing process, which aims to more effectively meet today's needs for efficient oil and water separation.

Membranes are a promising alternative to traditional separation methodologies. The numerous sources of oily wastewater and increasingly strict environmental guidelines necessitate a highly effective, economical, and durable membrane, with a long service life, for purifying waste streams and spills. The type of membrane used will depend on the waste stream composition, fouling potential, and the system employed for the separation (on-demand, gravity fed, high pressure, etc.). The form of oil, whether free or emulsified, will indicate the pore-size for the membrane and thus is directly related to the permeation rate through the membrane. All these parameters must be taken into account for utilizing membranes with selective wettability.

Chapter 2 explores my work in addressing several of these hurdles for membrane technology. I have developed a methodology for achieving the uncommon hydrophilic and oleophobic (HL/OP) wettability on a variety of industrially relevant substrates such as polymers, ceramics, and metal. The approach is applicable to a range of pore sizes from 5 nm to 25 μm and achieves three of the four major surface wettabilities on a single substrate with the addition of a single silane, in a very controlled manner. This meets the qualifications of using industrially available materials and being suitable for scaled up manufacturing at a reasonable cost. I demonstrate that these membranes can separate several forms of oil-contaminated water, including surfactant-stabilized oil-in-water emulsions and free oil & water, in batch and cross-flow operation with approximately 99.9% purity. The advantages and capability of these membranes to decrease membrane fouling is demonstrated, due to the dual nature of the low energy and hydrophilic components. The anti-fouling methodology increases the service life of membranes and

will help energy-saving membrane technology to expand its use in the many industries treating oily wastewater.

In addition to the separation of immiscible liquid components, Chapter 3 investigates how these HL/OP membranes enabled the development of the CLEANS methodology for the continuous, low energy extraction of miscible solutes from liquid mixtures. In pursuit of decreasing the intensive energy usage associated with industrial liquid separations, we developed this liquid-liquid extraction unit operation to emulsify and demulsify the feed and extractant continuously under gravity. This is the first system of its kind and it enhances extraction through the additional mass transfer surface area, created by emulsification with surfactant present. The purified feed (or raffinate) and extractant are recovered by two membranes operating in tandem; one allowing solely the non-polar phase to pass and the other allowing only the polar phase through. The CLEANS system is demonstrated using commercially important separations such as dye and sulfur removal from fuel, methanol removal from biofuel, and breaking an azeotrope.

The applications of surface science extend far beyond membrane technology. In Chapter 4, I discuss the scope and approaches to dealing with the everyday problem of fog formation. Fogged up windows, windshields, and glasses are a nuisance as well as dangerous. An ideal solution to this problem would involve a commercially applied coating which completely prevents the formation of fog in cold and warm conditions, while remaining entirely transparent and undetectable. I present a polymer coating that can be directly bonded to polycarbonate safety glasses and plates in a scalable manner, with high transparency and optical clarity. Our work in Chapter 2 also allowed us to achieve easy-clean properties on the anti-fog coating by post-treatment. The prototype

safety glasses are presented and are found to be highly useful in cold environments, such as a walk-in freezer, where the user's breath will readily fog up uncoated lenses.

Chapter 5 presents proof of concept for a new freeze concentration unit operation, which combines the crystallizer and separator into a single unit. This is achieved by selecting and designing membranes that can be actuated based on their breakthrough pressure. Liquid feed cannot pass through the membrane during the crystallization process, but after completion, vacuum pressure can actuate the membrane to recover the concentrate. This is demonstrated for apple juice, ethanol solution, and dyed water, which can benefit from freeze concentration in quality and energy efficiency.

1.5 References

1.   Kwon, G.; Post, E.; Tuteja, A., Membranes with selective wettability for the separation of oil–water mixtures. *MRS Commun.* **2015,** *5* (3), 475-494. 10.1557/mrc.2015.61

2.   Colombini, M. P.; Giachi, G.; Modugno, F.; Pallecchi, P.; Ribechini, E., The Characterization of Paints and Waterproofing Materials from the Shipwrecks Found at the Archaeological Site of the Etruscan and Roman Harbour of Pisa (Italy)*. *Archaeometry* **2003,** *45* (4), 659-674. 10.1046/j.1475-4754.2003.00135.x

3.   Jiang, T.; Guo, Z.; Liu, W., Biomimetic superoleophobic surfaces: focusing on their fabrication and applications. *J. Mater. Chem. A* **2015,** *3* (5), 1811-1827. 10.1039/C4TA05582A

4.   Kajitvichyanukul, P.; Hung, Y.-T.; Wang, L. K., *Handbook of Environmental Engineering, Vol 13: Membrane and Desalination Technologies*. The Humana Press Inc., New York 2011.

5.   *Office of the Federal Register: Code of Federal Regulations, Title 40 – Protection of Environment, Vol. 30, Part 435.13*. Washington, DC, 2014.

6.   Patterson, J. W., *Industrial Wastewater Treatment Technology*. 2nd ed.; Buttersworth, Stoneham, MA: 1985.

7.   Mason, T. G.; Wilking, J. N.; Meleson, K.; Chang, C. B.; Graves, S. M., Nanoemulsions: formation, structure, and physical properties. *J. Phys.: Condes. Matter* **2006,** *18* (41), R635-R666. 10.1088/0953-8984/18/41/r01

8.   Adebajo, M. O.; Frost, R. L.; Kloprogge, J. T.; Carmody, O.; Kokot, S., Porous materials for oil spill cleanup: A review of synthesis and absorbing properties. *J. Porous Mater.* **2003,** *10* (3), 159-170. 10.1023/A:1027484117065

9.   Cheryan, M.; Rajagopalan, N., Membrane processing of oily streams. Wastewater treatment and waste reduction. *J. Membr. Sci.* **1998,** *151* (1), 13-28. 10.1016/S0376-7388(98)00190-2

10.   Al-Shamrani, A. A.; James, A.; Xiao, H., Destabilisation of oil-water emulsions and separation by dissolved air flotation. *Water Res.* **2002,** *36* (6), 1503-1512. 10.1016/S0043-1354(01)00347-5

11.   Rubio, J.; Souza, M. L.; Smith, R. W., Overview of flotation as a wastewater treatment technique. *Miner. Eng.* **2002,** *15* (3), 139-155. 10.1016/S0892-6875(01)00216-3

12.   Ichikawa, T., Electrical demulsification of oil-in-water emulsion. *Colloids Surf. A: Physicochem. Eng. Asp.* **2007,** *302* (1-3), 581-586. 10.1016/j.colsurfa.2007.03.036

13.   Al-Shamrani, A. A.; James, A.; Xiao, H., Separation of oil from water by dissolved air flotation. *Colloids Surf. A: Physicochem. Eng. Asp.* **2002,** *209* (1), 15-26. 10.1016/S0927-7757(02)00208-X

14.   Toyoda, M.; Inagaki, M., Heavy oil sorption using exfoliated graphite - New application of exfoliated graphite to protect heavy oil pollution. *Carbon* **2000,** *38* (2), 199-210. 10.1016/S0008-6223(99)00174-8

15.   Gupta, V. K.; Carrott, P. J. M.; Carrott, M. M. L. R.; Suhas, Low-Cost Adsorbents: Growing Approach to Wastewater Treatmenta Review. *Crit. Rev. Env. Sci. Tec.* **2009,** *39* (10), 783-842. 10.1080/10643380801977610

16.   Rios, G.; Pazos, C.; Coca, J., Destabilization of cutting oil emulsions using inorganic salts as coagulants. *Colloids Surf. A: Physicochem. Eng. Asp.* **1998,** *138* (2-3), 383-389. 10.1016/S0927-7757(97)00083-6

17.   Loeb, S., The Loeb-Sourirajan Membrane: How It Came About. In *Synthetic Membranes*, American Chemical Society: 1981; Vol. 153, pp 1-9.

18.   Song, L. F., Flux decline in crossflow microfiltration and ultrafiltration: mechanisms and modeling of membrane fouling. *J. Membr. Sci.* **1998,** *139* (2), 183-200. 10.1016/S0376-7388(97)00263-9

19.   Kong, J.; Li, K., Oil removal from oil-in-water emulsions using PVDF membranes. *Sep. Purif. Technol.* **1999,** *16* (1), 83-93. 10.1016/S1383-5866(98)00114-2

20. Kai, M.; Ishii, K.; Tsugaya, H.; Miyano, T. In *Development of polyethersulfone ultrafiltration membranes*, Reverse Osmosis and Ultrafiltration, ACS Symposium Series, Sourirajan, S.; Matsuura, T., Eds. ACS Publications: , Washington, DC, 1985; pp 21-33.

21. Kota, A. K.; Choi, W.; Tuteja, A., Superomniphobic surfaces: Design and durability. *MRS Bull.* **2013,** *38* (5), 383-390. 10.1557/mrs.2013.101

22. Young, T., An Essay on the Cohesion of Fluids. *Philos. Trans. R. Soc.* **1805,** *95*, 65-87.

23. Tuteja, A.; Choi, W.; Ma, M. L.; Mabry, J. M.; Mazzella, S. A.; Rutledge, G. C.; McKinley, G. H.; Cohen, R. E., Designing superoleophobic surfaces. *Science* **2007,** *318* (5856), 1618-1622. 10.1126/science.1148326

24. Feng, X. J.; Jiang, L., Design and creation of superwetting/antiwetting surfaces. *Adv. Mater.* **2006,** *18* (23), 3063-3078. 10.1002/adma.200501961

25. Kota, A. K.; Kwon, G.; Tuteja, A., The design and applications of superomniphobic surfaces. *NPG Asia Mater.* **2014,** *6*, e109. 10.1038/am.2014.34

26. Wenzel, R. N., Resistance of Solid Surfaces to Wetting by Water. *Ind. Eng. Chem.* **1936,** *28*, 988-994. 10.1021/ie50320a024

27. Cassie, A. B. D.; Baxter, S., Wettability of porous surfaces. *Trans. Faraday Soc.* **1944,** *40*, 546. 10.1039/tf9444000546

28. Choi, W.; Tuteja, A.; Mabry, J. M.; Cohen, R. E.; McKinley, G. H., A modified Cassie–Baxter relationship to explain contact angle hysteresis and anisotropy on non-wetting textured surfaces. *J. Colloid Interface Sci.* **2009,** *339* (1), 208-216. 10.1016/j.jcis.2009.07.027

29. Dettre, R. H.; Johnson, R. E., Contact Angle Hysteresis. In *Contact Angle, Wettability, and Adhesion*, Fowkes, F. M., Ed. American Chemical Society: Washington, D.C., 1964; Vol. 43, pp 136-144.

30. Quere, D., Rough ideas on wetting. *Phys. A* **2002,** *313* (1-2), 32-46. 10.1016/S0378-4371(02)01033-6

31. McHale, G.; Shirtcliffe, N. J.; Newton, M. I., Contact-angle hysteresis on super-hydrophobic surfaces. *Langmuir* **2004,** *20* (23), 10146-10149. 10.1021/la0486584

32. Marmur, A., From hygrophilic to superhygrophobic: theoretical conditions for making high-contact-angle surfaces from low-contact-angle materials. *Langmuir* **2008,** *24*, 7573-9. 10.1021/la800304r

33. Marmur, A., Wetting on Hydrophobic Rough Surfaces: To Be Heterogeneous or Not To Be? *Langmuir* **2003,** *19*, 8343-8348. 10.1021/la0344682

34.   Tuteja, A.; Choi, W.; Mabry, J. M.; McKinley, G. H.; Cohen, R. E., Robust omniphobic surfaces. *Proc. Natl. Acad. Sci. USA* **2008,** *105* (47), 18200-5. 10.1073/pnas.0804872105

35.   Nosonovsky, M., Multiscale roughness and stability of superhydrophobic biomimetic interfaces. *Langmuir* **2007,** *23* (6), 3157-3161. 10.1021/la062301d

36.   Kota, A. K.; Kwon, G.; Choi, W.; Mabry, J. M.; Tuteja, A., Hygro-responsive membranes for effective oil-water separation. *Nat. Commun.* **2012,** *3*, 1025. 10.1038/ncomms2027

37.   Batchelor, G. K., *An Introduction to Fluid Dynamics*. Cambridge University Press: New York, NY, 2000.

38.   Choi, W.; Tuteja, A.; Chhatre, S.; Mabry, J. M.; Cohen, R. E.; McKinley, G. H., Fabrics with Tunable Oleophobicity. *Adv. Mater.* **2009,** *21* (21), 2190-+. 10.1002/adma.200802502

39.   Tuteja, A.; Choi, W.; McKinley, G. H.; Cohen, R. E.; Rubner, M. F., Design Parameters for Superhydrophobicity and Superoleophobicity. *MRS Bull.* **2008,** *33* (08), 752-758. 10.1557/mrs2008.161

40.   Chhatre, S. S.; Choi, W.; Tuteja, A.; Park, K.-C. K.; Mabry, J. M.; McKinley, G. H.; Cohen, R. E., Scale dependence of omniphobic mesh surfaces. *Langmuir* **2010,** *26*, 4027-35. 10.1021/la903489r

41.   Golovin, K.; Lee, D. H.; Mabry, J. M.; Tuteja, A., Transparent, Flexible, Superomniphobic Surfaces with Ultra-Low Contact Angle Hysteresis. *Angew. Chem. Int. Ed.* **2013,** *52* (49), 13007-13011. 10.1002/anie.201307222

42.   Hensel, R.; Finn, A.; Helbig, R.; Braun, H. G.; Neinhuis, C.; Fischer, W. J.; Werner, C., Biologically Inspired Omniphobic Surfaces by Reverse Imprint Lithography. *Adv. Mater.* **2014,** *26* (13), 2029-2033. 10.1002/adma.201305408

43.   Feng, L.; Zhang, Z.; Mai, Z.; Ma, Y.; Liu, B.; Jiang, L.; Zhu, D., A super-hydrophobic and super-oleophilic coating mesh film for the separation of oil and water. *Angew. Chem. Int. Ed.* **2004,** *43*, 2012-4. 10.1002/anie.200353381

44.   Feng, L.; Zhang, Z. Y.; Mai, Z. H.; Ma, Y. M.; Liu, B. Q.; Jiang, L.; Zhu, D. B., A super-hydrophobic and super-oleophilic coating mesh film for the separation of oil and water. *Angew. Chem. Int. Ed.* **2004,** *116* (15), 2046-2048. 10.1002/anie.200353381

45.   Cao, Y.; Zhang, X.; Tao, L.; Li, K.; Xue, Z.; Feng, L.; Wei, Y., Mussel-inspired chemistry and Michael addition reaction for efficient oil/water separation. *ACS Appl. Mater. Interfaces* **2013,** *5*, 4438-42. 10.1021/am4008598

46. Wu, J.; Chen, J.; Qasim, K.; Xia, J.; Lei, W.; Wang, B.-p., A hierarchical mesh film with superhydrophobic and superoleophilic properties for oil and water separation. *J. Chem. Technol. Biotechnol.* **2012,** *87*, 427-430. 10.1002/jctb.2746

47. Wang, Q. J.; Cui, Z.; Mao, Y.; Chen, Q. M., Stable highly hydrophobic and oleophilic meshes for oil-water separation. *Appl. Surf. Sci.* **2007,** *253* (23), 9054-9060. 10.1016/j.apsusc.2007.05.030

48. Wang, B.; Guo, Z., Superhydrophobic copper mesh films with rapid oil/water separation properties by electrochemical deposition inspired from butterfly wing. *Appl. Phys. Lett.* **2013,** *103*, 063704. 10.1063/1.4817922

49. Wang, C.; Yao, T.; Wu, J.; Ma, C.; Fan, Z.; Wang, Z.; Cheng, Y.; Lin, Q.; Yang, B., Facile approach in fabricating superhydrophobic and superoleophilic surface for water and oil mixture separation. *ACS Appl. Mater. Interfaces* **2009,** *1*, 2613-7. 10.1021/am900520z

50. Wang, S.; Song, Y.; Jiang, L., Microscale and nanoscale hierarchical structured mesh films with superhydrophobic and superoleophilic properties induced by long-chain fatty acids. *Nanotechnology* **2007,** *18*, 015103. 10.1088/0957-4484/18/1/015103

51. Liu, N.; Cao, Y.; Lin, X.; Chen, Y.; Feng, L.; Wei, Y., A facile solvent-manipulated mesh for reversible oil/water separation. *ACS Appl. Mater. Interfaces* **2014,** *6*, 12821-6. 10.1021/am502809h

52. Crick, C. R.; Gibbins, J. A.; Parkin, I. P., Superhydrophobic polymer-coated copper-mesh; membranes for highly efficient oil–water separation. *J. Mater. Chem. A* **2013,** *1*, 5943. 10.1039/c3ta10636e

53. Shang, Y.; Si, Y.; Raza, A.; Yang, L.; Mao, X.; Ding, B.; Yu, J., An in situ polymerization approach for the synthesis of superhydrophobic and superoleophilic nanofibrous membranes for oil-water separation. *Nanoscale* **2012,** *4*, 7847-54. 10.1039/c2nr33063f

54. Tang, X.; Si, Y.; Ge, J.; Ding, B.; Liu, L.; Zheng, G.; Luo, W.; Yu, J., In situ polymerized superhydrophobic and superoleophilic nanofibrous membranes for gravity driven oil-water separation. *Nanoscale* **2013,** *5*, 11657-64. 10.1039/c3nr03937d

55. Huang, M.; Si, Y.; Tang, X.; Zhu, Z.; Ding, B.; Liu, L.; Zheng, G.; Luo, W.; Yu, J., Gravity driven separation of emulsified oil–water mixtures utilizing in situ polymerized superhydrophobic and superoleophilic nanofibrous membranes. *J. Mater. Chem. A* **2013,** *1*, 14071. 10.1039/c3ta13385k

56. Zhang, W.; Shi, Z.; Zhang, F.; Liu, X.; Jin, J.; Jiang, L., Superhydrophobic and superoleophilic PVDF membranes for effective separation of water-in-oil

emulsions with high flux. *Adv. Mater.* **2013,** *25*, 2071-6. 10.1002/adma.201204520

57. Wang, S.; Li, M.; Lu, Q., Filter paper with selective absorption and separation of liquids that differ in surface tension. *ACS Appl. Mater. Interfaces* **2010,** *2*, 677-83. 10.1021/am900704u

58. Du, C.; Wang, J.; Chen, Z.; Chen, D., Durable superhydrophobic and superoleophilic filter paper for oil–water separation prepared by a colloidal deposition method. *Appl. Surf. Sci.* **2014,** *313*, 304-310. 10.1016/j.apsusc.2014.05.207

59. Asthana, A.; Maitra, T.; Büchel, R.; Tiwari, M. K.; Poulikakos, D., Multifunctional superhydrophobic polymer/carbon nanocomposites: graphene, carbon nanotubes, or carbon black? *ACS Appl. Mater. Interfaces* **2014,** *6*, 8859-67. 10.1021/am501649w

60. Shi, Z.; Zhang, W.; Zhang, F.; Liu, X.; Wang, D.; Jin, J.; Jiang, L., Ultrafast separation of emulsified oil/water mixtures by ultrathin free-standing single-walled carbon nanotube network films. *Adv. Mater.* **2013,** *25* (17), 2422-7. 10.1002/adma.201204873

61. Zhang, J.; Seeger, S., Polyester Materials with Superwetting Silicone Nanofilaments for Oil/Water Separation and Selective Oil Absorption. *Adv. Funct. Mater.* **2011,** *21*, 4699-4704. 10.1002/adfm.201101090

62. Li, J.; Shi, L.; Chen, Y.; Zhang, Y.; Guo, Z.; Su, B.-l.; Liu, W., Stable superhydrophobic coatings from thiol-ligand nanocrystals and their application in oil/water separation. *J. Mater. Chem.* **2012,** *22*, 9774. 10.1039/c2jm30931a

63. Kavalenka, M. N.; Hopf, A.; Schneider, M.; Worgull, M.; Hölscher, H., Wood-based microhaired superhydrophobic and underwater superoleophobic surfaces for oil/water separation. *RSC Adv.* **2014,** *4*, 31079. 10.1039/C4RA04029E

64. Maartens, A.; Jacobs, E. P.; Swart, P., UF of pulp and paper effluent: membrane fouling-prevention and cleaning. *J. Membr. Sci.* **2002,** *209* (1), 81-92. 10.1016/S0376-7388(02)00266-1

65. Hu, B.; Scott, K., Influence of membrane material and corrugation and process conditions on emulsion microfiltration. *J. Membr. Sci.* **2007,** *294* (1-2), 30-39. 10.1016/j.memsci.2007.02.002

66. Liu, M.; Wang, S.; Wei, Z.; Song, Y.; Jiang, L., Bioinspired Design of a Superoleophobic and Low Adhesive Water/Solid Interface. *Adv. Mater.* **2009,** *21* (6), 665-669. 10.1002/adma.200801782

67. Xue, Z. X.; Liu, M. J.; Jiang, L., Recent developments in polymeric superoleophobic surfaces. *J. Polym. Sci., Part B: Polym. Phys.* **2012,** *50* (17), 1209-1224. 10.1002/polb.23115

68. Xue, Z.; Wang, S.; Lin, L.; Chen, L.; Liu, M.; Feng, L.; Jiang, L., A Novel Superhydrophilic and Underwater Superoleophobic Hydrogel-Coated Mesh for Oil/Water Separation. *Adv. Mater.* **2011,** *23*, 4270-4273. 10.1002/adma.201102616

69. Teng, C.; Lu, X.; Ren, G.; Zhu, Y.; Wan, M.; Jiang, L., Underwater Self-Cleaning PEDOT-PSS Hydrogel Mesh for Effective Separation of Corrosive and Hot Oil/Water Mixtures. *Adv. Mater. Interfaces* **2014,** *1* (6), 1400099. 10.1002/admi.201400099

70. Zhang, S. Y.; Lu, F.; Tao, L.; Liu, N.; Gao, C. R.; Feng, L.; Wei, Y., Bio-Inspired Anti-Oil-Fouling Chitosan-Coated Mesh for Oil/Water Separation Suitable for Broad pH Range and Hyper-Saline Environments. *ACS Appl. Mater. Interfaces* **2013,** *5* (22), 11971-11976. 10.1021/am403203q

71. Lu, F.; Chen, Y. N.; Liu, N.; Cao, Y. Z.; Xu, L. X.; Wei, Y.; Feng, L., A fast and convenient cellulose hydrogel-coated colander for high-efficiency oil-water separation. *RSC Adv.* **2014,** *4* (61), 32544-32548. 10.1039/c4ra04464a

72. Jing, B. X.; Wang, H. T.; Lin, K. Y.; McGinn, P. J.; Na, C. Z.; Zhu, Y. X., A facile method to functionalize engineering solid membrane supports for rapid and efficient oil-water separation. *Polymer* **2013,** *54* (21), 5771-5778. 10.1016/j.polymer.2013.08.030

73. Dong, Y.; Li, J.; Shi, L.; Wang, X. B.; Guo, Z. G.; Liu, W. M., Underwater superoleophobic graphene oxide coated meshes for the separation of oil and water. *Chem. Commun.* **2014,** *50* (42), 5586-5589. 10.1039/c4cc01408a

74. Wen, Q.; Di, J. C.; Jiang, L.; Yu, J. H.; Xu, R. R., Zeolite-coated mesh film for efficient oil-water separation. *Chem. Sci.* **2013,** *4* (2), 591-595. 10.1039/c2sc21772d

75. Zeng, J. W.; Guo, Z. G., Superhydrophilic and underwater superoleophobic MFI zeolite-coated film for oil/water separation. *Colloids Surf. A: Physicochem. Eng. Asp.* **2014,** *444*, 283-288. 10.1016/j.colsurfa.2013.12.071

76. Liu, N.; Chen, Y.; Lu, F.; Cao, Y.; Xue, Z.; Li, K.; Feng, L.; Wei, Y., Straightforward oxidation of a copper substrate produces an underwater superoleophobic mesh for oil/water separation. *ChemPhysChem* **2013,** *14*, 3489-94. 10.1002/cphc.201300691

77. Zhu, Y. Z.; Zhang, F.; Wang, D.; Pei, X. F.; Zhang, W. B.; Jin, J., A novel zwitterionic polyelectrolyte grafted PVDF membrane for thoroughly separating

oil from water with ultrahigh efficiency. *J. Mater. Chem. A* **2013,** *1* (18), 5758-5765. 10.1039/c3ta01598j

78. Chen, P. C.; Xu, Z. K., Mineral-Coated Polymer Membranes with Superhydrophilicity and Underwater Superoleophobicity for Effective Oil/Water Separation. *Sci. Rep.* **2013,** *3*, 2776. 10.1038/srep02776

79. Yang, H.-C.; Liao, K.-J.; Huang, H.; Wu, Q.-Y.; Wan, L.-S.; Xu, Z.-K., Mussel-inspired modification of a polymer membrane for ultra-high water permeability and oil-in-water emulsion separation. *J. Mater. Chem. A* **2014,** *2*, 10225. 10.1039/c4ta00143e

80. Yang, H.-C.; Pi, J.-K.; Liao, K.-J.; Huang, H.; Wu, Q.-Y.; Huang, X.-J.; Xu, Z.-K., Silica-Decorated Polypropylene Microfiltration Membranes with a Mussel-Inspired Intermediate Layer for Oil-in-Water Emulsion Separation. *ACS Appl. Mater. Interfaces* **2014,** *6*, 12566-72. 10.1021/am502490j

81. Ahmed, F. E.; Lalia, B. S.; Hilal, N.; Hashaikeh, R., Underwater superoleophobic cellulose/electrospun PVDF-HFP membranes for efficient oil/water separation. *Desalination* **2014,** *344*, 48-54. 10.1016/j.desal.2014.03.010

82. Raza, A.; Ding, B.; Zainab, G.; El-Newehy, M.; Al-Deyab, S. S.; Yu, J. Y., In situ cross-linked superwetting nanofibrous membranes for ultrafast oil-water separation. *J. Mater. Chem. A* **2014,** *2* (26), 10137-10145. 10.1039/c4ta00806e

83. Liu, Q. S.; Patel, A. A.; Liu, L. Y., Superhydrophilic and Underwater Superoleophobic Poly(sulfobetaine methacrylate)-Grafted Glass Fiber Filters for Oil-Water Separation. *ACS Appl. Mater. Interfaces* **2014,** *6* (12), 8996-9003. 10.1021/am502302g

84. Chen, Y. N.; Xue, Z. X.; Liu, N.; Lu, F.; Cao, Y. Z.; Sun, Z. X.; Feng, L., Fabrication of a silica gel coated quartz fiber mesh for oil-water separation under strong acidic and concentrated salt conditions. *RSC Adv.* **2014,** *4* (22), 11447-11450. 10.1039/c3ra46661b

85. Yang, J.; Zhang, Z. Z.; Xu, X. H.; Zhu, X. T.; Men, X. H.; Zhou, X. Y., Superhydrophilic-superoleophobic coatings. *J. Mater. Chem.* **2012,** *22* (7), 2834-2837. 10.1039/c2jm15987b

86. Howarter, J. A.; Youngblood, J. P., Self-cleaning and anti-fog surfaces via stimuli-responsive polymer brushes. *Adv. Mater.* **2007,** *19* (22), 3838-+. 10.1002/adma.200700156

87. Zhang, L. B.; Zhong, Y. J.; Cha, D.; Wang, P., A self-cleaning underwater superoleophobic mesh for oil-water separation. *Sci. Rep.* **2013,** *3*, 2326. 10.1038/srep02326

88.   Gao, P.; Liu, Z. Y.; Sun, D. D.; Ng, W. J., The efficient separation of surfactant-stabilized oil-water emulsions with a flexible and superhydrophilic graphene-TiO2 composite membrane. *J. Mater. Chem. A* **2014,** *2* (34), 14082-14088. 10.1039/c4ta02039a

89.   Sawai, Y.; Nishimoto, S.; Kameshima, Y.; Fujii, E.; Miyake, M., Photoinduced underwater superoleophobicity of TiO2 thin films. *Langmuir* **2013,** *29* (23), 6784-9. 10.1021/la401382g

90.   Yang, J.; Song, H.; Yan, X.; Tang, H.; Li, C., Superhydrophilic and superoleophobic chitosan-based nanocomposite coatings for oil/water separation. *Cellulose* **2014,** *21*, 1851-1857. 10.1007/s10570-014-0244-0

91.   Zhu, X.; Loo, H.-E.; Bai, R., A novel membrane showing both hydrophilic and oleophobic surface properties and its non-fouling performances for potential water treatment applications. *J. Membr. Sci.* **2013,** *436*, 47-56. 10.1016/j.memsci.2013.02.019

92.   Zhu, X. Y.; Tu, W. T.; Wee, K. H.; Bai, R. B., Effective and low fouling oil/water separation by a novel hollow fiber membrane with both hydrophilic and oleophobic surface properties. *J. Membr. Sci.* **2014,** *466*, 36-44. 10.1016/j.memsci.2014.04.038

93.   Howarter, J. A.; Youngblood, J. P., Amphiphile grafted membranes for the separation of oil-in-water dispersions. *J. Colloid Interface Sci.* **2009,** *329* (1), 127-132. 10.1016/j.jcis.2008.09.068

94.   Yoon, H.; Na, S. H.; Choi, J. Y.; Latthe, S. S.; Swihart, M. T.; Al-Deyab, S. S.; Yoon, S. S., Gravity-driven hybrid membrane for oleophobic-superhydrophilic oil-water separation and water purification by graphene. *Langmuir* **2014,** *30* (39), 11761-9. 10.1021/la5031526

95.   Berge, B., Electrocapillarity and wetting of insulator films by water. *Comptes Rendus Acad. Sci. II* **1993,** *317* (2), 157-163.

96.   Kwon, G.; Kota, A. K.; Li, Y.; Sohani, A.; Mabry, J. M.; Tuteja, A., On-demand separation of oil-water mixtures. *Adv. Mater.* **2012,** *24* (27), 3666-71. 10.1002/adma.201201364

CHAPTER 2

Highly Versatile, Hydrophilic-Oleophobic Modification for Anti-Fouling Membranes

This chapter contains work adapted from a first author article pending publication. Gibum Kwon assisted with experiments and Mathew Boban assisted with LEXT.

2.1 Introduction

2.1.1 Motivation

Clean water access is one of the greatest challenges worldwide. Over one billion people do not have clean water and 3,900 children die each day due to unsafe water and poor sanitation.[1] Effective purification should be cheap, low energy, and be able to process many forms of contaminated water.[2] Oily wastewater treatment is of particular interest because it is generated in many fields including: petrochemical processing, metallurgy, crude oil recovery, sewage, food processing, and pharmaceuticals.[3-6] Floatable oil or unstable emulsions are separated by traditional methods such as flotation, hydrocyclone, electrocoagulation, electroflotation, and chemical treatment, but these methods take a very long time or do not work with stable emulsion drops, especially below 10 μm in diameter.[7] Membrane technology is an attractive option for stable emulsions owing to several factors. Compared to other separation unit operations, membranes require lower capital, use no added chemicals, are less energy intensive and easily automated in many industries, and have uniform permeate and a small equipment

footprint.[7-9] A small footprint is especially important for applications such as offshore oil rigs where water treatment must be efficient, light, and compact.[4] Membranes can also be selected and modified to separate based on oil droplet size and the chemical interactions with the surface.[5] Despite all the advantages of membranes, there has been one major limitation to their widespread use, which increases the operating cost and shortens membrane life.

2.1.2 Membrane Fouling

The decline in membrane flux due to fouling is the greatest limitation of membranes[7, 10-11] and has slowed their use in industrial applications such as membrane bioreactor treatment of wastewater.[12] Fouling can decrease flux to less than a tenth of the initial.[13] Certain membrane materials, such as ceramics which have good mechanical properties and stability under adverse conditions, have seen little use for wastewater because of the high fouling costs.[7] Fouling originates from concentration polarization or the build up of material, including adsorption and cake layer deposition. The focus is on preventing the build up of material because it is related to the membrane properties, which can be modified. Fouling results in increased membrane resistance due to blocked pores and less active area. Common foulants include organics, inorganics, colloids, and particles.[14] Oil adsorption is a severe problem because it quickly, and usually irreversibly, plugs pores or lowers the effective pore size. Surfactants may also do the same, even forming micelles in pores.[5, 7, 15-17] The pressure in the system may also force larger oil drops into the smaller pores.[3, 16] Beyond pore blocking, oil can form a hydrophobic barrier to water permeation by lowering the surface energy. These sources of membrane resistance will lower the permeate flux if a constant transmembrane pressure (TMP) is

maintained, or flux can be increased by increasing the TMP, which costs money.[14] In order to minimize operating costs, fouling must be prevented from occurring or dealt with through cleaning.

2.1.3 Traditional Fouling Prevention

Many approaches have been taken for filtration design and operation to limit fouling, especially the reversible cake layer. Turbulence promoters, including pulsed flow, backwash, and cross-flow, have been used to help prevent foulants or coalesced oil from accumulating at the membrane surface.[3, 14, 18-22] Pre-treating the feed and adjusting the operating pressure and temperature may also be useful. To limit adsorbed irreversible fouling, adequate cleaning is still necessary.[23] The frequency of cleaning is a cost balance between increasing TMP and cleaning (down time, chemicals, labor) to achieve the necessary flux. A study in the Orange County Water District showed that cleaning a reverse osmosis train costs almost $16,000 and may be performed more than once per year.[24] Even with rigorous cleaning, which may actually damage the membrane,[10] there is permeation loss due to irreversible fouling. In order to decrease the complexity and cost of filtration systems, new generations of membranes should have greater selectivity and self-cleaning ability for longer service lives and greater efficiency.[7, 9]

2.1.4 Fouling Prevention through Control of Wetting

Polymer membranes are typically hydrophobic and easily adsorb organic foulants, but adding hydrophilic character can reduce fouling and cleaning needs.[23] Much prior work has indicated that hydrophilic membranes show reduced fouling (compared to hydrophobic ones) due to the favorable interaction with water and decreased oil contact and attachment to the wetted surface.[7, 10, 12, 25] Many groups have successfully increased

the hydrophilicity of various metal meshes and polymer membranes by adsorbing, grafting, or blending in hydrophilic polymers, hydrogels, surfactants, polyelectrolytes, minerals, and zeolites.[10, 17, 26-36] These hydrophilic or superhydrophilic membranes show underwater oleophobicity (omniphilic in air), but due to their high surface energy, lower surface tension oils will spread easily without a hydration layer and are more difficult to clean once fouled.[25, 37] This contamination may occur because of operating pressure, initial startup, stop-and-go operation, or maintenance where the membrane loses water exposure. Therefore, this wettability has narrowed applications. It can be utilized for gravity-driven filtration, but will perform poorly with feeds containing high fractions of oil, such as free water-in-oil or water-in-oil emulsions, unless every pore is pre-wet by water and does not dehydrate. A more ideal membrane would be hydrophilic and oleophobic (HL/OP) in air and underwater.[8, 25 38]

The HL/OP wettability is counterintuitive and somewhat difficult to fabricate because the surface tension of water is much higher than oils; oils typically have much lower contact angles than water on most surfaces. A reversal in normal wetting allows water to undercut oils on a membrane and wash the foulant off more easily. A few groups have developed HL/OP surfaces through a couple approaches, which all involve a combination of a hydrophilic component and a low surface energy, fluorinated component. Polymers with hydrophilic and fluorinated segments have been blended into or grafted onto a membrane,[5, 11, 25, 37, 39-41] low energy fluorodecyl POSS has been blended with a hydrogel,[8] and fluorinated surfactant-polyelectrolyte complexes have been synthesized.[38, 42-43] These groups explain this type of wetting in a couple ways. The dual nature polymers can change conformation based on a solvent switching response or the

separate hydrophilic and low energy material can reconfigure based on the liquid present. Another explanation is that the low energy, fluorinated layer has small defects leading to the hydrophilic substrate. This allows the small water molecules to penetrate to interact favorably with the polar substrate, while repelling larger, non-polar oils. In summary, if the low energy material does not completely mask the polar substrate, polar liquids, or liquids with sufficient polar character, wet the surface and permeate through the membrane.[44-45] A HL/OP membrane, in air and underwater, provides duality in fouling prevention. Polar interactions with the hydrophilic character bring fouling resistance through the hydration layer (with sufficient water present), and the low energy groups allow for fouling release, even solely by a water rinse, by weakening the foulant-membrane interaction.[5-6, 40]

This work has focused on developing a methodology that would yield anti-fouling membranes, in air and underwater, from a variety of common substrates and pore sizes, without the synthesis of custom polymers. The simplicity and flexibility of our fabrication methods will aid in the implementation of these membranes within industrial settings. They allow for the treatment of surfactant-stabilized emulsions, at the nano- and micro-scale, and will extend the life of oil-water separators due to water displacing oil, even under heavy oil exposure. By being HL/OP, in air and underwater, fouling during startup and stop-and-go operation, as well as maintenance may be reduced. Our membranes' anti-fouling capability and separation performance were demonstrated in a batch apparatus as well as cross-flow filtration systems, using both tubular and flat sheet membranes.

2.2 Materials and Methods

2.2.1 Materials

(Heptadecafluoro-1,1,2,2-tetrahydrodecyl) triethoxysilane (SIH5841.2), 2-[methoxy(polyethyleneoxy)$_{6-9}$ propyl] trichlorosilane (SIM6492.66), *n*-octadecyltriethoxysilane (SIO6642.0), and bis(3-trimethoxysilylpropyl) amine (SIB1833.0) were purchased from Gelest. 0.2 μm and 0.45 μm regenerated cellulose and 0.8 μm cellulose acetate membrane filters were sourced from Sterlitech Corporation. Ultracel® 100kDa (~10 nm) regenerated cellulose, 0.45 μm hydrophilic nylon, and 0.45 μm Durapore® Hydrophobic PVDF membranes were purchased from EMD Millipore Corporation. Whatman #4 and #114 (25 μm), Whatman #5 (2.5 μm), and Whatman RC55 (0.45 μm) cellulose membrane filters were purchased from GE Healthcare. Cellulose film (P25) was provided by Innovia Films. 200 x 200 aluminum mesh was purchased from McMaster-Carr. Dichloromethane and Oil Red O were from Alfa Aesar. ≥ 99% *n*-dodecane and Solvent Blue 38 were from Sigma-Aldrich. Dodecane, mixture of isomers was purchased from Acros Organics. Sodium dodecyl sulfate (SDS) was from Hoefer, Inc. Laboratory grade isopropyl alcohol, anhydrous ethanol, and toluene were from Fisher. The U.S. Navy provided Navy Standard Bilge Mix (NSBM) #4 and Detergent Mix #4. Laboratory-scale, 0.005 μm Silica UF membranes (5 nm) and stainless-steel test housing were purchased from Veolia. A CF042 Teflon Crossflow Cell was purchased from Sterlitech Corporation (extensive equipment lists for flow studies located in Appendix A.3.3). A Scienceware desiccator was sourced from Bel-art Products and a Maximadry vacuum pump from Fisher Scientific. A Rocker 410 vacuum pump was acquired from the Lab Depot, Inc.

2.2.2 Select HL/OP Membrane Fabrication (see Appendix A.1)

2.2.2.1 Sterlitech 0.2 μm and 0.45 μm Regenerated Cellulose Membranes

The membranes were treated with 30 W oxygen plasma for 20 min and subsequently exposed to vapor phase (heptadecafluoro-1,1,2,2-tetrahydrodecyl) triethoxysilane, under 84 kPa vacuum, for 3 hours at 70°C.

2.2.2.2 Whatman RC55 0.45 μm Regenerated Cellulose Membranes (142 mm)

The membranes were treated with 30 W oxygen plasma for 20 min and subsequently exposed to vapor phase (heptadecafluoro-1,1,2,2-tetrahydrodecyl) triethoxysilane, under 84 kPa vacuum, for 40 minutes (also 10 or 20 min for anti-fouling work) at 70°C. These were treated with the backside of the membrane covered with the spacer paper (from the manufacturer's packaging) to minimize plasma and silane contact during treatment. This was intended to create asymmetry and increase water permeation after it passes the fully-silanized top, active surface contacting the emulsion during cross-flow separation.

2.2.2.3 HL/OP Veolia Ceramic Membranes (5 nm silica)

A 1 vol% silane in dichloromethane (DCM) solution was prepared with a silane ratio of 95:5 (SIM6492.66: SIH5841.2). After removing the gaskets from the ends of the module, it was pre-soaked in pure DCM for 15 min. It was then dipped in the silane solution for 1 min and cured at 80°C for 30 min. This dipping and curing was performed two additional times.

2.2.3 Membrane Testing Procedures

2.2.3.1 Small-scale Batch Separation Apparatus

Our batch separation apparatus is made from two glass tubes, with a membrane and

gasket clamped between them (Figure 2.7b). The lower half has a vacuum port and a stopcock for easy permeate recovery. If pre-fouling the membrane, add 5 mL of *n*-dodecane to the apparatus and apply 500 mmHg vacuum to pull the oil through. An oil-in-water emulsion of 20 vol% *n*-dodecane and 80 vol% water containing 0.1 mg SDS/mL water, as prepared in Appendix A.3.2.1, was separated using a 95 mmHg vacuum. Permeate was tested with differential scanning calorimetry (DSC) and dynamic light scattering (DLS).

2.2.3.2 Cross-flow, RC55 Flat Sheet Membrane Testing Apparatus (Figure 2.10).

The membrane was cut to size for the CF042 Teflon Crossflow Cell with a laser cutter and installed in the flow cell, pre-wetted with water due to some expansion upon wetting. The appropriate emulsion (Appendix A.3.2.3) was prepared in the reservoir. The Lab Egg mixer was operated at 50% power throughout the tests. The pump power was set to maintain a 6.0 kPa upstream pressure before the membrane (throughout operation), which resulted in a 4 gph flow rate. The aqueous permeate was collected into a beaker of known mass and the mass was recorded every minute. After 50 mL of permeate was collected, it was returned to the feed tank (alternating between two collection beakers of known mass) to maintain a consistent feed. The emulsion was continuously circulated back to the feed tank. After operating for two hours, the system was shut down, the emulsion was flushed (and removed), and the system was rinsed by flowing 9 L of deionized water through the system at 6 kPa. This was done to test how well the membranes could be cleaned without added chemicals, just water. After rinsing, the emulsion was returned to the feed tank and operated for two more hours. The rinse cycle was repeated again, and then operated for two final hours; a total of 6 h of operation and

2 rinses per membrane tested. Small permeate samples were taken after each run.

2.2.3.3 Ceramic Membrane Testing Apparatus (Figure 2.15c).

The membrane was installed and the appropriate emulsion (Appendix A.3.2.2) was prepared in the feed tank. The mixer was operated at 50% power (775 rpm) using a Variac throughout the tests. The gear pump speed controller was set to provide a constant 13 gpm volumetric flow to the membrane. A heat exchanger with cooling water maintained the emulsion at 20 ± 2°C. The oil-in-water emulsion was circulated through the cross-flow membrane and returned to the feed tank, along with the purified water permeate, to be continuously re-mixed. The purified water flow rate was recorded about every hour, during work hours. The degree of fouling was gauged by the decrease in the pure water permeation rate over more than 520 h. This experiment was done with untreated and HL/OP silica tubular membranes.

2.2.4 Contact Angle Measurements

All contact angle measurements were conducted with a Ramé–Hart 200-F1 goniometer by advancing and receding a small volume of liquid (≈ 2 μL) on the surface, using a 2 mL micrometer syringe (Gilmont). At least six measurements were performed on each substrate. The typical error in measurements was ± 2°. A glass container, full of *n*-dodecane, with a membrane attached to the bottom was used with this instrument to image a water droplet on a membrane under oil. A membrane was held upside down in water, with an inverted needle to apply *n*-dodecane, for oil contact angles underwater.

2.2.5 Oxygen Plasma

A Harrick Plasma Cleaner (PDC-001) was used to apply 30 W oxygen plasma to the samples at 0.4 SCCM oxygen flow and 240 mTorr.

2.2.6 Microscopy

The surface morphology of the membranes was characterized using a Hitachi SU8000 scanning electron microscope (SEM) at 2 kV and a Philips XL30 FEG at 2 kV. Samples were gold sputter coated (~550 Å) with a SPI-Module™ Sputter Coater using argon and settings of: 18 mA, 1 kV, and 180 s exposures. Surface roughness was determined from the average of three measurements with an Olympus OLS 4000 LEXT laser confocal microscope using the 10x lens.

2.2.7 X-ray Photoelectron Spectroscopy

The membrane surfaces were analyzed with a Kratos Axis Ultra XPS with a monochromated Al source. Survey scans were performed with 160 eV pass energy and a 90° take off angle.

2.2.8 Separation Efficiency and Droplet Size Distributions

The purity of both the dodecane-rich phase and the water-rich phase after separation was measured using a TA Discovery differential scanning calorimeter (DSC). 15 µL of the sample was frozen to -25°C and then thawed to 20°C at a rate of 0.5 °C/min. The heat flow into the sample was measured. When analyzing permeate, retentate, and feed components for quantitative purity, each sample was tested in triplicate and the purity was estimated using TA Instruments Trios v4.1.1.33073 Purity Analysis (ASTM E928). The melting points and purity were determined to a 95% confidence interval, and the separated phases were compared to their respective feed component. Emulsion size distributions were determined through dynamic light scattering (DLS) with a Malvern Instruments Zetasizer Nano Series: Nano-ZS.

2.2.9 *n*-Dodecane Breakthrough Pressure Tests

For the largest pore size Whatman 4 membrane, a column of dodecane (small version of glassware in Figure 2.8) was used to find the pressure. Dodecane was slowly added at 2 mL min^{-1} with a syringe pump until a drop of dodecane passed through the membrane. The height of the dodecane column at breakthrough was measured to calculate the hydraulic pressure at the membrane surface. This was repeated ten times. For the smaller pore sizes down to 10 nm, 0.5 mL of dodecane (1.1 cm) was added above the membrane and then vacuum was applied gradually, with a regulator, until the first drop of dodecane was pulled through the membrane by the pressure differential. The vacuum level at failure was noted and the breakthrough pressure was calculated (95% confidence level uncertainty) based on the contributions from the vacuum and the short column of dodecane. This was also repeated ten times. A^* was calculated from the experimental breakthrough pressure (P_b), shown in Table 2.2. $A^* = P_b/P_{ref}$, where $P_{ref} = 2\gamma_{LV}/l_{cap}$. γ_{LV} is the dodecane surface tension and l_{cap} is the capillary length. $l_{cap} = (\gamma_{LV}/\rho g)^{1/2}$, where ρ is density and g is the gravitational constant.

2.3 Scalable and Versatile HL/OP Methodology

After the discovery of stimuli-responsive membranes (HL/OP), it was desired to develop a methodology that would allow HL/OP membranes to be derived from a variety of common substrates and pore sizes using a simple procedure. In addition, a covalently bonded surface modification would be more robust against mechanical stresses. Once these objectives were achieved, I moved on to performing useful separations of free oil and water, nano-, and micron-sized emulsions, as well as demonstrating the anti-fouling performance of the membranes.

2.3.1 Synthetic Approach

It was discovered that treating hydrophilic, cellulose membranes with oxygen plasma, followed by controlled vapor-phase silanization with (heptadecafluoro-1,1,2,2-tetrahydrodecyl) triethoxysilane, formed surfaces that would absorb water, while repelling oils (Methods 2.2.2). With the vapor-phase deposition of this fluorinated silane (F-silane), three of the four major wettabilities in air can be achieved: hydrophilic/oleophilic (HL/OL), hydrophilic/oleophobic (HL/OP), and hydrophobic/oleophobic (HP/OP)[46] on a cellulose membrane with a single chemical addition (Figure 2.1). The fourth wettability, hydrophobic/oleophilic (HP/OL), can be obtained by switching to a non-polar silane (see Appendix A.2). The longer the fluorosilanization time, the greater the degree of surface functionalization and the lower the surface energy becomes. Three hours of silanization achieves the desired HL/OP surface, but if the time is too long (4 h), the fluorinated layer is too dense and the hydrophilic nature of the substrate is masked, creating an undesirable omniphobic membrane. A commercially available, smooth cellulose film is compared to the 0.2 μm cellulose membrane in Figure 2.1. The porosity (roughness) increases the dodecane advancing contact angle, while allowing water to permeate and also undercut the oil. As any superhydrophilic membrane, these membranes are superoleophobic when underwater (Figure 2.2 and Table 2.1). Despite adding hydrophobic character to the cellulose membranes with the low energy fluorosilane treatment, a hydration layer still forms, which assists in repelling oily contaminants, and allows for more easy removal in shear flow. This structure and wettability later proves useful for oil-water separation and fouling prevention/removal.
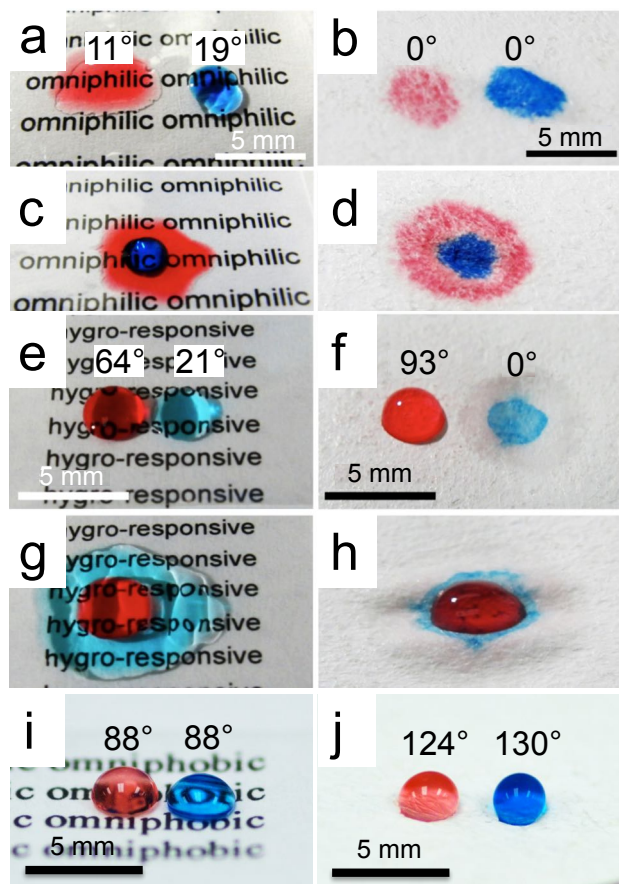
Figure 2.1: Wettability progression of cellulose film and a cellulose membrane. (a-d) Untreated, smooth cellulose film (left column) and 0.2 μm cellulose membrane (right column) advancing contact angles with dodecane (red) and water (blue) show HL/OL wettability and no oil displacement by water. (e-h) Both substrates treated for 3 hours of vapor-phase fluoro-silanization achieve the HL/OP wettability in air, where water can undercut the dodecane. (i-j) Both substrates treated for 4 hours are omniphobic (HP/OP).
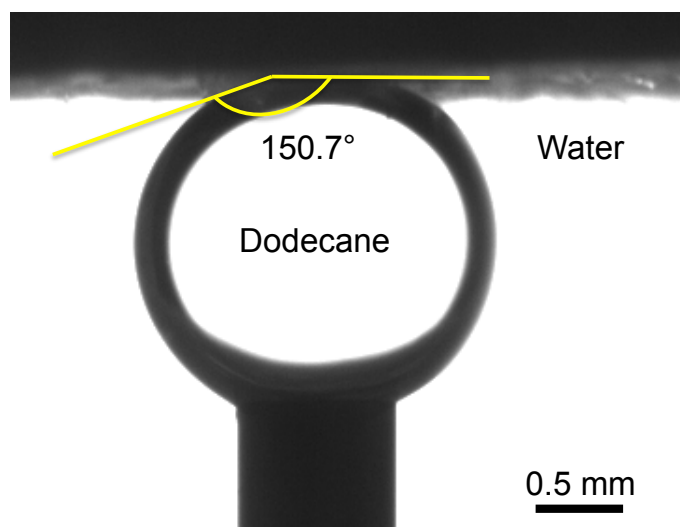
Figure 2.2: Dodecane on an underwater HL/OP Whatman #4 membrane using an inverted needle as described in Methods 2.2.4.

Table 2.1: Underwater *n*-dodecane angles on various HL/OP cellulose membranes

Cellulose Membrane Type	#4, 25 μm	#5, 2.5 μm	0.45 μm	0.2 μm	10 nm
Average Advancing Angle (°)	150.7	154.3	150.1	154.7	152.0
Advancing Standard Deviation (°)	3.6	2.4	3.4	1.7	4.5
Average Receding Angle (°)	146.9	150.2	148.5	152.6	126.6
Receding Standard Deviation (°)	3.3	2.3	3.9	2.0	9.2

2.3.2 Silane Durability and Versatility in Pore Size

The fluorosilane is covalently bonded to the surface, which is important for membrane integrity and durability, because fluorinated compounds have low surface energy and weak adhesion if used in a non-bonded coating.[47] These strong covalent bonds are necessary to maintain the surface modification during cleaning with solvents, whereas adsorbed materials can detach.[10, 39] Even after mechanical abrasion and extreme pH, the oil breakthrough pressure of the HL/OP membrane is not compromised (Chapter 3, section 3.3.2). During the silanization process, the use of ethoxysilane instead of chlorosilane is necessary to prevent embrittlement of the membrane substrate from hydrochloric acid generation. Another benefit of silanes is that membrane pores are not partially blocked by the coating (Figure 2.3) and even 10 nm sized pores can be treated, which is not possible with other high molecular weight coatings.[6, 10] The silane molecules are so small that they do not change the structural morphology of the membranes. This allows the nominal pore size to be readily known and the proper membrane can be matched to an application.

For effective membrane separations of emulsions, the pore diameter should be
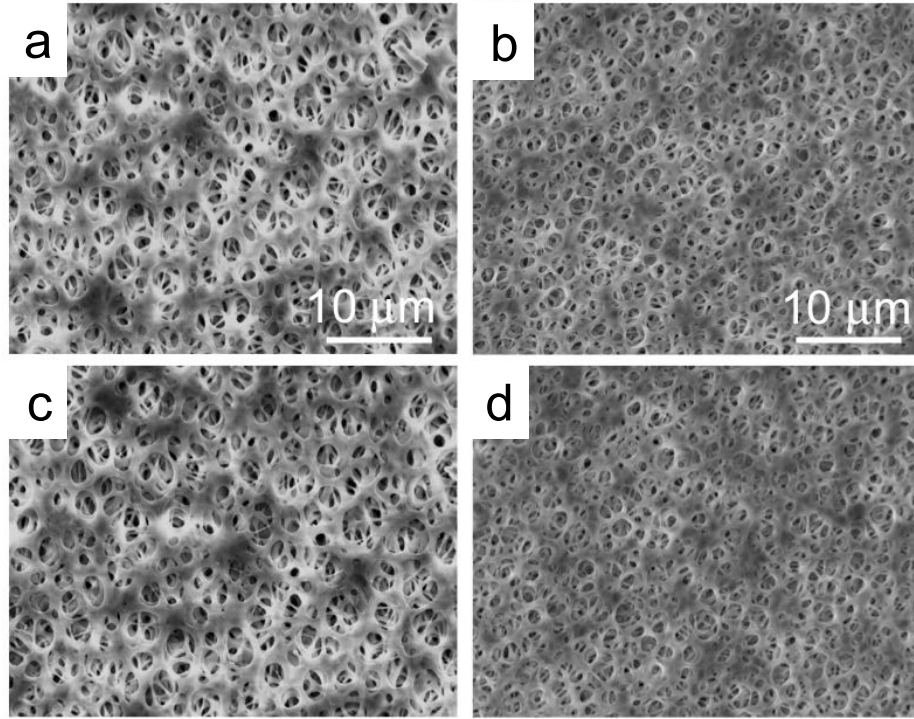
Figure 2.3: SEM images of untreated and silanized cellulose filter papers. (a) and (b) SEM images of untreated membranes with nominal pore sizes of 0.45 μm and 0.20 μm, respectively. (c) and (d) SEM images of silanized HL/OP membranes with nominal pore sizes of 0.45 and 0.20 μm, respectively.
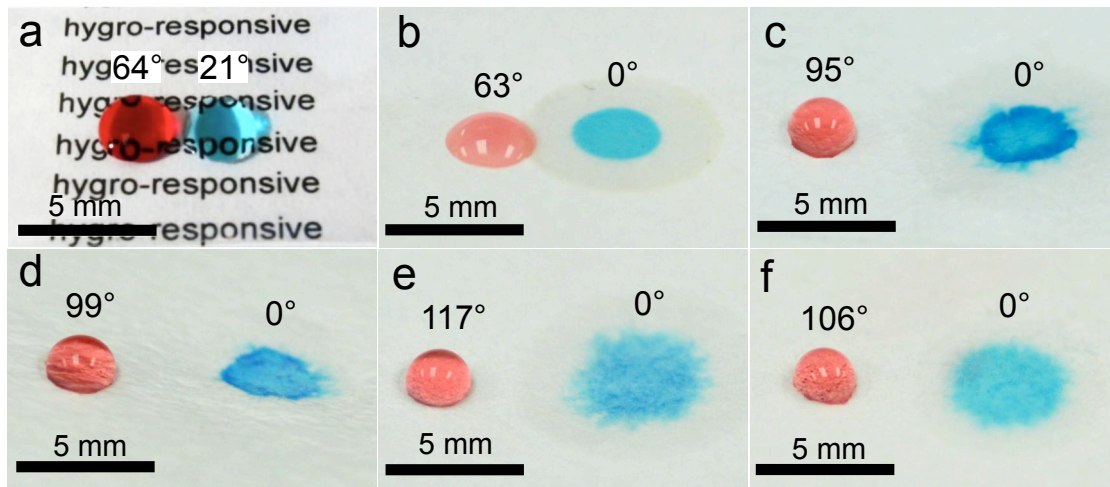
Figure 2.4: Versatility of HL/OP functionalization across several cellulose membrane pore sizes. (a) Cellulose film (non-porous), (b) 10 nm, (c) 0.2 μm, (d) 0.45 μm, (e) 2.5 μm, and (f) 25 μm effective pore diameters and their advancing contact angles. Dodecane is dyed red and water is dyed blue. The long-term stability of the coating was shown after measuring the same dodecane contact angle (Appendix Table A.1) on the HL/OP 2.5 μm membrane after more than 14 months of storage.

slightly smaller than the dispersed droplets being removed. However, from fluid dynamics, the Hagen-Poiseuille equation shows that volumetric flow decreases proportionally to the fourth power of a pore's radius, with other variables held constant.[48] To maintain the best possible permeation rates, the membrane pore size should be as large as possible, yet smaller than the emulsion droplets to be removed from the feed. By applying our F-silane deposition methodology to various cellulose membrane pore sizes (Figure 2.4), even down to effective diameter pores of 10 nm, there is increased flexibility in the feeds that may be treated with our new membranes.

2.3.3 Membrane Breakthrough Pressure and Roughness

Despite lower permeation rates, the smaller HL/OP membrane pore sizes do have the advantage of increased oil breakthrough pressure (Methods 2.2.9). Greater pressure can be applied before oil will be forced through the membrane and it fails. This is experimentally determined (Table 2.2) and quantified with the robustness factor, $A*$, which is the ratio of breakthrough pressure to a reference pressure.[8] When $A*$ is ≤ 1, it cannot prevent oil from wetting, but the membrane repels it more effectively the greater above one the robustness factor is. There is not a definitive breakthrough pressure

Table 2.2: n-Dodecane breakthrough pressure (P_b) on HL/OP membranes and the RMS Roughness values from LEXT

HL/OP Cellulose Membrane Type	Experimental P_b (kPa)	Experimental $A*$	RMS Roughness
Whatman #4, 25 μm	0.44 ± 0.05	16 ± 2	12.9 ± 0.3
Whatman #5, 2.5 μm	3.7 ± 0.1	137 ± 3	9.4 ± 0.5
Sterlitech 0.45 μm	11.7 ± 0.7	433 ± 27	6.0 ± 0.3
Sterlitech 0.2 μm	35.8 ± 0.7	1322 ± 27	7.7 ± 0.5
Ultracel® 10 nm	>88.4	>3270	3.5 ± 0.3

or $A*$ for the Ultracel® 10 nm because the breakthrough pressure was greater than the capability of our equipment.

The root mean square (RMS) roughness of the HL/OP membranes was found using 3 samples each with LEXT (Table 2.2; Methods 2.2.6). The general trend of larger pore sizes being rougher is shown. The hierarchy of support fibers and active surface leads to the higher uncertainty (Figure 2.5) and the break in the roughness trend with the 0.2 and 0.45 µm membranes.
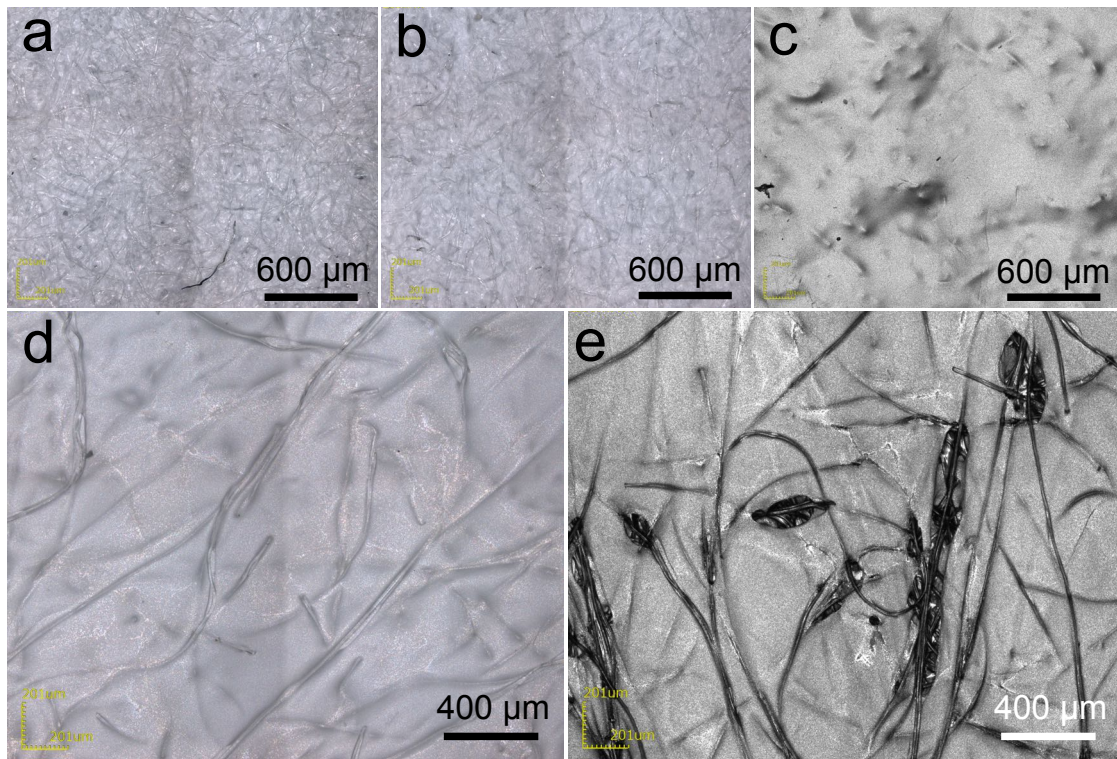
Figure 2.5: LEXT optical images at 10x. The surface structure of various cellulose membranes: (a) Whatman #4, (b) Whatman #5, (c) Ultracel® 100 kDa (~10 nm), (d) Sterlitech 0.45 µm, and (e) Sterlitech 0.2 µm. The variations due to supporting fibers can be seen, especially in (d) and (e). Sterlitech 0.2 µm roughness is higher than expected due to some surface holes around the reinforcing fibers (Table 2.2).

2.3.4 Substrate Adaptability of HL/OP Methodology

To further demonstrate the versatility of our methodology, in addition to cellulose, HL/OP membranes were made from cellulose acetate, hydrophilic nylon,
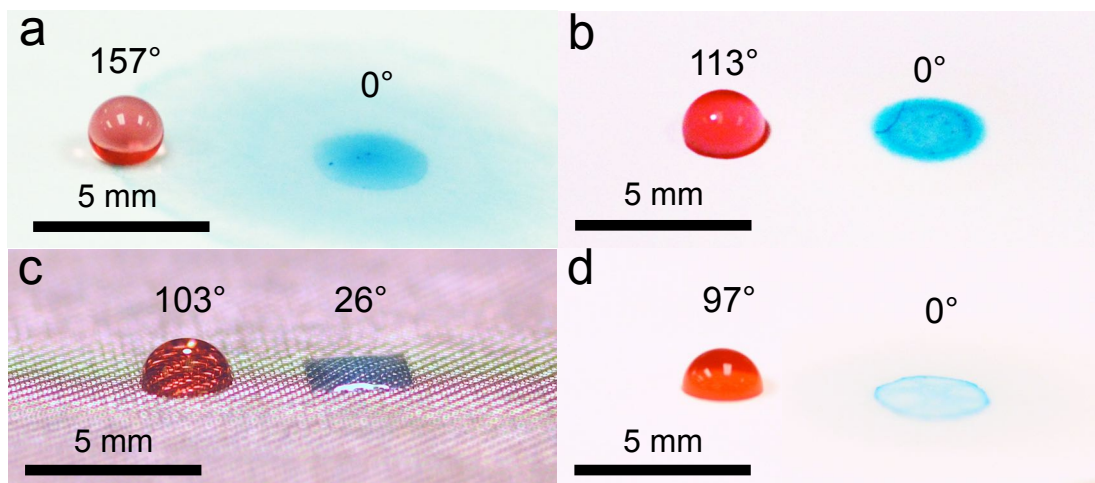
Figure 2.6: HL/OP modification of various substrates. (a) HL/OP 0.8 μm cellulose acetate membrane, (b) HL/OP 0.45 μm hydrophilic nylon membrane, (c) HL/OP 200-mesh aluminum membrane, and (d) HL/OP 0.45 μm PVDF membrane. Their respective advancing contact angles are provided. All have *n*-dodecane (dyed red) and water (dyed blue) droplets on them.

polyvinylidene difluoride (PVDF), 200-mesh aluminum (Figure 2.6), and a silica ceramic cross-flow membrane used in continuous emulsion separation (see Appendix A.1 for complete functionalization conditions). The cellulose acetate and hydrophilic nylon worked with the vapor-phase process, but the less hydrophilic aluminum mesh, the hydrophobic PVDF, and the rigid ceramic required a modified procedure. When forming HL/OP surfaces with solely F-silane, the best results were with hydrophilic polymer substrates, and membranes with greater pore sizes (generally rougher, shown by root mean square roughness – see Table 2.2) had greater oil contact angles, as expected.[38] In the cases where the substrate was less hydrophilic or rigid (no ability to reconfigure as discussed in the introduction), the HL/OP nature was arrived at through a blend of both

hydrophilic and fluorinated silanes. A surface with a silane blend would be reconfigurable and solvent responsive. Liquid-phase silanization was used due to the lower volatility of the 2-[methoxy(polyethyleneoxy)$_{6-9}$ propyl] trichlorosilane and the geometric complexity of certain treated surfaces. The chlorinated silane was chosen because of its greater hydrolysis rate and reactivity versus the ethoxy version.[49] This functionality, and a much greater fraction of hydrophilic silane in the reactive solution, encouraged it to react to the surface and prevented too much F-silane from binding, thereby avoiding an omniphobic surface. By adjusting the procedure, our methodology of a reconfigurable hydrophilic and low energy component surface allowed us to create a variety of HL/OP substrates with varying pore sizes. The usefulness of the HL/OP cellulose membranes was tested by analyzing the oil-water separation capability and the anti-fouling properties.

2.4 Anti-fouling and Separation Performance

2.4.1 Preliminary Anti-fouling Tests

Preliminary anti-fouling performance was tested by submerging a membrane in dodecane and also batch separating oil and water with a pre-fouled membrane. Figure 2.7a shows a water droplet over time on a dodecane submerged 0.2 μm HL/OP cellulose membrane. The dodecane does not permeate into the HL/OP membrane, but fully covers the surface. As the water touches the membrane, it displaces the oil and absorbs into the membrane in a few seconds. Furthermore, water can permeate through a HL/OP 0.45 μm cellulose membrane even if it is purposefully pre-fouled by forcing dodecane through it. The membrane is mounted in the small-scale batch apparatus, shown in Figure 2.7b, and 5 mL of dodecane is pulled through the membrane using 500 mmHg vacuum.
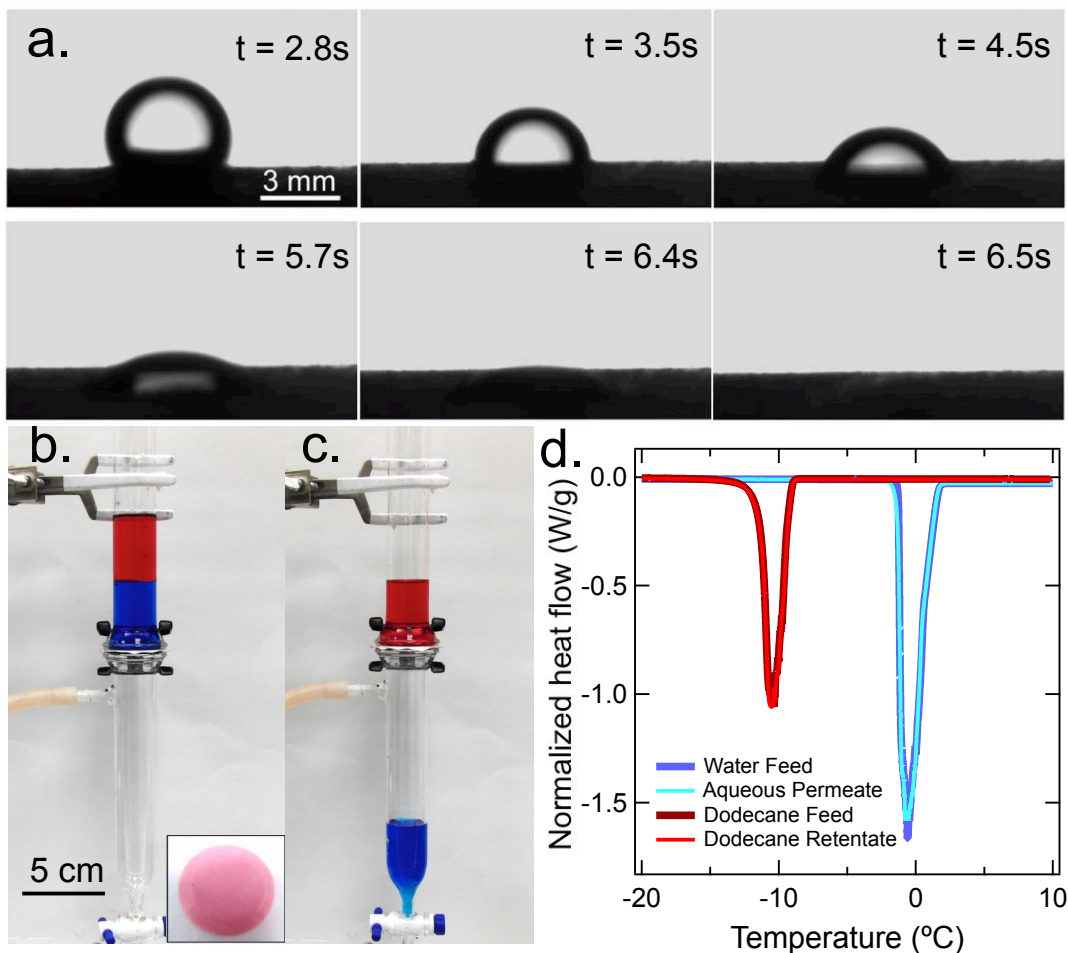
Figure 2.7: Stimuli-responsive membrane maintains and recovers oleophobicity (a) A stimuli-responsive 0.2 μm membrane is under oil (dodecane) for 1 h and then a water droplet is added. A series of snapshots shows how the water droplet displaces dodecane and penetrates into the membrane in a few seconds. (b) A separation apparatus with water (blue) and dodecane (red) above a HL/OP 0.45 μm membrane. The membrane sandwiched between the two glass tubes is pre-fouled with dodecane using sufficiently high pressure. Inset shows the membrane saturated with dodecane. (c) The water-rich permeate passes through the membrane while the dodecane-rich retentate remains above the membrane. (d) DSC data for the water-rich permeate and oil-rich retentate, and the as-obtained dodecane and water for comparison.

After fully wetting the membrane with oil, 20 mL of water and 20 mL of dodecane are added. 95 mmHg vacuum is applied (gravity is sufficient, but the permeation rate is slower) and the water passes, while the dodecane does not, showing the recovery of oleophobicity. Analysis of the water permeate by differential scanning calorimetry (DSC)

showed no significant difference between the permeate (>99.9% pure) and pure feed water (Appendix Figure A.8). These two tests are not definitive in proving the anti-fouling benefits of HL/OP membranes because untreated cellulose membranes show similar qualitative displacement of oil by water and oil repellency once a hydration layer forms. The effect of oil contact and fouling in the batch apparatus, as well as continuous systems later, was quantitatively analyzed through the permeation rates of water through HL/OP membranes and untreated controls.

2.4.2 The Effect of Pre-fouling on Gravity-driven, Batch Separation

In order to determine the quantitative improvement of HL/OP membranes in anti-fouling ability under heavy oil contact, 0.45 μm membranes (treated and untreated) were placed in the batch apparatus (see Figure 2.8). As *unfouled* controls, 20 mL of deionized water and 20 mL of dodecane (dyed red) were separated under gravity, with both the untreated (8 trials) and HL/OP (13 trials) membranes. More HL/OP membranes were tested in case of slight variations in the treatment process. The time for the 20 mL of water to permeate was recorded. For the oil-fouled trials, the membranes were exposed to 5 mL of dodecane for one minute, before adding 20 mL of deionized water and 15 mL of additional dodecane. One minute was short enough that the pre-fouling oil was just beginning to permeate through the untreated membrane. The same number of trials for each was performed as the control membranes. Figure 2.8d shows that a little oil passed through the untreated membrane before and during the separation process, but the HL/OP membrane allowed no oil through (Figure 2.8e). For the untreated membrane, the permeation time due to oil contact increased by 42 ± 13%, while the HL/OP membrane time only increased by 8 ± 15%, with 95% confidence intervals (Appendix Table A.3).

The prevention of oil permeation, and the negligible effect of the pre-fouling step on the

HL/OP membrane, shows the potential for fouling prevention with these membranes.
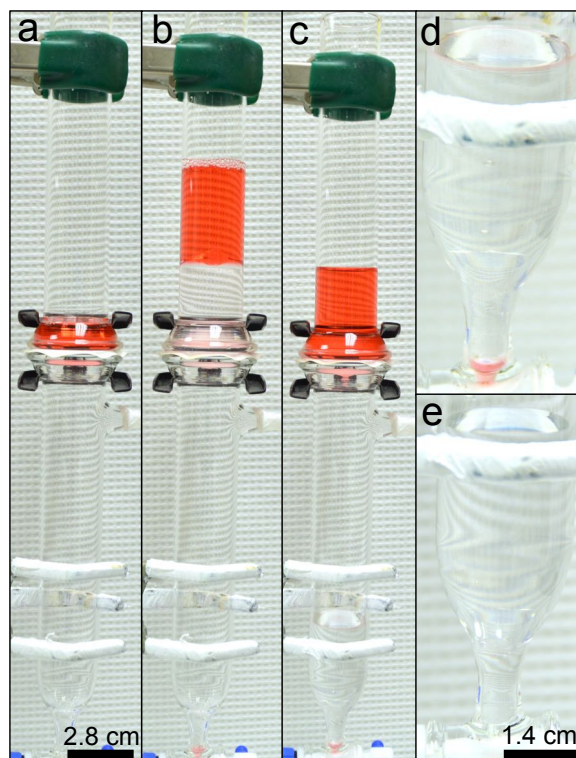
Figure 2.8: Effect of heavy *n*-dodecane pre-contact on 0.45 µm untreated versus HL/OP membrane performance with free dodecane and water. (a) 5 mL of dodecane (red) was added to each membrane for one minute. (b) A total volume of 20 mL of water and 20 mL of dodecane was added to each (untreated shown). (c) and (d) Completion of gravity separation with an untreated membrane shows some dodecane permeation and failure. (e) The HL/OP membrane did not allow any oil passage during the fouling or separation steps. Note that the permeation time was defined as the time when the last drop of water passed through the membrane (with no additional drops within one minute).

2.4.3 Batch Emulsion Separation

The separation performance with surfactant-stabilized, oil-in-water emulsions was

tested with the small-scale batch apparatus, before moving on to continuous systems. The

20 vol% dodecane-in-water emulsion preparation, using sodium dodecyl sulfate (SDS)

surfactant, is described in the Appendix A.3.2.1. This provided a range of droplet sizes

from tens of nm to over 800 nm (Figure 2.9c). An example separation is shown in Figures

2.9a-b where the HL/OP membrane is pre-fouled and the aqueous permeate is >99.9%

pure (Appendix Figure A.13). The separation was performed with 0.45 μm, 0.2 μm, and

10 nm pore-sized membranes, and the permeate from each was tested with dynamic light

scattering (DLS) to determine how effective the membranes were at demulsification

(Figures 2.9d-f). Only oil droplets smaller than the membrane pore-size permeated,
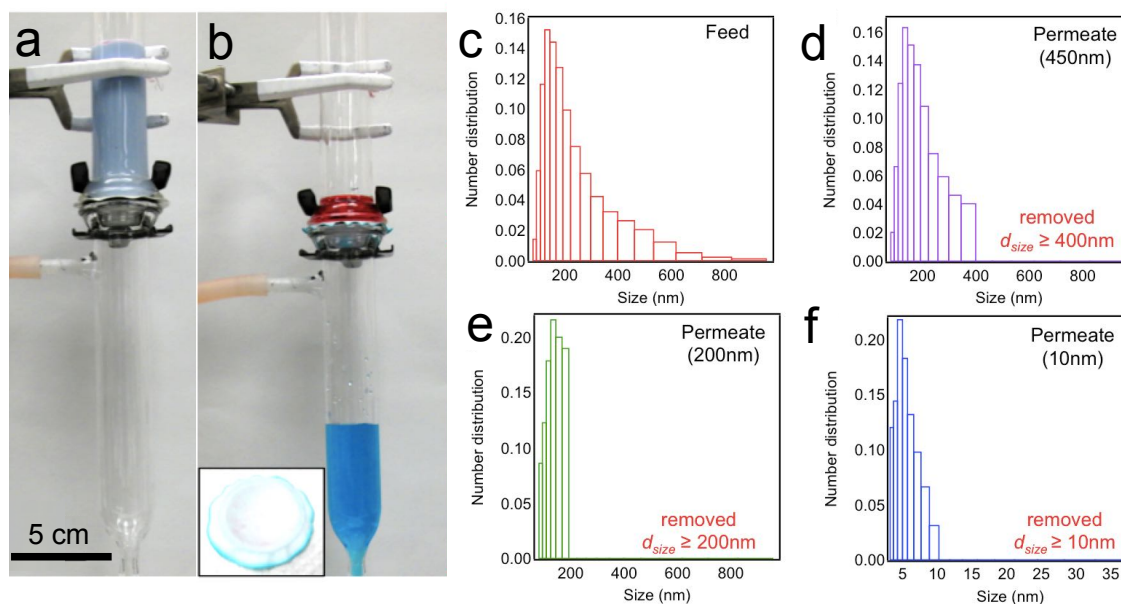
Figure 2.9: Emulsion separation with various pore sizes. (a) Separation apparatus with a 20:80 (v:v) dodecane-in-water emulsion (0.1 mg SDS mL^{-1} water) above the membrane. The 0.2 μm HL/OP membrane is pre-fouled by dodecane. Water is dyed blue and dodecane is dyed red. (b) The water-rich permeate passes through the membrane while the dodecane-rich retentate is retained above the membrane (DSC purity data is in Appendix A.3.4.2). (c) The number size distribution for the dodecane-in-water feed emulsion. (d), (e) and (f) The number size distributions for the permeates obtained from the separation of the dodecane-in-water feed emulsion using HL/OP membranes (not pre-fouled) with pore size = 0.45 μm, 0.2 μm, and 10 nm, respectively.

as expected, while the remainder was demulsified. Our HL/OP cellulose membranes

proved effective for the separation of surfactant-stabilized emulsions with a variety of

pore sizes. For industrial application, our membranes would need to show anti-fouling

ability for continuous flow equipment. Cross-flow equipment was tested because it is

commonly used and, as discussed earlier, its shear flow helps remove non-adhered foulants and prevent a cake layer.

2.4.4 Cross-flow, RC55 Sheet Membrane Emulsion Separation

Oil-in-water emulsion separation was chosen as a suitable process for testing our silanized cellulose sheet membranes in a continuous, cross-flow apparatus (Methods 2.2.3.2; Figure 2.10). The purification and anti-fouling abilities were assessed with
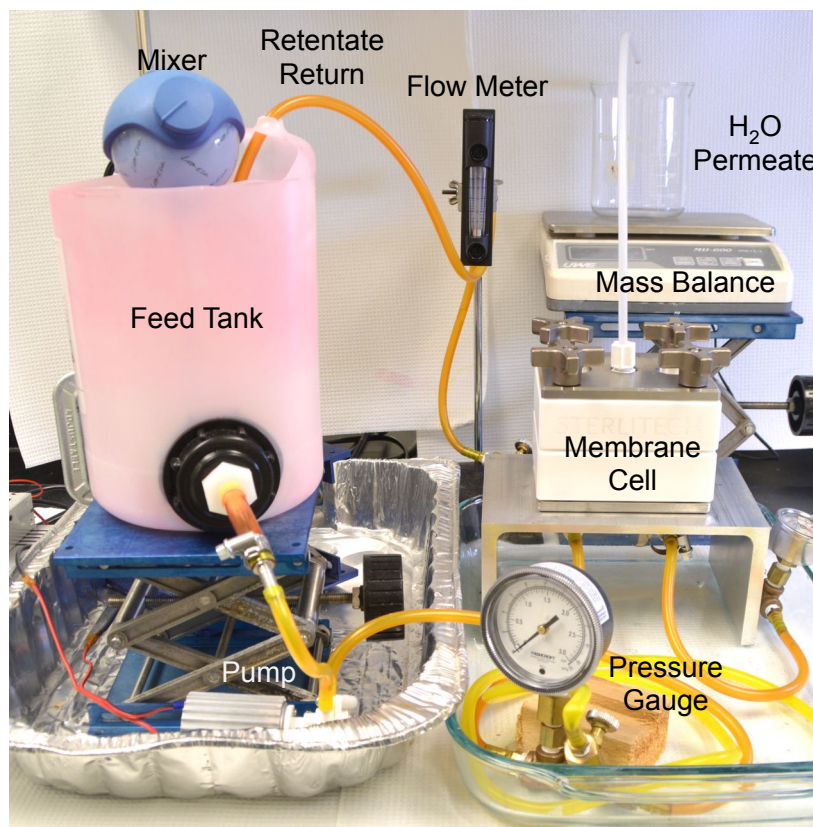
Figure 2.10: RC55 sheet membrane cross-flow equipment

a 20 vol% mixed isomer dodecane in water (surfactant concentration of 1 mg SDS mL^{-1} of water) over a 6 h operation, with a pure water flush every 2 h. The feed emulsion was characterized with DLS (Appendix Figure A.4), and 0.45 μm RC55 cellulose membranes were chosen to effectively treat the emulsion, whether as an untreated control or F_{17} silanized (SIH5841.2). The purified water permeate mass was measured over time to

quantify the degree of membrane fouling due to the oil. Untreated membranes, HL/OP membranes (40 min F_{17} functionalization), and under-functionalized (omniphilic) fluoro-membranes (10 min and 20 min F_{17} functionalization) were tested. It was discovered that the HL/OP membranes were not showing fouling resistance as expected, but were worse than the untreated controls by 18 ± 2 % (Figure 2.11). Prior work[50] indicates that excessive low energy material in membrane distillation surfaces has a negative impact on oil fouling resistance due to the increased hydrophobicity of the surface. The fluorinated
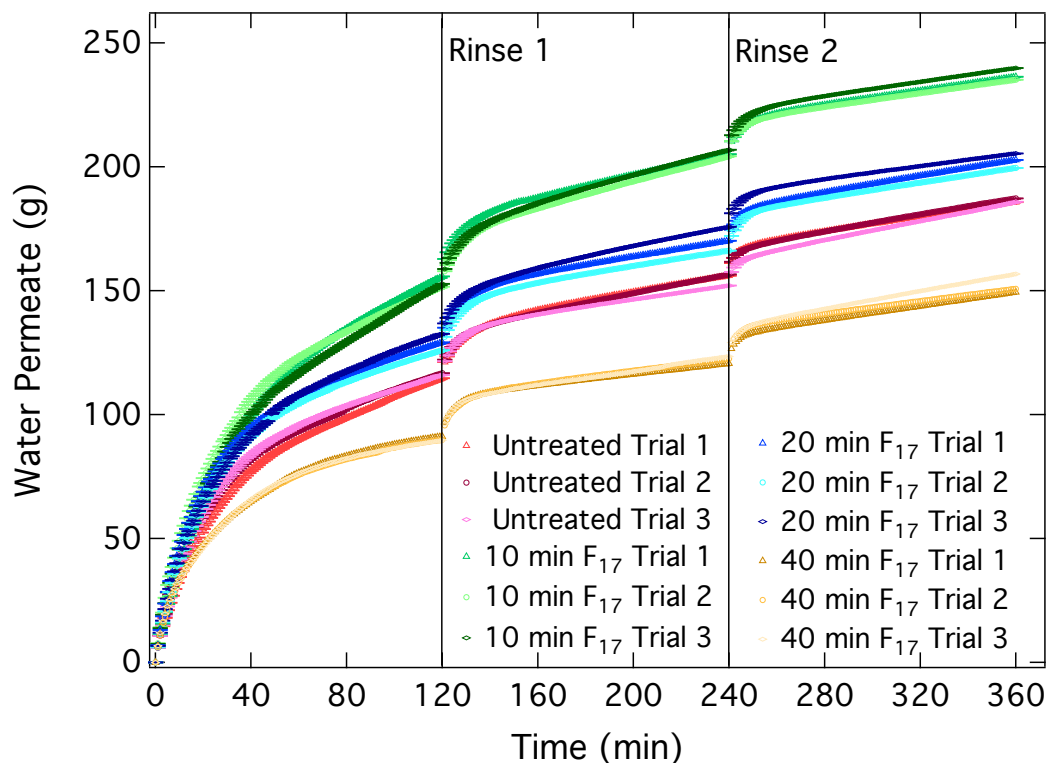
Figure 2.11: Cross-flow emulsion separation performance over extended time periods. The purified water permeate collected over 6 h, with pure water rinsing every 2 h, using 0.45 μm RC55 cellulose membranes (untreated and 10, 20, & 40 min F_{17} silane treated). The 10 and 20 min F_{17} treated membranes showed enhanced recovery, due to the anti-fouling property, over the untreated control, while the HL/OP (40 min) membrane performed poorly.

layer was too dense and the hydration layer was being compromised. Thus, in order to create a HL/OP-in-air membrane, the fluorinated layer was too dense and hampered oil-

in-water emulsion purification performance in cross-flow operation. The greatest increases in permeation over time were found with a 10 min F_{17} silane functionalization (Figure 2.11). This had significantly less surface fluorine content, according to XPS (Figure 2.12 and Appendix A.4), than the 20 min reaction. By adding the appropriate surface concentration of fluorosilane (10 min functionalization), increases in water permeation of $27 \pm 1\%$ were achieved over the control. The 20 min functionalization was increased by only $9 \pm 2\%$. The purified water is found to be >99.7% pure, for all cases, when compared to the original aqueous feed using DSC purity analysis, see Appendix
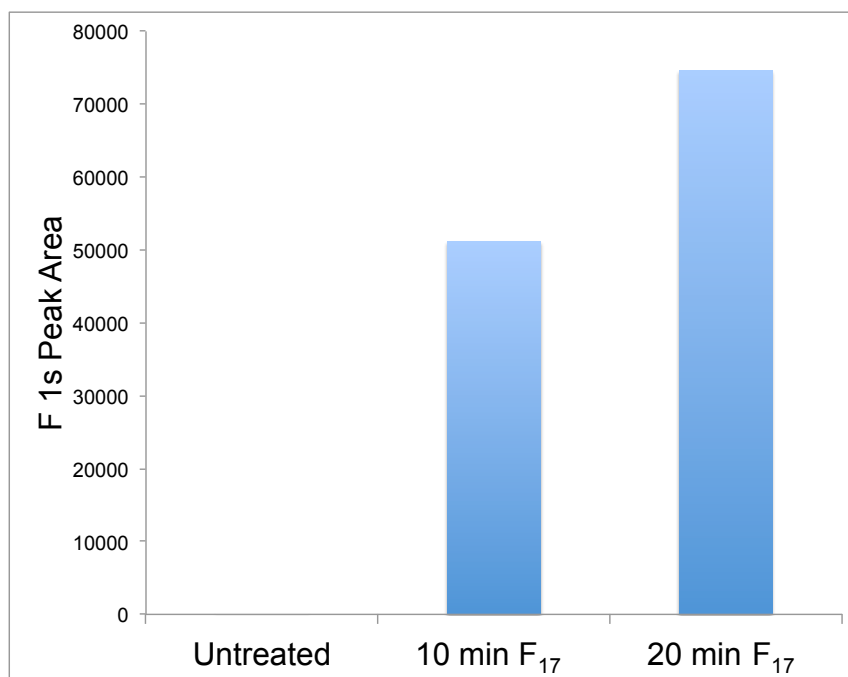
Figure 2.12: XPS F 1s peak areas for various levels of fluoro-silanization. The higher level of silane on the 20 min F_{17} membranes performed worse than 10 min F_{17}, but both showed enhanced performance over the untreated control.

A.3.4.3. In cross-flow conditions, permeation is better enhanced if less fluorosilane, than the amount required for HL/OP wetting in air, is used to ensure that the surface is not too hydrophobic. This allows a hydration layer to better form, while deterring oil adsorption and promoting oil droplet release in the cross-flow shear. With the appropriate surface

chemistry, a membrane can process more oil-in-water emulsion before an intensive cleaning or the end of its useful life.

2.4.5 Cross-flow, Ceramic Membrane Emulsion Separation

Ceramic membranes are very desirable due to their robustness, chemical resistance, and longer life spans.[51] With our anti-fouling methodology, we desired to further increase their useful life with silane modification. The substrate was a Veolia Ceramem® 5 nm silica UF membrane. It is a cross-flow membrane where the active separation layer is the thin, white silica layer (Figure 2.13c-e). In order to study the
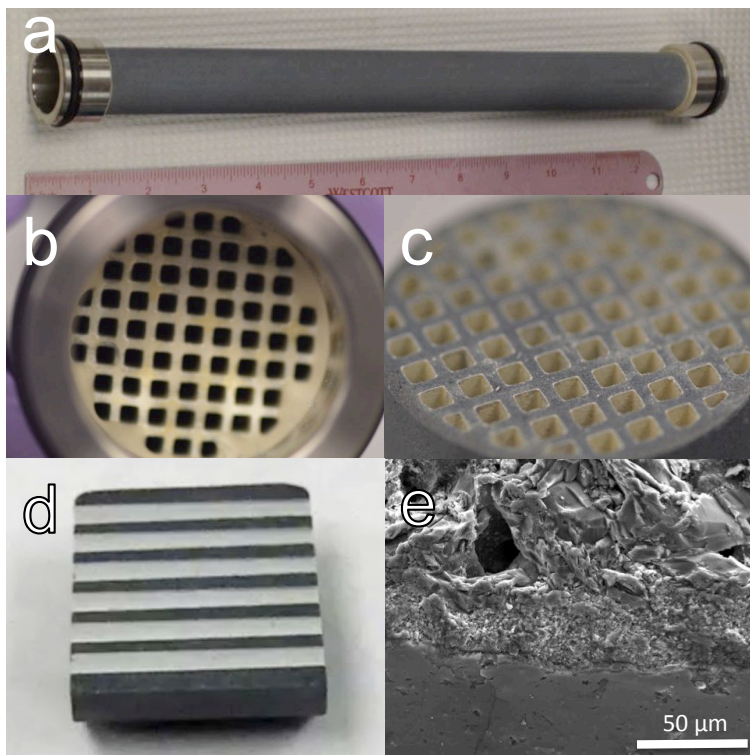
Figure 2.13: Ceramic membrane structure (a-b) Membrane size and channels. (c-d) The active, 5 nm pore sized layer, within the channels, is white and is shown in the cross section and halved membrane section. The support material is gray and has greater porosity, as shown by (e) the transition from the smooth, 5 nm pore sized layer to the support.

wettability of the active layer inside the channels, a membrane was cut into segments, which were then halved, with a diamond saw (Figure 2.13d). The untreated channels were omniphilic (Figure 2.14a-d), as expected, and testing with the F-silane (SIH5841.2) alone showed only a transition from HL/OL to HP/OL or HP/OP. We believe this is due
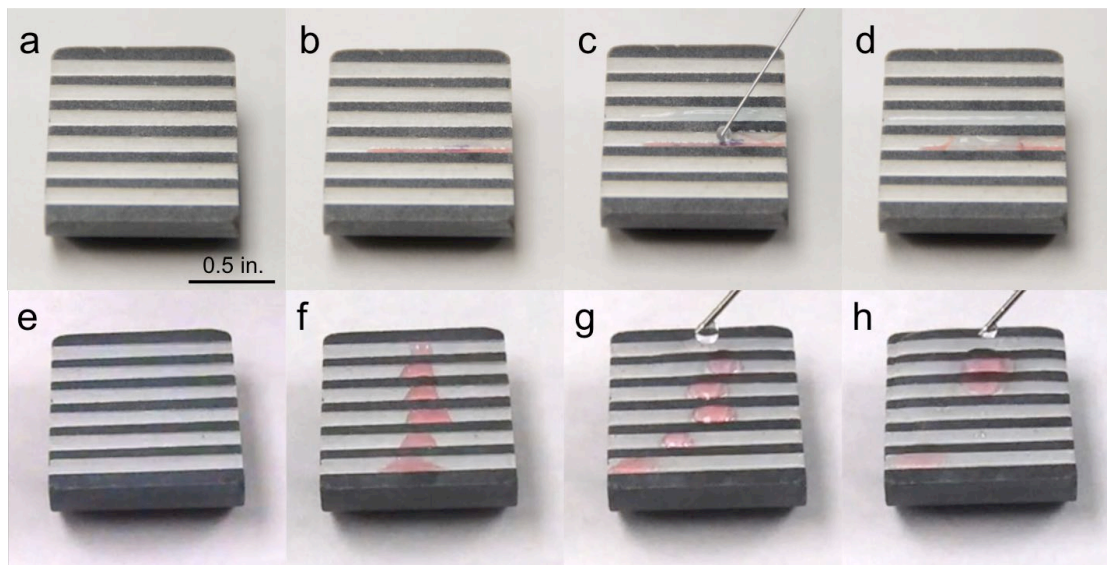
Figure 2.14: Untreated and silanized 5 nm silica UF membrane wetting properties. (a-d) A halved cross-section of the tubular cross-flow membrane shows that the white, silica channels are initially omniphilic. *n*-Dodecane (dyed red) and water both spread readily, and water cannot undercut and lift off the oil. (e-h) A halved cross-section of the silanized tubular cross-flow membrane shows that *n*-dodecane does not spread or absorb, while water can undercut the oil and remove it fully.

to the hydrophilic, ceramic substrate having only immobile, easily masked hydrophilic surface character. The f-POSS and x-PEGDA system[8] showed reconfiguration and the other HL polymers treated with F-silane were also non-rigid. A HL silane (SIM6492.66) was introduced and blended with the perfluorinated silane in dichloromethane for liquid-phase silanization. After trying several ratios of the two silanes in 1 vol% solutions, it was found that a 95 vol% HL silane to 5 vol% F-silane ratio yielded a channel where water spread and could undercut and lift off the repelled dodecane droplets (Figure 2.14e-h). This appeared to be HL/OP, but the channel contact angles could not be measured. Ratios lower than 95:5 were too hydrophobic and higher ratios allowed dodecane to absorb into the membrane surface. A full-sized ceramic module (Figure 2.13a) was treated as described in Methods 2.2.2.3.

The apparatus built for testing the membranes is shown in Figure 2.15c, and a

control membrane and coated membrane were tested with an oil-in-water emulsion specified by the U.S. Navy (see Appendix A.3.2.2 and Figure A.3) for over 520 hours. By comparing a membrane's permeate flux to its initial flux, I discovered that the coated membrane showed marked improvement over the control (Figure 2.15a). The control
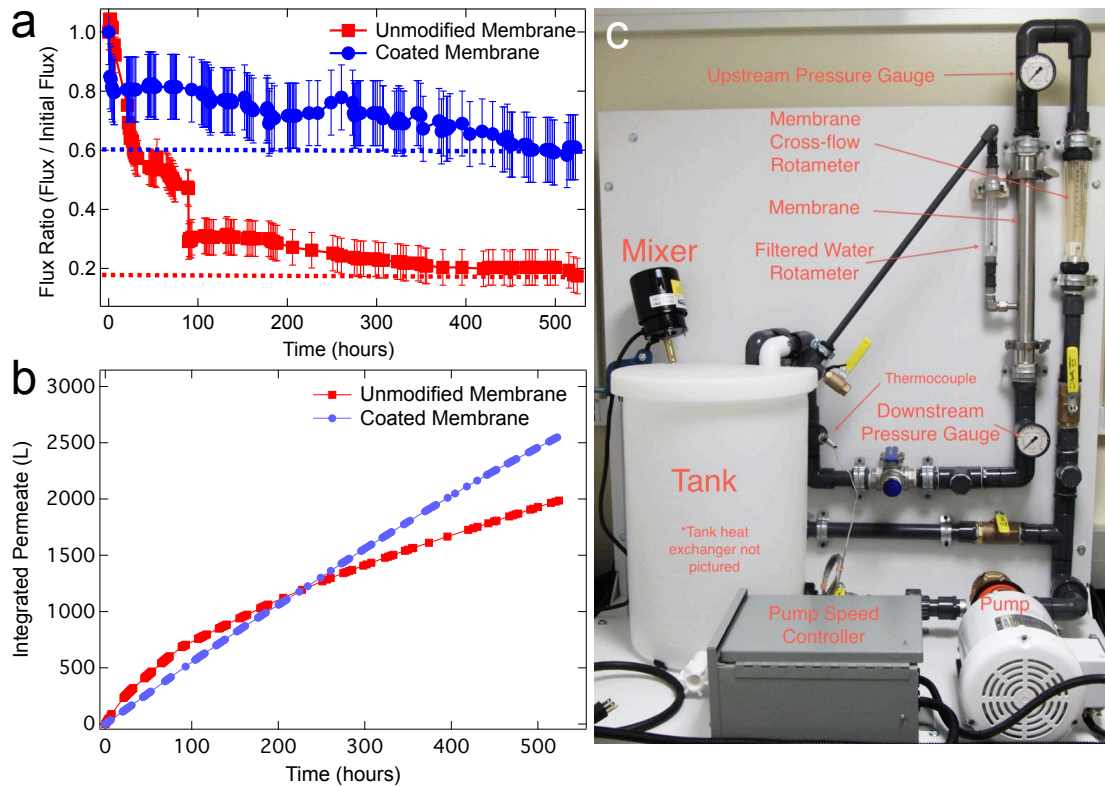
Figure 2.15: Untreated vs. Silanized Ceramic Membranes. (a) The anti-fouling property of the silanized 5 nm silica, cross-flow filtration membrane is shown during extended usage. The treated membrane shows more consistent water flux and resistance to fouling. The large decrease in the unmodified membrane at 89 h is due to an unexpected process shut down where the membrane dried out. This caused the oil contamination to adhere sooner than if the membrane had remained wet. (b) Total permeate collected, integrated from permeation rate data, by the coated membrane surpasses the untreated at about 225 h and continues to outperform. The initial flux of the treated membrane was lower than the untreated membrane, but this was shortly overcome due to fouling in the untreated membrane. (c). The testing apparatus for pumping the emulsion through the cross-flow membrane and measuring the permeate flow rate.

membrane decreased to 17% of its initial flux, while my modified membrane only decreased to 61% after 520 hours of operation. It should be noted that the initial flux of

the silanized membrane was not as high as the control membrane (113 mL/min versus 206 mL/min), but this was overcome in time due to the fouling in the untreated membrane. In Figure 2.15b, we see that the permeate collected over time by the treated membrane surpasses the untreated at about 225 h. At the end of the experiment, the treated membrane had collected 28% more permeate and would have continued to outperform at a permeation rate of 69 mL min^{-1} versus the control membrane's 36 mL min^{-1}. DSC showed that the permeate was >99.8% pure water, with either membrane (Appendix A.3.4.4). This experiment is directly comparable to an industrial application and shows that the principles learned from creating anti-fouling and HL/OP polymer membranes can be applied to other technologies, including ceramics, to extend the life of current membranes and decrease cleaning and replacement costs.

2.5 Conclusion

In conclusion, our methodology of treating membrane surfaces to have a blend of low energy perfluorosilane and hydrophilic components, whether from the substrate or silane, has allowed the creation of a variety of hydrophilic and oleophobic membranes, with many pores sizes. Silanes provide a durable bond that will not plug membrane pores, even 5-10 nm pores. Using polymers, metal, and ceramic, the membrane substrate and pore size can be optimized for a particular emulsion treatment application. The procedure is straightforward and uses commercially available components for more direct implementation. We demonstrated the utility of the HL/OP and partially fluorinated membranes for recovering water from surfactant-stabilized oil-in-water emulsions and preventing fouling due to oil adsorption. It was determined that HL/OP-in-air membranes prevent oil contamination (under heavy contact) and can have superior performance in

batch separation, but a lesser degree of fluorination may be necessary for enhanced performance in extended, continuous cross-flow operation with lesser oil content. Although, the seemingly HL/OP ceramic membrane showed definite enhancement. By maintaining water permeation rates significantly closer to initial flow rates, membranes can have longer service lives with less (and easier) cleaning, downtime, and replacement costs. We expect our anti-fouling methodology will allow energy-saving membrane technology to expand its use in the many industries treating oily wastewater.

2.6 References

1. UNICEF; WHO, Meeting the MDG Drinking Water and Sanitation Target: A Mid-Term Assessment of Progress. WHO/UNICEF 2004.

2. Shannon, M. A.; Bohn, P. W.; Elimelech, M.; Georgiadis, J. G.; Marinas, B. J.; Mayes, A. M., Science and technology for water purification in the coming decades. *Nature* **2008,** *452* (7185), 301-310. 10.1038/nature06599

3. Koltuniewicz, A. B.; Field, R. W.; Arnot, T. C., Cross-flow and dead-end microfiltration of oily-water emulsion. Part I: Experimental study and analysis of flux decline. *J. Membr. Sci.* **1995,** *102*, 193-207. 10.1016/0376-7388(94)00320-x

4. Arnot, T. C.; Field, R. W.; Koltuniewicz, A. B., Cross-flow and dead-end microfiltration of oily-water emulsions: Part II. Mechanisms and modelling of flux decline. *J. Membr. Sci.* **2000,** *169* (1), 1-15. 10.1016/S0376-7388(99)00321-X

5. Howarter, J. A.; Youngblood, J. P., Amphiphile grafted membranes for the separation of oil-in-water dispersions. *J. Colloid Interface Sci.* **2009,** *329* (1), 127-132. 10.1016/j.jcis.2008.09.068

6. Chen, W.; Su, Y.; Peng, J.; Zhao, X.; Jiang, Z.; Dong, Y.; Zhang, Y.; Liang, Y.; Liu, J., Efficient Wastewater Treatment by Membranes through Constructing Tunable Antifouling Membrane Surfaces. *Environ. Sci. Technol.* **2011,** *45* (15), 6545-6552. 10.1021/es200994n

7. Kajitvichyanukul, P.; Hung, Y.-T.; Wang, L. K., Membrane Technologies for Oil-Water Separation. In *Handbook of Environmental Engineering, Vol 13: Membrane and Desalination Technologies*, Wang, L. K.; Chen, J. P.; Hung, Y.-T.; Shammas, N. K., Eds. The Humana Press Inc., New York 2011.

8.   Kota, A. K.; Kwon, G.; Choi, W.; Mabry, J. M.; Tuteja, A., Hygro-responsive membranes for effective oil-water separation. *Nat. Commun.* **2012,** *3*, 1025. 10.1038/ncomms2027

9.   *Materials Research for Separations Technologies: Energy and Emission Reduction Opportunities*; Oak Ridge National Laboratory and BCS, Incorporated: 2005.

10.   Maartens, A.; Jacobs, E. P.; Swart, P., UF of pulp and paper effluent: membrane fouling-prevention and cleaning. *J. Membr. Sci.* **2002,** *209*, 81-92. 10.1016/S0376-7388(02)00266-1

11.   Howarter, J. A.; Genson, K. L.; Youngblood, J. P., Wetting Behavior of Oleophobic Polymer Coatings Synthesized from Fluorosurfactant-Macromers. *ACS Appl. Mater. Interfaces* **2011,** *3* (6), 2022-2030. 10.1021/am200255v

12.   Le-Clech, P.; Chen, V.; Fane, T. A. G., Fouling in membrane bioreactors used in wastewater treatment. *J. Membr. Sci.* **2006,** *284* (1–2), 17-53. 10.1016/j.memsci.2006.08.019

13.   Mueller, J.; Cen, Y.; Davis, R. H., Crossflow microfiltration of oily water. *J. Membr. Sci.* **1997,** *129* (2), 221-235. 10.1016/S0376-7388(96)00344-4

14.   Field, R., Fundamentals of Fouling. In *Membranes for Water Treatment*, Peinemann, K.-V.; Nunes, S. P., Eds. Wiley-VCH Verlag GmbH & Co. KGaA: Weinheim, 2010; pp 1-23.

15.   Bhattacharyya, D.; Jumawan, A. B.; Grieves, R. B.; Harris, L. R., Ultrafiltration Characteristics of Oil-Detergent-Water Systems: Membrane Fouling Mechanisms. *Sep. Sci. Technol.* **1979,** *14* (6), 529-549. 10.1080/01496397908068474

16.   Lee, S.; Aurelle, Y.; Roques, H., Concentration polarization, membrane fouling and cleaning in ultrafiltration of soluble oil. *J. Membr. Sci.* **1984,** *19* (1), 23-38. 10.1016/S0376-7388(00)80168-4

17.   Chakrabarty, B.; Ghoshal, A. K.; Purkait, M. K., Ultrafiltration of stable oil-in-water emulsion by polysulfone membrane. *J. Membr. Sci.* **2008,** *325* (1), 427-437. 10.1016/j.memsci.2008.08.007

18.   Winzeler, H. B.; Belfort, G., Enhanced performance for pressure-driven membrane processes: the argument for fluid instabilities. *J. Membr. Sci.* **1993,** *80* (1), 35-47. 10.1016/0376-7388(93)85130-O

19.   Li, H.-y.; Bertram, C. D.; Wiley, D. E., Mechanisms by which pulsatile flow affects cross-flow microfiltration. *AIChE J.* **1998,** *44* (9), 1950-1961. 10.1002/aic.690440903

20. Gupta, B. B.; Blanpain, P.; Jaffrin, M. Y., Permeate flux enhancement by pressure and flow pulsations in microfiltration with mineral membranes. *J. Membr. Sci.* **1992,** *70* (2), 257-266. http://dx.doi.org/10.1016/0376-7388(92)80111-V

21. Jönsson, A.-S., Influence of shear rate on the flux during ultrafiltration of colloidal substances. *J. Membr. Sci.* **1993,** *79* (1), 93-99. 10.1016/0376-7388(93)85020-W

22. Belfort, G.; Davis, R. H.; Zydney, A. L., The behavior of suspensions and macromolecular solutions in crossflow microfiltration. *J. Membr. Sci.* **1994,** *96* (1), 1-58. 10.1016/0376-7388(94)00119-7

23. Schrotter, J.-C.; Bozkaya-Schrotter, B., Current and Emerging Membrane Processes for Water Treatment. In *Membranes for Water Treatment*, Peinemann, K.-V.; Nunes, S. P., Eds. Wiley-VCH Verlag GmbH & Co. KGaA: Weinheim, 2010; pp 53-91.

24. Owens, E.; Patel, M., RO Cleaning Frequency: A Balance of Costs. *Water & Wastes Digest: Membrane Technology* 2010, pp 8-11.

25. Zhu, X.; Loo, H.-E.; Bai, R., A novel membrane showing both hydrophilic and oleophobic surface properties and its non-fouling performances for potential water treatment applications. *J. Membr. Sci.* **2013,** *436*, 47-56. 10.1016/j.memsci.2013.02.019

26. Liu, F.; Du, C.-H.; Zhu, B.-K.; Xu, Y.-Y., Surface immobilization of polymer brushes onto porous poly(vinylidene fluoride) membrane by electron beam to improve the hydrophilicity and fouling resistance. *Polymer* **2007,** *48* (10), 2910-2918. 10.1016/j.polymer.2007.03.033

27. Xue, Z.; Wang, S.; Lin, L.; Chen, L.; Liu, M.; Feng, L.; Jiang, L., A Novel Superhydrophilic and Underwater Superoleophobic Hydrogel-Coated Mesh for Oil/Water Separation. *Adv. Mater.* **2011,** *23*, 4270-4273. 10.1002/adma.201102616

28. Zhang, S. Y.; Lu, F.; Tao, L.; Liu, N.; Gao, C. R.; Feng, L.; Wei, Y., Bio-Inspired Anti-Oil-Fouling Chitosan-Coated Mesh for Oil/Water Separation Suitable for Broad pH Range and Hyper-Saline Environments. *ACS Appl. Mater. Interfaces* **2013,** *5* (22), 11971-11976. 10.1021/am403203q

29. Jing, B. X.; Wang, H. T.; Lin, K. Y.; McGinn, P. J.; Na, C. Z.; Zhu, Y. X., A facile method to functionalize engineering solid membrane supports for rapid and efficient oil-water separation. *Polymer* **2013,** *54* (21), 5771-5778. 10.1016/j.polymer.2013.08.030

30. Yang, H.-C.; Liao, K.-J.; Huang, H.; Wu, Q.-Y.; Wan, L.-S.; Xu, Z.-K., Mussel-inspired modification of a polymer membrane for ultra-high water permeability

and oil-in-water emulsion separation. *J. Mater. Chem. A* **2014,** *2*, 10225. 10.1039/c4ta00143e

31. Zhu, Y. Z.; Zhang, F.; Wang, D.; Pei, X. F.; Zhang, W. B.; Jin, J., A novel zwitterionic polyelectrolyte grafted PVDF membrane for thoroughly separating oil from water with ultrahigh efficiency. *J. Mater. Chem. A* **2013,** *1* (18), 5758-5765. 10.1039/c3ta01598j

32. Liu, Q. S.; Patel, A. A.; Liu, L. Y., Superhydrophilic and Underwater Superoleophobic Poly(sulfobetaine methacrylate)-Grafted Glass Fiber Filters for Oil-Water Separation. *ACS Appl. Mater. Interfaces* **2014,** *6* (12), 8996-9003. 10.1021/am502302g

33. Chen, Y. N.; Xue, Z. X.; Liu, N.; Lu, F.; Cao, Y. Z.; Sun, Z. X.; Feng, L., Fabrication of a silica gel coated quartz fiber mesh for oil-water separation under strong acidic and concentrated salt conditions. *RSC Adv.* **2014,** *4* (22), 11447-11450. 10.1039/c3ra46661b

34. Dong, Y.; Li, J.; Shi, L.; Wang, X. B.; Guo, Z. G.; Liu, W. M., Underwater superoleophobic graphene oxide coated meshes for the separation of oil and water. *Chem. Commun.* **2014,** *50* (42), 5586-5589. 10.1039/c4cc01408a

35. Chen, P. C.; Xu, Z. K., Mineral-Coated Polymer Membranes with Superhydrophilicity and Underwater Superoleophobicity for Effective Oil/Water Separation. *Sci. Rep.* **2013,** *3*, 2776. 10.1038/srep02776

36. Wen, Q.; Di, J. C.; Jiang, L.; Yu, J. H.; Xu, R. R., Zeolite-coated mesh film for efficient oil-water separation. *Chem. Sci.* **2013,** *4* (2), 591-595. 10.1039/c2sc21772d

37. Yang, J.; Zhang, Z. Z.; Xu, X. H.; Zhu, X. T.; Men, X. H.; Zhou, X. Y., Superhydrophilic-superoleophobic coatings. *J. Mater. Chem.* **2012,** *22* (7), 2834-2837. 10.1039/c2jm15987b

38. Brown, P. S.; Atkinson, O. D. L. A.; Badyal, J. P. S., Ultrafast Oleophobic–Hydrophilic Switching Surfaces for Antifogging, Self-Cleaning, and Oil–Water Separation. *ACS Appl. Mater. Interfaces* **2014,** *6* (10), 7504-7511. 10.1021/am500882y

39. Howarter, J. A.; Youngblood, J. P., Self-Cleaning and Anti-Fog Surfaces via Stimuli-Responsive Polymer Brushes. *Adv. Mater.* **2007,** *19* (22), 3838-3843. 10.1002/adma.200700156

40. Zhang, G.; Jiang, J.; Zhang, Q.; Gao, F.; Zhan, X.; Chen, F., Ultralow Oil-Fouling Heterogeneous Poly(ether sulfone) Ultrafiltration Membrane via Blending with Novel Amphiphilic Fluorinated Gradient Copolymers. *Langmuir* **2016,** *32* (5), 1380-1388. 10.1021/acs.langmuir.5b04044

41. Chen, W.; Su, Y.; Peng, J.; Dong, Y.; Zhao, X.; Jiang, Z., Engineering a Robust, Versatile Amphiphilic Membrane Surface Through Forced Surface Segregation for Ultralow Flux-Decline. *Adv. Funct. Mater.* **2011,** *21* (1), 191-198. 10.1002/adfm.201001384

42. Lampitt, R. A.; Crowther, J. M.; Badyal, J. P. S., Switching Liquid Repellent Surfaces. *J. Phys. Chem. B* **2000,** *104* (44), 10329-10331. 10.1021/jp002234a

43. Yoon, H.; Na, S. H.; Choi, J. Y.; Latthe, S. S.; Swihart, M. T.; Al-Deyab, S. S.; Yoon, S. S., Gravity-driven hybrid membrane for oleophobic-superhydrophilic oil-water separation and water purification by graphene. *Langmuir* **2014,** *30* (39), 11761-9. 10.1021/la5031526

44. Bellanger, H.; Darmanin, T.; Guittard, F., Surface Structuration (Micro and/or Nano) Governed by the Fluorinated Tail Lengths toward Superoleophobic Surfaces. *Langmuir* **2012,** *28* (1), 186-192. 10.1021/la2034356

45. Hansen, C. M., *Hansen Solubility Parameters: A User's Handbook*. 2nd ed.; CRC Press: Boca Raton, 2007.

46. Kwon, G.; Post, E.; Tuteja, A., Membranes with selective wettability for the separation of oil–water mixtures. *MRS Commun.* **2015,** *5* (3), 475-494. 10.1557/mrc.2015.61

47. Brown, P. S.; Bhushan, B., Durable superoleophobic polypropylene surfaces. *Philos. Trans. A Math Phys. Eng. Sci.* **2016,** *374* (2073). 10.1098/rsta.2016.0193

48. Batchelor, G. K., *An Introduction to Fluid Dynamics*. Cambridge University Press: New York, NY, 2000.

49. Naik, V. V.; Städler, R.; Spencer, N. D., Effect of Leaving Group on the Structures of Alkylsilane SAMs. *Langmuir* **2014,** *30* (49), 14824-14831. 10.1021/la503739j

50. Wang, Z.; Lin, S., The impact of low-surface-energy functional groups on oil fouling resistance in membrane distillation. *J. Membr. Sci.* **2017,** *527*, 68-77. 10.1016/j.memsci.2016.12.063

51. Dickhout, J. M.; Moreno, J.; Biesheuvel, P. M.; Boels, L.; Lammertink, R. G. H.; de Vos, W. M., Produced water treatment by membranes: A review from a colloidal perspective. *J. Colloid Interface Sci.* **2017,** *487*, 523-534. 10.1016/j.jcis.2016.10.013

CHAPTER 3

Continuous Liquid-Liquid Extraction and *In-situ* Membrane Separation of Miscible Liquid Mixtures

This chapter contains work adapted from an article, equally co-authored with Gibum Kwon, pending publication.

3.1 Introduction

Separation of miscible liquid mixtures is critical across a wide variety of manufacturing industries and accounts for about one quarter of all in-plant energy consumption in the United States.[1] Conventional separation operations require either thermal or chemical treatment, both of which have a large environmental impact and carbon footprint.[1] Consequently, there is a great need to develop sustainable, clean methodologies for separation of miscible liquid mixtures. The greatest opportunities to achieve this lie in replacing high-energy separation operations (e.g., distillation) with low-energy alternatives such as liquid-liquid extraction. One of the primary design challenges in liquid-liquid extraction is to maximize the interfacial area between two immiscible (e.g., polar and non-polar) liquids for efficient mass transfer. However, this often involves energy-intensive methods including ultrasonication[2-3], pumping the feed and the extractant through packed columns with high tortuosity[4], or using a supercritical fluid as an extractant.[5] Emulsifying the feed and the extractant[6-7], especially with a surfactant, offers a large interfacial area, but subsequent separation of emulsions can be

90

energy-intensive and less economical.[7-8] Thus, emulsions are typically avoided in conventional extraction operations.[9]

Herein, we discuss a novel, easily scalable, platform separation methodology termed CLEANS (Continuous Liquid-liquid Extraction And *iN-situ* membrane Separation). CLEANS integrates emulsion-enhanced extraction with continuous, gravity-driven, membrane-based separation of emulsions into a single unit operation. Our results demonstrate that the addition of a surfactant and emulsification significantly enhance extraction (by > 250% in certain cases), even for systems where the best extractants for miscible liquid mixtures are known. Utilizing the CLEANS methodology, we demonstrate continuous separation of a wide range of miscible liquid mixtures, including soluble organic molecules from oils, alcohols from esters, and even azeotropes.

Over 1,000 liquid-liquid extraction (LLE) systems are currently operating in the U.S. alone, with the recovery of pure ethanol from its aqueous azeotrope being one of the largest applications.[1] LLE systems are also prevalent in acetic acid, essential oil, and caprolactam recovery, as well as heat sensitive algae and fermentation broth purifications. Using LLE in bioethanol production can save ~ $0.35/gallon of fuel ethanol through acetic acid removal[10], which is a potential savings of $5.4 billion/yr, based on U.S. production capacity alone, from a single industrial LLE application.

After more than six decades of research and development, modifications to extraction columns, along with widespread implementation of industrial best practice programs, the liquid-liquid extraction unit operation is generally considered to have reached a mature state, with potential for only incremental improvements. Energy efficient separation of miscible liquids via extraction requires addressing two design

challenges: i) effective mixing between the feed (the liquid mixture from which a component is extracted) and the extractant to gain a large interfacial area for efficient mass transfer and ii) continuous separation of the extract (extractant with the preferentially extracted component of the feed) and raffinate (residual feed) phases.[11-12] This has led to various novel extraction methodologies[13] including the utilization of mixer-settler units, extraction columns, and centrifugal extractors. However, these methodologies still typically suffer from high-energy consumption or low extraction efficiency.[12, 14] Alternatively, for improved energy efficiency, membrane separation has been integrated with LLE. However, the efficiency of such systems has been relatively low either due to the necessity of having to separate emulsions in multiple steps after LLE[15-16] or the need to employ energy intensive cross-flow filtration for demulsification.[17] The ideal liquid-liquid extraction operation would enable emulsification within the extraction column for maximizing mass transport between the feed and the extractant, followed by rapid demulsification, with minimal or no external energy input, before recovering the extract and raffinate phases.

3.2 Materials and Methods

3.2.1 Materials

Cellulose-based filters (nominal pore sizes of 25 μm and 2.5 μm) and clean room wipes were obtained from Whatman and Contec, respectively. (Heptadecafluoro-1,1,2,2-tetrahydrodecyl) triethoxysilane and *n*-octadecyltrichlorosilane were obtained from Gelest. N,N-dimethylformamide (DMF), hydrochloric acid, methanol, ethanol, toluene, Methylene Blue, Oil Red O, and sodium dodecyl sulfate (SDS) were obtained from Fisher Scientific. Heptane and sodium hydroxide were purchased from J.T. Baker.

Hexadecane was obtained from Alfa Aesar. 1-Octanol was from Acros Organics. Dodecane, *n*-butanol, *n*-hexanol, Disperse Red 1, methyl oleate, benzothiophene, 2-methyl-2-propanethiol (*t*-butyl thiol) and poly(methyl methacrylate) (PMMA) were obtained from Sigma Aldrich. Asahiklin AK-225 was obtained from Structure Probe, Inc.

3.2.2 Membrane Fabrication

3.2.2.1 Stimuli-Responsive Membranes (HL/OP)

Cellulose-based filters or Contec wipes were treated with 30 W oxygen plasma for 5 min and subsequently exposed to vapor phase (heptadecafluoro-1,1,2,2-tetrahydrodecyl) triethoxysilane for 20 h at room temperature (22°C).

3.2.2.2 Hydrophobic and oleophilic membranes (HP/OL)

3.2.2.2.1 Used for the Extraction of Disperse Red 1, Sulfur Compounds, & Methanol

A solution (2.5 mg mL^{-1}) of *n*-octadecyltrichlorosilane was prepared in toluene. Cellulose-based filters (nominal pore size of 25 μm) were dip coated in the solution for 30 min and dried with nitrogen gas at room temperature (22°C) for 5 min. Dip-coated filter papers were then baked at 70°C for 2 h, followed by a thorough ethanol rinse. These HP/OL membranes allow dodecane or methyl oleate to permeate through while preventing permeation of DMF or water.

3.2.2.2.2 Used for the Extraction of Ethanol

A solution (10 mg ml^{-1}) of poly(methylmethacrylate) (PMMA) was prepared in Asahiklin AK-225. Cellulose-based filters (nominal pore size of 25 μm) were dip coated in the solution for 30 min and dried with nitrogen gas at room temperature (22°C) for 5 min. These membranes allow heptane to permeate through while preventing water permeation.

3.2.3 Membrane Characterization

3.2.3.1 Contact Angle Measurements

All contact angle measurements were conducted with a Ramé–Hart 200-F1 goniometer by advancing and receding a small volume of liquid (≈ 2 μL) on the surface, using a 2 mL micrometer syringe (Gilmont). At least three measurements were performed on each substrate and the typical error in the measurements was ± 2°.

3.2.3.2 Microscopy

The surface morphology of the membranes was characterized using a Hitachi SU8000 scanning electron microscope (SEM) at 2 kV. Optical microscopy of emulsions was conducted with an Olympus BH-2 optical microscope.

3.2.3.3 Breakthrough Pressure Test

Membrane samples were installed in a glass apparatus with a 25 cm glass tube (7.75 mm ID) above the membrane. Dodecane was added above the membrane with a KD Scientific syringe pump at a rate of 2 mL min^{-1} until 25 cm was reached or a drop of dodecane passed through the membrane (failure). The dodecane column height at failure was recorded.

3.2.4 Extraction Equipment

3.2.4.1 Batch Extraction Apparatus: Dye Removal

The batch separation apparatus consists of two vertical glass tubes with a stimuli-responsive membrane (nominal pore size of 2.5 μm) sandwiched between them (see Figure 3.7a). A 50:50 dodecane:DMF volume ratio emulsion was added to the upper tube to be gravity separated. The dodecane droplet number size distributions indicated that the greatest fractions were in the range of 1 - 20 μm and 100 - 300 nm (see Appendix B.1).

3.2.4.2 CLEANS Apparatus

The continuous separation apparatus consists of a chamber where the feed and the extractant, with or without dissolved SDS surfactant, are continuously fed using syringe pumps. SDS was chosen as the surfactant in the tested systems because it is immiscible with the desired pure phases. We adopted a gravity-driven countercurrent flow, with the lower density liquid fed from the bottom of the chamber, and the higher density liquid fed from the top. The feed and extractant are emulsified *in-situ* in the chamber by a mechanical stirrer. The chamber is equipped with two membranes operating in parallel – a stimuli-responsive membrane at the bottom and a hydrophobic and oleophilic (HP/OL) membrane on the sidewall (Figure 3.7c).

3.2.5 Quantifying Extraction Performance

3.2.5.1 Refractive Index Measurements

Refractive index measurements were conducted using a Reichert r^2i300 refractometer. A few drops of liquid sample ($\approx$ 300 μL) were applied and at least five measurements were performed. All measurements occurred at room temperature (22 ± 0.1°C) and the typical error in measurements was ± 0.0002.

3.2.5.2 UV-Vis Spectroscopy

The dye (Disperse Red 1) or benzothiophene content in the dodecane-rich phase after separations was measured using a Cary 50 Bio Ultraviolet-Visible spectrophotometer.

3.2.5.3 Aspen Plus V8.8 Simulation Software

The simulation of the one-stage, CLEANS apparatus was performed using a decanter block at 25°C and 1 atm. The feed and extractant, for the various systems, were

fed into the decanter to reach thermodynamic equilibrium at volumetric flow ratios of 90:10 to 50:50 (feed:extractant). The property method was chosen based on the chemical system and the correlation to experimental data. UNIFAC was used for the methanol, methyl oleate, and water system. NRTL was used for the ethanol, heptane, and water system. UNIF-LL was used for the benzothiophene, dodecane, and DMF system.

3.3 Stimuli-Responsive Membranes and Characterization

3.3.1 Development and Wetting

To engineer one of the first methodologies capable of such extraction, we first developed novel, stimuli-responsive membranes that dramatically alter their wettability when contacting polar liquids, but show no change when contacting non-polar liquids
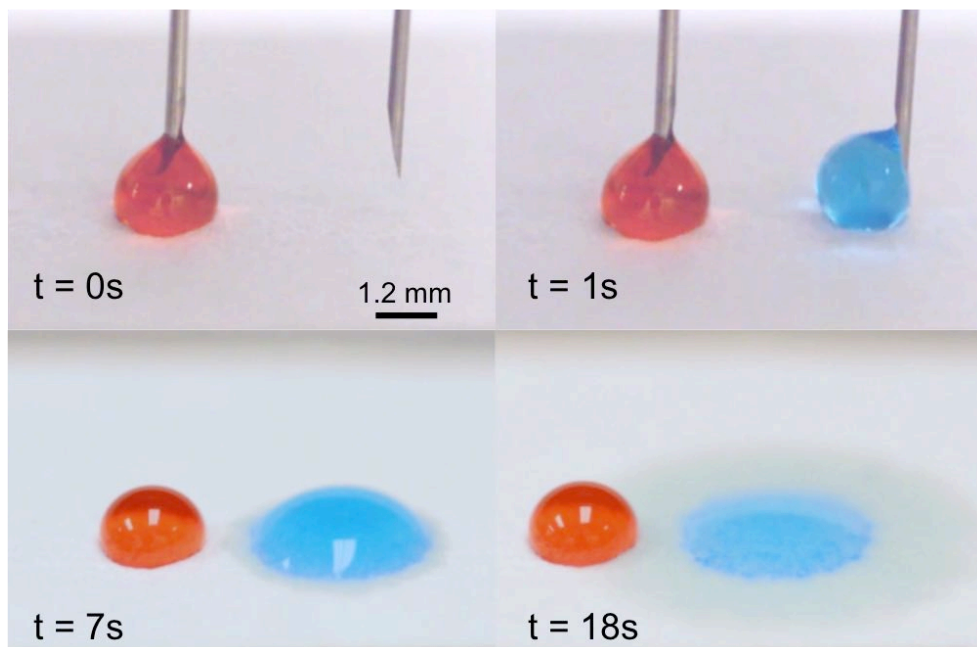
Figure 3.1: The stimuli-responsive nature of these hydrophilic/oleophobic membranes (2.5 μm) is shown by the nearly simultaneous addition of dodecane (dyed red) and water (dyed blue) droplets. Upon contact, water's polar interactions allow it to pass through the membrane, while dodecane is excluded. By adding dodecane first, the oil repellency in air is shown as well as underwater, as the water droplet can preferentially undercut the oil droplet.

(see Figure 3.1). We fabricated the membranes by controlled vapor-phase silanization of different cellulose-based porous substrates with a perfluorinated silane (see Methods 3.2.2.1 for the original silanization approach before the improved procedure discussed in Chapter 2), which creates a thin layer of covalently bonded silane on the membrane surface.[18-19] Consequently, the membrane's surface is robustly and homogeneously coated without clogging the filter pores. Scanning Electron Microscopy (SEM) images (Figure 3.2) clearly show that surface morphologies are unaffected by the coating.
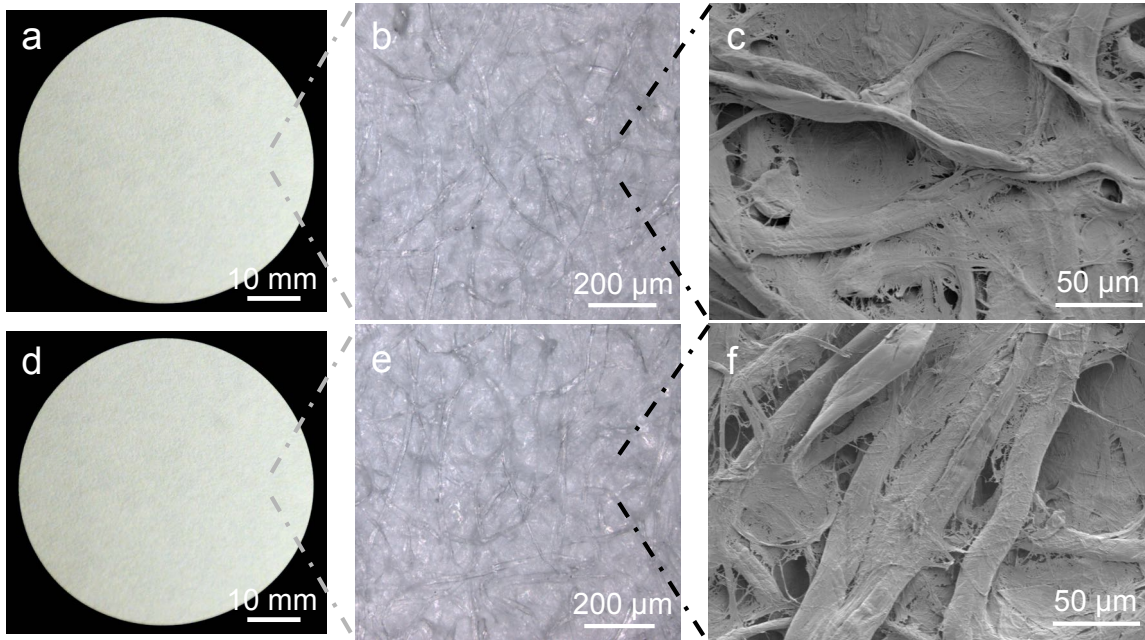
Figure 3.2: (a - c) Neat cellulose filter (nominal pore size of 2.5 μm) images at varying degrees of magnification, using optical and scanning electron microscopes. (d - f) Optical and SEM images of cellulose filters, with the same nominal pore size, after silane vapor treatment. Surface morphologies are unaffected by the silane treatment, unlike polymer coatings which could fill in the surface structures.

When a non-polar liquid droplet contacts the membranes, it cannot permeate through and displays a high apparent contact angle θ^* (i.e. contact angle on a textured surface, Figures 3.3a and b). For example, the advancing apparent contact angles for hexadecane and dodecane are $\theta^*_{hexadecane,adv} = 126°$ and $\theta^*_{dodecane,adv} = 113°$, respectively, on a membrane

fabricated using a 2.5 μm nominal pore size, cellulose filter. This is due to a combination

of the re-entrant texture of the membranes (insets in Figures 3.3a, b) and the low surface

energy of the perfluorinated groups on the surface.[20-21] In contrast, when a polar liquid

droplet contacts the membranes, it completely wets the surface and permeates through.

This is a direct consequence of hydrogen bonding and dipole-dipole interactions between

the polar liquid and the cellulose-based membrane surface.[21-24] Due to this preferential

wetting of polar liquids, counter-intuitively, a higher surface tension liquid like DMF (γ_{LV}

= 37.1 mN/m) wets the membrane surface, while a lower surface tension non-polar

liquid, dodecane (γ_{LV} = 25.3 mN/m), beads up (Figures 3.3a, b).
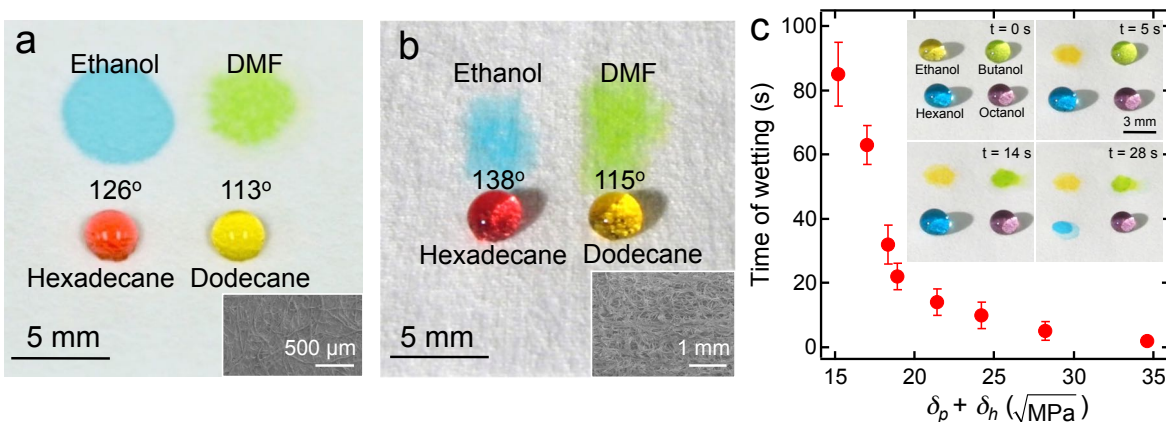
Figure 3.3: Selective wetting of polar liquids and non-polar liquids. (a) and (b) Droplets of ethanol (dyed blue), DMF (dyed light green), hexadecane (dyed red) and dodecane (dyed yellow) on the stimuli-responsive surfaces fabricated using a cellulose-based filter (nominal pore size of 2.5 μm) and a cellulose – polyester blend based Contec wipe, respectively. Insets show morphologies of the respective filter and wipe surfaces. (c) Time of wetting for a series of alcohols on the membrane shown in (a). Insets show sequential wetting of four alcohol droplets in the order of decreasing Hansen Polar and Hydrogen bonding parameters (δ_p+δ_h). The error bars denote standard deviation.

We also measured the time of wetting for a homologous series of alcohols with a

range of polar (δ_p) and hydrogen bonding (δ_h) Hansen solubility parameters on our

membranes (Figure 3.3c). Here, we define the time of wetting as the time required for a

liquid droplet to imbibe into the membrane. The data show that the more polar the liquid,

as indicated by higher values of δ_p and δ_h, the more readily it wets and permeates through the membrane solely under gravity. In contrast, non-polar liquids remain above the membrane with high apparent contact angles that do not change with time.

3.3.2 Stimuli-Responsive Membrane Durability

The silanized membranes displayed exceptional chemical and mechanical resistance, as demonstrated by consistent oil contact angles and breakthrough pressure. The resistance of our membranes against harsh chemical environments was tested through immersion in acids or bases for 24 hours, followed by thorough rinsing and drying. To evaluate the chemical resistance, we measured the contact angles with dodecane, a low surface tension liquid (γ_{LV} = 25.3 mN/m). Figure 3.4a shows the advancing contact angles for dodecane on the membranes after acid (hydrochloric acid, pH = 4) or base (sodium hydroxide, pH = 10) treatment. We found that our membranes still display high contact angles for dodecane ($\theta^*_{dodecane,adv}$ = 111° and $\theta^*_{dodecane,adv}$ = 110° after acid and base treatments, respectively) even after 24 hours of chemical exposure. This clearly indicates that the silane is not being cleaved from the surface and our membranes are highly resistant against chemical damage.

The mechanical durability of our membranes was tested using a linear abraser, Taber® Industries 5750. The membranes (nominal pore size of 2.5 μm) were mechanically abraded with CS-5 abradant (using a mass of 300 g at 60 cycles per minute) for up to 5,000 abrasion cycles. The breakthrough pressure of dodecane (i.e., the pressure required for dodecane to permeate through the membrane, Methods 3.2.3.3) was measured after the abrasion tests and found that it was almost constant ($P_{breakthrough}$ =
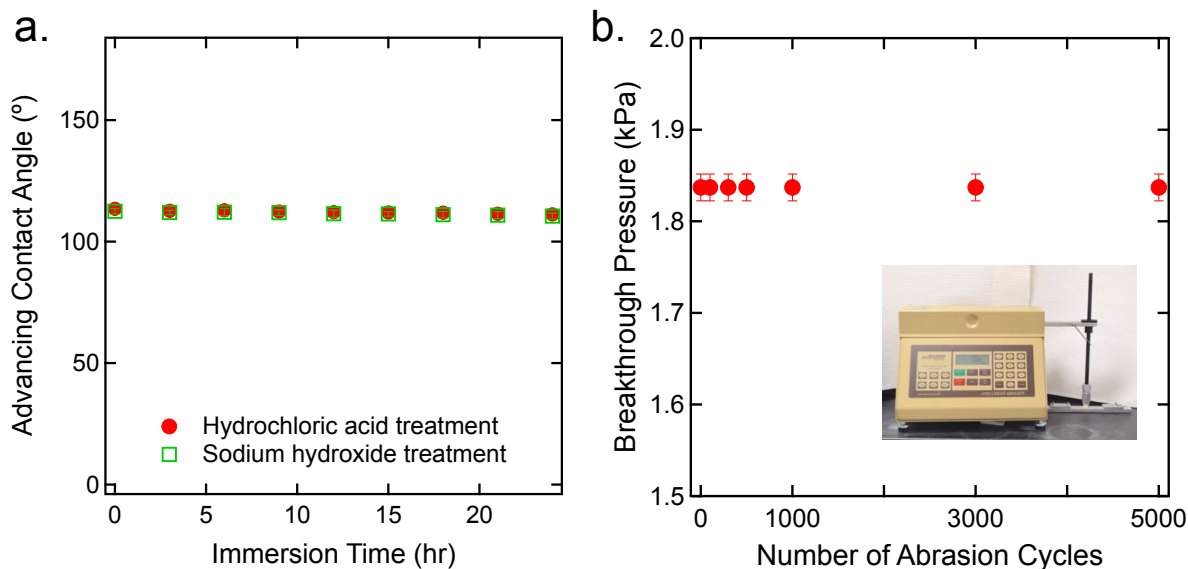
Figure 3.4: Membrane durability testing. (a) A plot of advancing contact angles for dodecane on membranes after immersion in hydrochloric acid (pH = 4) or in basic (pH = 10) solutions with varying immersion time. (b) A plot of breakthrough pressures for dodecane on membranes as a function of the number of abrasion cycles (inset shows the linear abraser).

1,840 Pa), for up to 5,000 cycles of abrasion (Figure 3.4b), indicating that the chemical modification of our membranes is mechanically robust.

3.4 Immiscible Liquid Separation

These stimuli-responsive membranes are capable of separating a range of immiscible liquid mixtures comprising a non-polar and a polar phase simply under gravity due to the density difference between the two immiscible phases, including free oil-water.

3.4.1 Non-emulsified Batch Separation

Figures 3.5a and b show the batch separation of a 50:50 (v:v) methanol (polar, dyed blue) and hexadecane (non-polar, dyed red) mixture. Our 2.5 μm membrane was sandwiched between the glass tubes, and the methanol-hexadecane mixture was added to the upper glass tube. After a few minutes, the methanol-rich phase permeated through the
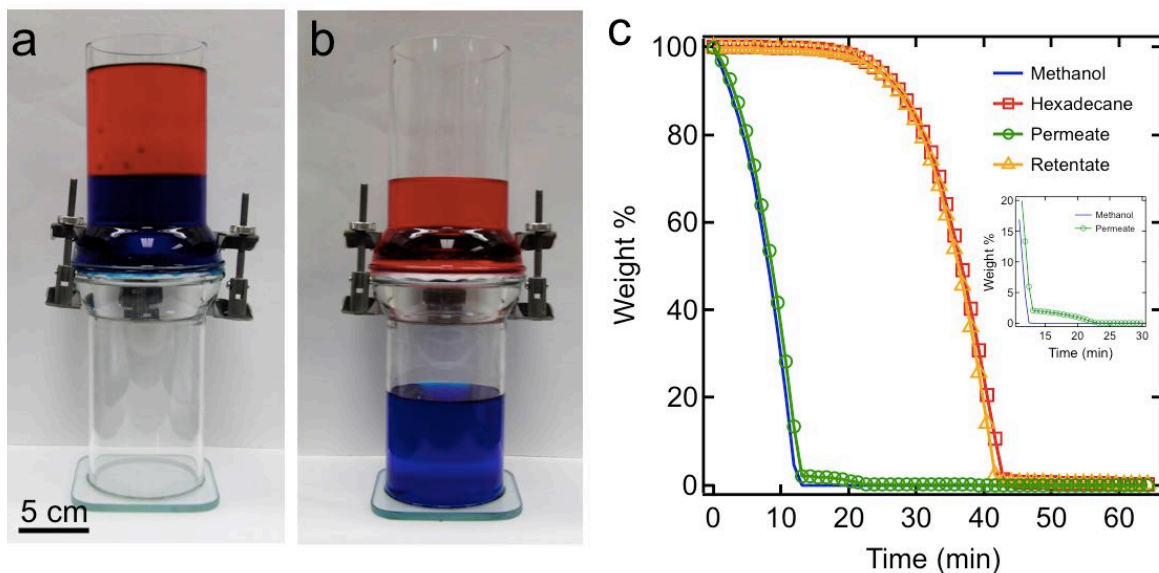
Figure 3.5: (a) A batch separation apparatus with a 50:50 (v:v) methanol-hexadecane mixture above the membrane. (b) Methanol-rich permeate (blue) passed through the membrane, while the hexadecane-rich phase (red) was retained. (c) TGA data for the methanol-rich permeate and hexadecane-rich retentate, with as obtained methanol and hexadecane data shown for comparison. The inset shows that the methanol-rich permeate contains ≈ 2 wt% hexadecane.

membrane whereas the hexadecane-rich retentate remained above the membrane (Figure 3.5b). After separation, the compositions of the methanol-rich permeate and hexadecane-rich retentate were measured using thermogravimetric analysis (TGA). Approximately 60 mg samples were heated from room temperature to 300°C for 40 min. Note that the boiling point of hexadecane is 287°C. The weight loss of the hexadecane-rich phase was compared to that of the as-obtained hexadecane to estimate the purity of the hexadecane-rich phase. Similarly, the weight loss of the methanol-rich phase was compared to that of the as-obtained methanol to estimate the purity of the methanol-rich phase. TGA data indicated that the methanol-rich permeate contained ≈ 2 wt% hexadecane, while hexadecane-rich retentate contained ≈ 0.1 wt% methanol (Figure 3.5c). These values are close to the mutual solubilities for methanol and hexadecane reported in literature.[25] Note that the TGA detection accuracy is 0.1 wt%.

3.4.2 Emulsified Batch Separation

Surprisingly, the fabricated stimuli-responsive membranes could also demulsify different emulsions (Figure 3.7a) without any external energy source, except for gravity. This again included oil-water emulsions (Figure 3.6), making this process one of the most energy efficient processes for oil-water separation.[26] Energy efficient separation of oil-water emulsions is critical for clean up of oil-spills, wastewater treatment, and fuel purification, amongst many other applications.[27-29]

To demonstrate the applicability of our membranes in oil-water separation, 500 mL of emulsion was formed by stirring 30 vol% dodecane (dyed with Sudan 1) and 70 vol% water (dyed with purple McCormick® food dye) with 0.1 mg sodium dodecyl sulfate (SDS)/mL water (see Figure 3.6a). The membrane demulsified the mixture under gravity (Figure 3.6b), and the permeate and retentate phases were tested for purity. Thermogravimetric analysis (TA Instruments Q5000IR) was used for the individual feed
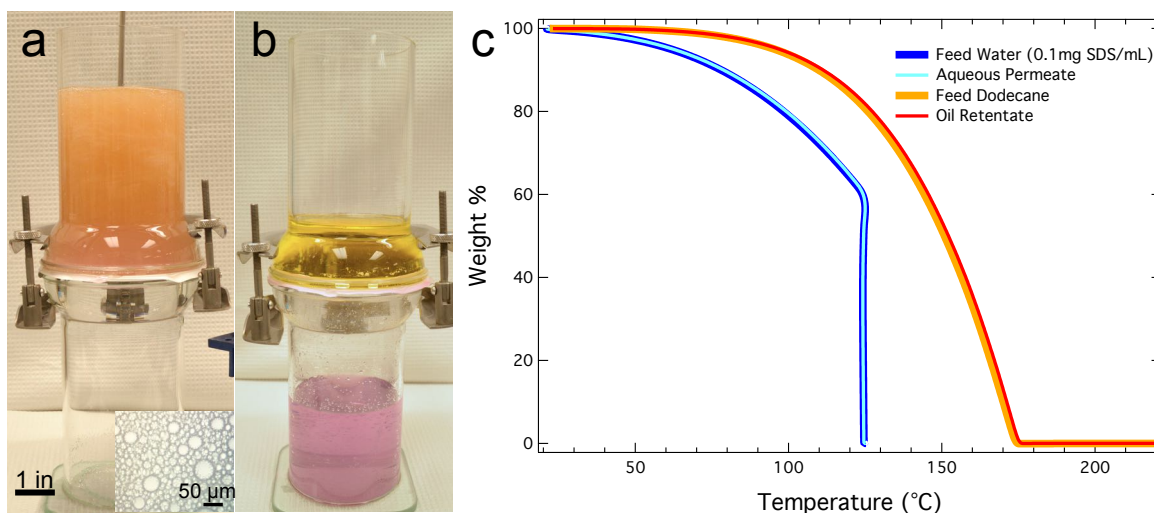
Figure 3.6: (a) and (b) Separation of a 30 vol% dodecane (dyed with Sudan 1) and 70 vol% water (dyed with purple food dye and 0.1 mg SDS/mL water) emulsion using the HL/OP stimuli-responsive membrane. Inset shows the emulsion droplet distribution. (c) Thermogravimetric analysis results for the individual feed components and the demulsified phases, showing that the permeate and retentate are > 99.9% pure.

components and the demulsified phases. Samples were heated at 25°C/min to 125°C for aqueous phases and 220°C for oil phases, and then held for 10 min at the final temperature. This showed that the permeate and retentate are > 99.9% pure, compared to the original feed components.

3.5 Miscible Liquid Component Extraction

Next, we studied the utility of these membranes for the separation of miscible liquids using liquid-liquid extraction. To conduct our extraction experiments, we first emulsified the feed with an immiscible liquid extractant using a surfactant. Typically the surfactant is chosen such that it has a very high solubility in the extractant, and negligible solubility in the raffinate. Emulsification ensures a large interfacial area from the small droplets, and shorter diffusion lengths between the feed and the extractant, thereby significantly enhancing the extraction efficiency.[30] Subsequently, we leverage the selective wettability of our stimuli-responsive membranes for solely gravity-driven separation of the immiscible raffinate and extract phases.

3.5.1 Batch Extraction of Dye

As an example, we first demonstrate a batch extraction of an oil-soluble dye, Disperse Red 1, from dodecane using dimethylformamide (DMF) as an extractant, and sodium dodecyl sulfate (SDS has negligible solubility in dodecane) as the surfactant. Dodecane containing dye (30 ppm) and DMF with dissolved SDS (1 mg mL^{-1}) were emulsified. The dodecane droplet number size distributions indicated that the greatest fractions were in the range of 1 - 20 μm and 100 - 300 nm (see Appendix B.1). Within a few minutes of adding the emulsion to a separation apparatus with a stimuli-
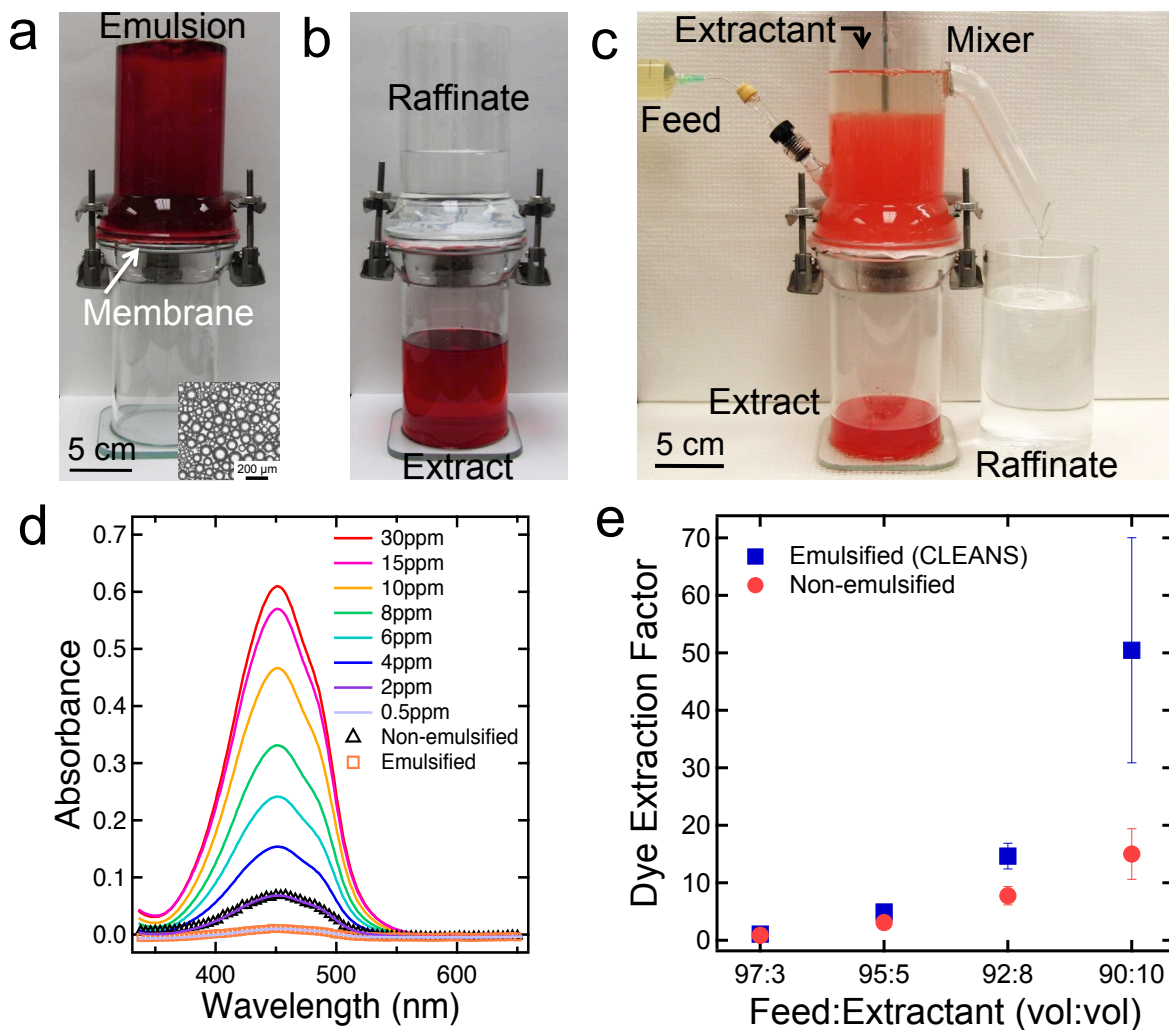
Figure 3.7: Disperse Red 1 dye extractions using a batch separation apparatus and CLEANS methodology. (a) A batch separation apparatus with SDS-stabilized, 50:50 vol:vol dodecane-in-DMF emulsion above the stimuli-responsive membrane. (b) The dye-enriched DMF phase permeates through the membrane, while the dye-depleted dodecane phase is retained. (c) An apparatus used for CLEANS methodology. The dye-enriched DMF phase continuously passes through the stimuli-responsive membrane at the bottom, while the dye-depleted dodecane phase passes through the HP/OL membrane on the sidewall. (d) UV-Vis absorbance data for the dodecane phases obtained from the CLEANS methodology using a 90:10 feed:extractant volumetric flow ratio. For comparison, UV-Vis absorbance data for various dye concentrations and the non-emulsified control (no surfactant) are also provided. (e) Dye extraction factors from separations using various feed:extractant volumetric flow ratios, with and without the CLEANS methodology. The error bars denote standard deviation.

responsive membrane sandwiched between glass tubes (see Figure 3.7a), the dye-enriched, polar DMF phase permeated through the membrane solely under gravity while the dye-depleted, non-polar dodecane phase was retained above the membrane (Figure 3.7b). After separation, the dodecane phase was almost completely transparent, indicating efficient dye extraction.

3.5.2 Continuous Extraction: "CLEANS"

In the batch separation described above, the extraction of dye using a surfactant-stabilized emulsion and the membrane separation of these emulsions are two separate unit operations. Additionally, in batch separation, as more emulsion is added, the dodecane phase will continue to accumulate above the membrane and eventually permeate through the membrane if the hydrostatic pressure is sufficiently high. In order to overcome these shortcomings and make the separation methodology scalable, we developed a continuous separation methodology that integrates emulsion-enhanced extraction and solely gravity-driven membrane separation into a single unit operation (see Figure 3.7c). We termed this methodology CLEANS (Continuous Liquid-liquid Extraction And *iN-situ* membrane Separation).

By integrating emulsified liquid-liquid extraction with these stimuli-responsive membranes that enable rapid demulsification[21, 31], our CLEANS methodology achieves extremely energy-efficient LLE in a single unit operation. The apparatus for CLEANS consists of an *in-situ* mixer (for emulsification) and two membranes operating in parallel – a stimuli-responsive membrane at the bottom and a hydrophobic (HP) and oleophilic (OL) membrane on the sidewall, designed to separate immiscible liquids based on their surface tension (Methods 3.2.4.2). While the stimuli-responsive membrane allows the

polar, higher surface tension liquid phase to pass through, it prevents the permeation of the non-polar liquid phase. Furthermore, the HP and OL membrane allows only the non-polar, lower surface tension liquid phase to pass through. Note that during operation, the feed emulsification and extraction occur continuously and simultaneously, along with the membrane-based extract-raffinate separation.

3.5.3 Dye Extraction from a Jet Fuel Proxy (Dodecane) with CLEANS

Utilizing our CLEANS methodology, we first separated a miscible red dye (Disperse Red 1, 30 ppm concentration) from dodecane (Figure 3.7c). Dye is put in jet fuel for identification purposes, but has been shown to damage engines. Therefore, an easy method for its removal is required. In steady-state operation, the polar, dye-enriched DMF phase continuously permeates through the stimuli-responsive membrane at the bottom, while the dye-depleted dodecane phase continuously passes through the HP/OL membrane on the side–wall. UV-Vis absorbance measurements indicate that the dye-depleted dodecane phase contains ≈ 0.5 ppm of dye. In contrast, the concentration of dye without emulsification was found to be ≈ 2 ppm (Figure 3.7d and 90:10 v:v ratio in Figure 3.7e). This clearly indicates that our methodology facilitates enhanced extraction due to the increased interfacial area between emulsified feed and extractant, as well as shorter diffusion lengths.

The CLEANS methodology allows for efficient liquid–liquid extraction even with a high volumetric flow ratio of the feed to extractant. Figure 3.7e shows the dye extraction factor (D_m) as a function of the feed:extractant volumetric flow ratio. The extraction factor[32] is the ratio of solute in the extractant to the solute in the raffinate, and is defined as:

$$\text{Extraction factor}(D_m) = \frac{m_{s,f} - m_{s,r}}{m_{s,r}} \qquad (3.1)$$

where $m_{s,r}$ is the mass of a solute in the raffinate after separation and $m_{s,f}$ is the initial mass of a solute in the feed. Figure 3.7e shows that the CLEANS methodology has led to a significant improvement in D_m. For a 90:10 feed:extractant volumetric flow ratio, the extraction factor using the CLEANS methodology is 50, which is about a 240% increase over the value obtained without emulsification. For a given volumetric ratio, this enhanced solute mass transfer to the extractant significantly reduces the number of stages in an extraction process and, consequently, the operating costs and energy consumption.

In addition to dye extraction, the simplicity and versatility of the CLEANS methodology enables the separation of a wide variety of commercially relevant miscible liquid mixtures. Next, we demonstrate the utility of CLEANS in separating three such liquid mixtures:

3.5.4 Extraction of Methanol from Biodiesel

Biodiesel, a renewable and biodegradable source of energy, is an alternative to fossil fuels.[33] Transesterification, the common biodiesel production process, converts vegetable oils or animal fats to fuel by chemically reacting them with alcohols (e.g., methanol).[34-35] This reaction produces methyl esters (biodiesel) and by-products, such as glycerol and excess methanol.[34-35] While glycerol can be easily separated from methyl esters through centrifugation or decantation, due to low miscibility and significant density difference[36-37], the separation of methanol often requires energy-intensive operations such as vacuum distillation.[36, 38]

Here, we demonstrate the separation of methanol from methyl oleate, a mimic of

biodiesel, using the CLEANS methodology. We separated methanol (10 vol%) from

methyl oleate using water as the extractant and SDS as the surfactant in the apparatus

shown in Figure 3.7c. The methanol remaining in the methyl oleate phase after separation

was determined by measuring its refractive index (Appendix B.2). Figure 3.8a shows the

methanol extraction factors using various feed:extractant volumetric flow ratios.

Compared to the separation operation without using a surfactant, the CLEANS

methodology greatly enhances the removal of methanol from methyl oleate, as

demonstrated by higher values of D_m for all feed:extractant volumetric flow ratios

considered. Simulations in Aspen Plus (Methods 3.2.5.3) reveal that the emulsification

helps a single-stage, CLEANS based extraction process approach the thermodynamic
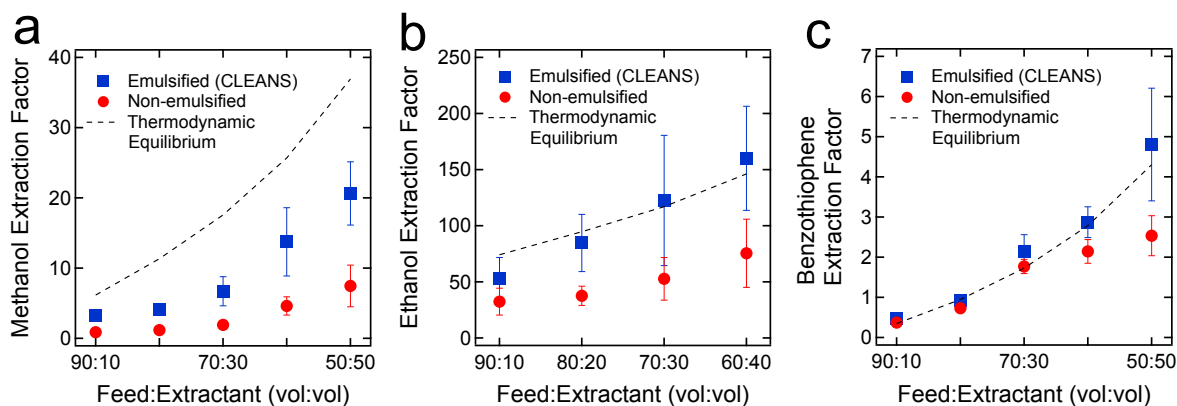
Figure 3.8: Separation of a range of commercially relevant liquid mixtures using the CLEANS methodology. (a) Methanol extraction factors obtained from the separation of methanol-methyl oleate mixtures, with and without CLEANS methodology, using different feed:extractant volumetric flow ratios. (b) Ethanol extraction factors from the separation of ethanol-heptane azeotropes. (c) Benzothiophene (BT) extraction factors from the separation of BT-dodecane mixtures. The dashed lines represent the maximum extraction factors once thermodynamic equilibrium is reached, as predicted using the Aspen Plus V8.8 simulation software. The error bars denote standard deviation.

limit for extraction between the two liquid phases. Further, the higher the feed:extractant

volumetric flow ratios (i.e., when lower extractant volumes are used), the higher the

utility of emulsification using a surfactant. At the highest feed to extractant ratio of 90:10

(the least favorable extraction conditions tested), emulsifying the system with surfactant increased the extraction factor from 0.9 to 3.3, which is about a 270% increase over the value obtained without emulsification. From operational and economics viewpoints, using reduced extractant volumes is highly desirable, especially if subsequent recovery of extractant requires energy-intensive techniques such as distillation.

3.5.5 Separation of an Ethanol-Heptane Azeotrope

Liquid-liquid extraction can serve as an alternative for the separation of azeotropes (i.e., constant boiling mixtures), which cannot be separated by simple distillation.[9, 14] Effective separation of completely miscible oil-alcohol mixtures, including azeotropes, is highly desirable in biodiesel production[33, 36-37], edible oils refining[39-40] and different petrochemical industries.[41-42]

We demonstrate the separation of an ethanol-heptane azeotrope (49 wt% ethanol : 51 wt% heptane)[43] using water as the extractant and SDS as the surfactant. Refractive index measurements were used to determine the ethanol concentration in the heptane-rich phase after separation (see Appendix B.3). Figure 3.8b shows the ethanol extraction factor as a function of feed:extractant volumetric flow ratio. At the highest feed to extractant ratio of 90:10, emulsifying the system with surfactant increased D_m from 32 to 53. It is clear from the data that the CLEANS process increases the extraction factors to near the thermodynamic limit.

3.5.6 Extraction of Sulfur from Oils

With tighter government mandates and environmental regulations, there is a significant push toward removing sulfur from fossil fuels.[44-45] Desulfurization of fuels is also important for producing clean fuel for solid-oxide fuel cell based mobile electric

power generators in remote defense bases. Hydrodesulfurization, the most common technology to remove sulfur compounds from oils, typically requires elevated temperatures and pressures which leads to high capital and operating costs.[46]

We demonstrate the extraction of 30 ppm benzothiophene, a common sulfur compound present in fuels, from dodecane using DMF as the extractant and SDS as the surfactant. UV-Vis absorbance measurements (see Appendix B.4) were used to analyze the concentration of benzothiophene in the dodecane-rich phase after extraction. Figure 3.8c shows the benzothiophene extraction factor as a function of feed:extractant volumetric flow ratio. From the data, it is clear that the CLEANS methodology can separate benzothiophene more effectively when compared to the separation operation without emulsification. At a feed to extractant ratio of 50:50, emulsifying the system with the surfactant increased D_m from 2.5 to 4.8. Again, the surfactant-enhanced extraction increases the extraction factors to near the thermodynamic limit. Another sulfur compound, *tert*-butyl thiol, was also successfully separated using the CLEANS methodology (see Appendix B.5). To our knowledge, the CLEANS methodology is one of the first high efficiency desulfurization technologies that operates at room temperature and atmospheric pressure.

3.6 Conclusion

In conclusion, we have developed a miscible liquid separation technology named Continuous Liquid-liquid Extraction And *iN-situ* membrane Separation (CLEANS) by combining emulsion-enhanced extraction and solely gravity-driven, membrane separation, into a single unit operation. Utilizing the CLEANS methodology, we demonstrate the efficient separation of a wide range of different liquid mixtures,

including organic dyes and sulfur compounds from oils, alcohols from esters, and azeotropes. The CLEANS process is capable of improving extraction to within range of the thermodynamic maximums, dramatically lowering extractant volumes, as well as lowering the costs associated with extraction. We anticipate that the CLEANS methodology will have numerous practical applications, including the production of ultra-low sulfur diesel, petroleum purification, separation and recovery of biofuels, removal of contaminants from fuels, separation of azeotropes, and wastewater treatment.

3.7 References

1. Oak Ridge National Laboratory; BCS Inc, Materials Research for Separations Technologies: Energy and Emission Reduction Opportunities. **2005**.

2. Delgado-Povedano, M. M.; de Castro, L., Ultrasound-assisted analytical emulsification-extraction. *TrAC-Trend. Anal. Chem.* **2013,** *45*, 1-13. 10.1016/j.trac.2012.12.011

3. Vilkhu, K.; Mawson, R.; Simons, L.; Bates, D., Applications and opportunities for ultrasound assisted extraction in the food industry - A review. *Innov. Food Sci. Emerg. Technol.* **2008,** *9* (2), 161-169. 10.1016/j.ifset.2007.04.014

4. Gabelman, A.; Hwang, S. T., Hollow fiber membrane contactors. *J. Membr. Sci.* **1999,** *159* (1-2), 61-106. 10.1016/S0376-7388(99)00040-X

5. *Separation and Purification Technologies in Biorefineries*. John Wiley & Sons, Ltd: Chichester, 2013.

6. Huebner, A.; Sharma, S.; Srisa-Art, M.; Hollfelder, F.; Edel, J. B.; Demello, A. J., Microdroplets: a sea of applications? *Lab Chip* **2008,** *8* (8), 1244-54. 10.1039/b806405a

7. Kralj, J. G.; Schmidt, M. A.; Jensen, K. F., Surfactant-enhanced liquid-liquid extraction in microfluidic channels with inline electric-field enhanced coalescence. *Lab Chip* **2005,** *5* (5), 531-5. 10.1039/b418815b

8. Chabrand, R. M.; Kim, H.-J.; Zhang, C.; Glatz, C. E.; Jung, S., Destabilization of the Emulsion Formed during Aqueous Extraction of Soybean Oil. *J. Am. Oil Chem. Soc.* **2008,** *85* (4), 383-390. 10.1007/s11746-008-1199-9

9. Treybal, R. E., *Mass-Transfer Operations*. 3rd ed.; McGraw-Hill: New York, 1980.

10. Aghazadeh, M.; Engelberth Abigail, S., Techno-economic analysis for incorporating a liquid–liquid extraction system to remove acetic acid into a proposed commercial scale biorefinery. *Biotechnol. Prog.* **2016,** *32* (4), 971-977. 10.1002/btpr.2325

11. Kralj, J. G.; Sahoo, H. R.; Jensen, K. F., Integrated continuous microfluidic liquid-liquid extraction. *Lab Chip* **2007,** *7* (2), 256-63. 10.1039/b610888a

12. Jaritsch, D.; Holbach, A.; Kockmann, N., Counter-Current Extraction in Microchannel Flow: Current Status and Perspectives. *J. Fluids Eng.* **2014,** *136* (9), 091211-091211-7. 10.1115/1.4026608

13. Müller, E.; Berger, R.; Blass, E.; Sluyts, D.; Pfennig, A., Liquid–Liquid Extraction. In *Ullmann's Encyclopedia of Industrial Chemistry*, Wiley-VCH Verlag GmbH & Co. KGaA: Weinheim, 2002.

14. Li, S.; Jing, S.; Luo, Q.; Chen, J.; Luo, G., Bionic system for countercurrent multi-stage micro-extraction. *RSC Adv.* **2012,** *2* (29), 10817-10820. 10.1039/C2RA21818F

15. Rodríguez, M.; González-Muñoz, M. J.; Luque, S.; Alvarez, J. R.; Coca, J., Extractive ultrafiltration for the removal of carboxylic acids. *J. Membr. Sci.* **2006,** *274* (1), 209-218. 10.1016/j.memsci.2005.08.012

16. Rodríguez, M.; Luque, S.; Alvarez, J. R.; Coca, J., Extractive ultrafiltration for the removal of valeric acid. *J. Membr. Sci.* **1996,** *120* (1), 35-43. 10.1016/0376-7388(96)00116-0

17. Scott, K.; McConvey, I. F.; Adhamy, A., Application of crossflow microfiltration to emulsion separation in extraction processes. *J. Membr. Sci.* **1992,** *72* (3), 245-257. 10.1016/0376-7388(92)85052-K

18. Ulman, A., Formation and structure of self-assembled monolayers. *Chem. Rev.* **1996,** *96* (4), 1533-1554. 10.1021/cr9502357

19. Wang, M. J.; Liechti, K. M.; Wang, Q.; White, J. M., Self-assembled silane monolayers: Fabrication with nanoscale uniformity. *Langmuir* **2005,** *21* (5), 1848-1857. 10.1021/la048483y

20. Tuteja, A.; Choi, W.; Mabry, J. M.; McKinley, G. H.; Cohen, R. E., Robust omniphobic surfaces. *Proc. Natl. Acad. Sci. USA* **2008,** *105* (47), 18200-5. 10.1073/pnas.0804872105

21. Kota, A. K.; Kwon, G.; Choi, W.; Mabry, J. M.; Tuteja, A., Hygro-responsive membranes for effective oil-water separation. *Nat. Commun.* **2012,** *3*, 1025. 10.1038/ncomms2027

22. Hansen, C. M., *Hansen Solubility Parameters: A User's Handbook*. 2nd ed.; CRC Press: Boca Raton, 2007.

23. Howarter, J. A.; Youngblood, J. P., Self-Cleaning and Anti-Fog Surfaces via Stimuli-Responsive Polymer Brushes. *Adv. Mater.* **2007,** *19* (22), 3838-3843. 10.1002/adma.200700156

24. Sawada, H.; Ikematsu, Y.; Kawase, T.; Hayakawa, Y., Synthesis and surface properties of novel fluoroalkylated flip-flop-type silane coupling agents. *Langmuir* **1996,** *12* (15), 3529-3530. 10.1021/la951041p

25. Won, D.-B.; Park, S.-J.; Han, K.-J.; Kim, C.-J., Liquid–liquid equilibria for methanol+ hexadecane+ heterocyclic nitrogen-containing compounds at 298.15 K. *Fluid Phase Equilib.* **2002,** *193* (1-2), 217-227. 10.1016/S0378-3812(01)00732-4

26. Kajitvichyanukul, P.; Hung, Y.-T.; Wang, L. K., Membrane Technologies for Oil-Water Separation. In *Handbook of Environmental Engineering, Vol 13: Membrane and Desalination Technologies*, Wang, L. K.; Chen, J. P.; Hung, Y.-T.; Shammas, N. K., Eds. The Humana Press Inc., New York 2011.

27. Shannon, M. A.; Bohn, P. W.; Elimelech, M.; Georgiadis, J. G.; Marinas, B. J.; Mayes, A. M., Science and technology for water purification in the coming decades. *Nature* **2008,** *452* (7185), 301-310. 10.1038/nature06599

28. Nordvik, A. B.; Simmons, J. L.; Bitting, K. R.; Lewis, A.; Strøm-Kristiansen, T., Oil and water separation in marine oil spill clean-up operations. *Spill Sci. Technol. Bull.* **1996,** *3* (3), 107-122. 10.1016/S1353-2561(96)00021-7

29. Atadashi, I. M., Purification of crude biodiesel using dry washing and membrane technologies. *Alexandria Eng. J.* **2015,** *54* (4), 1265-1272. 10.1016/j.aej.2015.08.005

30. Albers, W.; Overbeek, J. T. G., Stability of emulsions of water in oil: II. Charge as a factor of stabilization against flocculation. *J. Colloid Sci.* **1959,** *14* (5), 510-518. 10.1016/0095-8522(59)90016-9

31. Marmur, A., From hygrophilic to superhygrophobic: theoretical conditions for making high-contact-angle surfaces from low-contact-angle materials. *Langmuir* **2008,** *24* (14), 7573-9. 10.1021/la800304r

32. Rice, N. M.; Irving, H. M. N. H.; Leonard, M. A., Nomenclature for liquid-liquid distribution (solvent extraction) (IUPAC Recommendations 1993). *Pure Appl. Chem.* **1993,** *65* (11), 2373. 10.1351/pac199365112373

33. *The Biodiesel Handbook*. 2nd ed.; AOCS Press: Urbana, 2010.

34.   Meher, L. C.; Vidya Sagar, D.; Naik, S. N., Technical aspects of biodiesel production by transesterification—a review. *Renew. Sustain. Energy Rev.* **2006,** *10* (3), 248-268. 10.1016/j.rser.2004.09.002

35.   Kiss Anton, A.; Bildea Costin, S., A review of biodiesel production by integrated reactive separation technologies. *J. Chem. Technol. Biotechnol.* **2012,** *87* (7), 861-879. 10.1002/jctb.3785

36.   Atadashi, I. M.; Aroua, M. K.; Aziz, A. A., Biodiesel separation and purification: A review. *Renew. Energ.* **2011,** *36* (2), 437-443. 10.1016/j.renene.2010.07.019

37.   Berrios, M.; Skelton, R. L., Comparison of purification methods for biodiesel. *Chem. Eng. J.* **2008,** *144* (3), 459-465. 10.1016/j.cej.2008.07.019

38.   Kiss, A. A.; Ignat, R. M., Enhanced methanol recovery and glycerol separation in biodiesel production – DWC makes it happen. *Appl. Energ.* **2012,** *99*, 146-153. 10.1016/j.apenergy.2012.04.019

39.   *Edible Oil Processing*. 2nd ed.; John Wiley & Sons, Ltd: Chicester, 2013.

40.   Gupta, M. K., *Practical Guide to Vegetable Oil Processing*. AOCS Press: Urbana, 2008.

41.   Meyers, R. A., *Handbook of Petroleum Refining Processes*. 3rd ed.; McGraw-Hill: New York, 2004.

42.   Meyers, R. A., *Handbook of Petrochemicals Production Processes*. McGraw-Hill: New York, 2004.

43.   Speight, J. G., *Lange's Handbook of Chemistry*. 16th ed.; McGraw-Hill: New York, 2005.

44.   Song, C., An overview of new approaches to deep desulfurization for ultra-clean gasoline, diesel fuel and jet fuel. *Catal. Today* **2003,** *86* (1), 211-263. 10.1016/S0920-5861(03)00412-7

45.   Babich, I. V.; Moulijn, J. A., Science and technology of novel processes for deep desulfurization of oil refinery streams: A review. *Fuel* **2003,** *82* (6), 607-631. 10.1016/S0016-2361(02)00324-1

46.   Vasudevan, P. T.; Fierro, J. L. G., A Review of Deep Hydrodesulfurization Catalysis. *Catal. Rev.* **1996,** *38* (2), 161-188. 10.1080/01614949608006457

CHAPTER 4

Dually Functional Anti-Fog and Easy-Clean Polymer Spray Coating

This chapter contains work adapted from a first author article pending publication. Mathew Boban assisted with LEXT and AFM surface analysis.

4.1 Introduction

Every day around the world, fog formation is prevalent and ranges from being a nuisance to a real hazard. It is an aesthetic concern for food packaging and refrigerator/freezer doors, but a functional concern for mirrors, building windows, and greenhouses. Fogging becomes dangerous on safety equipment, such as eyewear, hazmat suits, and full-face helmets, and transportation windshields, including automobiles, aircraft, and boats. Solutions to prevent fogging must be devised in such a way that they will work for the lifetime of the product, as well as be readily cleaned of contaminants such as fingerprints.

Fog is formed when the temperature at the surface of a material reaches the dew point for a given air temperature and humidity. Water vapor condenses into many droplets covering the surface, which scatter light in all directions yielding a translucent or opaque surface.[1] If sufficiently cooled, ice crystals will also form and scatter light.[2] It has been shown that the shape of the water drops causes the scattering of light instead of the droplet size. In order to minimize light reflection and scattering, the droplet advancing

contact angle with the substrate should be less than 40° for a filmwise mode of condensation.[1, 3] By looking at Young's relation[4] for a smooth surface, the equilibrium contact angle (θ) can be lowered by increasing the surface energy of the substrate or decreasing the solid-water interfacial tension. These can both be accomplished by increasing the hydrophilicity or polarity of the substrate. Furthermore, the Wenzel equation[5] reveals that for a given hydrophilic substrate ($\theta_{water} < 90°$), increasing the surface roughness (r) will also lower the macroscopic, apparent contact angle (θ^*). The surface can even become superhydrophilic where water's angle approaches 0°, i.e. completely wetted.[6] During efforts to create effective hydrophilic surfaces for fog prevention, the goals of maintaining a highly transparent material with high optical clarity must be kept in mind. In addition, the surface treatment should be mechanically durable, well adhered to substrates, stable and functional over time, scalable, and economical.

Due to its importance, much research has been conducted on anti-fog treatments or coatings. It is divided into three general categories: 1. Direct treatment of a substrate, 2. Texturing a hydrophilic surface or chemically modifying a textured surface, and 3. Hydrophilic polymer coatings. Surfaces such as TiO_2 or ZnO can be photochemically activated by UV radiation to have a clean, hydrophilic surface, but this effect is temporary due to ambient contamination.[7-9] Implantation of argon or helium ions into polydiethylene glycol bis(allyl carbonate)[3] and oxygen plasma treatment of polymers, to create polar surface groups[10], are also both short-lived and revert within a day. The direct silanization of an oxide substrate with zwitterionic sulfobetaine silane yields a superhydrophilic surface.[11] Ionic molecules have shown good promise due to their high

polarity and are further discussed in the hydrophilic polymer coatings overview.

Textured hydrophilic coatings have been produced from SiO_2, ZrO_2, and colloidal SiO_2 spray-coated sol-gel[12], Al_2O_3 sol-gel[13], and porous TiO_2 sol-gel.[14] They are durable, but require high temperature calcination, which negates polymers as possible substrates. A lower temperature method involves binding silica nanoparticles to polyethylene terephthalate with glycidoxypropyltrimethoxysilane.[15] Mundo *et al.* first nanotextured polycarbonate with oxygen plasma, then deposited a "silica-like" surface on top using hexamethyldisiloxane plasma. This texture allowed it to remain superhydrophilic, despite an increase in the equilibrium contact angle from long aging periods.[16] Unfortunately, nanostructures are known to be easily damage by mechanical abrasion[17] and cross-linkable polymer coatings are much more durable.

A majority of anti-fog treatments have focused on hydrophilic polymer coatings. Some early work involved mixing non-ionic surfactants (sorbitan esters, polyoxyethylene esters, glycerol esters, and polyglycerol esters) into hydrophobic polymers and allowing them to migrate to the surface from the bulk. This makes the surface hydrophilic, but it has a limited functional life due to losses from cleaning and contamination.[18] Depositing cellulose nanocrystals on polymer films provided another functional, but poorly adhered coating.[19] Despite substrate adhesion issues, the non-covalent bonding between a coating made of polyvinylpyrollidone and aminopropyl-functionalized clay platelets showed anti-fog and self-healing abilities.[20] Pullulan, a naturally derived polysaccharide polymer, can be covalently bonded to LDPE substrates with azirine for greater durability.[21] Many examples of using layer-by-layer assembly of cationic and anionic polymers to form quality anti-fog coatings have been shown.[22-26] A few are held by electrostatic forces,

while others are covalently bonded to the substrate, as well as between the bilayers, and show high pencil hardness. This method is plagued by the need for the assembly of many bilayers for functionality, with extensive surface preparation and long dip and cure times. Anti-fog coatings that show the most promise for scalability and implementation are UV cross-linked due to their increased hardness and quick surface application in one step.

Yuan *et al.* synthesized a UV-curable acrylate with sulfonic acid groups that produced a durable, hydrophilic coating when blended and cured with additional cross-linker and diluents.[27] A further example of this approach is the synthesis of a quaternary ammonium salt (QAS) with methacrylate functionality. This charged species is very hydrophilic and a UV-initiated radical reaction quickly bonds it with poly(ethylene glycol) diacrylate and its substrate. QAS imparts anti-bacterial properties to the coating as well.[28] For enhanced wetting, silica nanoparticles can be blended into these UV curable polymer systems. Chang *et al.* blended silica into an acrylate primer and cross-linked the primer with the substrate followed by an anti-fog topcoat of methacrylate-modified Tween 20 surfactant.[29] By controlling texture, hydrophilicity, cross-link density, and substrate adhesion, one-step UV curable polymer coatings have a bright future in anti-fog coatings.

A secondary issue for anti-fog coatings is keeping them free of contaminants, especially low surface tension oils and fingerprints. This is a functional and cosmetic problem for many surfaces including windows, optics systems, packaging, eyewear lenses, and touch screens.[30-31] Preventing contamination or allowing for easy-clean properties (anti-staining, anti-soiling, anti-fingerprint) is forecasted to be the greatest coatings research need in the near future.[32] The main types of skin residue are sebum-rich

and eccrine-sweat rich materials, ranging in surface tension from 20 – 50 mN/m.[30] Surface wettability is the dominant factor in keeping surfaces clean, and omniphobicity is usually desired to reduce adhesion of fingerprint oil. For robust repellency and easy dynamic removal of oils, a combination of low surface energy materials and surface texture (hierarchical and/or re-entrant[33-36]) are typically used, although the mean surface roughness should be between 30 – 100 nm to maintain transparency.[37] This type of surface would appear to be in contrast to hydrophilic, higher surface energy anti-fog coatings, but the oil contacts angles do not need to be exceptionally high for repellency, as shown by slippery, liquid-like grafted surfaces that have very low oil sliding angles and low hysteresis, despite contact angles << 90°.[38-39] Studying the dynamics of receding oil is important due to the nature of fingerprint deposition. Residue is left behind on a surface as a finger is removed due to irregularities, pinning, and necking of oil along the contact line.[40] Coatings that have found success in showing anti-fingerprint, easy-clean, or low hysteresis properties include: textured and smooth fluorinated surfaces[41-49] and a couple textured non-fluorinated surfaces.[50-52] In this work, we find that practical post-processing of our UV-cured anti-fog formulation with low energy silane allows *n*-dodecane droplets to readily slide off and ease the cleaning of fingerprints, without hampering the anti-fog performance and transparency. This dually functional coating is expected to have many applications where it is necessary to keep anti-fog surfaces clean.

4.2 Materials and Methods

4.2.1 Materials

1,300 kDa polyvinylpyrrolidone (PVP), 99% benzophenone, and (3-aminopropyl) triethoxysilane were from Sigma-Aldrich. 30% H_2O_2, methanol (MeOH), isopropanol

(IPA), anhydrous ethanol, and safety glasses were from Fisher. 1,1,1-trimethylolpropane triacrylate (TMPTA) was from Polysciences, Inc. 99% 1-propanol was from Mallinckrodt Chemicals. $\geq$ 99.0% n-dodecane was from TCI. Polycarbonate 1" x 4ft strips were purchased from McMaster-Carr. (Heptadecafluoro-1,1,2,2-tetrahydrodecyl) triethoxysilane (SIH5841.2) and bis(3-trimethoxysilylpropyl) amine (SIB1833.0) were sourced from Gelest.

4.2.2 Anti-Fog Polymer Solution

The anti-fog coating solution was prepared by adding 1.32 g PVP, 50 mg benzophenone, 2 mL of 30% H_2O_2, and 2 mL of 0.0733 g TMPTA/mL MeOH (11.1 wt% TMPTA with respect to PVP) to 46.4 mL of 1-propanol and 3.08 mL of water (94 vol% 1-propanol). The 1-propanol/water mixed solvent was discovered using Hansen solubility parameter solvent optimization for PVP (HSPiP software).

4.2.3 Anti-Fog Sample Preparation

4.2.3.1 Polycarbonate Strips

Strips cut to 1" x 3" were cleaned with isopropanol and dried before treating with 30 W oxygen plasma for 5 min (Harrick Plasma Cleaner, PDC-001, at 0.4 SCCM oxygen flow and 240 mTorr vacuum). Immediately after surface activation with the plasma, the samples were spray coated with an ATD-6903 HVLP Mini Touch UP Spray Gun, 1.0 mm (solution from section 4.2.2). The conditions were 10 psig air pressure and 3 passes over the sample at a 6" distance. The samples were then cured for 10 min under UVC (UVP XX-40S Bench Lamp, 3.6 mW/cm^2) and UVA (UVP 100 W Longwave Mercury Spot Lamp) at a 5" distance from the sample. This spray-coating process allowed for highly uniform coatings with no optical distortion, unlike some of the initial drop-cast

samples using ethanol as the solvent.

4.2.3.2 Safety Glasses

The lenses were coated in the same manner, but the anti-scratch coating from the manufacturer required removal for good adhesion. It was removed through a series of sand paper grits from 1200 grit down to 200 nm silica polishing solution.

4.2.3.3 APTES Pre-treatment Procedure

Clean a polycarbonate slide with isopropanol (IPA) and dry, before treating with 30 W oxygen plasma for 5 min. Dip slide in 4 vol% (3-aminopropyl) triethoxysilane (APTES) in IPA and air dry for 3 min. Drop cast anti-fog solution (in ethanol solvent, initially) and hang dry 20 min before curing 10 min under UVA/UVC. This procedure was discontinued and the solvent system was adjusted for better performance and application later (Methods 4.2.2 and 4.2.3.1), after determining that APTES was unnecessary and hindered transparency (Section 4.3.2).

4.2.4 Easy-Clean Surface Modification

4.2.4.1 System A: Plasma + Silane Linker + 6 h F_{17} Silane (<u>final procedure</u>)

Treat cured anti-fog coating with 30 W oxygen plasma for 20 minutes and then soak in 2 wt% Gelest SIB1833.0 silane linker (40 mL ethanol, 0.625 mL silane, and 2 mL of pH = 2 acetic acid; stirred for 2 h before use) for 20 min. Rinse sample with ethanol to remove non-adhered silane and dry with nitrogen gas. Vapor-phase silanize the dry sample in a desiccator with (heptadecafluoro-1,1,2,2-tetrahydrodecyl) triethoxysilane, under 84 kPa vacuum, for 6 h at 70°C.

4.2.4.2 System B: Plasma + 6 h F_{17} Silane

Same as System A except no silane linker is used.

4.2.4.3 System C: Silane Linker + 6 h F$_{17}$ Silane

Same as System A except no oxygen plasma is used before the silane linker.

4.2.5 Cold Temperature Fog Test

For comparison of uncoated and coated polycarbonate slides, samples were placed on a -10°C Peltier thermoelectric cooling plate for 1 min and then breathed on. Coated safety glasses were placed in a Summit Appliances FS20LGL7DTHUMPH freezer operating at -15°C (34% relative humidity) for 5 min. They were then moved to room conditions of 22°C and 45% relative humidity for imaging of any fogging.

4.2.6 Durability Testing

A Taber$^{®}$ Industries 5750 Linear Abraser mechanically abraded the anti-fog coatings with CS-5 abradant and a mass of 300 g. Abrasion tests were performed at 60 cycles per minute, for up to 5,000 abrasion cycles. For the initial drop-cast samples, Taber$^{®}$ abrasion was performed in stages, and UV-Vis % transmittance (Methods 4.2.7) was measured after each degree of abrasion, until 500 cycles was reached. A Gardco 5021 Pencil Hardness Tester was used according to ASTM D3363-05 for identifying the hardness of the anti-fog coating.

4.2.7 UV-Vis % Transmittance

A Cary 50 Bio UV-Vis was used at 300-800 nm wavelengths with a medium scan rate. The UV-Vis measurement was zeroed to an empty chamber, and then polycarbonate (PC) control or anti-fog coated PC slides were measured.

4.2.8 Contact Angle Measurements

All measurements were conducted with a Ramé–Hart 200-F1 goniometer. Static contact angles were measured by dispensing a small volume of liquid ($\approx$ 2 μL) on the

surface, using a 2 mL micrometer syringe (Gilmont), and allowing it to equilibrate for 1 or 5 minutes. At least six measurements were performed on each substrate. Dodecane droplet sliding angles were performed by securing the sample to the leveled stage and tilting the instrument with the built-in mechanism (six measurements). Droplets for sliding angles were applied with either a Scilogex 0.1 – 2.5 μL or Fisherbrand 10 – 100 μL pipette.

4.2.9 Microscopy

The surface roughness was characterized with an Olympus OLS 4000 LEXT laser confocal microscope using the 50x lens. Coating thickness was analyzed with a Bruker Innova Atomic Force Microscope (AFM) in tapping mode using an RTESP-300 tip. A measurable cut was formed in the coating by spray coating over tape and removing the tape after curing.

4.2.10 Degree of Swelling Test

Four 1" x 3" polycarbonate slides, of known mass, were coated and the dry mass was recorded. The slides were then soaked in deionized water for 7 days. Free water was absorbed and the slide masses were again recorded. The mass swell ratio is the swollen mass divided by the dry mass.

4.2.11 Easy-Clean Fingerprint Test

To apply the fingerprint, a clean gloved finger was rubbed on the researcher's forehead (oily, sebum-rich[53]) and pressed onto the sample slide. To assess the ease of cleaning, a Taber® Industries 5750 Linear Abraser with a 300 g load, 1.5" strokes, and 3 cycles at 60 cycles min^{-1} was used. The abraser attachment was a 1 in^2 piece of Eco-fused

123

Microfiber cleaning cloth mounted on a flat adapter. The removal of the fingerprint was compared visually.

4.3 Anti-Fog Coating Development

4.3.1 System Specifications and Initial Formulation

In order to develop an anti-fog system that would be highly functional as well as feasible, we looked for a UV cross-linkable, hydrophilic polymer system that would perform in cold and warm conditions, specifically for polycarbonate eyewear. The coating system should be readily implementable industrially and work with complex eyewear geometries. Hydrophilic polymers such as, polyvinylpyrrolidone and poly(ethylene glycol),[2, 26] have already been known to absorb water into their structure and prevent it from freezing (non-freezing or 'unfreezable water').[54-56] Polyvinylpyrrolidone (PVP) is UV cross-linkable and readily available. Prior work has shown its usefulness in preventing the fogging of polystyrene.[2] Hydrogen peroxide initiates the radical cross-linking of the PVP under UVC radiation and benzophenone abstracts protons from the polystyrene surface under UVA radiation for covalent binding to the anti-fog coating. It was found that this system did not work for polycarbonate (PC), even if the PC was treated with 20 min of 30 W oxygen plasma before coating. The coating disintegrated readily when wetted and wiped, showing poor adhesion and integrity of the coating itself. Despite the mechanical issues, it showed excellent anti-fog ability. The sample would not fog up under warm, moist breath, similar to what glasses would experience while being worn.

4.3.2 Enhancing Coating Durability and Adhesion

The addition of a multi-functional cross-linker into the formulation was

investigated, as well as silane linker (coupling agent) pre-treatment of the polycarbonate for increased adhesion. The cross-linker should help maintain the integrity of the coating, increasing the durability and hardness[57-58], while the coating remains highly transparent and hydrophilic. UV-curable, tri-functional 1,1,1-trimethylolpropane triacrylate (TMPTA) was chosen, and I also experimented with pre-treating the polycarbonate with 4 vol% (3-aminopropyl)triethoxysilane (APTES) in isopropanol (Methods 4.2.3.3), which has shown to enhance bonding to polycarbonate.[59] The coating could no longer be rubbed off the polycarbonate, while still bonding to polystyrene as well, so we continued to optimize the optical properties of the coating. UV-Vis transmittance was used to quantify the effects of APTES and wt% TMPTA on transparency. 85% transmittance is usually considered transparent. A comparison of Figures 4.1 and 4.2 shows that APTES decreased transparency from > 85 %T to 60 – 70 %T for visible light, so it was
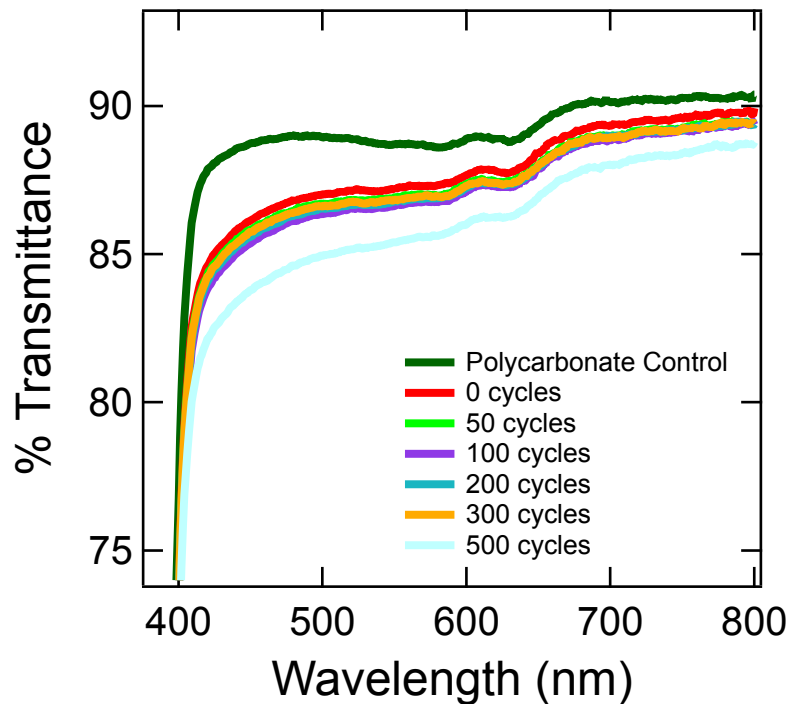
Figure 4.1: UV-Vis % Transmittance after various abrasion cycles for a drop-cast anti-fog coating with 11.1 wt% TMPTA (final formulation).
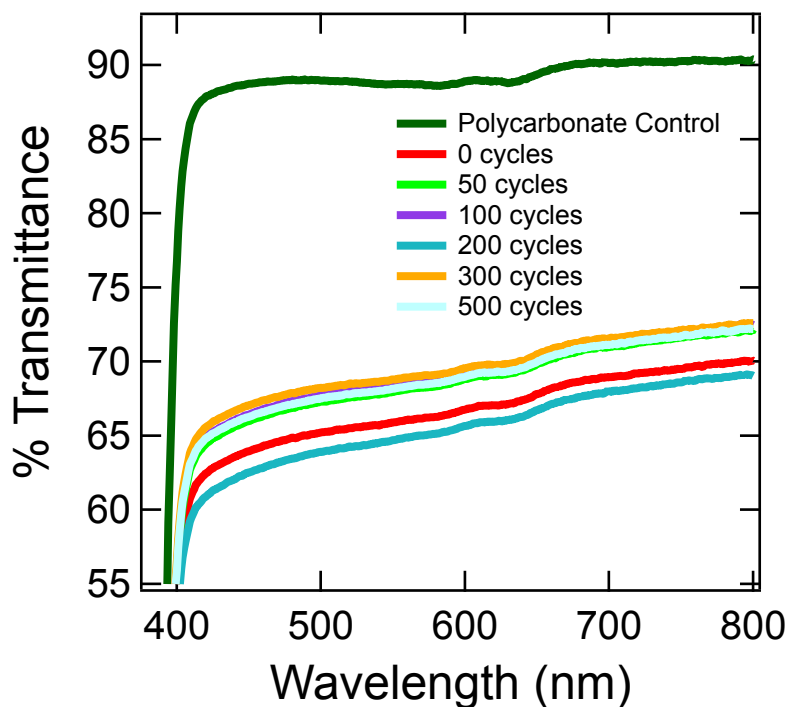
Figure 4.2: UV-Vis % Transmittance after various abrasion cycles for a polycarbonate slide pre-treated with APTES before drop casting the anti-fog coating with 11.1 wt% TMPTA. Due to the heterogeneous sampling area in the abraded area, the %T is not necessarily the lowest for the highest number of abrasion cycles.

discontinued. Furthermore, the integrity of the coating remained after removing APTES, indicating that the bulk integrity of the poorly cross-linked PVP (without TMPTA) was the issue rather than covalent adhesion to the polycarbonate substrate.

4.3.3 Coating Optimization

Comparison of Figures 4.1 and 4.3 shows that 11.1 wt% TMPTA is highly transparent through the visible light range, while 19.7 wt% has lower transparency. 11.1 wt% TMPTA (i.e. a cross-linking ratio of 0.042 – moles of cross-linker/moles of PVP repeat unit) was utilized in the final formulation as it was the highest amount tested, for greater durability, without adverse optical effects. This initial work was performed using ethanol, followed by methanol (better than ethanol), as the coating solvent, but was later switched to 94 vol% 1-propanol and 6 vol% water (much better solvent for PVP

according to Hansen solubility parameters) due to higher optical clarity (no wavy aberrations) and better leveling during spray coating. The spray-coated, final anti-fog
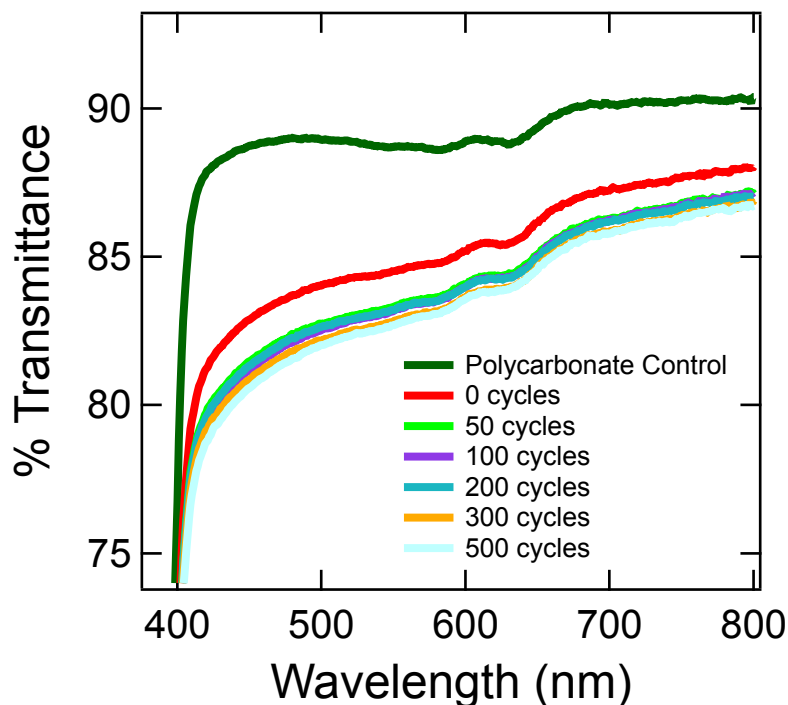
Figure 4.3: UV-Vis % Transmittance after various abrasion cycles for a drop-cast anti-fog coating with 19.7 wt% TMPTA.

formulation (Methods 4.2.2 and 4.2.3.1) showed ~90 % visible light transmittance (Figure 4.4a), nearly identical to polycarbonate, and with very low surface roughness (< 100 nm), shown by the LEXT laser confocal microscope (Figure 4.4b), to prevent light scattering. The spray-coated thickness was 1.8 ± 0.4 μm according to AFM.

4.3.4 Coating Durability

The mechanical durability was tested with Taber® abrasion and pencil hardness (Methods 4.2.6). Figure 4.1 shows that the coating transmittance is only slightly harmed by 500 cycles of abrasion with CS-5 abradant. This indicates that the coating will hold up well under routine cleaning. Up to 5,000 CS-5 abrasion cycles were performed on the anti-fog coating and a polycarbonate control (Figure 4.5). They both showed similar,
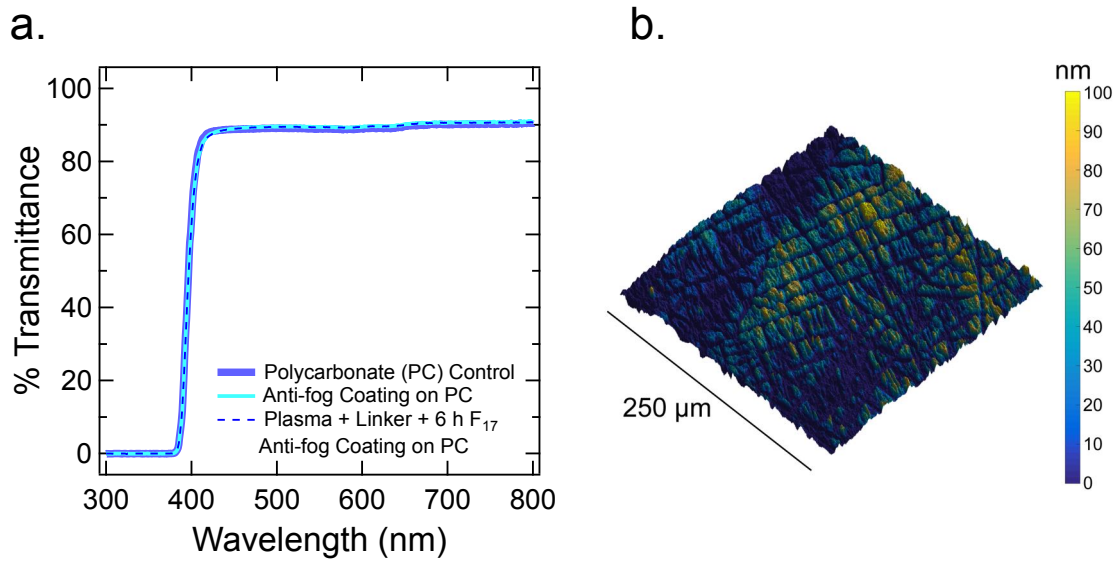
Figure 4.4: Properties of the anti-fog coating. (a) The UV-Vis % Transmittance shows that the anti-fog coating, as well as the easy-clean silane treatments, do not alter the optical properties of the highly transparent polycarbonate. (b) The LEXT profilometer scan of the anti-fog coating shows that it is quite smooth, with roughness features < 100 nm.
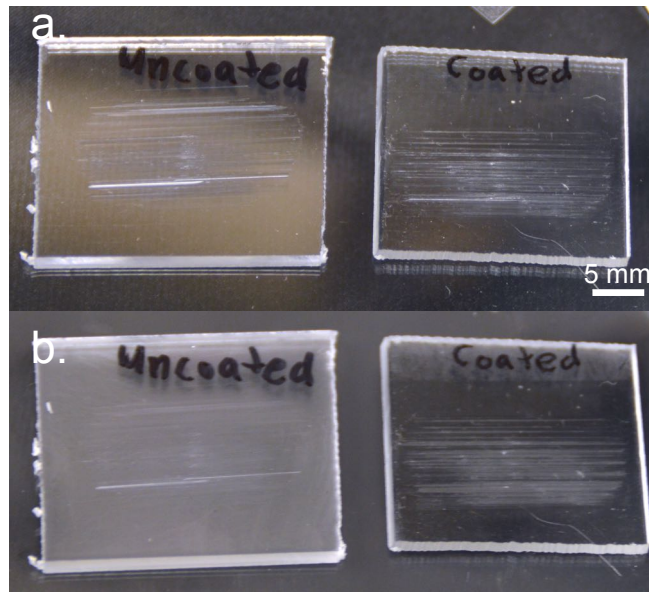
Figure 4.5: 5,000 continuous abrasion cycles. (a) 5,000 abrasion cycles on untreated polycarbonate (PC) to the left and our anti-fog coating on PC to the right. Similar scratching is seen due to comparable pencil hardness. (b) After breathing on the samples, fogging is still minimal on our anti-fog surface, while the PC is entirely fogged over. Note that the top edge of the coated sample is uncoated due to tape holding it while spraying.

minor scratching, but only our coating would not fog up under moist breath, despite the scratches. The pencil test hardness of the anti-fog coating with 11.1 wt% TMPTA was found to be 2B, as it failed the B test according to ASTM D3363-05. This indicates that the anti-fog coating has a similar or slightly higher hardness than untreated polycarbonate, which is also typically 2B or less. This agreed with the performance found using CS-5 abrasion. This is not extremely hard or scratch resistant and is an area for improvement in future work.

4.3.5 Anti-Fog Coating Wetting Properties

After achieving a mechanically sound anti-fog coating, the wetting properties were investigated. The static water contact angles on the surface were tested for 1 and 5 minute equilibration times. At 1 min, water's static angle was $46 \pm 6°$ and at 5 min, $29 \pm 6°$, while oil completely wet (Table 4.1). These angles agree with the work of Grube *et al.*[2] for PVP on polystyrene. This shows that the TMPTA does not significantly affect the wetting properties of the PVP surface and the coating is below the 40° contact angle upper boundary for the anti-fog property. Because these hydrophilic polymers uptake

Table 4.1: Water and dodecane contact angles on the anti-fog coating

Water Static Angle, 1 min. equilibrium (°)	$46 \pm 6°$	Dodecane Static Angle, 1 min. equilibrium (°)	$0 \pm 0°$
Water Static Angle, 5 min. equilibrium (°)	$29 \pm 6°$	Dodecane Static Angle, 5 min. equilibrium (°)	$0 \pm 0°$
Water Advancing Angle (°)	$100 \pm 3°$	Dodecane Advancing Angle (°)	$11 \pm 1°$
Water Receding Angle (°)	$0 \pm 0°$	Dodecane Receding Angle (°)	$0 \pm 0°$

water, the capacity of our cross-linked film was tested and found to have a mass swell ratio of 3.8 ± 0.3 when comparing the swollen film mass to the freshly UV-cured film (Appendix C.1). This is about three times the film's mass in water uptake.

4.3.6 Anti-Fog Testing

To test the anti-fog ability in more grueling conditions, we chilled samples well below 0°C and exposed them to humid air. In Figure 4.6, polycarbonate and anti-fog samples were chilled to -10°C and then breathed on. Fog formation was entirely prevented on coated samples and they were entirely transparent to the printed letters
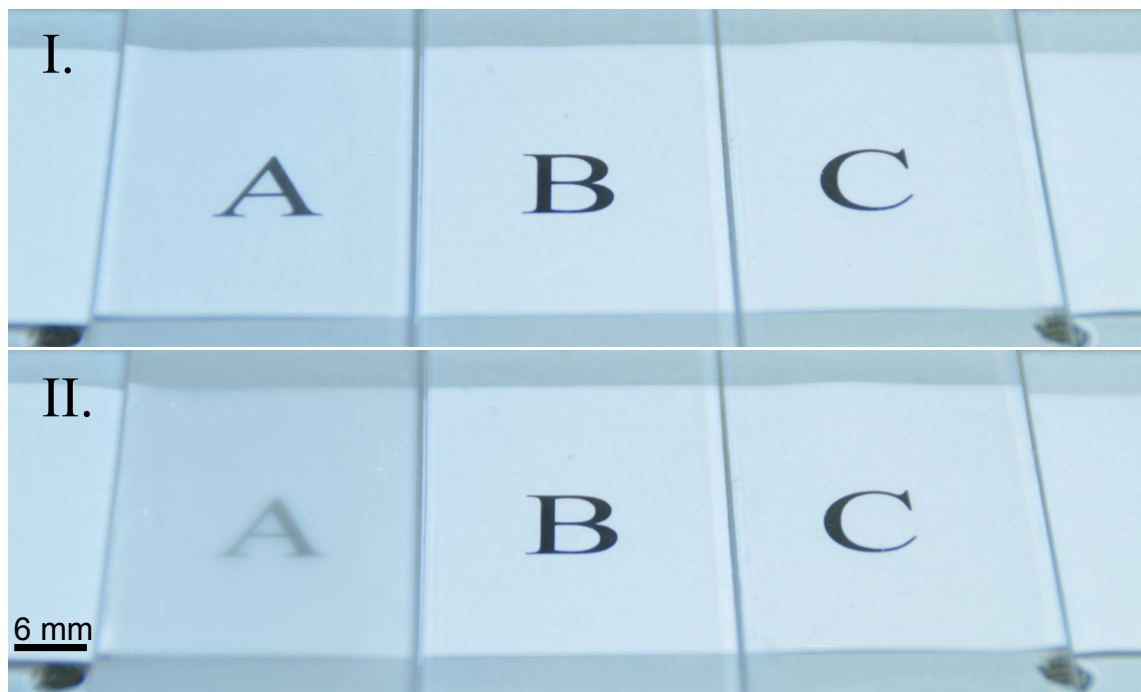
Figure 4.6: Comparison of uncoated polycarbonate (A), Anti-fog (B), and Plasma + Linker + 6 h F_{17} Easy-Clean Anti-fog (C) performance. Frame I shows the slides on a -10°C Peltier plate. Frame II shows the cooled slides after exposure to moist breath. The easy-clean treatment does not harm its anti-fog performance (Section 4.4).

beneath. Additionally, we spray coated lab safety glasses (Methods 4.2.3.2) on both sides of the lenses for a real world test. We set our laboratory freezer to -15°C (34% relative humidity) and placed coated and uncoated glasses inside for 5 minutes. We did not observe any opaque areas on the coated lenses, indicating no frozen water in the coating. After removing both glasses to atmospheric lab conditions (22°C and 45% relative humidity), the cold, uncoated lenses fogged up thoroughly, while the anti-fog lenses were

perfectly transparent (Figure 4.7). This same effect is experienced while entering and exiting a -20°C walk-in laboratory freezer. It saves the user much frustration by providing clear visibility, while untreated lenses inhibit workflow.
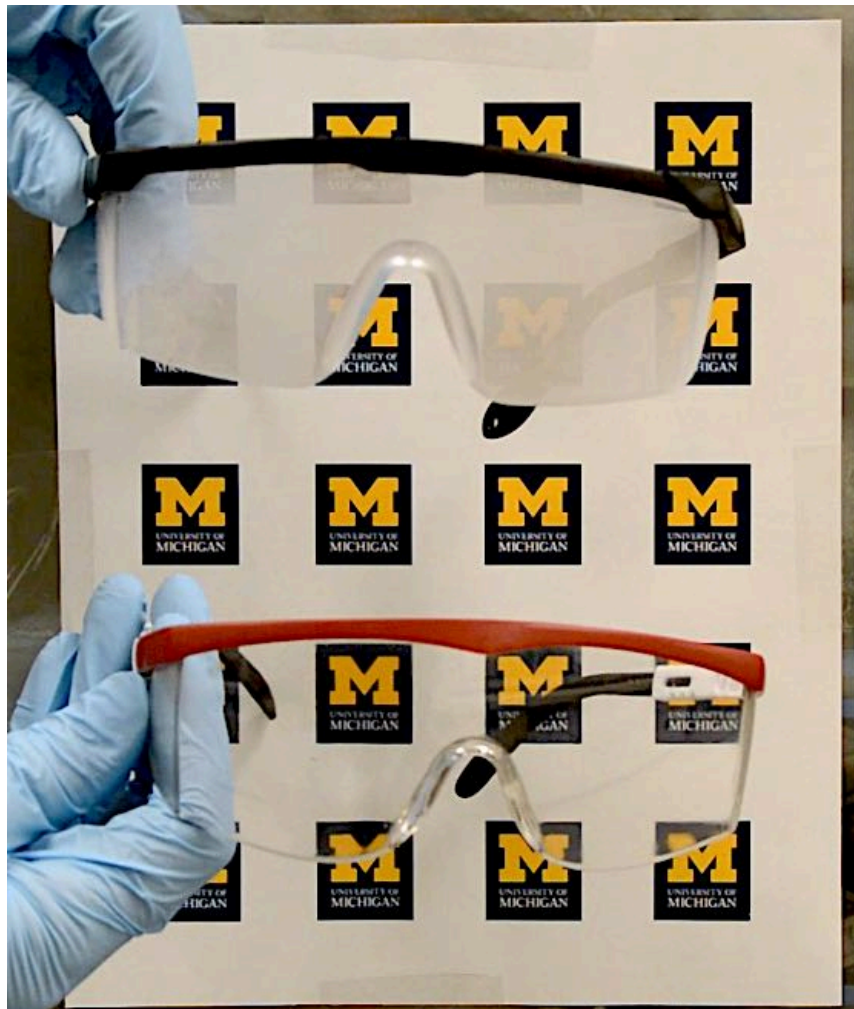
Figure 4.7: Anti-fog coating on safety glasses. Polycarbonate safety glasses were placed in a freezer at -15°C (34% relative humidity) for 5 minutes and removed to a room temperature of 22°C and 45% relative humidity. The top pair of glasses is untreated, while the bottom is coated inside and out.

4.4 Easy-Clean, Oil Repellent Modification

The final performance hurdle was providing the anti-fog coating with oil repellency and easy-clean abilities. The functionalization must be performed in a way

that oil repellency will remain after rinsing with cleaning solvent (ethanol) and fingerprint testing (Methods 4.2.11). As described earlier, low energy silanes are an effective means of robustly lowering surface energy.[60] We studied how to effectively apply (heptadecafluoro-1,1,2,2-tetrahydrodecyl) triethoxysilane to the anti-fog coating and analyzed its easy-clean property. As described in the methods, the first rendition utilized low energy oxygen plasma to oxidize the surface and increase its reactivity to the vapor-phase reaction of the fluoro-silane. This achieved $75 \pm 2°$ advancing and $41 \pm 5°$ receding angles with dodecane (still anti-fogging), but after rinsing with ethanol and drying with nitrogen, the angles reduced to $32 \pm 11°$ advancing and no receding (see Table 4.2 for the angles of all fluoro-silanization procedures). With no oil receding angle, the oil cannot be readily removed from the surface, and this indicates that the silane rinses off and is not bonded well.

To enhance bonding, a dipodal linker silane (bis(3-trimethoxysilylpropyl) amine) primer was applied before the fluoro-silane (Methods 4.2.4.1). This achieved $54 \pm 3°$ advancing and $44 \pm 1°$ receding angles with dodecane (remains anti-fogging), and after rinsing with ethanol and drying with nitrogen, the angles were still $30 \pm 3°$ and $18 \pm 1°$, respectively. Accordingly, it showed a 10 μL dodecane droplet sliding angle of $6 \pm 1°$, and even a 2 μL dodecane droplet could slide at $37 \pm 6°$ (Table 4.3). The predicted sliding angles were calculated using the Furmidge equation (Appendix C.2).[61] This surface is a form of a low angle, low hysteresis surface where oil droplets can be shed despite low contact angles. This Linker + 6 h F_{17} Anti-fog system allowed for easier fingerprint cleaning as shown in Figure 4.8 (b, e, h). Fingerprints could be entirely removed from this surface using a microfiber cleaning cloth attachment with the Taber®

Table 4.2: Variations of easy-clean, anti-fog coatings: Contact angles before and after ethanol rinsing

Sample	Unrinsed					
	Water			Dodecane		
	Advancing	Receding	Static	Advancing	Receding	Static
Plasma + 6 h F_{17} silane (no Silane Linker)	149 ± 4°	0 ± 0°	106 ± 6°	75 ± 2°	41 ± 5°	72 ± 1°
Silane Linker + 6 h F_{17} silane (no Plasma)	141 ± 2°	0 ± 0°	98 ± 1°	54 ± 3°	44 ± 1°	53 ± 2°
Plasma + Silane Linker + 6 h F_{17} silane	143 ± 4°	0 ± 0°	108 ± 1°	60 ± 1°	47 ± 2°	58 ± 1°

Sample	Ethanol Rinsed					
	Water			Dodecane		
	Advancing	Receding	Static	Advancing	Receding	Static
Plasma + 6 h F_{17} silane (no Silane Linker)	83 ± 6°	0 ± 0°	36 ± 3°	32 ± 11°	0 ± 0°	28 ± 9°
Silane Linker + 6 h F_{17} silane (no Plasma)	126 ± 5°	0 ± 0°	86 ± 3°	30 ± 3°	18 ± 1°	25 ± 3°
Plasma + Silane Linker + 6 h F_{17} silane	138 ± 3°	0 ± 0°	108 ± 2°	41 ± 1°	27 ± 2°	37 ± 1°

Table 4.3: Variations of easy-clean, anti-fog coatings: Dodecane sliding angles after rinsing

Sample	Ethanol Rinsed, 10 μL Dodecane Sliding (°)	Predicted 10 μL Sliding Angle (°)	Ethanol Rinsed, 2 μL Dodecane Sliding (°)	Predicted 2 μL Sliding Angle (°)
Plasma + 6 h F_{17} silane (no Silane Linker)	No sliding, pinned	-	No sliding, pinned	-
Silane Linker + 6 h F_{17} silane (no Plasma)	6 ± 1°	11 ± 4°	37 ± 6°	32 ± 12°
Plasma + Silane Linker + 6 h F_{17} silane	11 ± 1°	17 ± 2°	40 ± 8°	27 ± 6°

Industries 5750 Linear Abraser (Methods 4.2.11), while the standard anti-fog coating

remained smudged with fingerprint oil. This system's downfall was that after three

fingerprint cleaning tests, the dodecane contact angles reduced to 19 ± 3° advancing
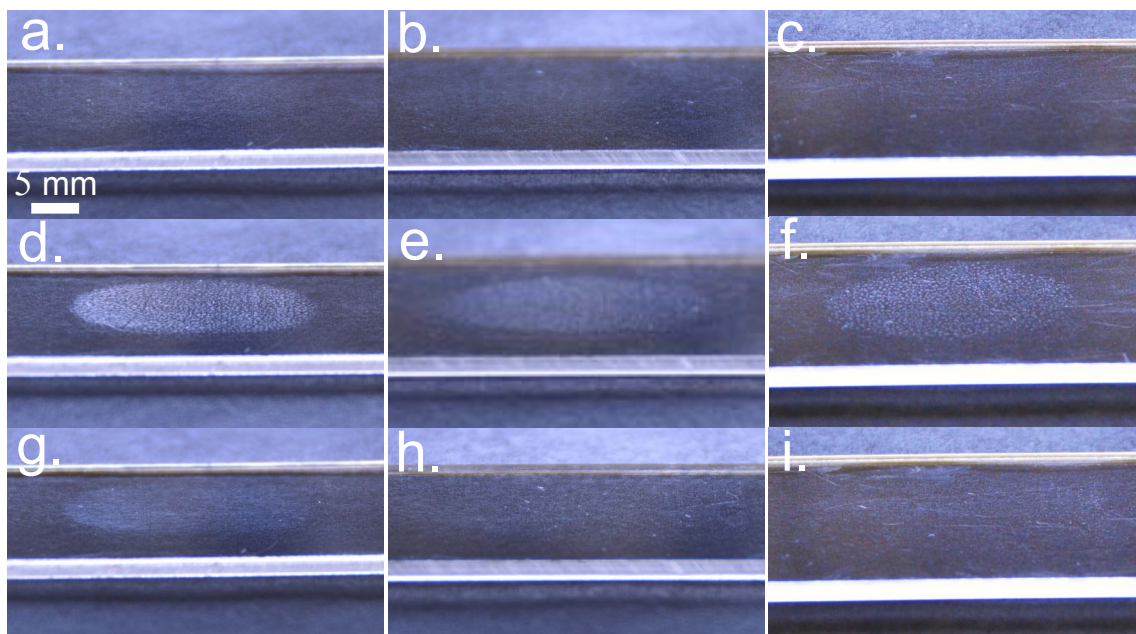
Figure 4.8: Anti-fog and easy-clean anti-fog coatings fingerprint tests. (a-c) The clean coated slides, where the left column is the anti-fog coating, the middle column is the Linker + 6 h F_{17} Anti-fog, and the right column is the Plasma + Linker + 6 h F_{17} Anti-fog coating. (d-f) An oily fingerprint is applied to each slide. After our standard microfiber-wiping test, a smudged fingerprint remains on the anti-fog coating (g), while the print is cleanly removed on the two easy-clean variations (h-i).

Table 4.4: Easy-clean, anti-fog coating durability (after 3 fingerprint, FP, tests) with and without oxygen plasma before the silane linker

Sample	Rinsed, Dodecane Angles			Dodecane Angles after 3 FP tests			After 3 FP tests, 10 µL Dodecane Sliding Angles (°)	Predicted 10 µL Sliding Angle (°)
	Adv.	Rec.	Static	Adv.	Rec.	Static		
Silane Linker + 6 h F_{17} silane	30 ± 3°	18 ± 1°	25 ± 3°	19 ± 3°	0 ± 0°	14 ± 1°	No sliding, pinned	-
Plasma + Silane Linker + 6 h F_{17} silane	41 ± 1°	27 ± 2°	37 ± 1°	32 ± 1°	16 ± 1°	28 ± 2°	10 ± 2°	15 ± 2°

and no receding (or sliding) as listed in Table 4.4.

To remedy this low durability, our final system was Plasma + Silane Linker + 6 h F_{17} silane, where oxygen plasma treatment of the anti-fog coating preceded the silane linker primer. $60 \pm 1°$ advancing and $47 \pm 2°$ receding angles with dodecane (still anti-fogging, Figure 4.6) were attained, and after rinsing with ethanol and drying with nitrogen, the angles were still $41 \pm 1°$ and $27 \pm 2°$, respectively. Accordingly, it showed a 10 µL dodecane droplet sliding angle of $11 \pm 1°$ (Figure 4.9a-c), and a 2 µL dodecane droplet could slide at $40 \pm 8°$ (Figure 4.9d-f). The easy-clean ability is demonstrated in Figure 4.8 (c, f, i), and after three fingerprint tests, dodecane could advance at $32 \pm 1°$, recede at $16 \pm 1°$, and slide at $10 \pm 2°$ (Table 4.4). After three fingerprint (FP) tests, only
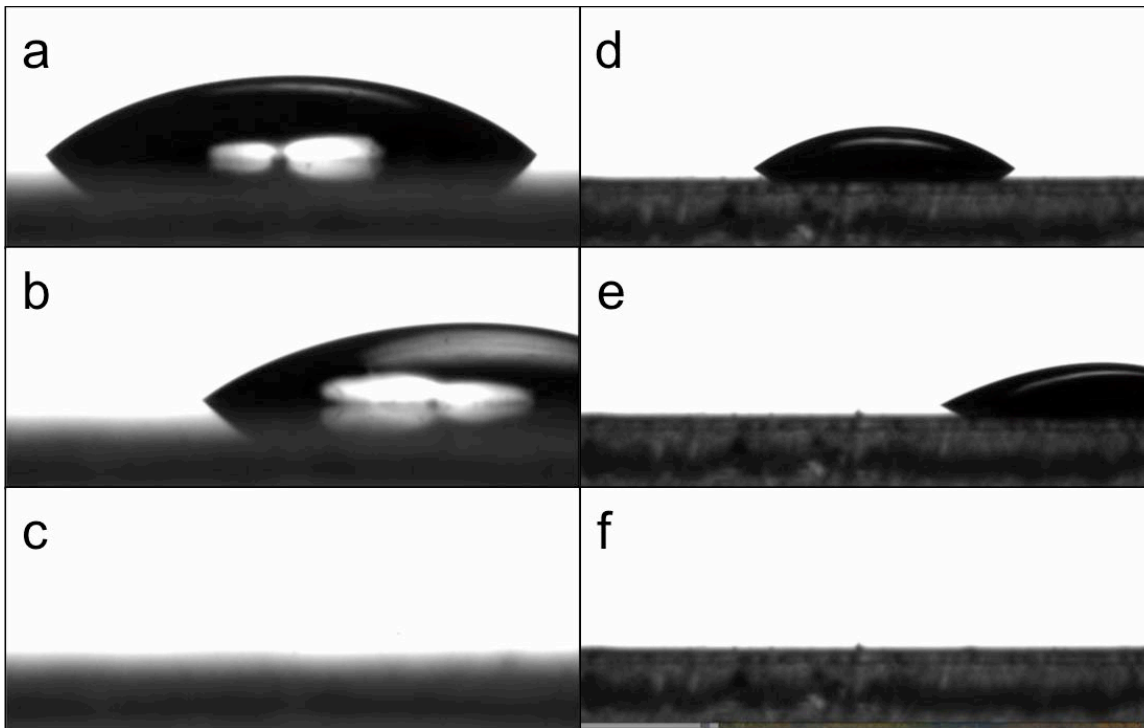
Figure 4.9: 10 and 2 µL dodecane droplets sliding on an ethanol rinsed, Plasma + Silane Linker + 6 h F_{17} easy-clean anti-fog coating. (a-c) The 10 µL droplet sliding angle is 11° here, and it cleanly leaves the surface without pearling or any satellite drops left behind. (d-f) The 2 µL droplet sliding angle is 42° here, and it also cleanly leaves the surface without pearling or any satellite drops left behind.

samples treated with oxygen plasma before the silane linker and then fluoro-silane maintained dodecane receding and sliding angles. The surface functionalization was too damaged on the other surfaces to maintain easy-clean properties.

The longevity of our easy-clean anti-fog coating was achieved through a combination of oxygen plasma, a silane linker, and fluoro-silane deposition. This yielded a surface that could be cleaned with alcohol and a cleaning cloth repeatedly without losing its oil repellency. The easy-clean modification of the surface was found to not hinder the transparency or the anti-fog property, as shown in Figures 4.4a and 4.6 respectively.

4.5 Conclusion

In conclusion, an anti-fog coating was developed that covalently bonds to polycarbonate, as well as polystyrene, for providing superior fog prevention of safety glasses and other transparent polycarbonate sheeting, even at low temperatures. The TMPTA cross-linker yields a stable, adhered film capable of being cleaned/rubbed with common lens cleaning solvents without damage or inhibition of performance. The hydrophilic, cross-linked PVP successfully prevents frost formation in the coating and water wets it in a filmwise mode to prevent fog at warmer, everyday conditions. This transparent, one-step UV-curable polymer system can be spray coated onto flat or curved surfaces without difficulty. The ability to post-treat the anti-fog coating with our easy-clean methodology further enhances the coating performance by ready removal of oily contaminants such as fingerprints. We expect this coating to be readily implementable and scalable for commercial use.

4.6 References

1. Briscoe, B. J.; Galvin, K. P., The effect of surface fog on the transmittance of light. *Sol. Energy* **1991,** *46* (4), 191-197. 10.1016/0038-092X(91)90063-3

2. Grube, S.; Siegmann, K.; Hirayama, M., A moisture-absorbing and abrasion-resistant transparent coating on polystyrene. *J. Coat. Technol. Res.* **2015,** *12* (4), 669-680. 10.1007/s11998-015-9678-z

3. Grosu, G.; Andrzejewski, L.; Veilleux, G.; Ross, G. G., Relation between the size of fog droplets and their contact angles with CR39 surfaces. *J. Phys. D: Appl. Phys.* **2004,** *37* (23), 3350. 10.1088/0022-3727/37/23/019

4. Young, T., An Essay on the Cohesion of Fluids. *Phil. Trans. R. Soc. Lond.* **1805,** *95*, 65-87. 10.1098/rstl.1805.0005

5. Wenzel, R. N., Resistance of Solid Surfaces to Wetting by Water. *Ind. Eng. Chem.* **1936,** *28*, 988-994. 10.1021/ie50320a024

6. McHale, G.; Shirtcliffe, N. J.; Aqil, S.; Perry, C. C.; Newton, M. I., Topography Driven Spreading. *Phys. Rev. Lett.* **2004,** *93* (3), 036102. 10.1103/PhysRevLett.93.036102

7. Wang, R.; Hashimoto, K.; Fujishima, A.; Chikuni, M.; Kojima, E.; Kitamura, A.; Shimohigoshi, M.; Watanabe, T., Photogeneration of Highly Amphiphilic TiO$_2$ Surfaces. *Adv. Mater.* **1998,** *10* (2), 135-138. 10.1002/(SICI)1521-4095(199801)10:2<135::AID-ADMA135>3.0.CO;2-M

8. Guan, K.; Lu, B.; Yin, Y., Enhanced effect and mechanism of SiO2 addition in super-hydrophilic property of TiO2 films. *Surf. Coat. Technol.* **2003,** *173* (2), 219-223. 10.1016/S0257-8972(03)00521-8

9. Liu, H.; Feng, L.; Zhai, J.; Jiang, L.; Zhu, D., Reversible Wettability of a Chemical Vapor Deposition Prepared ZnO Film between Superhydrophobicity and Superhydrophilicity. *Langmuir* **2004,** *20* (14), 5659-5661. 10.1021/la036280o

10. Min, N.; Patel, P.; Kai, S.; Meng, D. D. In *Superhydrophilic anti-fog polyester film by oxygen plasma treatment*, 2009 4th IEEE International Conference on Nano/Micro Engineered and Molecular Systems, 5-8 Jan. 2009; 2009; pp 1017-1020. 10.1109/NEMS.2009.5068746

11. Huang, K.-T.; Yeh, S.-B.; Huang, C.-J., Surface Modification for Superhydrophilicity and Underwater Superoleophobicity: Applications in Antifog, Underwater Self-Cleaning, and Oil–Water Separation. *ACS Appl. Mater. Interfaces* **2015,** *7* (38), 21021-21029. 10.1021/acsami.5b07362

12. Ogawa, T.; Murata, N.; Yamazaki, S., Development of Anti-Fogging Mirror Coated with SiO$_2$-ZrO$_2$-Colloidal SiO$_2$ Film by the Sol-Gel Process. *J. Sol-Gel Sci. Technol.* **2003,** *27* (2), 237-238. 10.1023/A:1023719105484

13. Tadanaga, K.; Morinaga, J.; Minami, T., Formation of Superhydrophobic-Superhydrophilic Pattern on Flowerlike Alumina Thin Film by the Sol-Gel Method. *J. Sol-Gel Sci. Technol.* **2000,** *19* (1), 211-214. 10.1023/A:1008732204421

14. Huang, W.; Chen, Y.; Yang, C.; Situ, Y.; Huang, H., pH-driven phase separation: Simple routes for fabricating porous TiO$_2$ film with superhydrophilic and anti-fog properties. *Ceram. Int.* **2015,** *41* (6), 7573-7581. 10.1016/j.ceramint.2015.02.081

15. Song, K.-C.; Park, J.-K.; Kang, H.-U.; Kim, S.-H., Synthesis of Hydrophilic Coating Solution for Polymer Substrate Using Glycidoxypropyltrimethoxysilane. *J. Sol-Gel Sci. Technol.* **2003,** *27* (1), 53-59. 10.1023/A:1022679910313

16. Di Mundo, R.; d'Agostino, R.; Palumbo, F., Long-Lasting Antifog Plasma Modification of Transparent Plastics. *ACS Appl. Mater. Interfaces* **2014,** *6* (19), 17059-17066. 10.1021/am504668s

17. Yonghao, X.; Yan, L.; Dennis, W. H.; Wong, C. P., Mechanically robust superhydrophobicity on hierarchically structured Si surfaces. *Nanotechnology* **2010,** *21* (15), 155705. 10.1088/0957-4484/21/15/155705

18. Plasman, V.; Caulier, T.; Boulos, N., Polyglycerol esters demonstrate superior antifogging properties for films. *Plast. Additives Compound.* **2005,** *7* (2), 30-33. 10.1016/S1464-391X(05)00359-4

19. Li, F.; Biagioni, P.; Bollani, M.; Maccagnan, A.; Piergiovanni, L., Multi-functional coating of cellulose nanocrystals for flexible packaging applications. *Cellulose* **2013,** *20* (5), 2491-2504. 10.1007/s10570-013-0015-3

20. England, M. W.; Urata, C.; Dunderdale, G. J.; Hozumi, A., Anti-Fogging/Self-Healing Properties of Clay-Containing Transparent Nanocomposite Thin Films. *ACS Appl. Mater. Interfaces* **2016,** *8* (7), 4318-4322. 10.1021/acsami.5b11961

21. Introzzi, L.; Fuentes-Alventosa, J. M.; Cozzolino, C. A.; Trabattoni, S.; Tavazzi, S.; Bianchi, C. L.; Schiraldi, A.; Piergiovanni, L.; Farris, S., "Wetting Enhancer" Pullulan Coating for Antifog Packaging Applications. *ACS Appl. Mater. Interfaces* **2012,** *4* (7), 3692-3700. 10.1021/am300784n

22. Cebeci, F. Ç.; Wu, Z.; Zhai, L.; Cohen, R. E.; Rubner, M. F., Nanoporosity-Driven Superhydrophilicity: A Means to Create Multifunctional Antifogging Coatings. *Langmuir* **2006,** *22* (6), 2856-2862. 10.1021/la053182p

23. Chevallier, P.; Turgeon, S.; Sarra-Bournet, C.; Turcotte, R.; Laroche, G., Characterization of Multilayer Anti-Fog Coatings. *ACS Appl. Mater. Interfaces* **2011,** *3* (3), 750-758. 10.1021/am1010964

24. Florea-Spiroiu, M.; Achimescu, D.; Stanculescu, I.; Purica, M.; Gavrila, R.; Peretz, S., Anti-fog chitosan/sodium lauryl ether sulfate films. *Polym. Bull.* **2013,** *70* (12), 3305-3316. 10.1007/s00289-013-1023-z

25. Nuraje, N.; Asmatulu, R.; Cohen, R. E.; Rubner, M. F., Durable Antifog Films from Layer-by-Layer Molecularly Blended Hydrophilic Polysaccharides. *Langmuir* **2011,** *27* (2), 782-791. 10.1021/la103754a

26. Lee, H.; Alcaraz, M. L.; Rubner, M. F.; Cohen, R. E., Zwitter-Wettability and Antifogging Coatings with Frost-Resisting Capabilities. *ACS Nano* **2013,** *7* (3), 2172-2185. 10.1021/nn3057966

27. Yuan, Y.; Liu, R.; Wang, C.; Luo, J.; Liu, X., Synthesis of UV-curable acrylate polymer containing sulfonic groups for anti-fog coatings. *Prog. Org. Coat.* **2014,** *77* (4), 785-789. 10.1016/j.porgcoat.2014.01.001

28. Tang, R.; Muhammad, A.; Yang, J.; Nie, J., Preparation of antifog and antibacterial coatings by photopolymerization. *Polym. Adv. Technol.* **2014,** *25* (6), 651-656. 10.1002/pat.3267

29. Chang, C.-C.; Huang, F.-H.; Chang, H.-H.; Don, T.-M.; Chen, C.-C.; Cheng, L.-P., Preparation of Water-Resistant Antifog Hard Coatings on Plastic Substrate. *Langmuir* **2012,** *28* (49), 17193-17201. 10.1021/la304176k

30. Belhadjamor, M.; El Mansori, M.; Belghith, S.; Mezlini, S., Anti-fingerprint properties of engineering surfaces: a review. *Surf. Eng.* **2018,** *34* (2), 85-120. 10.1080/02670844.2016.1258449

31. Fiore, D.; Wilson, B. In *Hydrophobic and oleophobic coating technologies for polymer optics*, SPIE Optical Engineering + Applications, SPIE: 2012; p 7.

32. Uhlmann, P.; Frenzel, R.; Voit, B.; Mock, U.; Szyszka, B.; Schmidt, B.; Ondratschek, D.; Gochermann, J.; Roths, K., Research agenda surface technology: Future demands for research in the field of coatings materials. *Prog. Org. Coat.* **2007,** *58* (2), 122-126. 10.1016/j.porgcoat.2006.08.020

33. Tuteja, A.; Choi, W.; Ma, M.; Mabry, J. M.; Mazzella, S. A.; Rutledge, G. C.; McKinley, G. H.; Cohen, R. E., Designing superoleophobic surfaces. *Science* **2007,** *318* (5856), 1618-22. 10.1126/science.1148326

34. Bellanger, H.; Darmanin, T.; Guittard, F., Surface Structuration (Micro and/or Nano) Governed by the Fluorinated Tail Lengths toward Superoleophobic Surfaces. *Langmuir* **2012,** *28* (1), 186-192. 10.1021/la2034356

35. Liu, T. L.; Kim, C.-J. C., Turning a surface superrepellent even to completely wetting liquids. *Science* **2014,** *346* (6213), 1096. 10.1126/science.1254787

36. Michael, N.; Bhushan, B., Hierarchical roughness makes superhydrophobic states stable. *Microelectron. Eng.* **2007,** *84* (3), 382-386. 10.1016/j.mee.2006.10.054

37. Nakajima, A.; Fujishima, A.; Hashimoto, K.; Watanabe, T., Preparation of Transparent Superhydrophobic Boehmite and Silica Films by Sublimation of Aluminum Acetylacetonate. *Adv. Mater.* **1999,** *11* (16), 1365-1368. 10.1002/(SICI)1521-4095(199911)11:16<1365::AID-ADMA1365>3.0.CO;2-F

38. Cheng, D. F.; Urata, C.; Yagihashi, M.; Hozumi, A., A Statically Oleophilic but Dynamically Oleophobic Smooth Nonperfluorinated Surface. *Angew. Chem. Int. Ed.* **2012,** *51* (12), 2956-2959. 10.1002/anie.201108800

39. Fadeev, A. Y.; McCarthy, T. J., Trialkylsilane Monolayers Covalently Attached to Silicon Surfaces: Wettability Studies Indicating that Molecular Topography Contributes to Contact Angle Hysteresis. *Langmuir* **1999,** *15* (11), 3759-3766. 10.1021/la981486o

40. Scruton, B.; Robins, B. W.; Blott, B. H., The deposition of fingerprint films. *J. Phys. D: Appl. Phys.* **1975,** *8* (6), 714.

41. Wu, L. Y. L.; Ngian, S. K.; Chen, Z.; Xuan, D. T. T., Quantitative test method for evaluation of anti-fingerprint property of coated surfaces. *Appl. Surf. Sci.* **2011,** *257* (7), 2965-2969. 10.1016/j.apsusc.2010.10.101

42. Wang, G.; Wang, H.; Guo, Z., A robust transparent and anti-fingerprint superhydrophobic film. *Chem. Commun.* **2013,** *49* (66), 7310-7312. 10.1039/C3CC43677B

43. Chang, S. W.; Chen, C. M.; He, J. L., Power Modulated Plasma-Polymerized Anti-Fingerprint Transparent Protective Coating with a Gradient Composition. *Adv. Mater. Res.* **2012,** *509*, 132-134. 10.4028/www.scientific.net/AMR.509.132

44. Rabnawaz, M.; Liu, G., Graft-Copolymer-Based Approach to Clear, Durable, and Anti-Smudge Polyurethane Coatings. *Angew. Chem. Int. Ed.* **2015,** *54* (22), 6516-6520. 10.1002/anie.201501360

45. Macoretta, D.; Rabnawaz, M.; Grozea, C. M.; Liu, G.; Wang, Y.; Crumblehulme, A.; Wyer, M., Clear Antismudge Unimolecular Coatings of Diblock Copolymers on Glass Plates. *ACS Appl. Mater. Interfaces* **2014,** *6* (23), 21435-21445. 10.1021/am5064348

46. Kondo, H.; Sungkil, L.; Hanaoka, H., Durable Anti-Smudge Materials for Display Terminals. *Tribol. T.* **2008,** *52* (1), 29-35. 10.1080/10402000802044357

47.   Howarter, J. A.; Youngblood, J. P., Self-Cleaning and Anti-Fog Surfaces via Stimuli-Responsive Polymer Brushes. *Adv. Mater.* **2007,** *19* (22), 3838-3843. 10.1002/adma.200700156

48.   Brown, P. S.; Atkinson, O. D. L. A.; Badyal, J. P. S., Ultrafast Oleophobic–Hydrophilic Switching Surfaces for Antifogging, Self-Cleaning, and Oil–Water Separation. *ACS Appl. Mater. Interfaces* **2014,** *6* (10), 7504-7511. 10.1021/am500882y

49.   Wang, Y.; Dong, Q.; Wang, Y.; Wang, H.; Li, G.; Bai, R., Investigation on RAFT Polymerization of a Y‑Shaped Amphiphilic Fluorinated Monomer and Anti‑Fog and Oil‑Repellent Properties of the Polymers. *Macromol. Rapid Commun.* **2010,** *31* (20), 1816-1821. 10.1002/marc.201000243

50.   Kesmez, Ö.; Tamsü Selli, N.; Tunali, A.; Akarsu, E.; Akarsu, M.; Arpaç, E., Fingerprint resistant coatings for stainless steel substrates. *Prog. Org. Coat.* **2017,** *112*, 51-56. 10.1016/j.porgcoat.2017.07.003

51.   Rabnawaz, M.; Liu, G.; Hu, H., Fluorine-Free Anti-Smudge Polyurethane Coatings. *Angew. Chem. Int. Ed.* **2015,** *54* (43), 12722-12727. 10.1002/anie.201504892

52.   Siriviriyanun, A.; Imae, T., Anti-fingerprint properties of non-fluorinated organosiloxane self-assembled monolayer-coated glass surfaces. *Chem. Eng. J.* **2014,** *246*, 254-259. 10.1016/j.cej.2014.02.066

53.   Thomas, G. L., The physics of fingerprints and their detection. *J. Phys. E: Sci. Instrum.* **1978,** *11* (8), 722.

54.   Wolfe, J.; Bryant, G.; Koster, K. L., What is 'unfreezable water', how unfreezable is it and how much is there? *Cryoletters* **2002,** *23* (3), 157-166.

55.   Ping, Z. H.; Nguyen, Q. T.; Chen, S. M.; Zhou, J. Q.; Ding, Y. D., States of water in different hydrophilic polymers — DSC and FTIR studies. *Polymer* **2001,** *42* (20), 8461-8467. 10.1016/S0032-3861(01)00358-5

56.   Hatakeyama, H.; Hatakeyama, T., Interaction between water and hydrophilic polymers. *Thermochim. Acta* **1998,** *308* (1), 3-22. 10.1016/S0040-6031(97)00325-0

57.   Krumova, M.; López, D.; Benavente, R.; Mijangos, C.; Pereña, J. M., Effect of crosslinking on the mechanical and thermal properties of poly(vinyl alcohol). *Polymer* **2000,** *41* (26), 9265-9272. 10.1016/S0032-3861(00)00287-1

58.   Schwartz, C. J.; Bahadur, S.; Mallapragada, S. K., Effect of crosslinking and Pt–Zr quasicrystal fillers on the mechanical properties and wear resistance of UHMWPE for use in artificial joints. *Wear* **2007,** *263* (7), 1072-1080. 10.1016/j.wear.2006.10.023

59.	Aran, K.; Sasso, L. A.; Kamdar, N.; Zahn, J. D., Irreversible, direct bonding of nanoporous polymer membranes to PDMS or glass microdevices. *Lab Chip* **2010,** *10* (5), 548-552. 10.1039/B924816A

60.	Lessel, M.; Bäumchen, O.; Klos, M.; Hähl, H.; Fetzer, R.; Paulus, M.; Seemann, R.; Jacobs, K., Self‐assembled silane monolayers: an efficient step‐by‐step recipe for high‐quality, low energy surfaces. *Surf. Interface Anal.* **2015,** *47* (5), 557-564. 10.1002/sia.5729

61.	Furmidge, C. G. L., Studies at phase interfaces. I. The sliding of liquid drops on solid surfaces and a theory for spray retention. *J. Colloid Sci.* **1962,** *17* (4), 309-324. 10.1016/0095-8522(62)90011-9

CHAPTER 5

Actuatable Membrane Enabled Freeze Concentration

This chapter contains work adapted from a first author article pending publication. Rishabh Tennankore assisted with experiments.

5.1 Introduction

Frozen concentrated fruit juices generated $1.19 billion in revenue in the United States in 2017 and was 37.1% of the total frozen fruit market.[1] In order to concentrate fruit juice, low pressure and high temperatures in an evaporator are commonly used to remove a large fraction of the water. Unfortunately, this evaporation step removes volatile components associated with good aroma and flavor. A percentage of fresh juice can be added back to help recover desirable flavor.[2] Freeze concentration is an alternative to evaporation for water removal. By utilizing low temperatures, heat sensitive and volatile components are not lost or damaged for better taste, aroma, and nutrition.[3] The process works by chilling a solution in a controlled manner to nucleate ice crystals that do not trap the desirable solutes, such as juice sugar molecules.[4-6] Furthermore, removing water in the form of ice is much more energy efficient than vapor due to its heat of fusion = 6.008 J/mol being much lower than its heat of vaporization = 40.66 J/mol.[7] Pre-concentration of wastewater prior to incineration can achieve a 77% energy savings.[8] This approach has been researched and utilized for several industrial applications

143

including: desalination, fruit juices and food, *p*-xylene production, paper processing, wastewater treatment, and brewing.[4, 7-12]

The two most important unit operations in the freeze concentration process are the crystallizer and the separator, which control the freezing process and the subsequent ice crystal removal from the concentrate.[7] By carefully cooling the solution, ice crystals nucleate and grow while excluding the valuable solutes, such as sugars, without homogeneously freezing the solution at the eutectic temperature. An indirect chiller system is preferred so that the product is never in contact with the refrigerant. As this process continues, the solution freezing point continues to decrease as the solutes concentrate, so lower temperatures are required to continue increasing the concentration.
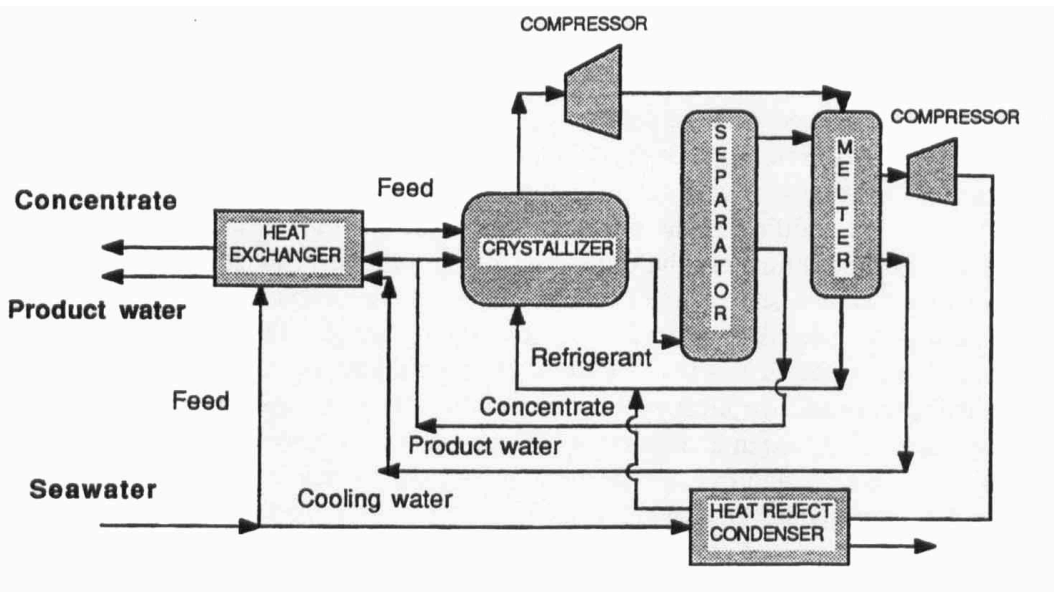
Figure 5.1: A typical freeze concentration process flow diagram.[7]

To limit solute entrainment and ease the mechanical separation of ice crystals, larger ice crystals are preferred due to lower surface area per mass and greater diameter. This can be accomplished by using lower subcooling, which promotes crystal growth, instead of nucleation, and lower surface area disk shapes versus needles/dendrites.[5-6] To

initiate crystallization, a small seed crystal of ice is often added. The two main modes of crystallization are suspension crystallization, in which crystals grow in solution by Ostwald ripening, and progressive freeze concentration, where ice grows on a chilled surface.[4, 13] After crystallization, the separator unit operation mechanically removes the ice from the liquid concentrate using presses, centrifuges, and wash columns[8-9] for suspensions or scraped-surface heat exchangers for progressive freeze concentration[7], which are expensive. A process diagram for a typical industrial freeze concentration system is shown in Figure 5.1.

In this work, a methodology integrating the crystallizer and separator unit operations into one freeze concentration system was developed. This is made possible by understanding liquid breakthrough pressure on a porous, liquid-repellent surface and designing an actuatable membrane to be incorporated into the unit. The feed is held in the apparatus chamber, with an indirect cooling jacket to prevent product contamination, by a membrane with a breakthrough pressure greater than that of the feed's hydraulic pressure. With controlled subcooling and ice crystal seeding, ice progressively forms and the concentrate (i.e. mother liquor) is recovered by applying a differential pressure greater than the membrane's breakthrough pressure. This technique is utilized for the concentration of two valuable commodities, apple juice and ethanol, and dye to purify contaminated water.

5.2 Materials and Methods

5.2.1 Materials

Dimethyldimethoxysilane (SID4123.1) was purchased from Gelest. Tetraethyl orthosilicate (TEOS) and 200 proof ethanol were from Sigma-Aldrich. Isopropanol,

sulfuric acid, and Fast Green FCF dye were from Fisher Scientific. Kroger brand 100% Apple Juice was sourced at Kroger. Ethylene glycol, for the chiller, was from Dynalene, Inc. Whatman 114 (25 μm) wet-strengthened membranes were from GE Healthcare and 0.45 μm Durapore® Hydrophobic PVDF membranes were from EMD Millipore Corporation. A ½ HP Glycol Chiller was from Penguin Chillers (50 vol% ethylene glycol coolant), and two 0.6 kW cartridge heaters with a MS Lauda 1.1 kW immersion heater temperature controller (13 L/min flow rate) fine-tuned the coolant temperature. An SMC vacuum regulator (Model # IRV10-N07BG) was purchased from Grainger Industrial Supply. A high accuracy, vacuum range pressure transducer (PX409-015VV) and precision meter (DP25B) were from Omega Engineering.

5.2.2 Hydrophobic Whatman 114 Membranes

The Whatman 114 membranes were treated with 30 W oxygen plasma (Methods 5.2.4) for 20 min and then dipped in TEOS three times. Afterward, the membranes were dipped in a 10 wt% dimethlydimethoxysilane in isopropanol solution (1 wt% sulfuric acid) for 5 s.[14] Free solution was gently shaken off and the membrane was cured at 75°C for 10 min. The membranes were then rinsed with water, isopropanol, and then toluene. Lastly, nitrogen gas was used to dry the membranes and achieve a highly hydrophobic surface.

5.2.3 Breakthrough Pressure Testing

5.2.3.1 Apple Juice on Hydrophobic Whatman 114 (Methods 5.2.2)

0.5 mL of apple juice (1.1 cm) was added above the membrane and then vacuum was applied gradually, with a regulator, until the first drop of juice was pulled through the membrane by the pressure differential. The vacuum level at failure was noted and the

breakthrough pressure was calculated (95% confidence level uncertainty) based on the contributions from the vacuum and the short column of dodecane. This was repeated five times.

5.2.3.2 Ethanol Solution on 0.45 μm PVDF

The as-received membranes were tested in the same manner as in 5.2.3.1 with varying wt% ethanol solutions instead of apple juice.

5.2.4 Oxygen Plasma

A Harrick Plasma Cleaner (PDC-001) was used to apply 30 W oxygen plasma to the samples at 0.4 SCCM oxygen flow and 240 mTorr.

5.2.5 Refractive Index and Brix Measurements

Refractive index and Brix measurements were conducted using a Reichert r^2i300 refractometer. A few drops of liquid sample ($\approx$ 300 μL) were applied and six measurements were performed. All measurements occurred at room temperature (23.5 ± 0.3°C). The refractive index is accurate to ± 0.0001 and Brix is accurate to ± 0.1°.

5.2.6 UV-Vis Spectroscopy

The Fast Green FCF dye content in the water was measured using a Cary 50 Bio Ultraviolet-Visible spectrophotometer from 300 – 800 nm wavelengths. The peak of maximum absorbance was at 625 nm, and the peak area (calculated with Origin 2018b) was used with the calibration curve in Appendix D.4 to find the dye concentration (ppm).

5.2.7 Differential Scanning Calorimetry

The apple juice's freezing point was found using a TA Discovery differential scanning calorimeter (DSC). ~15 μL of the sample was frozen to -20°C and then thawed

to 20°C at a rate of 5°C/min. The heat flow into the sample was measured and the melting point was analyzed with TA Trios v4.1.1.33073 software.

5.2.8 Freeze Concentration Apparatus and Process Conditions

5.2.8.1 Apparatus Assembly

The top half of the apparatus consists of a custom-made freeze concentration chamber. It was made from a 19/22 Kimax 190 mm distillation condenser with a gasket fitting mounted at the base to hold a membrane in place (see Figure 5.3). A clamp holds a membrane and gasket between the top and bottom halves. The bottom is fitted with a vacuum port and a Teflon stopcock for liquid recovery. Tygon® tubing connects the chiller with 50 vol% ethylene glycol to the condenser. The chiller inlet is at the bottom, near the membrane, and the outlet is at the top of the column.

5.2.8.2 Apple Juice Freeze Concentration

After assembling the apparatus (Methods 5.2.8.1), 18.5 mL of apple juice (mass measured each time) was added to the condenser column, where the 20 cm tall column of liquid is held in place by the hydrophobic membrane at the bottom (Methods 5.2.2). The chiller ran continuously with the immersion heaters used to precisely tune the coolant temperature to ± 0.1°C. After equilibrating the system to -2.0°C, an ice crystal (formed from 10 μL deionized water droplets frozen on PVDF) was added to the top of the column, which was then covered to contain the system. This temperature was held for 1 h. The temperature was decreased to -3.0, -4.0, -5.0, -6.0, -7.0, -8.0, and -9.0°C, while holding the system at each temperature for 30 min. After the temperature program was completed, the chiller equipment was turned off and a vacuum pressure of 40.3 kPa was applied for 5 min to actuate the hydrophobic membrane and recover the liquid

concentrate from the column. After shutting off the vacuum, the permeate was recovered into a vial, of known mass, using the stopcock. The frozen retentate was allowed to melt and that too was recovered in a similar manner. The mass of each phase was recorded and 6 Brix measurements were performed on each phase after warming to room temperature.

5.2.8.3 Ethanol Freeze Concentration

After assembling the apparatus (Methods 5.2.8.1), 18 mL of 3.5 ± 0.2 wt% ethanol solution (mass measured each time) was added to the condenser column, where it was held in place by the 0.45 μm PVDF membrane at the bottom. The feed solution was prepared by mixing 7.5 ± 0.1 mL of 200 proof ethanol and 142.5 ± 0.7 mL of deionized water, and the actual concentration was precisely determined using refractive index and a calibration curve (see Appendix D.2). The freezing process used the same temperature program as the apple juice process, but the recovery and actuation processes differed. With the chiller at -9.0°C, the vacuum was set to 56.8 kPa. Next, the chiller was set back to -2°C to aid in recovering trapped permeate. After the chiller reached -2.0°C (a couple minutes), the vacuum was immediately increased to 70.8 kPa, at which liquid breakthrough occurred. To continue collecting permeate, the vacuum was returned to 56.8 kPa for 3.5 min to complete the recovery. After recovery, the phase masses were recorded and the refractive index was measured 6 times, after the liquids warmed to room temperature. The ethanol-in-water calibration curve (Appendix D.2) was used to determine permeate and retentate concentrations.

5.2.8.4 Dye Removal and Water Purification

After assembling the apparatus (Methods 5.2.8.1), 17 mL of 19.3 ± 0.1 ppm Fast Green FCF dye in water (mass measured each time) was added to the condenser column,

where it was held in place by the hydrophobic membrane at the bottom (Methods 5.2.2). The operating procedure was similar to 5.2.8.2, but the system was equilibrated at -0.4°C, seeded with a 10 μL ice crystal, and held for 42 min. At exactly 42 min, the membrane was actuated at 5.8 kPa vacuum pressure, while the chiller was set to 0°C. The bulk of the concentrate permeated in a few seconds and the adsorbed dye, on the surface of the ice, was washed into the concentrate with 0.75 mL of added water. After 1.25 min, the recovery was completed. The purified ice was collected and allowed to melt, before measuring the mass and testing both liquid phases with UV-Vis (Methods 5.2.6).

5.3 Apple Juice Concentration

Apple juice is one of several fruit products that can benefit from freeze concentration, due to superior aroma, taste, and nutrition from avoiding high processing temperatures and low pressures. The degree of concentration is quantified by degrees Brix (°Bx), which describes the soluble solids and is equal to the percentage of sucrose by weight, and can be measured by a refractometer.[4] The Kroger 100% Apple Juice was measured to be 11.8 ± 0.1°Bx, as received.

Our novel freeze concentration apparatus was designed to decrease the equipment unit operations and the number of processing steps by integrating both the crystallizer and separator. This was made possible by an actuatable hydrophobic membrane. The membrane holds the column of apple juice in the crystallizing chamber because the membrane's breakthrough pressure was greater than the hydrostatic pressure from the juice. The unconcentrated apple juice breakthrough pressure on the hydrophobic Whatman 114 was 6.7 ± 0.3 kPa (Methods 5.2.3.1) and the hydrostatic pressure was only 2.0 kPa. Furthermore, the breakthrough pressure was not so great that we could not

150

actuate the membrane with vacuum pressure. The combination of the hydrostatic pressure and vacuum pressure beneath the membrane exceeded the hydrophobic membrane breakthrough pressure to recover the concentrated apple juice permeate from the ice after completing the freezing process (Methods 5.2.8.2).

Our apparatus (Figure 5.2) is a type of progressive freeze concentrator where the ice begins nucleating at the seed ice crystal and continues to form along the chilled feed chamber walls. It is an indirect system so there is no contamination of the edible product from any coolant contact. The feed chamber's flared base near the membrane was filled with cross-linked PDMS (while leaving a cylindrical opening) to limit the "non-freezing" volume beneath the coolant level, which still contains 5 mL of solution from the 18.5 mL total feed volume. This dilutes the concentrate and is a limitation of the current equipment.
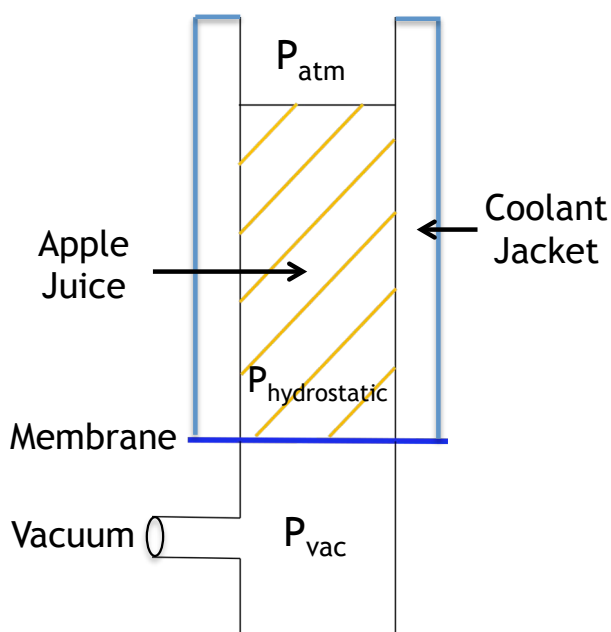
Figure 5.2: Actuatable Freeze Concentration Apparatus Diagram: Crystallizer and Separator

As discussed in Section 5.1, the freezing process is very important to the purity and form of ice crystals. In order to encourage the growth of larger and purer ice for greater recoveries of the concentrated apple juice, our freezing process began at -2°C (Methods 5.2.8.2) because it is higher than the bulk apple juice freezing point of -5.37°C (Appendix D.1), but cold enough to start growing ice upon the addition of a seed crystal.

151

The low degree of subcooling from the freezing point of water helps prevent the entrapment of the solutes through slower growth. For this reason, the system was kept at this initial temperature of -2°C for 1 hour versus 30 min for the remaining temperatures. As concentration occurred, the freezing point of the remaining liquid was depressed, so the temperature was decreased by one degree every half hour, after the initial 1 h at -2°C. Figure 5.3 shows the various stages in the freeze concentration process.

Tables 5.1 – 5.3 show the Brix measurements, mass and sugar content of each phase, and the % sugar recovered in the concentrate for three separate experiments. The
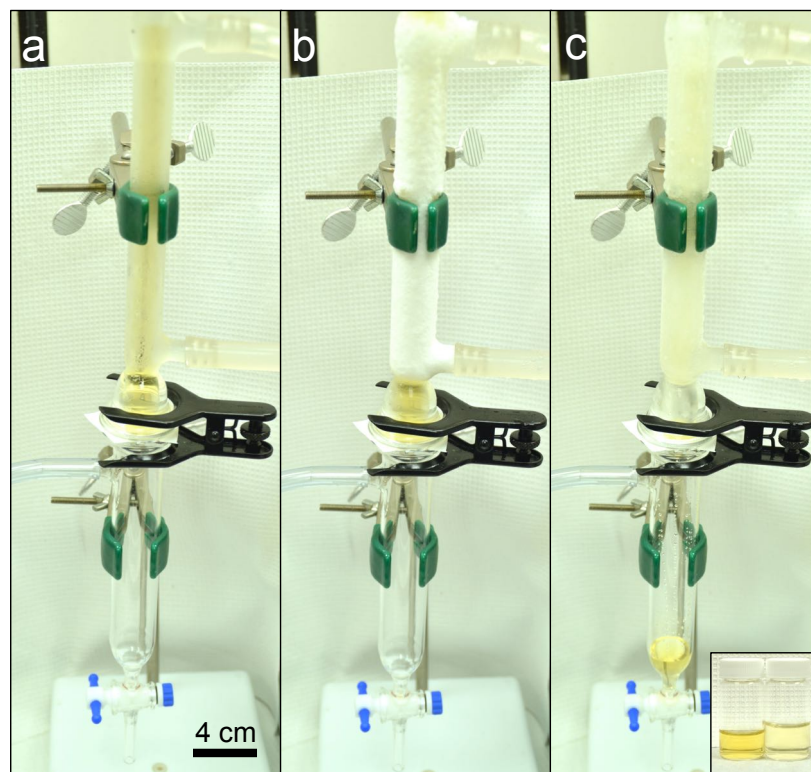
Figure 5.3: The actuatable freeze concentration apparatus. (a) The feed chamber is charged with apple juice and equilibrated at -2°C. (b) The end of the chiller program at -9°C, just before actuation and recovery of the permeate. Frost collected on the outside of the apparatus from moisture in the air. (c) The concentrate (permeate) was recovered in the lower half of the apparatus. The frost, on the outside, began melting with the chiller off. The inset shows the concentrate (darker yellow, left) and the retentate (right).

average concentration of the permeate was 19.8 ± 0.6°Bx, a 68 ± 2% increase. Calculated from the mass and Brix values, 73 ± 1% of the sugar (on average with 95% confidence) was recovered from the three freeze concentration trials. By successfully concentrating apple juice, proof of principle is shown for the usage of actuating membranes in progressive freeze concentration. In the future, further temperature control and studies in the freezing kinetics could enhance the concentration for even more efficient recoveries. Suggestions for further improving this work can be found in Chapter 6 regarding the current shortcomings in the equipment and parameter manipulation.

Table 5.1: Apple Juice Concentration Trial #1: Phase Mass and Concentration Data

Freeze Trial #1	Permeate		Retentate	
Measurement #	Brix (°)	Sample T (°C)	Brix (°)	Sample T (°C)
1	19.5	23.8	6.1	23.6
2	19.6	23.8	5.8	23.6
3	19.6	23.8	5.8	23.6
4	19.6	23.8	5.8	23.6
5	19.6	23.8	5.8	23.6
6	19.7	23.8	5.8	23.6
Phase:	Permeate	Retentate		Feed
Mass (g)	8.2026 ± 0.0001	9.9099 ± 0.0001		19.0916 ± 0.0001
Sugar Content (g)	1.6077 ± 0.0082	0.5797 ± 0.0099		2.2528 ± 0.0191
% of Feed Sugar Recovered in Phase	71.36 ± 0.71	25.73 ± 0.49		-

Table 5.2: Apple Juice Concentration Trial #2: Phase Mass and Concentration Data

Freeze Trial #2	Permeate		Retentate	
Measurement #	Brix (°)	Sample T (°C)	Brix (°)	Sample T (°C)
1	20.6	23.2	5.1	23.3
2	20.6	23.2	5.0	23.3
3	20.6	23.1	5.0	23.3
4	20.6	23.1	5.1	23.2
5	20.6	23.1	5.0	23.2
6	20.6	23.1	5.1	23.2
Phase:	Permeate	Retentate		Feed
Mass (g)	8.2658 ± 0.0001	10.0967 ± 0.0001		19.1747 ± 0.0001
Sugar Content (g)	1.7028 ± 0.0083	0.5099 ± 0.0101		2.2626 ± 0.0192
% of Feed Sugar Recovered in Phase	75.26 ± 0.73	22.54 ± 0.49		-

Table 5.3: Apple Juice Concentration Trial #3: Phase Mass and Concentration Data

Freeze Trial #3	Permeate		Retentate	
Measurement #	Brix (°)	Sample T (°C)	Brix (°)	Sample T (°C)
1	19.4	23.7	6.2	23.7
2	19.3	23.7	6.2	23.7
3	19.3	23.7	6.1	23.7
4	19.3	23.7	6.1	23.7
5	19.3	23.7	6.1	23.7
6	19.3	23.7	6.1	23.8
Phase:	Permeate	Retentate		Feed
Mass (g)	8.4660 ± 0.0001	10.3975 ± 0.0001		19.2159 ± 0.0001
Sugar Content (g)	1.6353 ± 0.0085	0.6377 ± 0.0104		2.2675 ± 0.0192
% of Feed Sugar Recovered in Phase	72.12 ± 0.72	28.12 ± 0.52		-

5.4 Ethanol Concentration

Approximately 15.5 billion gallons of ethanol are fermented and recovered from corn in the United States for fuel each year.[15] During fermentation, the ethanol becomes toxic to the yeast upon reaching about 8 wt% and must be recovered from the aqueous broth after recovering the yeast cells by centrifuge or filtration.[16-18] Dewatering the broth to recover the ethanol is very energy intensive with distillation, and freeze concentration is a potential solution.

In this section, I extend the application of actuatable membrane freeze concentration from fruit juice to aqueous ethanol solutions. As described in Methods 5.2.8.3, the apparatus was prepared in a similar manner as with apple juice, but the membrane was switched to a 0.45 μm PVDF membrane. This was because the surface tension of ethanol solutions drops rapidly (Appendix D.3) and the membranes could self-actuate before reaching much higher ethanol concentrations. To increase the breakthrough pressure, low surface energy PVDF (25 mN/m)[19] with significantly smaller pores (0.45 μm versus 25 μm) was used, as described in Chapter 1 concerning breakthrough pressure and A^*.

To understand how this new PVDF membrane would perform, Figure 5.4 shows the breakthrough pressure (Method 5.2.3) of various ethanol solutions. It was found that only pure water (> 87.7 kPa breakthrough) could not permeate through the membrane under the vacuum pressure applied by our equipment. The pressure required for breakthrough of a particular ethanol solution drops quickly as the wt% ethanol increases. As mentioned earlier in the chapter, breakthrough occurs when the combined pressure from the hydrostatic pressure (the 20 cm height equals about 1.5 to 1.9 kPa,
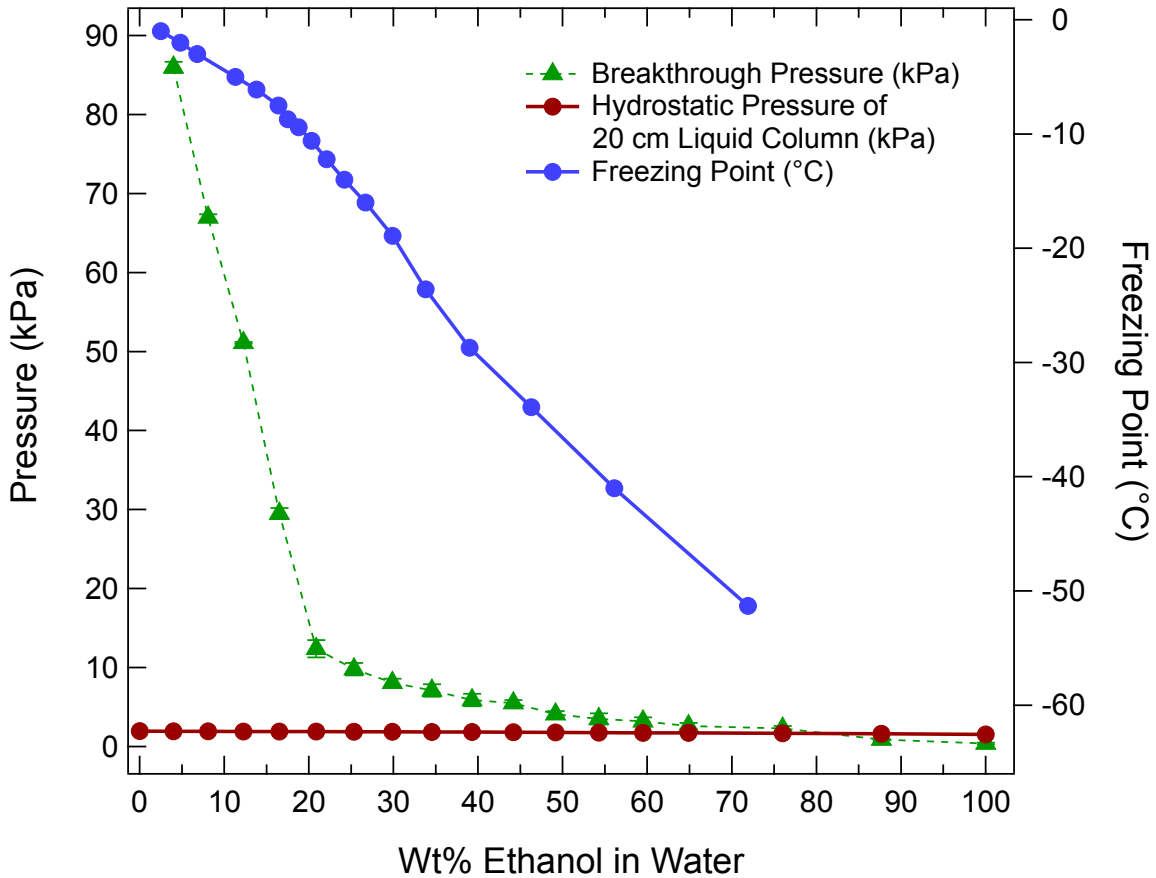
Figure 5.4: Pertinent ethanol solution properties for membrane-based freeze concentration. The experimental breakthrough pressure on the 0.45 μm PVDF membrane must be greater than the hydrostatic pressure for the liquid to be held in the feed chamber. The solution freezing point drops quickly as the wt% ethanol increases (right Y axis).[20]

depending on the ethanol concentration) and the vacuum pressure reaches the membrane's breakthrough pressure. If the breakthrough pressure (green in Figure 5.4) is not greater than the hydrostatic pressure (dark red in Figure 5.4), the membrane will fail and leak during the concentration process. In theory, the membrane will automatically actuate upon reaching an ethanol concentration of approximately 80 wt%, as the breakthrough pressure equals the hydrostatic pressure at this point. This may have an application as a sensor in other work, but this region was beyond the capability of our current equipment. -25.7°C was the lower limit for the current chiller and the freezing

point of 80 wt% is below -50°C (blue in Figure 5.4). Due to the chiller's temperature limitation, a lower, 3.5 wt% ethanol feed solution was used for demonstrating freeze concentration proof of principle.

In a manner similar to the freeze concentration of juice, the apparatus was assembled, charged with feed, and slowly freeze concentrated (Methods 5.2.8.3). Tables 5.4 – 5.6 show the permeate and retentate phase information (refractive index, mass measurements, ethanol concentration) for three trials of the ethanol freeze concentration process. From averaging the results of the three trials, the aqueous ethanol feed was concentrated from 3.5 ± 0.2 wt% to 6.0 ± 0.2 wt% ethanol, which is a $71 \pm 2\%$ increase in concentration (95% confidence level in uncertainties). From this freeze concentration process, $80 \pm 6\%$ of the feed ethanol was recovered in the permeate.

Table 5.4: Ethanol Solution Concentration Trial #1: Phase Mass and Concentration Data

Freeze Trial #1	Permeate		Retentate	
Measurement #	Refractive Index	Sample T (°C)	Refractive Index	Sample T (°C)
1	1.3367	23.4	1.3338	23.3
2	1.3368	23.3	1.3338	23.3
3	1.3367	23.3	1.3338	23.4
4	1.3367	23.3	1.3338	23.3
5	1.3367	23.3	1.3338	23.3
6	1.3368	23.3	1.3338	23.3

Phase:	Permeate	Retentate	Feed
Mass (g)	8.1568 ± 0.0001	8.9925 ± 0.0001	17.6459 ± 0.0001
EtOH Content (g)	0.4849 ± 0.0080	0.1452 ± 0.0133	0.5975 ± 0.0260
EtOH wt%	5.9443 ± 0.0984	1.6146 ± 0.1476	3.3858 ± 0.1476
% of Feed EtOH Recovered in Phase	81 ± 4	24 ± 2	-

Table 5.5: Ethanol Solution Concentration Trial #2: Phase Mass and Concentration Data

Freeze Trial #2	Permeate		Retentate	
Measurement #	Refractive Index	Sample T (°C)	Refractive Index	Sample T (°C)
1	1.3367	23.6	1.3332	23.6
2	1.3366	23.6	1.3332	23.6
3	1.3366	23.6	1.3332	23.6
4	1.3367	23.6	1.3331	23.7
5	1.3367	23.5	1.3332	23.7
6	1.3367	23.6	1.3331	23.7

Phase:	Permeate	Retentate	Feed
Mass (g)	8.4015 ± 0.0001	8.2518 ± 0.0001	17.7056 ± 0.0001
EtOH Content (g)	0.4905 ± 0.0120	0.0561 ± 0.0162	0.6256 ± 0.0305
EtOH wt%	5.8383 ± 0.2268	0.6798 ± 0.1968	3.5334 ± 0.1722
% of Feed EtOH Recovered in Phase	78 ± 4	9 ± 3	-

Table 5.6: Ethanol Solution Concentration Trial #3: Phase Mass and Concentration Data

Freeze Trial #3	Permeate		Retentate	
Measurement #	Refractive Index	Sample T (°C)	Refractive Index	Sample T (°C)
1	1.3369	23.3	1.3337	23.3
2	1.3368	23.3	1.3336	23.3
3	1.3368	23.3	1.3336	23.3
4	1.3368	23.3	1.3336	23.4
5	1.3368	23.3	1.3337	23.4
6	1.3368	23.3	1.3336	23.3

Phase:	Permeate	Retentate	Feed
Mass (g)	8.2633 ± 0.0001	9.0429 ± 0.0001	17.6793 ± 0.0001
EtOH Content (g)	0.5014 ± 0.0102	0.1238 ± 0.0089	0.6247 ± 0.0304
EtOH wt%	6.0673 ± 0.1230	1.3686 ± 0.0984	3.5334 ± 0.1722
% of Feed EtOH Recovered in Phase	80 ± 4	20 ± 2	-

5.5 Dye Removal from Contaminated Water

In order to visualize the freeze concentration process and demonstrate a highly pure product, Fast Green FCF was removed from water (Methods 5.2.8.4) and the desired product was the ice instead of the concentrate, unlike prior separations. It is a unique system because the exclusion of the dye to the concentrate can be readily viewed throughout the freezing process. Figure 5.5 shows how the light blue color narrows and darkens as the colorless, pure ice grows from the walls of the chamber and isolates the dye in the concentrate.
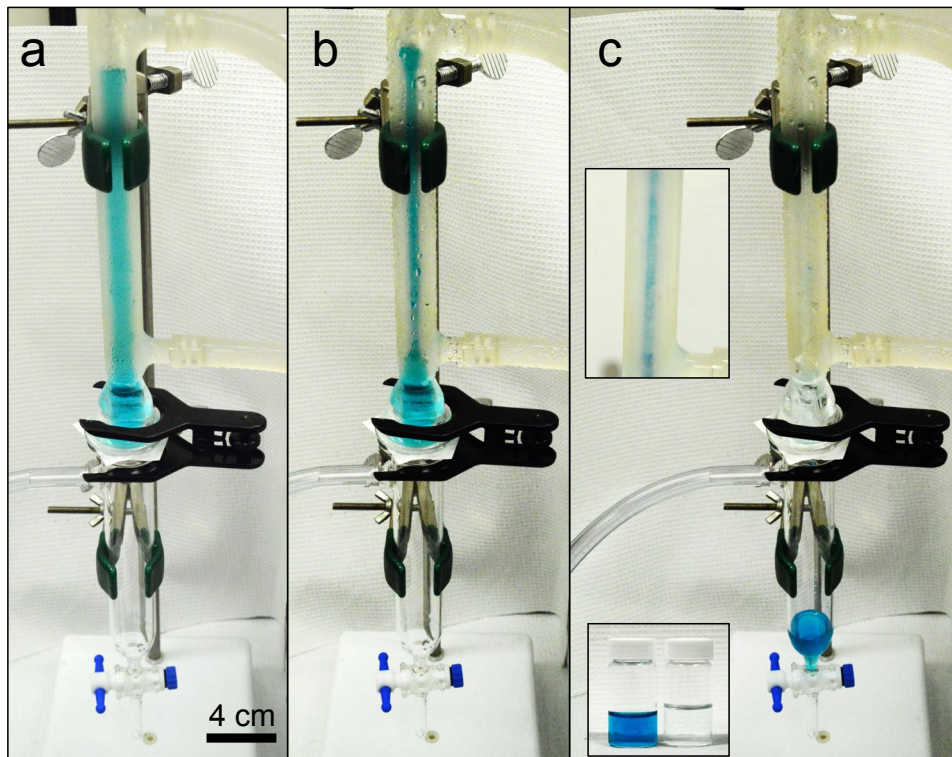
Figure 5.5: Freeze concentration of dye from water. (a) The feed is supplied to the freezing chamber and equilibrated at -0.4°C. (b) In the midst of the freezing process, the exclusion of the dye from the ice to the liquid core is observed. (c) After membrane actuation and washing, essentially pure ice remains in the chamber. The insets show a close-up of the excluded dye before actuation and a visual comparison of vials containing the recovered concentrate (left) and purified water (right).

As with apple juice concentration, a hydrophobic Whatman 114 membrane was

used with the aqueous dye solution, but only a subcooling to -0.4°C was required to keep the ice growing throughout the experiment. With this system, the ice being formed was pure and dense, so the 42 min at -0.4°C was very important to prevent complete solidification of the column, while recovering the most ice. If the column was allowed to solidify, the last bit of concentrated dye became encapsulated in the ice, rather than being removed by the wash step. Furthermore, the formation of a solid plug made membrane actuation difficult because air could not easily replace the volume held by the permeating liquid in the system beneath the ice plug. This was due to a lower pressure (vacuum) below the membrane and no path for air to vent through the ice from above.

After the freezing process was complete and the bulk of the concentrate was removed by actuation, a wash step was introduced due to the low interfacial tension between the ice and remaining adsorbed liquid concentrate.[21] Only a small volume, 0.75 mL, of water was necessary to displace the highly concentrated liquid remaining on the surface of the narrow channel running through the ice plug. Table 5.7 shows the data from three purification replicates. On average, 98.0 ± 0.3% of the dye was removed from

Table 5.7: Water Purification Trials Data

	Trial #1	Trial #2	Trial #3
% Dye Removed from Water	98.1 ± 0.5	96.4 ± 0.5	99.3 ± 0.5
Wt% of Purified Water Recovered from Feed	54.5798 ± 0.0006	50.1810 ± 0.0006	49.8964 ± 0.0006
Purified Water Dye Concentration (ppm)	0.3 ± 0.1	0.7 ± 0.1	0.1 ± 0.1
Dye Concentration in the Concentrate (ppm)	34.9 ± 0.1	33.7 ± 0.1	32.5 ± 0.1
Feed Dye Concentration (ppm)	19.3 ± 0.1	19.3 ± 0.1	19.3 ± 0.1
Feed Mass, including Wash Water (g)	17.6567	17.4335	17.6163
Purified Water Mass (g)	9.6370	8.7483	8.7899
Concentrate Mass (g)	7.7204	8.0631	8.0154

the purified water, recovered in the ice phase, and 51.6 wt% of the water, within the feed, was reclaimed. This work visibly demonstrates that even dilute contaminants, such as dye, can be removed with our membrane-based freeze concentration apparatus to yield high purity product.

5.6 Conclusion

In summary, proof of concept was shown for a new approach to freeze concentration enabled by an actuatable membrane. Combining the crystallizer and separator operations into one unit minimized the equipment footprint, and indirect cooling prevented contamination of the product with coolant. Aqueous ethanol and apple juice concentration demonstrated that the sugar and ethanol concentrations could be increased by about 70%, while recovering 70-80% of the product, and significantly decreased the water content of the solutions. Furthermore, the frozen fraction can yield highly pure ice as demonstrated by the removal of 98% of the dye from water. The removal of water as ice, instead of by evaporation, provides a significant energy savings due to the much lower enthalpy of fusion vs. vaporization, and valuable flavor and aroma components are not lost in this process. With further optimization, this unit operation could be valuable in the recovery and purification of multiple industrial commodities and waste streams.

5.7 References

1.   Stivaros, C. *IBISWorld Industry Report OD4628 Frozen Fruit & Juice Production in the US*; September 2017.

2.   Matthews, R. F. *Frozen Concentrated Orange Juice From Florida Oranges*; University of Florida: 1994.

3. Braddock R, J.; Marcy J, E., Quality of Freeze Concentrated Orange Juice. *J. Food Sci.* **2006,** *52* (1), 159-162. 10.1111/j.1365-2621.1987.tb13995.x

4. Sánchez, J.; Ruiz, Y.; Raventós, M.; Auleda, J. M.; Hernández, E., Progressive freeze concentration of orange juice in a pilot plant falling film. *Innov. Food Sci. Emerg. Technol.* **2010,** *11* (4), 644-651. 10.1016/j.ifset.2010.06.006

5. Stocking, J. H.; King, C. J., Secondary nucleation of ice in sugar solutions and fruit juices. *AIChE J.* **2004,** *22* (1), 131-140. 10.1002/aic.690220116

6. Shirai, Y.; Sugimoto, T.; Hashimoto, M.; Nakanishi, K.; Matsuno, R., Mechanism of Ice Growth in a Batch Crystallizer with an External Cooler for Freeze Concentration. *Agric. Biol. Chem.* **1987,** *51* (9), 2359-2366. 10.1080/00021369.1987.10868410

7. Englezos, P., The Freeze Concentration Process and its Applications. *Dev. Chem. Eng. Min. Process.* **1994,** *2* (1), 3-15. 10.1002/apj.5500020102

8. Lemmer, S.; Klomp, R.; Ruemekorf, R.; Scholz, R., Preconcentration of Wastewater through the Niro Freeze Concentration Process. *Chem. Eng. Technol.* **2001,** *24* (5), 485-488. 10.1002/1521-4125(200105)24:5<485::AID-CEAT485>3.0.CO;2-H

9. Hartel, R. W.; Espinel, L. A., Freeze concentration of skim milk. *J. Food Eng.* **1993,** *20* (2), 101-120. 10.1016/0260-8774(93)90009-9

10. Holt, S., The role of freeze concentration in waste water disposal. *Filtr. Sep.* **1999,** *36* (10), 34-35. 10.1016/S0015-1882(00)80052-X

11. Hernández, E.; Raventós, M.; Auleda, J. M.; Ibarz, A., Concentration of apple and pear juices in a multi-plate freeze concentrator. *Innov. Food Sci. Emerg. Technol.* **2009,** *10* (3), 348-355. 10.1016/j.ifset.2009.02.001

12. Nazir, S.; Farid, M. M., Modeling ice removal in fluidized‐bed freeze concentration of apple juice. *AIChE J.* **2008,** *54* (11), 2999-3006. 10.1002/aic.11602

13. Huige, N. J. J.; Thijssen, H. A. C., Production of large crystals by continuous ripening in a stirrer tank. *J. Cryst. Growth* **1972,** *13-14*, 483-487. 10.1016/0022-0248(72)90285-0

14. Wang, L.; McCarthy Thomas, J., Covalently Attached Liquids: Instant Omniphobic Surfaces with Unprecedented Repellency. *Angew. Chem. Int. Ed.* **2015,** *55* (1), 244-248. 10.1002/anie.201509385

15. Hill, S.; Hanson, S. *U.S. fuel ethanol production continues to grow in 2017*; U.S. Energy Information Administration: 2017.

16.   Pfeffer, M.; Wukovits, W.; Beckmann, G.; Friedl, A., Analysis and decrease of the energy demand of bioethanol-production by process integration. *Appl. Therm. Eng.* **2007,** *27* (16), 2657-2664. 10.1016/j.applthermaleng.2007.04.018

17.   Bai, F. W.; Anderson, W. A.; Moo-Young, M., Ethanol fermentation technologies from sugar and starch feedstocks. *Biotechnol. Adv.* **2008,** *26* (1), 89-105. 10.1016/j.biotechadv.2007.09.002

18.   Martins da Matta, V.; de Andrade Medronho, R., A new method for yeast recovery in batch ethanol fermentations: Filter aid filtration followed by separation of yeast from filter aid using hydrocyclones. *Bioseparation* **2000,** *9* (1), 43-53. 10.1023/A:1008145419175

19.   Liu, F.; Hashim, N. A.; Liu, Y.; Abed, M. R. M.; Li, K., Progress in the production and modification of PVDF membranes. *J. Membr. Sci.* **2011,** *375* (1), 1-27. 10.1016/j.memsci.2011.03.014

20.   Speight, J. G.; Lange, N. A., *Lange's Handbook of Chemistry*. 16th ed.; McGraw-Hill Professional: Maidenhead, 2005.

21.   Shwartz, J.; Probstein, R. F., An analysis of counterwashers for freeze-distillation desalination. *Desalination* **1968,** *4* (1), 5-29. 10.1016/S0011-9164(00)84032-1

CHAPTER 6

Closing Remarks and Future Work

6.1 Closing Remarks

As discussed throughout my dissertation, there are four major selective wettabilities to choose from, and many different methods for achieving each one of them. The type of membrane used will depend on the waste stream composition, fouling potential, and the system employed for the separation (on-demand, gravity fed, high pressure, etc.). In wastewater purification, the form of oil, whether free or emulsified, will indicate the pore-size for the membrane and thus is directly related to the permeation rate through the membrane. All these parameters must be taken into account for utilizing membranes with selective wettability.

A multitude of selective wettability systems have been used to successfully separate oil and water mixtures with greater than 99.9% efficiency, but the future lies in imparting these wetting properties to membranes that withstand high trans-membrane pressures, have greater permeation rates of the desired liquid, are anti-fouling, and can be scalably manufactured at a reasonable cost. Developing a selective wettability membrane with all these characteristics will require creative solutions, and provides a range of intellectual and research challenges. Such membranes will help meet the growing needs for waste and byproduct treatment in a wide variety of fields.

In this work, I contributed incrementally to a variety of applications and

methodologies dependent on the careful control of liquid wetting. In Chapter 2, a versatile and scalable approach to achieving counterintuitive, hydrophilic and oleophobic (HL/OP) membranes was presented. These membranes separated surfactant-stabilized emulsions into their original components with extremely high purity, in batch and continuous operation. Due to their oil repellency in air and underwater, these membranes showed significant increases in product recovery over time and extended life times due to their anti-fouling capability produced by a combination of hydrophilic and low surface energy components.

Chapter 3 described how a HL/OP membrane could be used in tandem with a hydrophobic and oleophilic membrane to enable the novel methodology of Continuous Liquid-Liquid Extraction and *In-situ* Membrane Separation. The effective gravity-driven, membrane separation of surfactant-enhanced emulsions allows for increased extraction factors due to the greater surface area of emulsions. This allows our system to achieve extractions of miscible components much closer to the thermodynamic limit, than without surfactant present.

Chapter 4 explored the formulation of a new anti-fog coating, which can be post-functionalized for oil repellency and easy fingerprint removal. It is spray coated and directly bonded to polycarbonate for ease of application and durability. It does not delaminate from the surface and performs in warm and cold environments. The addition of fluoro-silane enables dodecane droplets to slide cleanly from the surface and fingerprints to wipe cleanly away, without compromising the anti-fog performance. Lastly, Chapter 5 presented proof of concept for a new form of freeze concentration enabled by actuating hydrophobic membranes. Instead of separating two liquid phases,

remaining liquid is separated from ice crystals to achieve higher concentrations of liquids, such as fruit juice and ethanol, without the additional energy required for evaporating the water.

6.2 Future Work

Each project throughout this dissertation was conceived due to recurring problems in life, and several solutions were discovered, but several interesting paths remain for future work in perfecting these discoveries. The ideal hydrophilic and oleophobic membrane would never allow oil through, never get contaminated with oil or other foulants, and have a very high and constant permeation rate. One struggle is that very small membrane pore sizes are required to remove nanometer sized emulsion droplets, which decreases the flow rate through the membrane. The pressure could be increased to enhance the flow rate, but then oil droplets could be forced through if the breakthrough pressure is exceeded. Secondly, I found that increasing the oil repellency (and breakthrough pressure) of the membranes could decrease the water permeation rate. With the 0.45 μm cellulose sheet membranes, I found that the truly HL/OP membranes (40 min silanization) actually performed worse than the control in the cross-flow separation. The fluorosilane density was too great and the hydrophilic nature of the substrate was masked. Oil contamination was worse and the flow rate compromised, unless the silane content was lowered. The 10 and 20 min functionalization times showed anti-fouling ability, but these were oleophilic in air and the permeation rate still decreased with time in operation. Furthermore, the HL/OP ceramic membrane had worse performance initially, but outperformed the control after about the first 225 hours. Anti-fouling ability was shown in these systems, but they are far from the ideal HL/OP membrane. Future work should

166

look into preventing oil adhesion and contamination without preventing high water permeation rates, whether only initially or long term, in the purification of oil contaminated water.

In our work on the extraction of miscible liquid components with CLEANS, further analysis of the results revealed that certain systems had greater improvements in extraction than others. It would be important to determine which chemical systems would stand to benefit the most from implementing this methodology, as well as which extractant/surfactant system to use. The system that benefited the most from CLEANS in our study, but with room for further improvement toward equilibrium, was the extraction of methanol from methyl oleate using water with 1 mg SDS mL^{-1} as the extractant. One aspect that stood out was the higher viscosity of methyl oleate (Table 6.1). 90 vol% of the feed was methyl oleate, and the volume ratio of feed to extractant was between 50:50 and 90:10, so the overall viscosity of this system was much higher than the others. High viscosity lowers the diffusion coefficient and decreases the mass transfer rate of a solute through a solvent as shown by the Stokes-Einstein equation[1]:

$$D_{AB} = \frac{RT}{6\pi\mu_B R_A N_A} \tag{6.1}$$

where R is the gas constant, T is temperature, μ_B is solvent viscosity, R_A is solute molecular radius, and N_A is Avogadro's number. Fick's law of diffusion shows that for a given concentration gradient, the only way to increase flux (diffusion coefficient times the concentration gradient) is by increasing the diffusion coefficient, D_{AB}. Raising the temperature is undesirable and the chemicals in the system determine the viscosity. The effect of viscosity, in both the feed and extractant phases, on the CLEANS emulsified methodology is a key fundamental area of interest.

Table 6.1: Component viscosities in the various LLE experiments using CLEANS

System	Solute	Viscosity (cP)	Extractant	Viscosity (cP)	Feed Solvent	Viscosity (cP)
Figure 3.8a	Methanol 10 feed vol% (25°C)[2]	0.544	Water (25°C)[2]	0.890	Methyl Oleate (40°C)[3]	3.94
Figure 3.8b	Ethanol 49 feed wt% (25°C)[2]	1.074	Water (25°C)[2]	0.890	Heptane (25°C)[2]	0.387
Figure 3.8c	Benzothiophene 30ppm in feed (35°C)[4]	2.517	DMF (25°C)[2]	0.794	Dodecane (25°C)[2]	1.383

A promising extraction feed for isolating the effect of viscosity on CLEANS performance is 30 ppm Sudan 1 dye in varying viscosities of silicone oil (5, 10, and 20 cSt). All the silicone oils are chemically similar and only vary in molecular weight to alter the viscosity. Sudan 1 was chosen because it is mutually soluble in the polar extractant, ethylene glycol (16.06 cP at 25°C).[2] Ethylene glycol (EG) is used because it is one of the few solvents that is both denser than silicone oil and immiscible with it. For the surfactant-enhanced emulsion, the surfactant is Silube® CS-1 (dimethicone PEG-8 succinate), which is deprotonated with NH_4OH to pH = 7 to ensure that it remains solely in the polar EG phase. It was confirmed that EG permeates through the stimuli-responsive membranes and silicone oil is repelled. After continuous extraction with CLEANS, the concentration of dye in each phase will be determined by UV-Vis and calibration curves. By using EG (with and without surfactant) and varying the silicone oil viscosity, detailed understanding of the effect on LLE and the exact benefit of CLEANS for viscous systems will be known. The effect of the emulsion mixing rate and droplet size could also be investigated during this process. Overall, we will be able to determine the extent of benefit for CLEANS in diffusion-limited viscous, extraction systems.

For my anti-fog coating, the number one area of investigation will be enhancing the mechanical durability and scratch resistance of the coating. The coating is highly effective in preventing fog due to its ability to take water vapor into its structure, and it is well bonded to the polycarbonate substrate, but it has about the same scratch resistance and hardness as its polycarbonate substrate, as shown in Chapter 4. Glasses lenses usually have a scratch resistant coating on them and this would be replacing that coating as the outermost layer in order to prevent fog. Options for increasing the cross-linking and loading of nanoparticles should be explored to boost the coating's hardness. Preferably, the coating should still be UV cross-linkable and any particles should be well dispersed to achieve uniformity and prevent clogging of the spray applicator. The greatest concern is achieving this without hindering the transparency of the surface.

My final project showed proof of concept for combining an actuatable membrane with freeze concentration. Concentration of industrially relevant commodities (apple juice and ethanol) and dyed water was demonstrated, but there are several areas for improvement in the procedure and equipment. With greater time, the freezing process could be optimized for increased ice purity. Further studies on the control of ice formation in this cylindrical geometry could be performed to determine the best temperatures and times for the freezing process. Heat transfer modeling could be done collaboratively. During the permeate recovery phase, the temperature setting of the chiller during actuation should be better analyzed. If the column is frozen too solidly, remaining permeate is entrapped in the structure. We found that shutting off the chiller, or increasing its temperature, during the short time needed for permeate recovery allowed

the ice structure to become more porous and release the concentrate for the apple juice and ethanol systems. This is at the expense of possible concentrate dilution.

Additionally, the apparatus design could be substantially improved. The conical area, near the clamped membrane, holds feed liquid that is not in contact with a chilled surface. To minimize the volume in the conical base, PDMS was cross-linked to fill the cavity except for a column of the same diameter as the condenser's inner diameter. This still left ~5 mL of volume that is not freezing, of a total 17 - 18.5 mL feed volume. This leaves a significant fraction of the feed to dilute the concentrated liquid. The freeze concentration column should be re-designed so that coolant reaches the total length of the column, all the way to the membrane at the bottom, so that there is no 'non-freezing' area to dilute the concentrate. This will allow the apparatus to achieve higher effective concentrations than we have shown. Also, utilizing a chiller that can go lower than -25.7°C will allow higher wt% ethanol feed solutions to be used and concentrated. Lastly, re-designing the batch system to a continuous system would also be an interesting engineering problem.

6.3 References

1.   Seader, J. D.; Henley, E. J.; Roper, D. K., *Separation Process Principles: Chemical and Biochemical Operations*. 3rd ed.; John Wiley & Sons, Inc.: 2011.

2.   *CRC Handbook of Chemistry and Physics 95th Edition*. CRC Press: 2014.

3.   Knothe, G.; Steidley, K. R., Kinematic viscosity of biodiesel fuel components and related compounds. Influence of compound structure and comparison to petrodiesel fuel components. *Fuel* **2005,** *84* (9), 1059-1065. 10.1016/j.fuel.2005.01.016

4.   Haines, W. E.; Helm, R. V.; Cook, G. L.; Ball, J. S., Purification and Properties of Ten Organic Sulfur Compounds-Second Series. *J. Phys. Chem.* **1956,** *60* (5), 549-555. 10.1021/j150539a009

APPENDICES

Appendix A

Chapter 2 Supplementary Information

A.1 HL/OP Membrane Fabrication & Contact Angles in Air

A comprehensive list of all the substrates modified to be hydrophilic and oleophobic, including polymers, metal, and ceramic, and their respective contact angles (Table A.1) are presented in this section. All of the HL/OP samples maintained *n*-dodecane contact angles in air > 90° and prevented the oil from absorbing into the surface, with a couple exceptions. The very smooth Ultracel® 100 kDa cellulose membrane and the Innovia cellulose film prevented oil absorption, but the angles were below 90°. Also, the HL/OP 0.45 μm PVDF's oil repellency was quite temporary as the dodecane soaked in after a few minutes of exposure. Nonetheless, it is interesting that the silane treatment can reverse the oil-water wetting of an inherently hydrophobic membrane with just silanes. Initially, it was HP/OL with a 121 ± 4° advancing water contact angle (dodecane wet) and it switched to HL/OP with a 97 ± 5° dodecane advancing angle (water wet). Note that the cellulose acetate contact angle was very high due to a fine, powdery and rough texture, as received from the manufacturer (Chapter 2, Figure 2.6a).

A.1.1 Sterlitech 0.2 μm and 0.45 μm regenerated cellulose membranes were treated with 30 W oxygen plasma for 20 min and subsequently exposed to vapor phase

172

(heptadecafluoro-1,1,2,2-tetrahydrodecyl) triethoxysilane, under 84 kPa vacuum, for 3 hours at 70°C.

A.1.2 Ultracel® 100 kDa (~10 nm) cellulose membranes were treated with 30 W oxygen plasma for 20 min and subsequently exposed to vapor phase (heptadecafluoro-1,1,2,2-tetrahydrodecyl) triethoxysilane, under 84 kPa vacuum, for 19 hours at 70°C.

A.1.3 Whatman #4 and #5 were treated with 30 W oxygen plasma for 20 min and subsequently exposed to vapor phase (heptadecafluoro-1,1,2,2-tetrahydrodecyl) triethoxysilane, under 84 kPa vacuum, for 40 minutes (#4) and 50 minutes (#5) at 70°C.

A.1.4 Whatman #114 wet-strengthened cellulose membranes were treated with 30 W oxygen plasma for 20 min and subsequently exposed to vapor phase (heptadecafluoro-1,1,2,2-tetrahydrodecyl) triethoxysilane, under 84 kPa vacuum, for 21 minutes at 70°C.

A.1.5 Whatman RC55 0.45 μm regenerated cellulose membranes (142 mm) were treated with 30 W oxygen plasma for 20 min and subsequently exposed to vapor phase (heptadecafluoro-1,1,2,2-tetrahydrodecyl) triethoxysilane, under 84 kPa vacuum, for 40 minutes (also 10 or 20 min for anti-fouling work) at 70°C. These were treated with the backside of the membrane covered with the spacer paper (from the manufacturer's packaging) to minimize plasma and silane contact during treatment. This was intended to create asymmetry and increase water permeation after it passed the fully silanized top, active surface contacting the emulsion during cross-flow separation.

A.1.6 Millipore 0.45 μm nylon membranes were treated with 30 W oxygen plasma for 20 min and subsequently exposed to vapor phase (heptadecafluoro-1,1,2,2-tetrahydrodecyl) triethoxysilane, under 84 kPa vacuum, for 68 minutes at 70°C.

A.1.7 Sterlitech 0.8 µm cellulose acetate membranes were treated with 30 W oxygen plasma for 60 min and subsequently exposed to vapor phase (heptadecafluoro-1,1,2,2-tetrahydrodecyl) triethoxysilane, under 84 kPa vacuum, for 3 h 50 min. at 70°C.

A.1.8 Innovia P25 cellulose film was treated with 30 W oxygen plasma for 20 min and subsequently exposed to vapor phase (heptadecafluoro-1,1,2,2-tetrahydrodecyl) triethoxysilane, under 84 kPa vacuum, for 3 hours at 70°C.

A.1.9 200 x 200 aluminum mesh was treated with 30 W oxygen plasma for 20 min and dipped for 5 min in a 1 vol% silane in isopropyl alcohol solution. The solution was 90:10 (SIM6492.66 : SIH5841.2) by volume. The membrane was removed from solution and placed in a glass desiccator under 84 kPa vacuum. The desiccator was heated at 110°C for 10 min.

A.1.10 0.45 µm Durapore® hydrophobic PVDF was dipped in 2 wt% bis(3-trimethoxysilylpropyl) amine (SIB1833.0) in ethanol (12.5 mL ethanol, 195 µL silane, 0.63 mL of pH = 2 acetic acid solution; stirred for 2 h before use) for 20 min. The silane linker aids in the adhesion of the hydrophilic and fluoro silanes to the PVDF. This was dried with nitrogen and then dipped in 30:70 (SIM6492.66 : SIH5841.2) by volume in dichloromethane (1 vol% silane in DCM) for 30 min. Again, this was dried with nitrogen and placed in a desiccator at 70°C for 30 min.

A.1.11 HL/OP Veolia ceramic membranes (5 nm silica): A 1 vol% silane in dichloromethane (DCM) solution was prepared with a silane ratio of 95:5 (SIM6492.66 : SIH5841.2). After removing the gaskets from the ends of the module, it was pre-soaked in pure DCM for 15 min. It was then dipped in the silane solution for 1 min and cured at 80°C for 30 min. This dipping and curing was performed two additional times.

Table A.1: *n*-Dodecane contact angles on the various HL/OP membranes.

HL/OP Membrane Type	Pore size (μm)	Dodecane Advancing Contact Angle (°)	Contact Angle Standard Deviation (°)
Whatman #4 Cellulose	25	106.4	7.6
Whatman #5 Cellulose	2.5	116.6	3.4
Whatman #5 Cellulose, after 14 months storage	2.5	116.5	2.8
Sterlitech Cellulose	0.45	99.5	5.3
Sterlitech Cellulose	0.2	95.5	3.7
Ultracel® 100 kDa Cellulose	0.01	63.5	1.1
Whatman RC55 Cellulose	0.45	121.8	2.3
Cellulose Acetate	0.8	157.4	6.1
Hydrophilic Nylon	0.45	113.2	1.8
Whatman #114 Cellulose	25	110.1	3.3
Innovia Cellulose Film	-	64.5	2.2
Hydrophobic PVDF	0.45	96.5	5.2
200-Mesh Aluminum	74	103.2	2.0
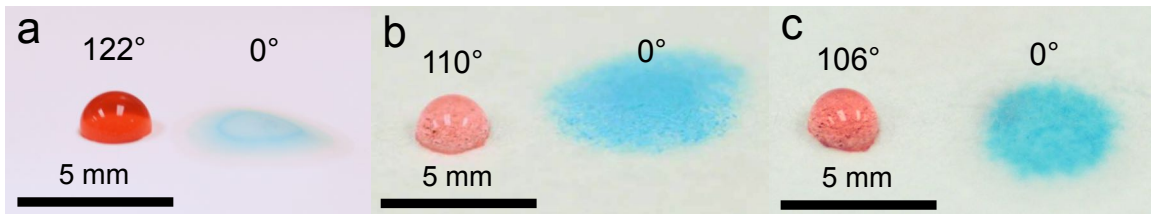
Figure A.1: Additional HL/OP cellulose membranes. (a) 0.45 μm RC55 HL/OP cellulose membrane for cross-flow testing, (b) HL/OP Whatman #114 (wet-strengthened), and (c) HL/OP Whatman #4, again, for comparison to the #114. They are the same effective pore size (25 μm), but the #114 has an 8.9 psi wet burst while #4 is only 0.22 psi. Their respective advancing contact angles are provided. All have *n*-dodecane (dyed red) and water (dyed blue) droplets on them.

A.2 Hydrophobic and Oleophilic (HP/OL) Membranes

A solution (3.0 mg mL^{-1}) of *n*-octadecyltriethoxysilane was prepared in toluene. Whatman #5 cellulose filters were treated with 30 W oxygen plasma for 20 min and then dip coated in the solution for 2 h. They were air dried for 2 h. 0.2 μm and P25 film were dipped in 6.0 mg mL^{-1} *n*-octadecyltriethoxysilane in toluene for 67.5 hours and air dried for 2 h (see Table A.2 for angles). This allows cellulose to have the fourth major wettability by switching to a non-polar silane from the fluorosilane (Figure A.2).

Table A.2: Water contact angles on the various HP/OL membranes.

HP/OL Membrane Type	Pore size (μm)	Water Advancing Contact Angle (°)	Contact Angle Standard Deviation (°)
Whatman #5 Cellulose	2.5	154.9	2.2
Sterlitech Cellulose	0.2	128.1	4.0
Innovia Cellulose Film	-	94.0	3.2
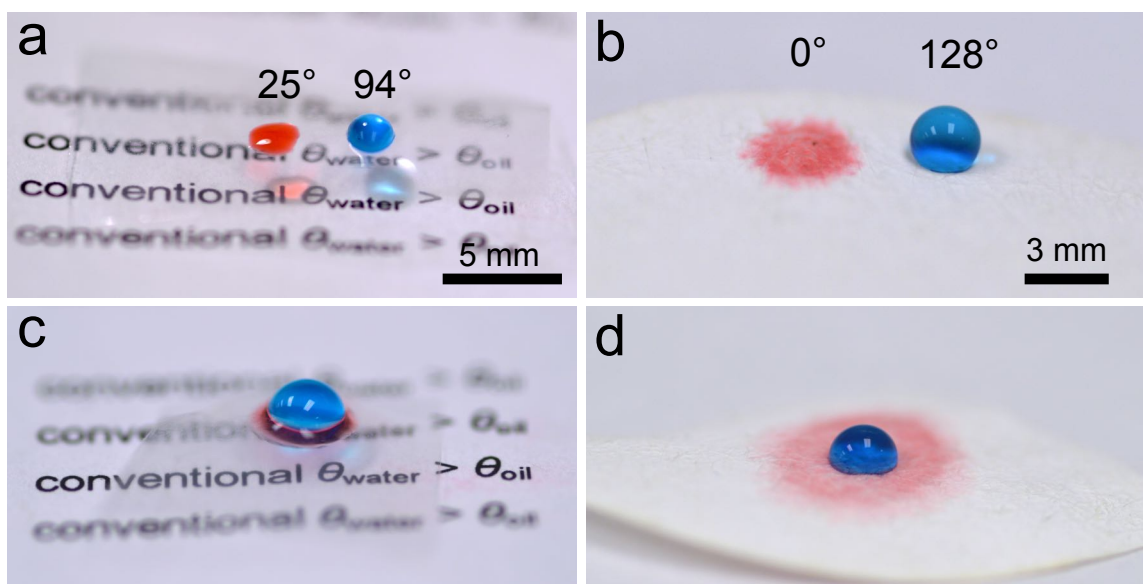
Figure A.2: HP/OL cellulose surfaces with $\theta_{water} > \theta_{oil}$. Advancing contact angles for droplets of water (dyed blue) and *n*-dodecane (dyed red) on (a) cellulose film and (b) cellulose filter paper with 0.2 μm pore size. Both surfaces have been treated with *n*-octadecyltriethoxysilane. (c) and (d) Water spreads on top of dodecane, preventing the surface from being self-cleaning.

A.3 Membrane Performance Testing and Data

A.3.1 Batch, Pre-fouled Free Oil and Water Separation Comparison

Table A.3: Water permeation times for untreated and HL/OP 0.45 μm cellulose membranes, with and without heavy pre-contact with *n*-dodecane.

Trial #	Untreated Permeation Time (min)	Untreated, Oil Pre-Contact Permeation Time (min)	HL/OP Permeation Time (min)	HL/OP, Oil Pre-contact Permeation Time (min)
1	12.7	16.9	11.4	20.6
2	12.2	17.5	21.2	17.8
3	13.8	16.6	16.6	14.6
4	11.8	14.9	17.4	13.8
5	11.3	17.4	18.4	17.0
6	10.5	15.6	18.3	17.3
7	9.1	17.0	13.9	14.7
8	11.2	15.5	16.8	16.2
9	-	-	12.1	14.4
10	-	-	16.9	21.2
11	-	-	14.1	20.2
12	-	-	12.9	14.7
13	-	-	15.0	18.8
Average	11.6	16.4	15.8	17.0
Standard Deviation	1.4	1.0	2.8	2.6
Uncertainty (95% confidence interval)	1.2	0.8	1.7	1.5
% Increase in Permeation Time (Propagated Uncertainty)	42 ± 13%		8 ± 15%	

A.3.2 Detailed Emulsion Preparation

A.3.2.1 Batch polymer membrane testing (nano-sized):

20 vol% *n*-dodecane and 80 vol% water containing 0.1 mg SDS mL^{-1} water were mixed and then ultrasonicated with a Heat Systems, Inc. Sonicator® Ultrasonic Processor

XL2020 with a CL4 Ultrasonic Converter and microtip (1/8") on power two for two minutes (see Figure 2.9c for DLS data).

A.3.2.2 Tubular, ceramic membrane testing:

100 ppm NSBM#4 (3.05 mL) and 25 ppm Detergent Mix #4 (765 µL), both by volume, were added to distilled water (30.498 L) and mixed at 775 rpm for 30 minutes in the feed tank. NSBM#4 (Navy Standard Bilge Mix) is 50 vol% Diesel Fuel Marine (MIL-PRF-16884K), 25 vol% TEP Steam Lube Oil (MIL-PRF-17331H(3)), and 25 vol% Diesel Lube Oil (MIL-PRF-9000H). Detergent Mix #4 is 50 vol% Type 1 General Purpose Detergent (MIL-D-16791G), 25 vol% Tide detergent, and 25 vol% Degreasing Solvent (MIL-PRF-680, Type III). See Figure A.3 for DLS data.
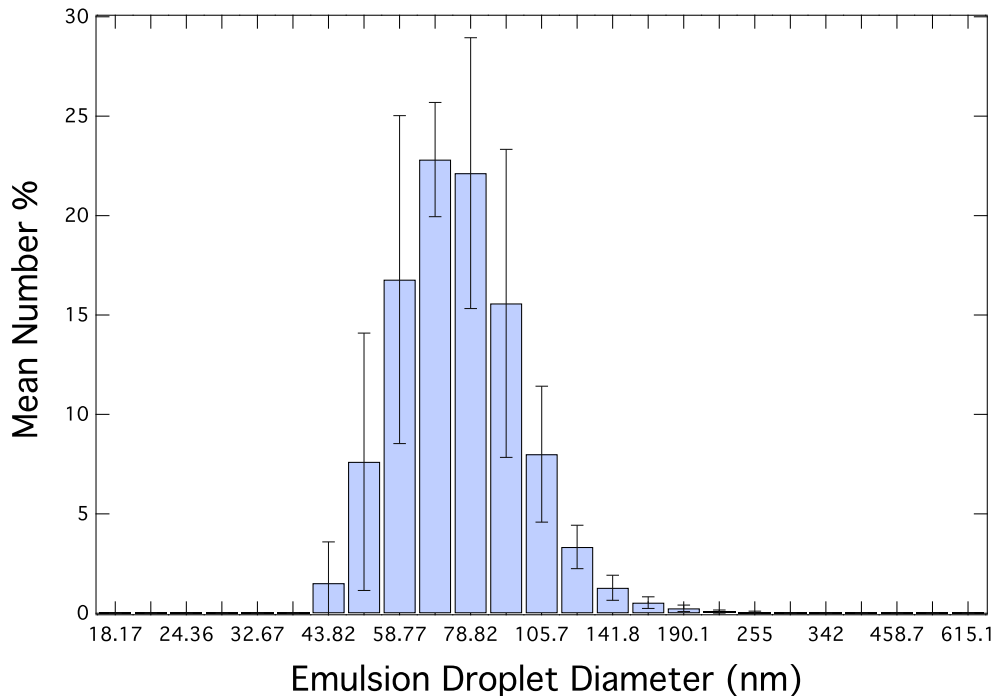
Figure A.3: DLS data for ceramic membrane test emulsion. Six measurements of the feed emulsion were taken and averaged. The error bars denote standard deviation.

A.3.2.3 Cross-flow cellulose RC55 sheet membrane testing:

20 vol% dodecane, mixture of isomers (240 mL) and 80 vol% water with 1 mg

SDS mL^{-1} (960 mL water + 960 mg SDS) were mixed for 10 min with the Lab Egg mixer

at 50% power. See Figure A.4 for DLS data.
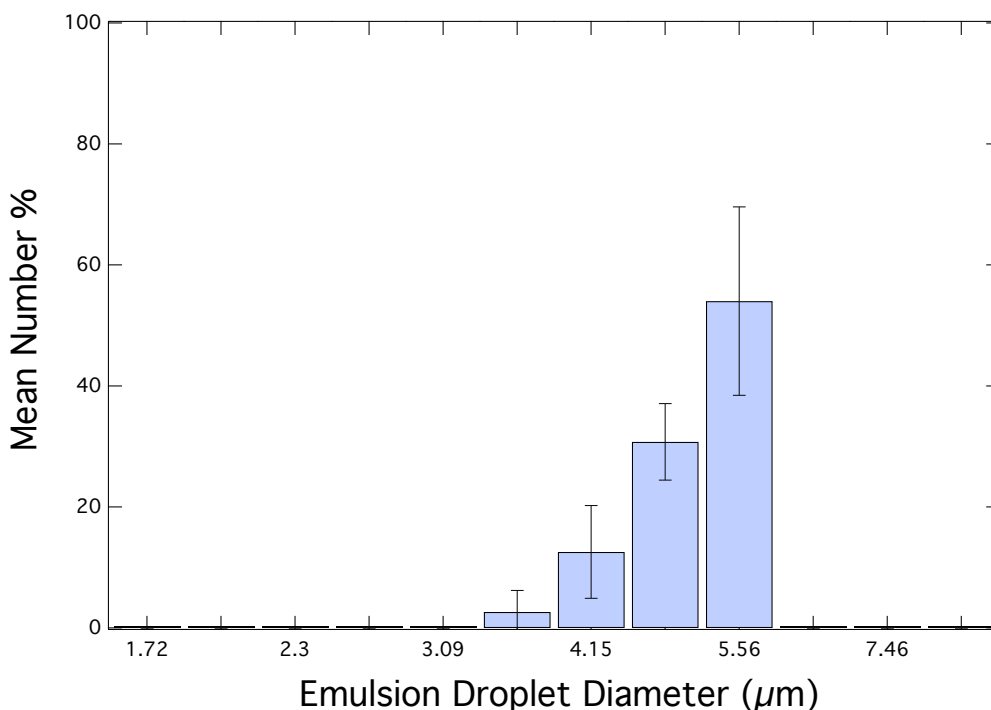
Figure A.4: DLS data for RC55 sheet membrane test emulsion. Seven measurements of the feed emulsion were taken and averaged. The error bars denote standard deviation.

A.3.3 Cross-flow Equipment Lists and Apparatus Diagrams

A.3.3.1 RC55 sheet membrane cross-flow equipment list:
Sterlitech CF042 Teflon Crossflow Cell, 0.67 GPM Miniature Gear Pump PQ-12DC Lab Model, Ashcroft 14902.5 Dual-Scale Low-Pressure Gauge 0 to 21 kPa with added brass pulsation-damping snubber, Low-Flow Shatter-Resistant Flowmeter 4-40 gph (Model MR3L22SNVT), Tygon F-4040-A Fuel & Lubricant Tubing (3/16" ID), IKA Lab Egg RW-11 mixer (0-2000 rpm), and UWE MII-600 mass balance (see Figure A.5).
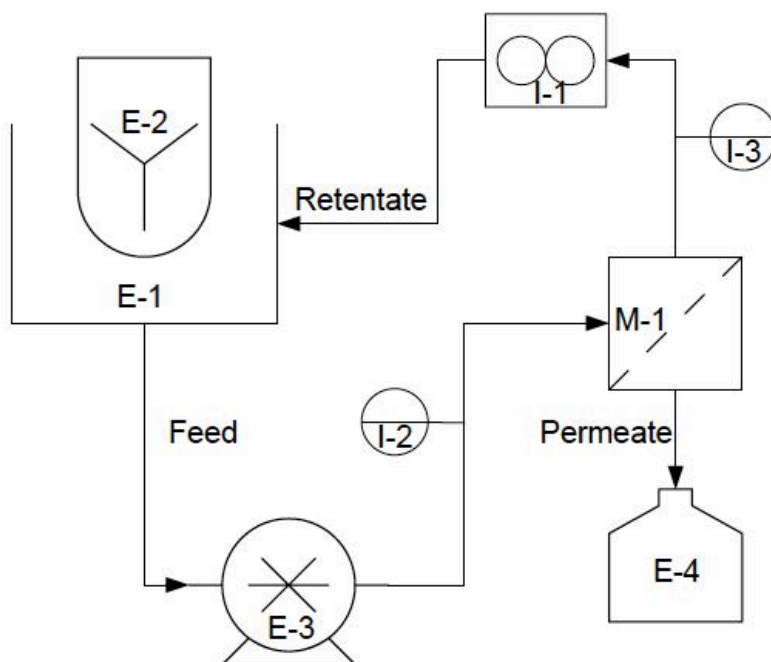
Equipment List

Label	Description
E-1	Feed Tank
E-2	Mixer
E-3	Pump
E-4	Water Permeate
M-1	Membrane Holder

Instrument List

Label	Description
I-1	Flowmeter
I-2	Upstream Pressure Gauge
I-3	Downstream Pressure Gauge

Figure A.5: RC55 sheet membrane cross-flow testing equipment P&ID diagram.

A.3.3.2 Ceramic cross-flow equipment list:

Veolia Ceramem Lab-Scale Test Modules: 5 nm Silica UF Membranes and their stainless steel holder, Pentair Water Shurflo GMBN6VC73T bronze gear pump with a Leeson Electric 3 hp motor, Dayton AC Motor Speed Control Model 13E648, Neptune Chemical Pump Co. 1/20 hp L-1-CL Mixer (0-1550 rpm) powered with a lab Variac at 50%, King Instrument Company (2-20 gpm) 7330 series flowmeter with Teflon float, Gilmont Compact Shielded Flowmeter Model GF-2360 (3-300 mL/min), Omega HH147U Data Logger and Omega TC-E-NPT-U-72 Thermocouple Probe, NoShok 900 series 25-910 60 psi liquid filled gauges with Ashcroft 1/4-1106B Pulsation Dampeners, and Schedule 80 PVC pipe (see Figure A.6).
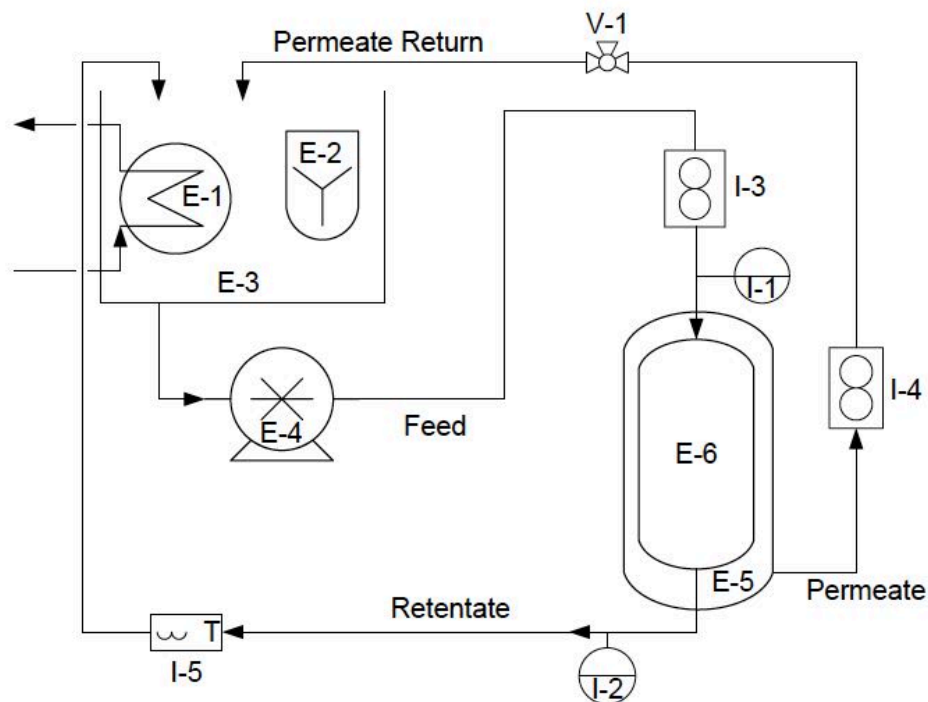
Equipment List		Instrument List	
Label	**Description**	**Label**	**Description**
E-1	Heat Exchanger	I-1	Upstream Pressure Gauge
E-2	Mixer	I-2	Downstream Pressure Gauge
E-3	Covered Feed Tank	I-3	Feed Flowmeter
E-4	Gear Pump	I-4	Permeate Flowmeter
E-5	Stainless Membrane Housing	I-5	Emulsion Thermocouple
E-6	Ceramic Membrane		
V-1	Permeate Sampling Port		

Figure A.6: Ceramic cross-flow testing equipment P&ID diagram.

A.3.4 Feed, Permeate, and Retentate Purity Analysis using DSC

Purity analysis, in triplicate, was performed using the DSC melting peaks and the

TA Instruments Trios software for purity analysis, as described in Chapter 2 (Methods

2.2.8).

A.3.4.1 *n*-Dodecane pre-fouled HL/OP 0.45 µm cellulose membrane batch separation (Chapter 2, Figure 2.7b) of free dodecane and water: DSC analysis of feed components, retentate, and permeate.
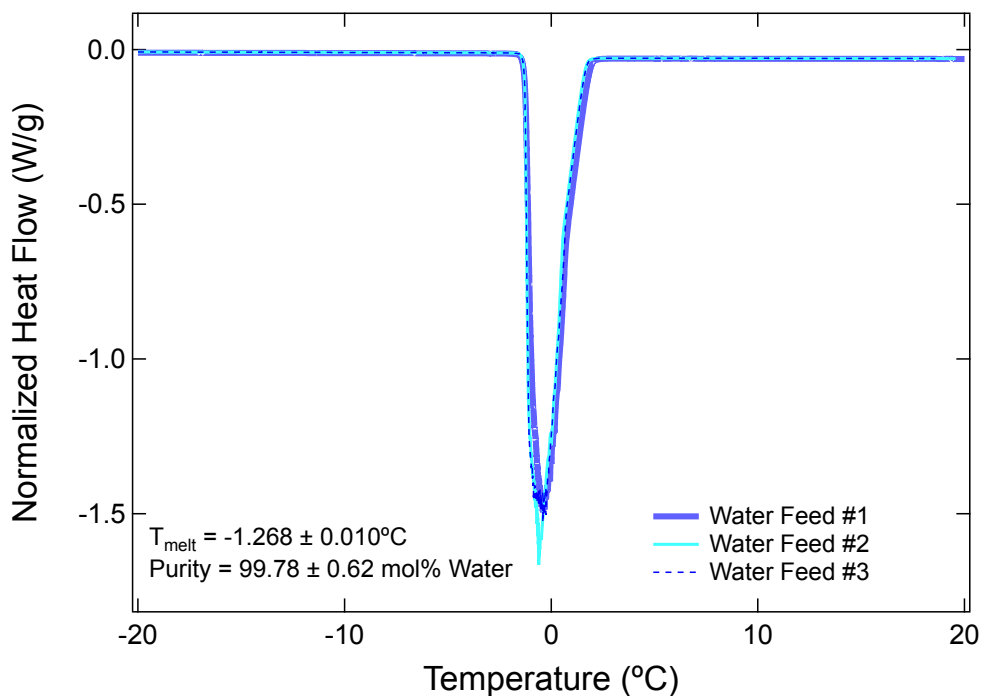
Figure A.7: DSC purity analysis of pure deionized water. The water is analyzed to be compared to the membrane permeate. Uncertainties use a 95% confidence interval.
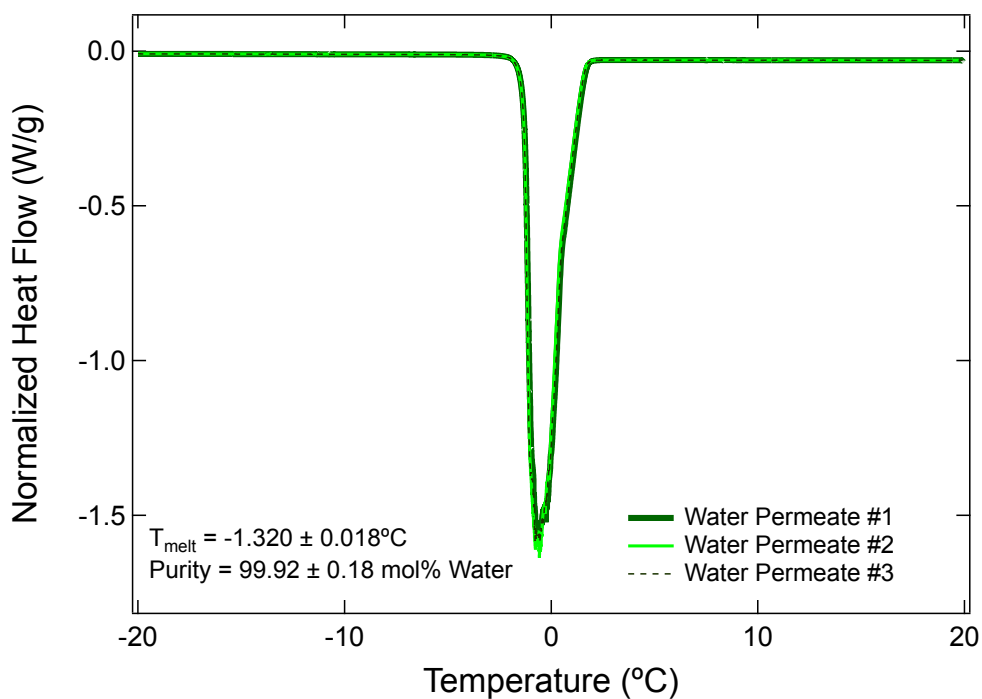
Figure A.8: DSC purity analysis of the water permeate. The permeate is to be compared to pure water (Figure A.7). Uncertainties use a 95% confidence interval.
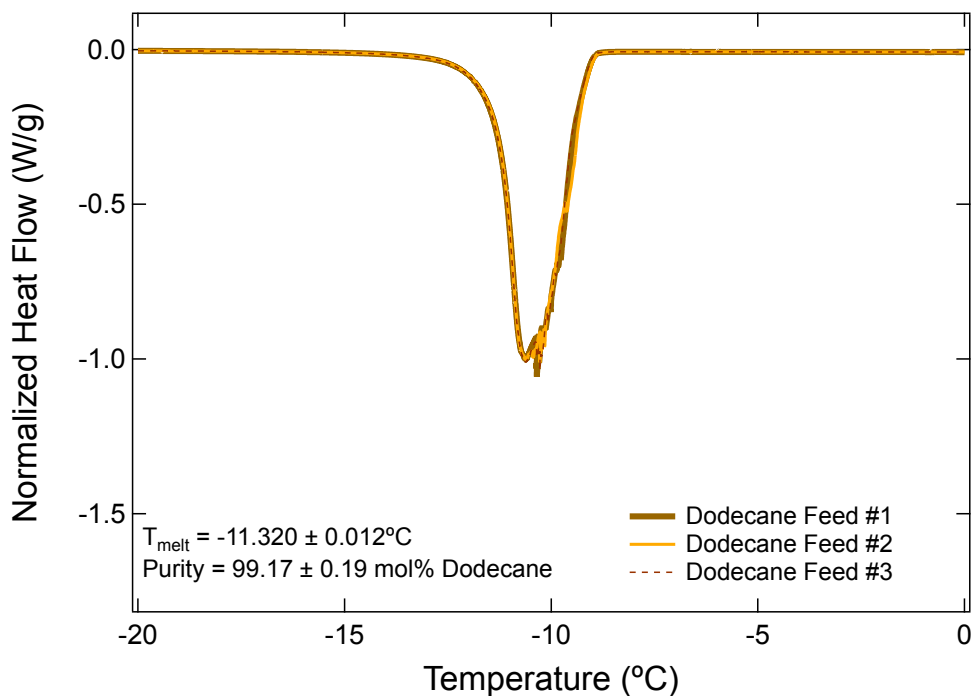
Figure A.9: DSC purity analysis of >99% pure *n*-dodecane. The dodecane is to be compared to dodecane retentate. Uncertainties use a 95% confidence interval.
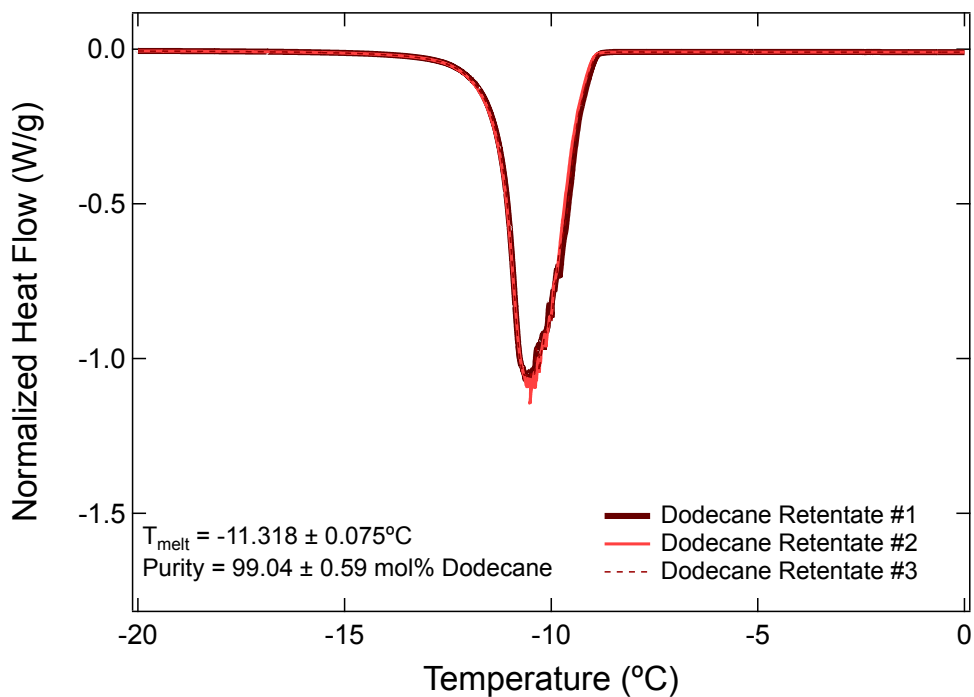
Figure A.10: DSC purity analysis of the dodecane retentate. The retentate is to be compared to pure dodecane (Figure A.9). Uncertainties use a 95% confidence interval.

A.3.4.2 *n*-Dodecane pre-fouled HL/OP 0.2 μm cellulose membrane batch separation (Chapter 2, Figure 2.9a) of emulsified dodecane/water: DSC analysis of feed, retentate, and permeate.
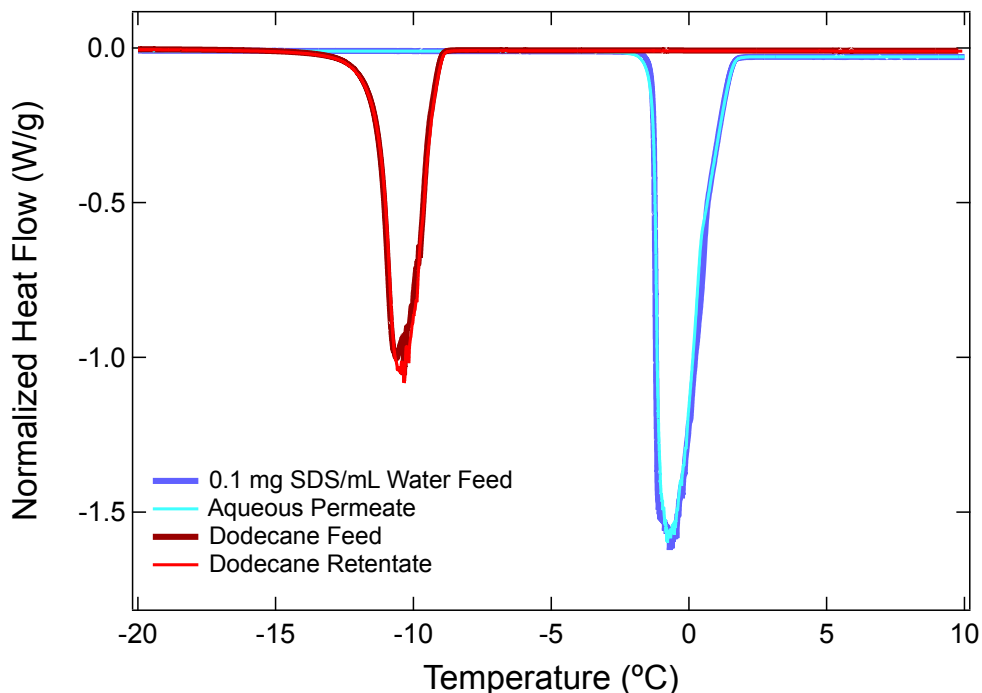
Figure A.11: DSC comparison of feed components and separated phases. The peaks are almost identical, indicating high purity after emulsion separation.
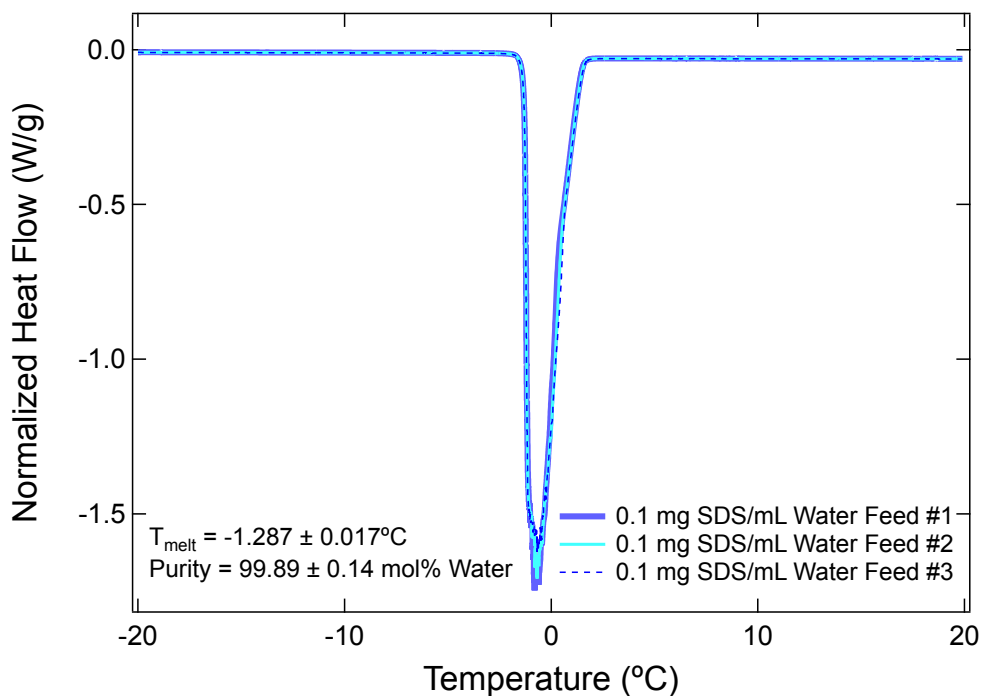
Figure A.12: DSC purity analysis of 0.1 mg SDS/mL water. The 0.1 mg SDS/mL water is compared to the water permeate. Uncertainties use a 95% confidence interval.
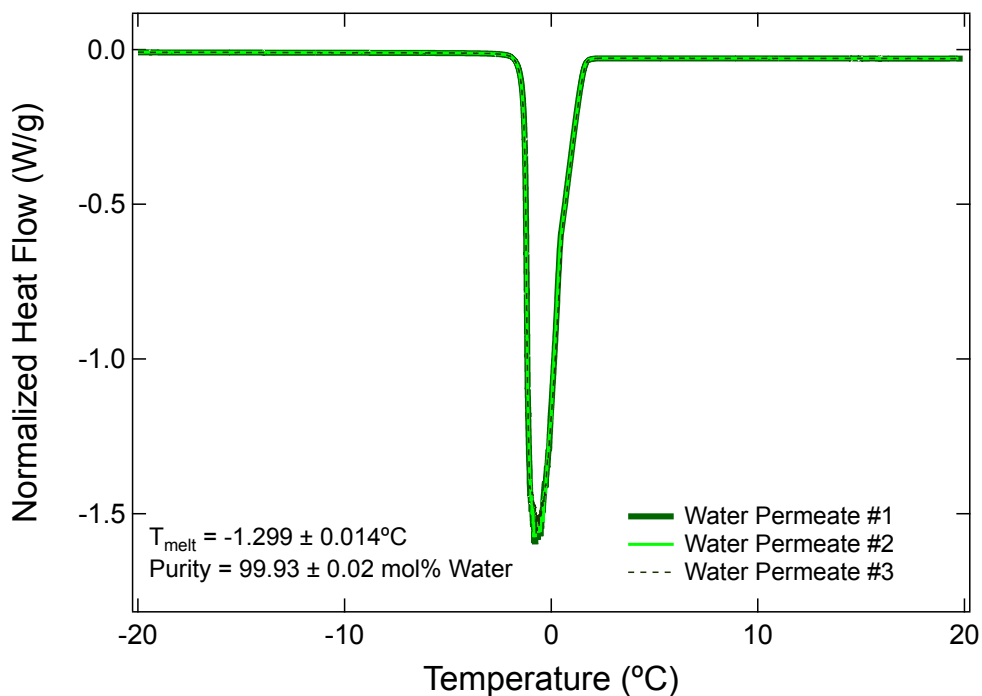
Figure A.13: DSC purity analysis of aqueous permeate. The permeate is to be compared to 0.1 mg SDS/mL water (Figure A.12). Uncertainties use a 95% confidence interval.
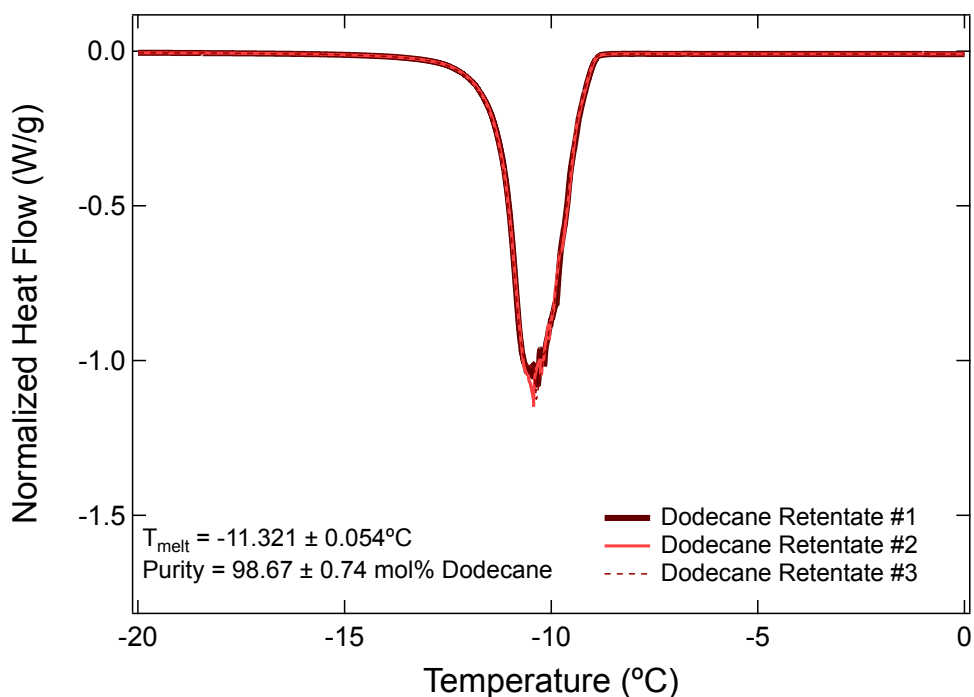
Figure A.14: DSC purity analysis of the dodecane retentate. The retentate is to be compared to pure *n*-dodecane (Figure A.9). Uncertainties use a 95% confidence interval.

A.3.4.3 RC55 sheet membrane feed and permeate purity analysis using DSC
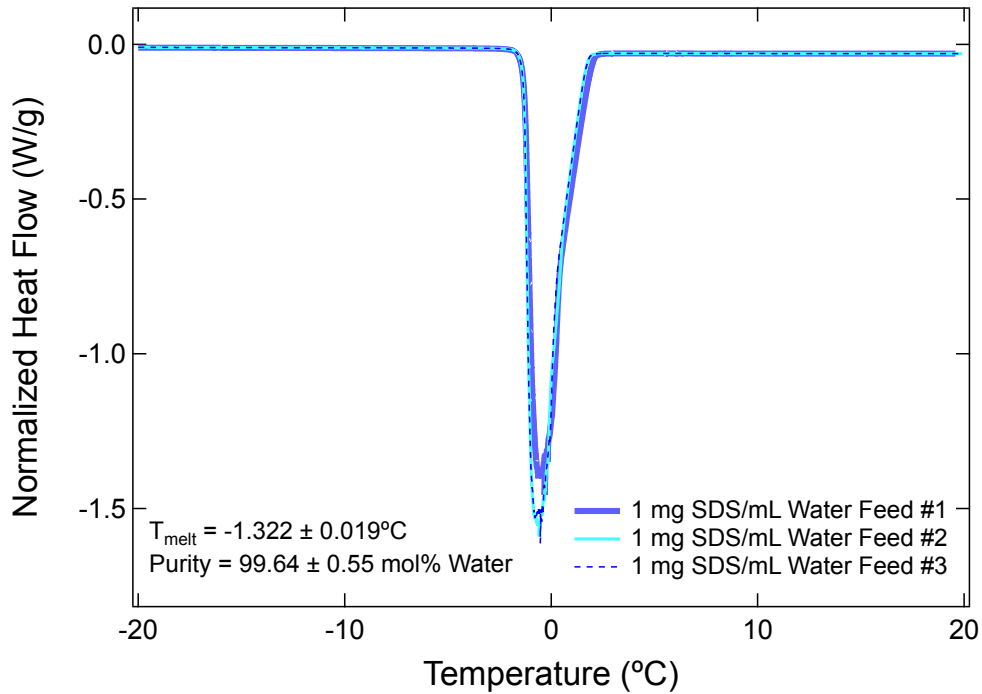
Figure A.15: DSC purity analysis of 1 mg SDS/mL water feed. The aqueous portion of the feed is to be compared to permeate. Uncertainties use a 95% confidence interval.
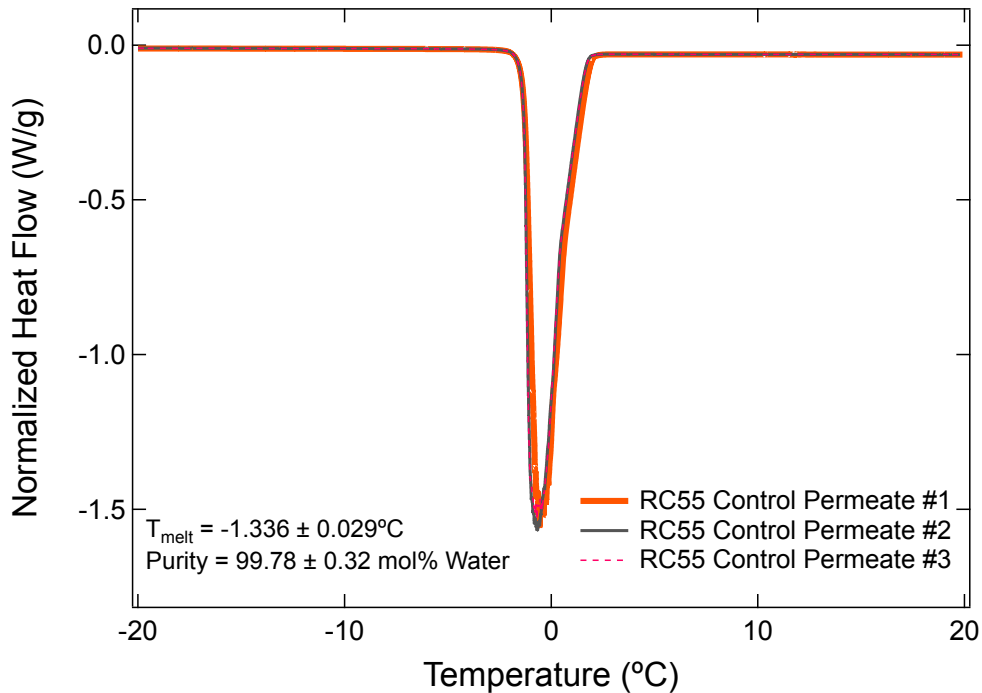
Figure A.16: DSC purity analysis of untreated RC55 control membrane permeate. The control permeate is as pure as the aqueous feed when compared to Figure A.15. Uncertainties use a 95% confidence interval.
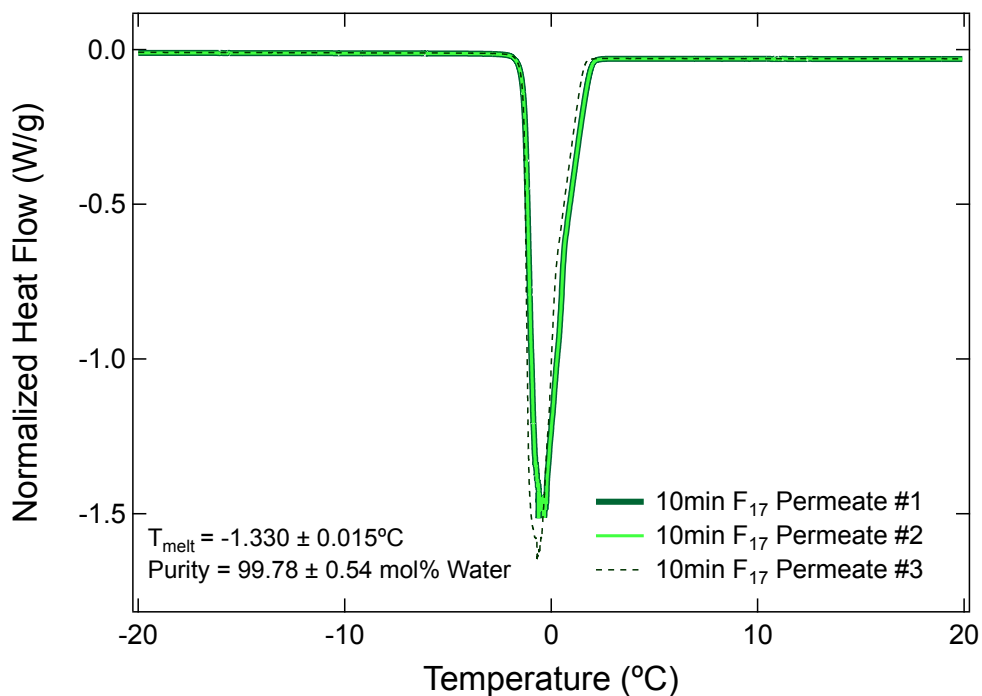
Figure A.17: DSC purity analysis of 10min F_{17} RC55 membrane permeate. The permeate is as pure as the aqueous feed when compared to Figure A.15. Uncertainties use a 95% confidence interval.
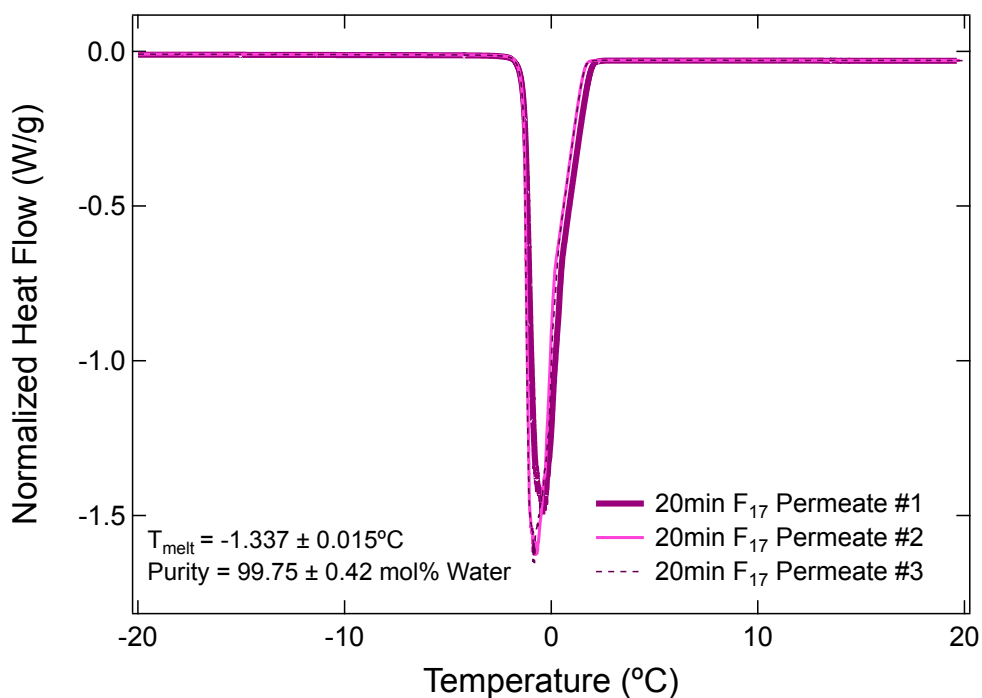
Figure A.18: DSC purity analysis of 20min F_{17} RC55 membrane permeate. The permeate is as pure as the aqueous feed when compared to Figure A.15. Uncertainties use a 95% confidence interval.

A.3.4.4 Ceramic silica membrane feed and permeate purity analysis using DSC
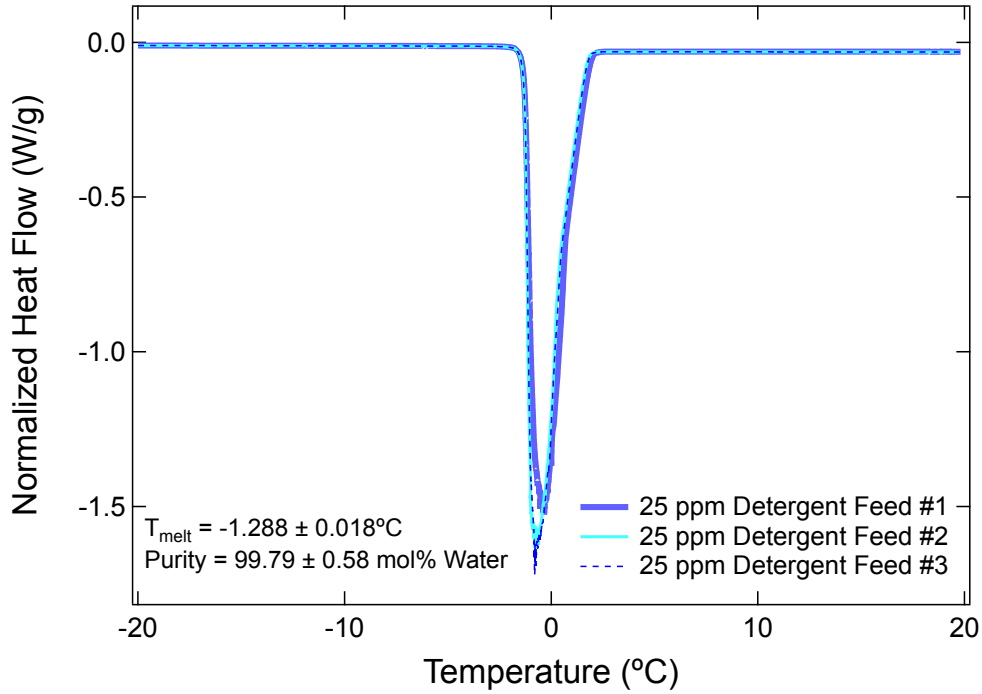
Figure A.19: DSC purity analysis of 25 ppm detergent in water feed. The aqueous portion of the feed for the tubular ceramic membrane apparatus is to be compared to the membrane permeate. Uncertainties use a 95% confidence interval.
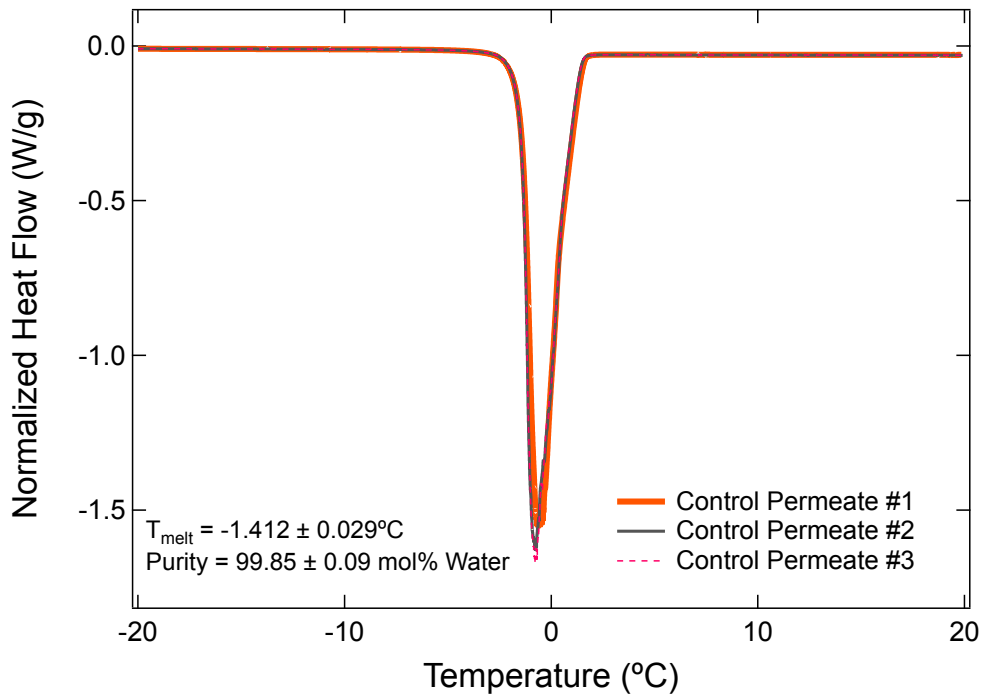
Figure A.20: DSC purity analysis for untreated silica control membrane permeate. The control permeate is as pure as the aqueous feed when compared to Figure A.19. Uncertainties use a 95% confidence interval.
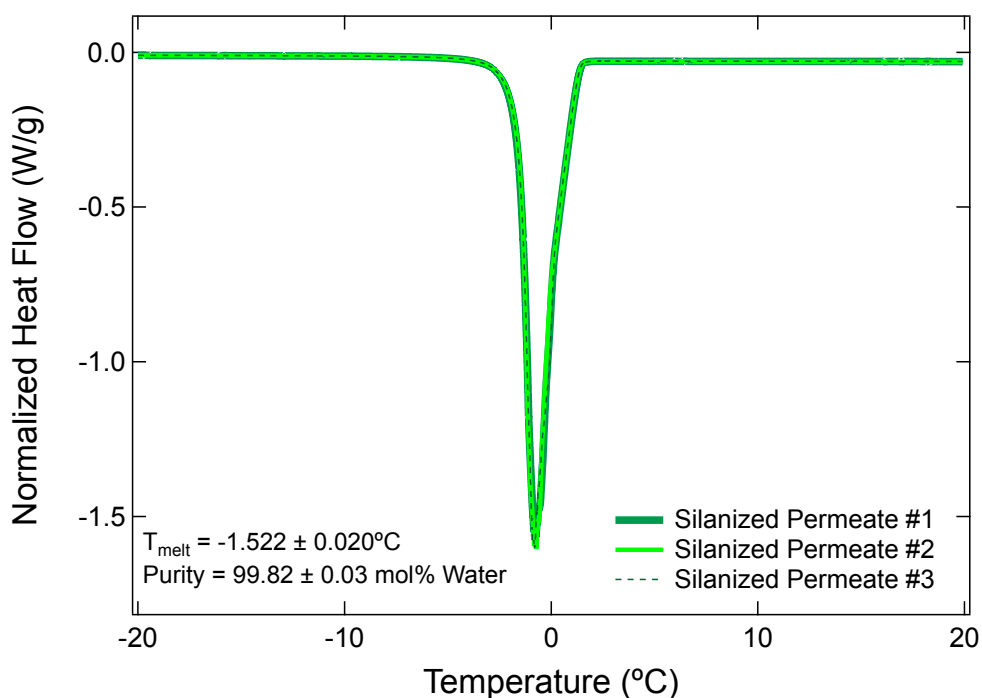
Figure A.21: DSC purity analysis of the HL/OP silica membrane permeate. The permeate is as pure as the aqueous feed when compared to Figure A.19. Uncertainties use a 95% confidence interval.

A.3.5 Raw RC55 Sheet Membrane Permeate Data for Figure 2.11

Table A.4: Untreated Trial 1: Collected Permeate Over Time

Time (min)	Permeate (g)	Time (min)	Permeate (g)	Time (min)	Permeate (g)	Time (min)	Permeate (g)
1.0	6.5	91.0	103.2	181.0	146.2	271.0	172.5
2.0	10.9	92.0	103.6	182.0	146.4	272.0	172.6
3.0	14.6	93.0	104.0	183.0	146.6	273.0	172.8
4.0	18.0	94.0	104.5	184.0	146.7	274.0	173.0
5.0	21.1	95.0	105.0	185.0	146.9	275.0	173.1
6.0	24.1	96.0	105.5	186.0	147.1	276.0	173.3
7.0	26.9	97.0	105.9	187.0	147.3	277.0	173.4
8.0	29.6	98.0	106.4	188.0	147.5	278.0	173.6
9.0	32.1	99.3	106.9	189.0	147.7	279.0	173.7
10.0	34.5	100.0	107.2	190.0	147.8	280.0	173.9
11.0	36.8	101.0	107.6	191.0	148.0	281.0	174.1
12.0	39.0	102.0	108.0	192.0	148.2	282.0	174.2
13.0	41.1	103.0	108.4	193.0	148.3	283.0	174.3
14.0	43.1	104.0	108.8	194.0	148.5	284.0	174.5
15.0	45.1	105.0	109.2	195.0	148.7	285.0	174.7
16.0	46.9	106.0	109.5	196.0	148.8	286.0	174.9
17.0	48.8	107.0	109.9	197.0	149.0	287.0	175.0
18.0	50.4	108.0	110.3	198.0	149.2	288.0	175.2

19.2	52.4	109.0	110.6	199.0	149.3	289.0	175.3
20.0	53.8	110.0	111.0	200.0	149.5	290.0	175.5
21.0	55.3	111.0	111.4	201.0	149.7	291.0	175.6
22.0	56.8	112.0	111.7	202.0	149.8	292.0	175.8
23.0	58.3	113.0	112.1	203.0	150.0	293.0	175.9
24.0	59.7	114.0	112.5	204.0	150.2	294.0	176.1
25.0	61.0	115.0	112.8	205.0	150.3	295.0	176.2
26.0	62.3	116.0	113.2	206.0	150.5	296.0	176.4
27.0	63.6	117.0	113.6	207.0	150.7	297.0	176.6
28.0	64.8	118.0	113.9	208.0	150.9	298.0	176.7
29.0	66.0	119.0	114.3	209.0	151.0	299.0	176.9
30.0	67.1	120.0	114.7	210.0	151.2	300.0	177.0
31.0	68.3	121.0	121.2	211.0	151.4	301.0	177.2
32.0	69.4	122.0	123.5	212.0	151.6	302.0	177.3
33.2	70.7	123.0	125.2	213.0	151.7	303.0	177.4
34.0	71.6	124.0	126.6	214.0	151.9	304.0	177.6
35.0	72.6	125.0	127.7	215.0	152.1	305.0	177.7
36.0	73.6	126.0	128.6	216.0	152.3	306.0	177.9
37.0	74.5	127.0	129.5	217.0	152.4	307.0	178.0
38.0	75.4	128.0	130.3	218.0	152.5	308.0	178.2
39.0	76.4	129.0	131.0	219.0	152.7	309.0	178.4
40.0	77.2	130.0	131.7	220.0	152.9	310.0	178.5
41.0	78.0	131.0	132.3	221.0	153.0	311.0	178.7
42.0	78.8	132.0	132.9	222.0	153.2	312.0	178.8
43.0	79.6	133.0	133.4	223.0	153.4	313.0	179.0
44.0	80.5	134.0	133.9	224.0	153.6	314.0	179.1
45.0	81.2	135.0	134.5	225.0	153.7	315.0	179.3
46.0	81.9	136.0	134.9	226.0	153.9	316.0	179.5
47.0	82.6	137.0	135.4	227.0	154.0	317.0	179.6
48.0	83.3	138.0	135.8	228.0	154.2	318.0	179.7
49.0	84.0	139.0	136.2	229.0	154.3	319.0	179.8
50.0	84.6	140.0	136.6	230.0	154.5	320.0	180.0
51.0	85.2	141.0	137.0	231.0	154.7	321.0	180.1
52.0	85.8	142.0	137.2	232.0	154.8	322.0	180.3
53.0	86.3	143.0	137.6	233.0	155.0	323.0	180.4
54.0	86.9	144.0	138.0	234.0	155.2	324.0	180.6
55.0	87.5	145.0	138.3	235.0	155.3	325.0	180.8
56.0	88.0	146.0	138.5	236.0	155.5	326.0	180.9
57.0	88.5	147.0	138.8	237.0	155.6	327.0	181.1
58.0	89.0	148.0	139.1	238.0	155.8	328.0	181.2
59.0	89.5	149.0	139.5	239.0	156.0	329.0	181.4
60.0	90.0	150.0	139.7	240.0	156.1	330.0	181.5
61.0	90.5	151.0	140.0	241.0	161.2	331.0	181.7
62.0	90.9	152.0	140.3	242.0	163.3	332.0	181.7
63.0	91.4	153.0	140.5	243.0	164.6	333.0	181.9
64.0	91.9	154.0	140.8	244.0	165.5	334.0	182.1
65.0	92.3	155.0	141.0	245.0	166.2	335.0	182.2
66.0	92.8	156.0	141.3	246.0	166.9	336.0	182.4
67.0	93.3	157.0	141.5	247.0	167.4	337.0	182.5
68.0	93.7	158.0	141.7	248.0	167.7	338.0	182.7
69.0	94.1	159.0	142.0	249.0	168.0	339.0	182.8
70.0	94.6	160.0	142.2	250.0	168.3	340.0	182.9

71.0	95.0	161.0	142.4	251.0	168.6	341.0	183.1
72.0	95.4	162.0	142.6	252.0	168.9	342.0	183.3
73.0	95.8	163.0	142.8	253.0	169.1	343.0	183.4
74.0	96.2	164.0	143.0	254.0	169.4	344.0	183.5
75.0	96.6	165.0	143.2	255.0	169.6	345.0	183.7
76.0	97.1	166.0	143.4	256.0	169.8	346.0	183.8
77.0	97.5	167.0	143.6	257.0	170.0	347.0	184.0
78.0	97.9	168.0	143.8	258.0	170.2	348.0	184.1
79.0	98.4	169.0	144.0	259.0	170.3	349.0	184.2
80.0	98.7	170.0	144.2	260.0	170.5	350.0	184.4
81.0	99.1	171.0	144.4	261.0	170.7	351.0	184.5
82.0	99.6	172.0	144.6	262.0	170.9	352.0	184.7
83.0	100.0	173.0	144.8	263.0	171.1	353.0	184.8
84.0	100.3	174.0	144.9	264.0	171.3	354.0	184.9
85.0	100.8	175.0	145.1	265.0	171.5	355.0	185.1
86.0	101.2	176.0	145.3	266.0	171.6	356.0	185.2
87.0	101.6	177.0	145.5	267.0	171.8	357.0	185.4
88.0	102.0	178.0	145.7	268.0	172.0	358.0	185.6
89.0	102.4	179.0	145.9	269.0	172.2	359.0	185.6
90.0	102.8	180.0	146.1	270.0	172.3	360.0	185.8

Table A.5: Untreated Trial 2: Collected Permeate Over Time

Time (min)	Permeate (g)	Time (min)	Permeate (g)	Time (min)	Permeate (g)	Time (min)	Permeate (g)
1.0	5.9	91.0	107.0	181.0	145.3	271.0	172.3
2.0	10.8	92.0	107.4	182.0	145.5	272.0	172.5
3.0	15.3	93.0	107.7	183.0	145.7	273.0	172.6
4.0	19.6	94.0	108.1	184.0	145.9	274.0	172.8
5.0	23.6	95.0	108.5	185.0	146.1	275.0	173.0
6.0	27.4	96.0	108.8	186.0	146.3	276.0	173.2
7.0	30.8	97.0	109.2	187.0	146.5	277.0	173.4
8.0	33.8	98.0	109.5	188.0	146.7	278.0	173.5
9.3	37.3	99.0	109.9	189.0	146.8	279.0	173.7
10.0	39.2	100.0	110.2	190.0	147.0	280.0	173.9
11.0	41.5	101.0	110.5	191.0	147.2	281.0	174.1
12.0	43.9	102.0	110.8	192.0	147.4	282.0	174.2
13.0	46.4	103.0	111.2	193.0	147.6	283.0	174.5
14.0	48.7	104.0	111.6	194.0	147.8	284.0	174.6
15.0	50.8	105.0	111.9	195.0	148.0	285.0	174.8
16.0	52.9	106.0	112.2	196.0	148.2	286.0	175.0
17.0	54.7	107.0	112.5	197.0	148.4	287.0	175.1
18.0	56.5	108.0	112.9	198.0	148.6	288.0	175.3
19.0	58.2	109.0	113.2	199.0	148.8	289.0	175.5
20.0	59.8	110.0	113.5	200.0	149.0	290.0	175.7
21.0	61.4	111.0	113.8	201.0	149.2	291.0	175.8
22.0	62.9	112.0	114.2	202.0	149.4	292.0	176.0
23.0	64.3	113.0	114.5	203.0	149.6	293.0	176.2
24.0	65.7	114.0	114.8	204.0	149.8	294.0	176.4
25.0	67.0	115.0	115.1	205.0	150.0	295.0	176.6
26.0	68.4	116.0	115.4	206.0	150.2	296.0	176.7
27.0	69.6	117.0	115.8	207.0	150.4	297.0	176.9
28.0	70.8	118.0	116.1	208.0	150.6	298.0	177.0

29.0	72.0	119.0	116.4	209.0	150.8	299.0	177.3
30.0	73.2	120.0	116.7	210.0	151.0	300.0	177.4
31.0	74.2	121.0	122.2	211.0	151.2	301.0	177.6
32.0	75.3	122.0	124.4	212.0	151.3	302.0	177.8
33.2	76.5	123.0	126.0	213.0	151.5	303.0	178.0
34.0	77.4	124.0	127.3	214.0	151.7	304.0	178.1
35.0	78.3	125.0	128.5	215.0	151.9	305.0	178.3
36.0	79.2	126.0	129.4	216.0	152.1	306.0	178.5
37.0	80.1	127.0	130.2	217.0	152.3	307.0	178.7
38.0	80.9	128.0	131.0	218.0	152.5	308.0	178.8
39.0	81.7	129.0	131.7	219.0	152.7	309.0	179.0
40.0	82.4	130.0	132.3	220.0	152.9	310.0	179.2
41.0	83.2	131.0	132.9	221.0	153.1	311.0	179.3
42.0	83.9	132.0	133.4	222.0	153.2	312.0	179.5
43.3	84.8	133.0	133.8	223.0	153.4	313.0	179.7
44.0	85.2	134.3	134.4	224.0	153.6	314.0	179.9
45.0	85.8	135.0	134.7	225.0	153.8	315.0	180.0
46.0	86.4	136.0	135.1	226.0	154.0	316.0	180.1
47.0	87.0	137.0	135.4	227.0	154.2	317.0	180.4
48.2	87.7	138.0	135.7	228.0	154.4	318.0	180.5
49.0	88.1	139.0	136.0	229.0	154.5	319.0	180.7
50.0	88.7	140.3	136.4	230.0	154.7	320.0	180.8
51.0	89.2	141.0	136.6	231.0	154.9	321.0	181.0
52.2	89.8	142.0	136.9	232.0	155.1	322.0	181.2
53.0	90.2	143.3	137.2	233.0	155.3	323.0	181.4
54.0	90.7	144.0	137.5	234.0	155.5	324.0	181.5
55.0	91.2	145.0	137.7	235.0	155.7	325.0	181.7
56.0	91.7	146.0	137.9	236.0	155.9	326.0	181.9
57.0	92.2	147.0	138.2	237.0	156.0	327.0	182.0
58.0	92.7	148.0	138.4	238.0	156.2	328.0	182.2
59.0	93.1	149.0	138.6	239.0	156.4	329.0	182.3
60.0	93.5	150.0	138.9	240.0	156.6	330.0	182.5
61.0	94.0	151.0	139.1	241.0	161.7	331.0	182.6
62.0	94.4	152.0	139.3	242.0	163.3	332.0	182.8
63.0	94.9	153.0	139.5	243.0	164.4	333.0	183.0
64.0	95.3	154.0	139.7	244.0	165.2	334.0	183.1
65.0	95.7	155.0	140.0	245.0	165.8	335.0	183.3
66.0	96.1	156.0	140.2	246.0	166.4	336.0	183.5
67.0	96.5	157.0	140.5	247.0	166.7	337.0	183.6
68.0	96.9	158.0	140.7	248.0	167.1	338.0	183.8
69.0	97.3	159.0	140.9	249.0	167.4	339.0	184.0
70.0	97.7	160.0	141.1	250.0	167.7	340.0	184.2
71.0	98.1	161.0	141.3	251.0	168.0	341.0	184.3
72.0	98.6	162.0	141.5	252.0	168.3	342.0	184.5
73.0	98.9	163.0	141.7	253.0	168.5	343.0	184.6
74.0	99.3	164.0	141.9	254.0	168.8	344.0	184.8
75.0	99.7	165.0	142.1	255.0	169.0	345.0	185.0
76.3	100.3	166.0	142.3	256.0	169.2	346.0	185.2
77.0	100.9	167.0	142.5	257.0	169.4	347.0	185.3
78.2	101.6	168.0	142.7	258.0	169.7	348.0	185.4
79.2	102.2	169.0	142.9	259.0	169.9	349.0	185.6
80.0	102.5	170.0	143.1	260.0	170.1	350.0	185.7

81.0	103.0	171.0	143.3	261.0	170.3	351.0	185.9
82.0	103.4	172.0	143.5	262.0	170.5	352.0	186.0
83.0	103.8	173.0	143.7	263.0	170.7	353.0	186.2
84.0	104.3	174.0	143.9	264.0	170.9	354.0	186.4
85.0	104.7	175.0	144.1	265.0	171.1	355.0	186.5
86.3	105.2	176.0	144.3	266.0	171.3	356.0	186.7
87.0	105.4	177.0	144.5	267.0	171.5	357.0	186.8
88.0	105.8	178.0	144.7	268.0	171.7	358.0	187.0
89.0	106.2	179.0	144.9	269.0	171.9	359.0	187.1
90.0	106.6	180.0	145.1	270.0	172.1	360.0	187.3

Table A.6: Untreated Trial 3: Collected Permeate Over Time

Time (min)	Permeate (g)	Time (min)	Permeate (g)	Time (min)	Permeate (g)	Time (min)	Permeate (g)
1.0	5.9	91.0	107.2	181.0	143.8	271.0	168.6
2.0	10.7	92.0	107.6	182.0	143.9	272.0	168.8
3.0	15.0	93.0	107.9	183.0	144.1	273.0	169.0
4.0	18.8	94.0	108.2	184.0	144.2	274.0	169.3
5.0	22.6	95.0	108.5	185.0	144.4	275.0	169.5
6.0	26.2	96.0	108.8	186.0	144.6	276.0	169.7
7.0	29.6	97.0	109.1	187.0	144.7	277.0	169.9
8.0	32.9	98.0	109.4	188.0	144.8	278.0	170.1
9.0	36.2	99.0	109.7	189.0	144.9	279.0	170.3
10.0	38.8	100.0	110.0	190.0	145.1	280.0	170.5
11.0	41.5	101.0	110.3	191.0	145.2	281.0	170.6
12.0	43.9	102.0	110.6	192.0	145.4	282.0	170.8
13.0	46.4	103.0	110.9	193.0	145.5	283.0	171.0
14.0	48.7	104.0	111.2	194.0	145.6	284.0	171.2
15.0	50.9	105.0	111.5	195.0	145.8	285.0	171.4
16.0	53.0	106.0	111.8	196.0	146.0	286.0	171.6
17.0	55.0	107.0	112.1	197.0	146.1	287.0	171.8
18.0	56.8	108.0	112.4	198.0	146.2	288.0	172.0
19.0	58.6	109.0	112.7	199.0	146.4	289.0	172.2
20.0	60.3	110.0	113.0	200.0	146.5	290.0	172.4
21.0	61.9	111.0	113.3	201.0	146.7	291.0	172.6
22.0	63.6	112.0	113.6	202.0	146.8	292.0	172.8
23.0	65.2	113.0	114.0	203.0	146.9	293.0	173.0
24.0	66.8	114.0	114.3	204.0	147.1	294.0	173.2
25.0	68.2	115.0	114.6	205.0	147.2	295.0	173.4
26.0	69.5	116.0	114.9	206.0	147.3	296.0	173.6
27.0	70.8	117.0	115.2	207.0	147.5	297.0	173.8
28.0	72.1	118.0	115.5	208.0	147.6	298.0	174.0
29.0	73.2	119.0	115.8	209.0	147.8	299.0	174.1
30.0	74.4	120.0	116.0	210.0	147.9	300.0	174.3
31.0	75.4	121.0	121.5	211.0	148.0	301.0	174.5
32.0	76.5	122.0	123.9	212.0	148.2	302.0	174.7
33.0	77.6	123.0	125.6	213.0	148.3	303.0	174.9
34.0	78.6	124.0	127.0	214.0	148.5	304.0	175.1
35.0	79.5	125.0	128.2	215.0	148.6	305.0	175.2
36.0	80.5	126.0	129.2	216.0	148.7	306.0	175.4
37.0	81.4	127.0	130.1	217.0	148.9	307.0	175.6
38.0	82.3	128.0	130.8	218.0	149.0	308.0	175.9

39.0	83.0	129.0	131.6	219.0	149.2	309.0	176.1
40.0	83.8	130.0	132.2	220.0	149.3	310.0	176.2
41.0	84.6	131.0	132.8	221.0	149.4	311.0	176.5
42.0	85.3	132.0	133.4	222.0	149.6	312.0	176.6
43.0	86.0	133.0	133.9	223.0	149.7	313.0	176.8
44.0	86.8	134.0	134.4	224.0	149.9	314.0	177.0
45.0	87.5	135.0	134.7	225.0	150.0	315.0	177.2
46.0	88.1	136.0	135.2	226.0	150.1	316.0	177.4
47.0	88.7	137.0	135.5	227.0	150.3	317.0	177.6
48.0	89.4	138.0	135.8	228.0	150.4	318.0	177.7
49.0	90.0	139.0	136.1	229.0	150.6	319.0	178.0
50.0	90.5	140.0	136.4	230.0	150.7	320.0	178.1
51.0	91.0	141.0	136.7	231.0	150.8	321.0	178.3
52.0	91.6	142.0	136.9	232.0	151.0	322.0	178.5
53.0	92.1	143.0	137.2	233.0	151.1	323.0	178.7
54.0	92.6	144.0	137.4	234.0	151.2	324.0	178.8
55.0	93.1	145.0	137.6	235.0	151.4	325.0	179.0
56.0	93.6	146.0	137.8	236.0	151.5	326.0	179.2
57.0	94.2	147.0	138.1	237.0	151.7	327.0	179.4
58.0	94.7	148.0	138.3	238.0	151.8	328.0	179.6
59.0	95.2	149.0	138.5	239.0	152.0	329.0	179.8
60.0	95.7	150.0	138.7	240.0	152.1	330.0	180.0
61.0	96.1	151.0	138.9	241.0	157.6	331.0	180.2
62.0	96.6	152.0	139.0	242.0	159.4	332.0	180.3
63.0	97.0	153.0	139.2	243.0	160.6	333.0	180.5
64.0	97.5	154.0	139.4	244.0	161.4	334.0	180.7
65.0	97.9	155.0	139.6	245.0	162.0	335.0	180.9
66.0	98.3	156.0	139.8	246.0	162.5	336.0	181.1
67.0	98.7	157.0	139.9	247.0	162.9	337.0	181.3
68.0	99.1	158.0	140.1	248.0	163.2	338.0	181.5
69.0	99.5	159.0	140.3	249.0	163.6	339.0	181.6
70.0	99.9	160.0	140.5	250.0	163.9	340.0	181.8
71.0	100.3	161.0	140.6	251.0	164.1	341.0	182.0
72.0	100.7	162.0	140.8	252.0	164.4	342.0	182.2
73.0	101.1	163.0	140.9	253.0	164.7	343.0	182.4
74.0	101.5	164.0	141.1	254.0	164.9	344.0	182.6
75.0	101.8	165.0	141.3	255.0	165.2	345.0	182.8
76.0	102.2	166.0	141.5	256.0	165.4	346.0	183.0
77.0	102.6	167.0	141.6	257.0	165.7	347.0	183.2
78.0	102.9	168.0	141.8	258.0	165.9	348.0	183.4
79.0	103.2	169.0	141.9	259.0	166.1	349.0	183.6
80.0	103.6	170.0	142.1	260.0	166.3	350.0	183.8
81.0	104.0	171.0	142.3	261.0	166.6	351.0	183.9
82.0	104.3	172.0	142.4	262.0	166.7	352.0	184.1
83.0	104.6	173.0	142.5	263.0	166.9	353.0	184.4
84.0	105.0	174.0	142.7	264.0	167.2	354.0	184.6
85.0	105.3	175.0	142.9	265.0	167.4	355.0	184.8
86.0	105.6	176.0	143.0	266.0	167.6	356.0	185.0
87.0	106.0	177.0	143.2	267.0	167.8	357.0	185.2
88.0	106.3	178.0	143.3	268.0	168.0	358.0	185.4
89.0	106.6	179.0	143.5	269.0	168.2	359.0	185.6
90.0	106.9	180.0	143.6	270.0	168.4	360.0	185.9

Table A.7: 10 min F_{17} Trial 1: Collected Permeate Over Time

Time (min)	Permeate (g)	Time (min)	Permeate (g)	Time (min)	Permeate (g)	Time (min)	Permeate (g)
1.0	6.5	91.0	140.9	181.0	192.6	271.0	223.6
2.0	11.4	92.0	141.4	182.0	192.8	272.0	223.8
3.0	15.7	93.0	142.0	183.0	193.0	273.0	224.0
4.2	20.4	94.0	142.5	184.0	193.3	274.0	224.2
5.1	23.6	95.0	143.0	185.0	193.5	275.0	224.3
6.0	26.8	96.0	143.5	186.0	193.7	276.0	224.4
7.0	30.1	97.0	144.1	187.0	193.9	277.0	224.6
8.0	33.5	98.0	144.6	188.0	194.2	278.0	224.8
9.0	36.3	99.0	145.1	189.0	194.4	279.0	224.9
10.0	39.7	100.0	145.7	190.0	194.6	280.0	225.1
11.0	42.8	101.0	146.2	191.0	194.8	281.0	225.2
12.0	45.7	102.0	146.7	192.0	195.1	282.0	225.4
13.0	48.6	103.0	147.2	193.0	195.3	283.0	225.5
14.0	51.2	104.0	147.7	194.0	195.5	284.0	225.7
15.0	53.8	105.0	148.2	195.0	195.7	285.0	225.9
16.0	56.3	106.0	148.8	196.0	196.0	286.0	226.0
17.0	58.8	107.0	149.3	197.0	196.2	287.0	226.1
18.0	61.1	108.0	149.8	198.0	196.4	288.0	226.3
19.0	63.3	109.0	150.3	199.0	196.6	289.0	226.4
20.0	65.4	110.0	150.8	200.0	196.8	290.0	226.5
21.0	67.4	111.0	151.3	201.0	197.0	291.0	226.7
22.3	69.9	112.0	151.8	202.0	197.2	292.0	226.9
23.0	71.6	113.0	152.3	203.0	197.4	293.0	227.0
24.0	73.3	114.0	152.9	204.0	197.6	294.0	227.1
25.0	75.1	115.0	153.3	205.0	197.8	295.0	227.3
26.3	77.4	116.0	153.8	206.0	198.0	296.0	227.4
27.1	79.1	117.0	154.3	207.0	198.3	297.0	227.5
28.0	80.8	118.0	154.8	208.0	198.5	298.0	227.7
29.0	82.7	119.0	155.2	209.0	198.7	299.0	227.8
30.2	84.9	120.0	155.8	210.0	198.9	300.0	227.9
31.3	87.0	121.0	162.8	211.0	199.1	301.0	228.1
32.0	88.1	122.0	165.5	212.0	199.3	302.0	228.2
33.0	89.7	123.0	167.5	213.0	199.5	303.0	228.3
34.0	91.4	124.0	169.1	214.0	199.7	304.0	228.5
35.0	92.8	125.0	170.4	215.0	200.0	305.0	228.7
36.0	94.3	126.0	171.7	216.0	200.2	306.0	228.8
37.3	96.1	127.0	172.7	217.0	200.3	307.0	228.9
38.0	97.3	128.0	173.8	218.0	200.6	308.0	229.1
39.0	98.4	129.0	174.6	219.0	200.8	309.0	229.2
40.0	99.7	130.0	175.5	220.0	201.0	310.0	229.4
41.0	101.0	131.0	176.3	221.0	201.2	311.0	229.5
42.0	102.3	132.0	177.0	222.0	201.4	312.0	229.6
43.0	103.5	133.0	177.7	223.0	201.6	313.0	229.7
44.0	104.7	134.0	178.4	224.0	201.8	314.0	229.9
45.0	105.9	135.0	179.0	225.0	202.0	315.0	230.0
46.0	107.0	136.0	179.6	226.0	202.2	316.0	230.2
47.0	108.1	137.0	180.2	227.0	202.4	317.0	230.3
48.0	109.3	138.0	180.6	228.0	202.6	318.0	230.5
49.0	110.3	139.0	181.1	229.0	202.8	319.0	230.6
50.0	111.4	140.0	181.6	230.0	203.0	320.0	230.7

51.0	112.4	141.0	182.0	231.0	203.2	321.0	230.9
52.0	113.5	142.0	182.4	232.0	203.4	322.0	231.0
53.0	114.4	143.0	182.8	233.0	203.6	323.0	231.1
54.3	115.6	144.0	183.2	234.0	203.8	324.0	231.3
55.0	116.4	145.0	183.6	235.0	204.0	325.0	231.5
56.0	117.2	146.0	184.0	236.0	204.2	326.0	231.6
57.0	118.0	147.0	184.3	237.0	204.4	327.0	231.7
58.0	119.0	148.0	184.7	238.0	204.6	328.0	231.8
59.0	119.8	149.0	185.0	239.0	204.9	329.0	232.0
60.0	120.6	150.0	185.3	240.0	205.1	330.0	232.1
61.0	121.5	151.0	185.6	241.0	210.3	331.0	232.3
62.0	122.3	152.0	185.9	242.0	212.0	332.0	232.4
63.0	123.1	153.0	186.1	243.0	213.3	333.0	232.6
64.0	123.9	154.0	186.2	244.0	214.4	334.0	232.7
65.0	124.6	155.0	186.3	245.0	215.4	335.0	232.8
66.0	125.3	156.0	186.6	246.0	216.2	336.0	232.9
67.0	126.1	157.0	186.8	247.0	216.8	337.0	233.1
68.0	126.9	158.0	187.1	248.0	217.4	338.0	233.2
69.0	127.5	159.0	187.3	249.0	218.0	339.0	233.4
70.0	128.2	160.0	187.6	250.0	218.5	340.0	233.5
71.3	129.0	161.0	187.8	251.0	219.0	341.0	233.6
72.0	129.5	162.0	188.1	252.0	219.4	342.0	233.8
73.0	130.2	163.0	188.3	253.0	219.7	343.0	233.9
74.0	130.8	164.0	188.6	254.0	220.0	344.0	234.1
75.0	131.4	165.0	188.8	255.0	220.4	345.0	234.2
76.0	132.1	166.0	189.1	256.0	220.6	346.0	234.4
77.0	132.6	167.0	189.3	257.0	220.9	347.0	234.5
78.0	133.2	168.0	189.6	258.0	221.2	348.0	234.6
79.0	133.9	169.0	189.8	259.0	221.4	349.0	234.8
80.0	134.5	170.0	190.0	260.0	221.6	350.0	234.9
81.0	135.0	171.0	190.3	261.0	221.8	351.0	235.1
82.0	135.6	172.0	190.5	262.0	222.1	352.0	235.2
83.0	136.3	173.0	190.7	263.0	222.2	353.0	235.4
84.0	136.8	174.0	191.0	264.0	222.4	354.0	235.5
85.0	137.4	175.0	191.2	265.0	222.6	355.0	235.7
86.0	138.0	176.0	191.4	266.0	222.8	356.0	235.8
87.0	138.6	177.0	191.7	267.0	223.0	357.0	235.9
88.0	139.2	178.0	191.9	268.0	223.2	358.0	236.1
89.0	139.7	179.0	192.1	269.0	223.4	359.0	236.2
90.0	140.3	180.0	192.3	270.0	223.5	360.0	236.4

Table A.8: 10 min F_{17} Trial 2: Collected Permeate Over Time

Time (min)	Permeate (g)	Time (min)	Permeate (g)	Time (min)	Permeate (g)	Time (min)	Permeate (g)
1.0	7.7	91.0	139.0	181.0	189.0	271.0	222.8
2.0	14.2	92.0	139.4	182.0	189.3	272.0	223.0
3.0	20.1	93.0	139.9	183.0	189.6	273.0	223.2
4.1	26.1	94.0	140.4	184.0	189.9	274.0	223.3
5.2	31.3	95.0	140.9	185.0	190.1	275.0	223.5
6.0	34.7	96.0	141.3	186.0	190.4	276.0	223.6
7.0	38.5	97.0	141.8	187.0	190.7	277.0	223.8
8.0	42.3	98.0	142.2	188.0	191.0	278.0	223.9
9.1	46.1	99.0	142.6	189.0	191.2	279.0	224.0

10.0	49.1	100.0	143.1	190.0	191.5	280.0	224.2
11.0	52.2	101.0	143.5	191.0	191.8	281.0	224.4
12.0	55.2	102.0	144.0	192.0	192.0	282.0	224.5
13.0	58.2	103.0	144.4	193.0	192.4	283.0	224.7
14.2	61.1	104.0	144.8	194.0	192.6	284.0	224.8
15.0	63.3	105.0	145.2	195.0	192.9	285.0	225.0
16.0	65.7	106.0	145.6	196.0	193.2	286.0	225.1
17.0	68.0	107.0	146.2	197.0	193.4	287.0	225.2
18.3	71.0	108.0	146.6	198.0	193.7	288.0	225.3
19.0	72.4	109.0	147.0	199.0	193.9	289.0	225.5
20.0	74.4	110.0	147.4	200.0	194.1	290.0	225.6
21.0	76.4	111.0	147.8	201.0	194.4	291.0	225.8
22.0	78.3	112.0	148.3	202.0	194.7	292.0	225.9
23.0	80.2	113.0	148.7	203.0	194.9	293.0	226.0
24.1	82.2	114.0	149.1	204.0	195.1	294.0	226.2
25.0	83.9	115.0	149.6	205.0	195.4	295.0	226.3
26.0	85.4	116.0	150.0	206.0	195.7	296.0	226.4
27.0	87.1	117.0	150.4	207.0	195.9	297.0	226.6
28.3	89.2	118.0	150.8	208.0	196.2	298.0	226.7
29.0	90.2	119.0	151.2	209.0	196.5	299.0	226.8
30.0	91.8	120.0	151.7	210.0	196.7	300.0	227.0
31.0	93.4	121.0	157.9	211.0	197.0	301.0	227.1
32.0	94.7	122.0	160.4	212.0	197.2	302.0	227.3
33.0	96.1	123.0	162.4	213.0	197.5	303.0	227.5
34.0	97.5	124.0	164.1	214.0	197.7	304.0	227.6
35.0	98.9	125.0	165.4	215.0	198.0	305.0	227.7
36.0	101.0	126.0	166.7	216.0	198.2	306.0	227.8
37.0	102.5	127.0	167.9	217.0	198.5	307.0	228.0
38.0	103.9	128.0	168.8	218.0	198.7	308.0	228.1
39.0	105.2	129.0	169.8	219.0	198.9	309.0	228.2
40.0	106.4	130.0	170.6	220.0	199.2	310.0	228.4
41.0	107.5	131.0	171.5	221.0	199.4	311.0	228.5
42.0	108.5	132.0	172.3	222.0	199.7	312.0	228.6
43.0	109.5	133.0	173.0	223.0	199.9	313.0	228.8
44.0	110.5	134.0	173.6	224.0	200.2	314.0	228.9
45.0	111.6	135.0	174.2	225.0	200.4	315.0	229.1
46.0	112.5	136.0	174.8	226.0	200.7	316.0	229.2
47.0	113.6	137.0	175.3	227.0	201.0	317.0	229.3
48.0	114.3	138.0	175.9	228.0	201.2	318.0	229.4
49.0	115.1	139.0	176.3	229.0	201.4	319.0	229.6
50.0	115.9	140.0	176.7	230.0	201.7	320.0	229.7
51.0	116.7	141.0	177.2	231.0	201.9	321.0	229.9
52.0	117.4	142.0	177.6	232.0	202.1	322.0	230.0
53.0	118.2	143.0	178.0	233.0	202.4	323.0	230.1
54.0	118.9	144.0	178.3	234.0	202.7	324.0	230.2
55.0	119.8	145.0	178.6	235.0	203.0	325.0	230.4
56.0	120.6	146.0	179.0	236.0	203.3	326.0	230.6
57.0	121.2	147.0	179.4	237.0	203.5	327.0	230.7
58.0	121.9	148.0	179.7	238.0	203.8	328.0	230.8
59.0	122.5	149.0	180.0	239.0	204.0	329.0	230.9
60.0	123.1	150.0	180.3	240.0	204.3	330.0	231.1
61.0	123.7	151.0	180.6	241.0	210.4	331.0	231.2
62.0	124.3	152.0	180.9	242.0	212.3	332.0	231.4
63.0	124.8	153.0	181.2	243.0	213.6	333.0	231.5

64.3	125.5	154.0	181.5	244.0	214.6	334.0	231.6
65.0	125.9	155.0	181.8	245.0	215.4	335.0	231.8
66.0	126.5	156.0	182.1	246.0	216.2	336.0	231.9
67.0	127.0	157.0	182.3	247.3	216.9	337.0	232.0
68.0	127.7	158.0	182.6	248.0	217.3	338.0	232.2
69.0	128.2	159.0	182.9	249.0	217.8	339.0	232.3
70.0	128.7	160.0	183.2	250.0	218.2	340.0	232.4
71.0	129.2	161.0	183.5	251.0	218.6	341.0	232.6
72.0	129.7	162.0	183.7	252.0	219.0	342.0	232.7
73.0	130.2	163.0	184.1	253.0	219.2	343.0	232.9
74.0	130.8	164.0	184.4	254.0	219.5	344.0	233.0
75.2	131.3	165.0	184.7	255.0	219.8	345.0	233.2
76.0	131.7	166.0	184.9	256.0	220.0	346.0	233.3
77.0	132.2	167.0	185.2	257.0	220.2	347.0	233.4
78.0	132.7	168.0	185.5	258.0	220.4	348.0	233.6
79.0	133.2	169.0	185.8	259.0	220.7	349.0	233.7
80.0	133.6	170.0	186.1	260.0	220.9	350.0	233.9
81.0	134.1	171.0	186.4	261.0	221.1	351.0	234.0
82.2	134.6	172.0	186.7	262.0	221.3	352.0	234.1
83.0	135.0	173.0	187.0	263.0	221.5	353.0	234.2
84.0	135.5	174.0	187.2	264.0	221.7	354.0	234.4
85.3	136.0	175.0	187.5	265.0	221.9	355.0	234.5
86.0	136.5	176.0	187.7	266.0	222.1	356.0	234.6
87.0	137.0	177.0	188.0	267.0	222.2	357.0	234.8
88.0	137.5	178.0	188.3	268.0	222.4	358.0	234.9
89.0	138.0	179.0	188.6	269.0	222.6	359.0	235.0
90.0	138.5	180.0	188.8	270.0	222.7	360.0	235.2

Table A.9: 10 min F_{17} Trial 3: Collected Permeate Over Time

Time (min)	Permeate (g)	Time (min)	Permeate (g)	Time (min)	Permeate (g)	Time (min)	Permeate (g)
1.0	7.5	91.0	135.9	181.0	191.6	271.0	227.1
2.0	13.8	92.0	136.4	182.0	191.9	272.0	227.3
3.0	19.2	93.0	137.0	183.0	192.2	273.0	227.5
4.0	23.9	94.0	137.7	184.0	192.4	274.0	227.6
5.0	28.3	95.0	138.3	185.0	192.7	275.0	227.8
6.0	32.2	96.0	138.9	186.0	193.0	276.0	227.9
7.0	35.8	97.0	139.5	187.0	193.3	277.0	228.1
8.0	39.2	98.0	140.1	188.0	193.5	278.0	228.2
9.0	42.5	99.0	140.7	189.0	193.8	279.0	228.4
10.0	45.6	100.0	141.3	190.0	194.1	280.0	228.5
11.2	49.0	101.0	141.9	191.0	194.3	281.0	228.7
12.2	51.6	102.0	142.6	192.0	194.6	282.0	228.9
13.0	53.8	103.0	143.2	193.0	194.9	283.0	229.0
14.0	56.2	104.0	143.8	194.0	195.1	284.0	229.2
15.0	58.6	105.0	144.4	195.0	195.4	285.0	229.3
16.0	60.8	106.0	145.0	196.0	195.7	286.0	229.5
17.0	62.9	107.0	145.5	197.0	195.9	287.0	229.6
18.0	64.9	108.0	146.1	198.0	196.2	288.0	229.8
19.0	66.9	109.0	146.7	199.0	196.4	289.0	229.9
20.0	68.9	110.0	147.3	200.0	196.7	290.0	230.1
21.8	72.2	111.0	147.8	201.0	197.0	291.0	230.2
22.0	72.6	112.0	148.4	202.0	197.2	292.0	230.4

23.0	74.3	113.0	148.9	203.0	197.5	293.0	230.5
24.0	76.1	114.0	149.5	204.0	197.8	294.0	230.6
25.0	77.8	115.0	150.0	205.0	198.1	295.0	230.8
26.0	79.4	116.0	150.6	206.0	198.3	296.0	231.0
27.0	81.0	117.0	151.1	207.0	198.5	297.0	231.1
28.0	82.5	118.0	151.6	208.0	198.8	298.0	231.2
29.0	85.1	119.0	152.2	209.0	199.0	299.0	231.3
30.0	87.0	120.0	152.8	210.0	199.3	300.0	231.5
31.0	88.6	121.0	158.8	211.0	199.5	301.0	231.6
32.0	90.2	122.0	161.3	212.0	199.8	302.0	231.8
33.0	91.6	123.0	163.2	213.0	200.1	303.0	231.9
34.0	92.8	124.0	164.9	214.0	200.3	304.0	232.1
35.0	94.1	125.0	166.2	215.0	200.6	305.0	232.2
36.0	95.4	126.0	167.5	216.0	200.8	306.0	232.3
37.0	96.6	127.0	168.5	217.0	201.1	307.0	232.5
38.0	97.7	128.0	169.6	218.0	201.3	308.0	232.6
39.0	98.8	129.0	170.7	219.0	201.6	309.0	232.8
40.3	100.2	130.0	171.6	220.0	201.9	310.0	232.9
41.2	101.1	131.0	172.4	221.0	202.1	311.0	233.1
42.0	102.0	132.0	173.2	222.0	202.4	312.0	233.2
43.3	103.2	133.0	173.9	223.0	202.7	313.0	233.3
44.0	103.8	134.0	174.5	224.0	202.9	314.0	233.5
45.2	104.9	135.0	175.2	225.0	203.2	315.0	233.6
46.0	106.1	136.0	175.7	226.0	203.4	316.0	233.8
47.0	107.2	137.0	176.3	227.0	203.6	317.0	233.9
48.0	108.1	138.0	176.9	228.0	203.9	318.0	234.0
49.0	108.9	139.0	177.3	229.0	204.2	319.0	234.2
50.0	109.7	140.0	177.8	230.0	204.4	320.0	234.3
51.0	110.4	141.0	178.3	231.0	204.7	321.0	234.5
52.0	111.1	142.0	178.8	232.0	204.9	322.0	234.6
53.0	111.8	143.0	179.2	233.0	205.2	323.0	234.7
54.0	112.6	144.0	179.6	234.0	205.4	324.0	234.9
55.0	113.3	145.0	180.0	235.0	205.6	325.0	235.0
56.0	114.0	146.0	180.4	236.0	205.9	326.0	235.2
57.0	114.7	147.0	180.8	237.0	206.1	327.0	235.3
58.0	115.3	148.0	181.2	238.0	206.4	328.0	235.5
59.0	116.0	149.0	181.5	239.0	206.6	329.0	235.6
60.0	116.8	150.0	181.9	240.0	206.9	330.0	235.7
61.0	117.5	151.0	182.2	241.0	212.8	331.0	235.9
62.0	118.1	152.0	182.6	242.0	214.8	332.0	236.0
63.0	118.8	153.0	183.0	243.0	216.2	333.0	236.2
64.0	119.4	154.0	183.3	244.0	217.4	334.0	236.3
65.0	120.1	155.0	183.6	245.0	218.4	335.0	236.4
66.0	120.7	156.0	184.0	246.0	219.1	336.0	236.6
67.0	121.4	157.0	184.3	247.0	219.9	337.0	236.7
68.0	122.0	158.0	184.7	248.0	220.6	338.0	236.9
69.0	122.7	159.0	185.0	249.0	221.1	339.0	237.0
70.0	123.3	160.0	185.3	250.0	221.6	340.0	237.1
71.0	123.9	161.0	185.7	251.0	222.1	341.0	237.3
72.0	124.5	162.0	186.0	252.0	222.5	342.0	237.4
73.0	125.1	163.0	186.3	253.0	222.9	343.0	237.5
74.0	125.7	164.0	186.6	254.0	223.3	344.0	237.7
75.0	126.3	165.0	186.9	255.0	223.6	345.0	237.8
76.0	127.0	166.0	187.2	256.0	223.9	346.0	238.0

77.0	127.6	167.0	187.5	257.0	224.2	347.0	238.1
78.0	128.2	168.0	187.9	258.0	224.5	348.0	238.3
79.0	128.8	169.0	188.2	259.0	224.8	349.0	238.4
80.0	129.4	170.0	188.4	260.0	225.0	350.0	238.5
81.0	130.0	171.0	188.7	261.0	225.2	351.0	238.7
82.0	130.6	172.0	189.0	262.0	225.4	352.0	238.8
83.0	131.2	173.0	189.3	263.0	225.6	353.0	238.9
84.0	131.8	174.0	189.6	264.0	225.8	354.0	239.1
85.0	132.4	175.0	189.9	265.0	226.0	355.0	239.2
86.0	132.9	176.0	190.2	266.0	226.2	356.0	239.4
87.0	133.5	177.0	190.5	267.0	226.4	357.0	239.5
88.0	134.1	178.0	190.8	268.0	226.6	358.0	239.6
89.0	134.7	179.0	191.1	269.0	226.7	359.0	239.7
90.0	135.3	180.0	191.4	270.0	226.9	360.0	239.9

Table A.10: 20 min F_{17} Trial 1: Collected Permeate Over Time

Time (min)	Permeate (g)	Time (min)	Permeate (g)	Time (min)	Permeate (g)	Time (min)	Permeate (g)
1.0	7.0	91.0	119.9	181.0	160.6	271.0	188.0
2.0	13.1	92.0	120.2	182.0	160.8	272.0	188.2
3.0	18.6	93.0	120.6	183.0	161.0	273.0	188.4
4.0	23.8	94.0	120.9	184.0	161.1	274.0	188.6
5.0	28.5	95.0	121.3	185.0	161.3	275.0	188.7
6.0	32.8	96.0	121.6	186.0	161.4	276.0	188.9
7.0	36.4	97.0	122.0	187.0	161.6	277.0	189.1
8.0	39.7	98.0	122.3	188.0	161.8	278.0	189.3
9.0	43.0	99.0	122.6	189.0	161.9	279.0	189.5
10.0	46.0	100.0	123.0	190.0	162.1	280.0	189.7
11.0	48.7	101.0	123.3	191.0	162.3	281.0	189.8
12.0	51.4	102.0	123.6	192.0	162.5	282.0	190.0
13.0	53.9	103.0	124.0	193.0	162.6	283.0	190.2
14.0	56.4	104.0	124.3	194.0	162.8	284.0	190.4
15.0	58.7	105.0	124.6	195.0	162.9	285.0	190.5
16.0	61.0	106.0	124.9	196.0	163.1	286.0	190.7
17.2	63.4	107.0	125.2	197.0	163.3	287.0	190.9
18.0	65.1	108.0	125.5	198.0	163.5	288.0	191.0
19.0	67.1	109.0	125.8	199.0	163.6	289.0	191.2
20.0	68.9	110.0	126.1	200.0	163.7	290.0	191.4
21.0	70.6	111.0	126.5	201.0	163.9	291.0	191.6
22.3	73.0	112.0	126.8	202.0	164.1	292.0	191.8
23.0	74.0	113.0	127.1	203.0	164.2	293.0	191.9
24.0	75.6	114.0	127.4	204.0	164.4	294.0	192.1
25.0	77.1	115.0	127.7	205.0	164.5	295.0	192.3
26.0	78.7	116.0	128.0	206.0	164.7	296.0	192.4
27.0	80.3	117.0	128.3	207.0	164.9	297.0	192.6
28.3	82.0	118.0	128.6	208.0	165.0	298.0	192.8
29.0	83.0	119.0	128.9	209.0	165.1	299.0	192.9
30.0	84.2	120.0	129.2	210.0	165.3	300.0	193.1
31.2	85.5	121.0	135.1	211.0	165.5	301.0	193.2
32.0	86.5	122.0	137.6	212.0	165.6	302.0	193.4
33.0	87.6	123.0	139.5	213.0	165.7	303.0	193.6
34.0	88.7	124.0	141.1	214.0	165.9	304.0	193.8
35.0	89.7	125.0	142.5	215.0	166.1	305.0	193.9

36.0	90.7	126.0	143.6	216.0	166.3	306.0	194.1
37.0	91.6	127.0	144.6	217.0	166.5	307.0	194.3
38.0	92.6	128.0	145.5	218.0	166.6	308.0	194.4
39.0	93.6	129.0	146.2	219.0	166.8	309.0	194.6
40.5	94.8	130.0	146.9	220.0	166.9	310.0	194.8
41.0	95.3	131.0	147.5	221.0	167.1	311.0	194.9
42.0	96.0	132.0	148.1	222.0	167.2	312.0	195.1
43.0	96.8	133.0	148.7	223.0	167.4	313.0	195.3
44.0	97.6	134.0	149.2	224.0	167.6	314.0	195.4
45.0	98.4	135.0	149.6	225.0	167.8	315.0	195.6
46.0	99.0	136.0	150.1	226.0	167.9	316.0	195.7
47.0	99.6	137.0	150.5	227.0	168.1	317.0	195.9
48.0	100.2	138.0	150.8	228.0	168.2	318.0	196.1
49.0	100.9	139.0	151.3	229.0	168.4	319.0	196.3
50.0	101.6	140.0	151.7	230.0	168.6	320.0	196.4
51.0	102.3	141.0	152.1	231.0	168.7	321.0	196.6
52.0	102.9	142.0	152.4	232.0	168.9	322.0	196.7
53.0	103.5	143.0	152.7	233.0	169.0	323.0	196.9
54.0	104.1	144.0	153.0	234.0	169.2	324.0	197.0
55.0	104.7	145.0	153.3	235.0	169.4	325.0	197.2
56.0	105.1	146.0	153.6	236.0	169.5	326.0	197.3
57.0	105.7	147.0	153.9	237.0	169.7	327.0	197.5
58.0	106.2	148.0	154.1	238.0	169.8	328.0	197.6
59.0	106.7	149.0	154.4	239.0	170.0	329.0	197.8
60.0	107.2	150.0	154.7	240.0	170.2	330.0	198.0
61.0	107.7	151.0	154.9	241.0	174.7	331.0	198.2
62.0	108.2	152.0	155.1	242.0	176.8	332.0	198.3
63.0	108.7	153.0	155.4	243.0	178.3	333.0	198.5
64.0	109.2	154.0	155.6	244.0	179.5	334.0	198.6
65.0	109.7	155.0	155.8	245.0	180.4	335.0	198.8
66.0	110.2	156.0	156.0	246.0	181.2	336.0	198.9
67.0	110.7	157.0	156.2	247.0	181.9	337.0	199.1
68.0	111.1	158.0	156.4	248.0	182.4	338.0	199.3
69.0	111.6	159.0	156.6	249.0	182.8	339.0	199.4
70.0	112.0	160.0	156.8	250.0	183.3	340.0	199.6
71.0	112.4	161.0	157.0	251.0	183.6	341.0	199.8
72.0	112.8	162.0	157.2	252.0	184.0	342.0	199.9
73.0	113.2	163.0	157.4	253.0	184.2	343.0	200.1
74.0	113.6	164.0	157.6	254.0	184.6	344.0	200.2
75.0	114.0	165.0	157.8	255.0	184.8	345.0	200.4
76.0	114.4	166.0	158.0	256.0	185.0	346.0	200.6
77.0	114.8	167.0	158.2	257.0	185.2	347.0	200.8
78.0	115.2	168.0	158.4	258.0	185.5	348.0	200.9
79.0	115.5	169.0	158.5	259.0	185.7	349.0	201.1
80.0	116.0	170.0	158.7	260.0	185.9	350.0	201.2
81.0	116.4	171.0	158.8	261.0	186.1	351.0	201.3
82.0	116.7	172.0	159.0	262.0	186.3	352.0	201.5
83.0	117.1	173.0	159.2	263.0	186.5	353.0	201.7
84.0	117.4	174.0	159.4	264.0	186.7	354.0	201.8
85.0	117.8	175.0	159.6	265.0	186.9	355.0	202.0
86.0	118.1	176.0	159.7	266.0	187.1	356.0	202.1
87.0	118.5	177.0	159.9	267.0	187.3	357.0	202.3
88.0	118.9	178.0	160.1	268.0	187.5	358.0	202.5
89.0	119.2	179.0	160.3	269.0	187.7	359.0	202.6

| 90.0 | 119.6 | 180.0 | 160.4 | 270.0 | 187.8 | 360.0 | 202.8 |

Table A.11: 20 min F_{17} Trial 2: Collected Permeate Over Time

Time (min)	Permeate (g)	Time (min)	Permeate (g)	Time (min)	Permeate (g)	Time (min)	Permeate (g)
1.0	6.1	91.0	117.1	181.0	157.0	271.0	186.0
2.1	11.7	92.0	117.4	182.0	157.1	272.0	186.2
3.0	16.2	93.0	117.7	183.0	157.3	273.0	186.4
4.0	20.6	94.0	118.1	184.0	157.4	274.0	186.5
5.0	24.7	95.0	118.4	185.0	157.6	275.0	186.7
6.0	28.4	96.0	118.7	186.0	157.8	276.0	186.9
7.0	32.0	97.0	119.0	187.0	157.9	277.0	187.0
8.0	35.6	98.0	119.4	188.0	158.1	278.0	187.2
9.0	39.0	99.0	119.7	189.0	158.3	279.0	187.3
10.0	42.0	100.0	120.1	190.0	158.5	280.0	187.5
11.2	45.4	101.0	120.3	191.0	158.6	281.0	187.6
12.3	48.4	102.0	120.6	192.0	158.8	282.0	187.8
13.0	50.2	103.0	120.9	193.0	158.9	283.0	188.0
14.0	52.5	104.0	121.2	194.0	159.1	284.0	188.1
15.0	54.7	105.0	121.5	195.0	159.2	285.0	188.3
16.0	56.8	106.0	121.9	196.0	159.4	286.0	188.5
17.0	58.8	107.0	122.2	197.0	159.5	287.0	188.6
18.0	60.7	108.0	122.5	198.0	159.7	288.0	188.8
19.0	62.7	109.0	122.8	199.0	159.9	289.0	188.9
20.0	64.7	110.0	123.0	200.0	160.0	290.0	189.1
21.0	66.5	111.0	123.4	201.0	160.2	291.0	189.3
22.0	68.3	112.0	123.7	202.0	160.4	292.0	189.4
23.0	70.1	113.0	123.9	203.0	160.5	293.0	189.6
24.0	71.8	114.0	124.2	204.0	160.6	294.0	189.7
25.0	73.3	115.0	124.5	205.0	160.8	295.0	189.9
26.0	75.2	116.0	124.8	206.0	161.0	296.0	190.0
27.0	76.8	117.0	125.1	207.0	161.2	297.0	190.2
28.0	78.2	118.0	125.4	208.0	161.3	298.0	190.3
29.0	79.7	119.0	125.7	209.0	161.5	299.0	190.5
30.0	81.0	120.0	126.0	210.0	161.6	300.0	190.6
31.0	82.1	121.0	131.4	211.0	161.8	301.0	190.8
32.0	83.3	122.0	134.1	212.0	161.9	302.0	190.9
33.0	84.4	123.0	135.9	213.0	162.1	303.0	191.1
34.0	85.5	124.0	137.4	214.0	162.2	304.0	191.3
35.0	86.7	125.0	138.8	215.0	162.4	305.0	191.4
36.0	87.7	126.0	139.9	216.0	162.6	306.0	191.6
37.0	88.7	127.0	140.9	217.0	162.7	307.0	191.7
38.0	89.7	128.0	141.8	218.0	162.9	308.0	191.9
39.0	90.5	129.0	142.7	219.0	163.0	309.0	192.0
40.0	91.4	130.0	143.5	220.0	163.2	310.0	192.2
41.0	92.3	131.0	144.1	221.0	163.3	311.0	192.3
42.0	93.1	132.0	144.7	222.0	163.5	312.0	192.5
43.0	93.9	133.0	145.4	223.0	163.6	313.0	192.6
44.0	94.9	134.0	145.9	224.0	163.8	314.0	192.7
45.0	95.8	135.0	146.4	225.0	163.9	315.0	192.9
46.0	96.6	136.0	146.8	226.0	164.1	316.0	193.0
47.0	97.4	137.0	147.2	227.0	164.3	317.0	193.2
48.0	98.1	138.0	147.6	228.0	164.4	318.0	193.4

49.0	98.7	139.0	148.0	229.0	164.5	319.0	193.5
50.0	99.3	140.0	148.4	230.0	164.6	320.0	193.6
51.0	100.0	141.0	148.7	231.0	164.8	321.0	193.8
52.0	100.6	142.0	149.0	232.0	165.0	322.0	193.9
53.0	101.1	143.0	149.3	233.0	165.1	323.0	194.1
54.0	101.7	144.0	149.6	234.0	165.3	324.0	194.2
55.0	102.2	145.0	149.9	235.0	165.4	325.0	194.4
56.0	102.7	146.0	150.1	236.0	165.5	326.0	194.5
57.0	103.3	147.0	150.4	237.0	165.8	327.0	194.7
58.0	103.7	148.0	150.7	238.0	165.9	328.0	194.8
59.0	104.3	149.0	150.9	239.0	166.0	329.0	194.9
60.0	104.8	150.0	151.1	240.0	166.2	330.0	195.1
61.0	105.3	151.0	151.3	241.0	172.1	331.0	195.3
62.0	105.8	152.0	151.6	242.0	174.4	332.0	195.4
63.0	106.2	153.0	151.7	243.0	175.9	333.0	195.6
64.0	106.6	154.0	151.9	244.0	177.3	334.0	195.7
65.0	107.1	155.0	152.2	245.0	178.3	335.0	195.8
66.0	107.5	156.0	152.4	246.0	179.2	336.0	196.0
67.0	107.9	157.0	152.6	247.0	179.9	337.0	196.1
68.0	108.3	158.0	152.8	248.0	180.6	338.0	196.3
69.0	108.7	159.0	153.0	249.0	181.0	339.0	196.5
70.0	109.0	160.0	153.2	250.0	181.5	340.0	196.6
71.0	109.6	161.0	153.4	251.0	181.9	341.0	196.8
72.0	110.1	162.0	153.6	252.0	182.2	342.0	196.9
73.0	110.6	163.0	153.8	253.0	182.6	343.0	197.1
74.0	111.0	164.0	154.0	254.0	182.8	344.0	197.2
75.0	111.4	165.0	154.2	255.0	183.0	345.0	197.4
76.0	111.8	166.0	154.4	256.0	183.3	346.0	197.5
77.0	112.2	167.0	154.5	257.0	183.5	347.0	197.7
78.0	112.5	168.0	154.7	258.0	183.7	348.0	197.8
79.0	112.8	169.0	154.9	259.0	183.9	349.0	198.0
80.0	113.2	170.0	155.1	260.0	184.1	350.0	198.1
81.0	113.6	171.0	155.3	261.0	184.3	351.0	198.3
82.0	113.9	172.0	155.5	262.0	184.5	352.0	198.5
83.0	114.3	173.0	155.6	263.0	184.6	353.0	198.6
84.0	114.7	174.0	155.7	264.0	184.8	354.0	198.7
85.0	115.1	175.0	156.0	265.0	185.0	355.0	198.9
86.0	115.4	176.0	156.1	266.0	185.2	356.0	199.0
87.0	115.7	177.0	156.3	267.0	185.3	357.0	199.2
88.0	116.0	178.0	156.5	268.0	185.5	358.0	199.3
89.0	116.4	179.0	156.6	269.0	185.7	359.0	199.5
90.0	116.8	180.0	156.8	270.0	185.8	360.0	199.6

Table A.12: 20 min F_{17} Trial 3: Collected Permeate Over Time

Time (min)	Permeate (g)	Time (min)	Permeate (g)	Time (min)	Permeate (g)	Time (min)	Permeate (g)
1.0	6.7	91.0	122.1	181.0	164.0	271.0	193.7
2.0	12.0	92.0	122.6	182.0	164.3	272.0	193.9
3.0	16.9	93.0	123.0	183.0	164.4	273.0	194.0
4.0	21.5	94.0	123.4	184.0	164.7	274.0	194.1
5.0	25.7	95.0	123.8	185.0	164.9	275.0	194.3
6.0	29.7	96.0	124.2	186.0	165.2	276.0	194.4
7.0	33.3	97.0	124.5	187.0	165.4	277.0	194.6

8.0	36.7	98.0	125.0	188.0	165.6	278.0	194.7
9.0	40.0	99.3	125.4	189.0	165.8	279.0	194.9
10.0	43.1	100.0	125.7	190.0	166.0	280.0	195.0
11.0	45.8	101.0	126.1	191.0	166.3	281.0	195.2
12.0	48.3	102.0	126.4	192.0	166.5	282.0	195.3
13.3	51.5	103.0	126.8	193.0	166.6	283.0	195.5
14.0	52.9	104.0	127.1	194.0	166.9	284.0	195.6
15.3	55.7	105.0	127.5	195.0	167.1	285.0	195.8
16.0	57.2	106.0	127.9	196.0	167.3	286.0	195.9
17.1	59.4	107.0	128.2	197.0	167.5	287.0	196.0
18.0	61.2	108.0	128.6	198.0	167.7	288.0	196.1
19.0	63.1	109.0	128.9	199.0	167.9	289.0	196.3
20.0	64.9	110.0	129.3	200.0	168.1	290.0	196.4
21.3	67.3	111.0	129.6	201.0	168.3	291.0	196.6
22.0	68.5	112.0	129.9	202.0	168.5	292.0	196.7
23.5	70.9	113.0	130.3	203.0	168.7	293.0	196.9
24.2	72.0	114.0	130.6	204.0	168.9	294.0	197.0
25.0	73.3	115.0	130.9	205.0	169.1	295.0	197.1
26.0	74.8	116.0	131.3	206.0	169.3	296.0	197.2
27.0	76.3	117.0	131.6	207.0	169.5	297.0	197.3
28.0	77.8	118.0	132.0	208.0	169.7	298.0	197.4
29.0	79.2	119.0	132.4	209.0	169.8	299.0	197.6
30.0	80.7	120.0	132.6	210.0	170.1	300.0	197.7
31.3	82.3	121.0	136.8	211.0	170.3	301.0	197.9
32.0	83.2	122.0	139.1	212.0	170.5	302.0	198.0
33.0	84.5	123.0	140.9	213.0	170.6	303.0	198.2
34.3	85.9	124.0	142.4	214.0	170.9	304.0	198.3
35.0	86.7	125.0	143.8	215.0	171.0	305.0	198.4
36.0	87.9	126.0	144.8	216.0	171.2	306.0	198.6
37.0	88.8	127.0	145.8	217.0	171.4	307.0	198.7
38.0	89.8	128.0	146.7	218.0	171.6	308.0	198.8
39.0	90.8	129.0	147.5	219.0	171.8	309.0	198.9
40.3	92.0	130.0	148.2	220.0	172.0	310.0	199.0
41.0	92.6	131.0	148.9	221.0	172.2	311.0	199.1
42.0	93.5	132.0	149.5	222.0	172.4	312.0	199.3
43.0	94.3	133.0	150.1	223.0	172.6	313.0	199.4
44.0	95.1	134.0	150.7	224.0	172.8	314.0	199.5
45.0	95.9	135.0	151.1	225.0	173.0	315.0	199.6
46.0	96.6	136.0	151.6	226.0	173.2	316.0	199.8
47.0	97.4	137.0	152.0	227.0	173.3	317.0	199.9
48.5	100.3	138.0	152.5	228.0	173.5	318.0	200.1
49.0	100.8	139.0	152.9	229.0	173.7	319.0	200.2
50.0	101.8	140.0	153.3	230.0	173.9	320.0	200.3
51.0	102.5	141.0	153.7	231.0	174.1	321.0	200.4
52.3	103.5	142.0	154.0	232.0	174.3	322.0	200.6
53.0	103.9	143.0	154.3	233.0	174.5	323.0	200.7
54.0	104.6	144.0	154.6	234.0	174.7	324.0	200.8
55.0	105.2	145.0	154.9	235.0	174.9	325.0	201.0
56.0	105.9	146.0	155.2	236.0	175.0	326.0	201.1
57.0	106.5	147.0	155.5	237.0	175.2	327.0	201.2
58.0	107.1	148.0	155.8	238.0	175.4	328.0	201.3
59.0	107.6	149.0	156.1	239.0	175.6	329.0	201.5
60.0	108.1	150.0	156.4	240.0	175.8	330.0	201.6
61.2	108.7	151.0	156.7	241.0	181.3	331.0	201.7

62.3	109.2	152.0	157.0	242.0	183.1	332.0	201.9
63.2	109.7	153.0	157.3	243.0	184.5	333.0	202.0
64.3	110.2	154.0	157.6	244.0	185.6	334.0	202.1
65.0	110.6	155.0	157.8	245.0	186.4	335.0	202.2
66.0	111.1	156.0	158.1	246.0	187.2	336.0	202.4
67.0	111.5	157.0	158.4	247.0	187.8	337.0	202.5
68.3	112.1	158.0	158.6	248.0	188.4	338.0	202.7
69.0	112.5	159.0	158.9	249.0	188.8	339.0	202.8
70.0	112.9	160.0	159.1	250.0	189.2	340.0	202.9
71.0	113.4	161.0	159.4	251.0	189.6	341.0	203.1
72.0	113.8	162.0	159.7	252.0	190.0	342.0	203.2
73.0	114.3	163.0	160.0	253.0	190.3	343.0	203.3
74.0	114.7	164.0	160.2	254.0	190.5	344.0	203.4
75.0	115.5	165.0	160.4	255.0	190.8	345.0	203.5
76.0	115.9	166.0	160.7	256.0	191.0	346.0	203.7
77.0	116.3	167.0	160.9	257.0	191.2	347.0	203.8
78.0	116.7	168.0	161.1	258.0	191.4	348.0	203.9
79.0	117.1	169.0	161.3	259.0	191.6	349.0	204.0
80.0	117.5	170.0	161.6	260.0	191.8	350.0	204.2
81.0	117.9	171.0	161.8	261.0	192.0	351.0	204.3
82.0	118.3	172.0	162.0	262.0	192.2	352.0	204.4
83.0	118.8	173.0	162.3	263.0	192.3	353.0	204.6
84.0	119.1	174.0	162.5	264.0	192.5	354.0	204.7
85.0	119.5	175.0	162.7	265.0	192.7	355.0	204.8
86.0	119.9	176.0	162.9	266.0	192.9	356.0	204.9
87.0	120.3	177.0	163.1	267.0	193.0	357.0	205.1
88.0	120.7	178.0	163.4	268.0	193.2	358.0	205.2
89.0	121.0	179.0	163.6	269.0	193.4	359.0	205.3
90.0	121.7	180.0	163.8	270.0	193.5	360.0	205.4

Table A.13: 40 min F_{17} Trial 1: Collected Permeate Over Time

Time (min)	Permeate (g)	Time (min)	Permeate (g)	Time (min)	Permeate (g)	Time (min)	Permeate (g)
1.0	6.7	91.0	86.1	181.0	114.2	271.0	136.8
2.0	11.7	92.0	86.4	182.0	114.4	272.0	136.9
3.0	16.1	93.0	86.6	183.0	114.5	273.0	137.0
4.0	19.8	94.0	86.8	184.0	114.6	274.0	137.2
5.0	23.0	95.0	87.0	185.0	114.7	275.0	137.3
6.0	25.7	96.0	87.2	186.0	114.8	276.0	137.5
7.0	28.1	97.0	87.4	187.0	114.9	277.0	137.6
8.0	30.3	98.0	87.6	188.0	115.0	278.0	137.8
9.0	32.3	99.0	87.8	189.0	115.1	279.0	137.9
10.0	34.1	100.0	88.0	190.0	115.2	280.0	138.1
11.0	35.7	101.0	88.2	191.0	115.3	281.0	138.2
12.0	37.3	102.0	88.4	192.0	115.4	282.0	138.4
13.3	39.1	103.0	88.5	193.0	115.6	283.0	138.5
14.0	40.0	104.0	88.7	194.0	115.7	284.0	138.7
15.0	41.4	105.0	88.9	195.0	115.8	285.0	138.8
16.0	42.7	106.0	89.1	196.0	115.9	286.0	139.0
17.0	44.0	107.0	89.3	197.0	116.0	287.0	139.1
18.0	45.3	108.0	89.4	198.0	116.1	288.0	139.3
19.0	46.4	109.0	89.6	199.0	116.2	289.0	139.4
20.0	47.6	110.0	89.7	200.0	116.3	290.0	139.5

21.0	48.7	111.0	89.9	201.0	116.4	291.0	139.7
22.0	49.7	112.0	90.1	202.0	116.5	292.0	139.9
23.0	50.7	113.0	90.2	203.0	116.6	293.0	140.0
24.0	51.8	114.0	90.3	204.0	116.7	294.0	140.1
25.0	52.7	115.0	90.5	205.0	116.9	295.0	140.3
26.0	53.7	116.0	90.7	206.0	117.0	296.0	140.4
27.0	54.7	117.0	90.8	207.0	117.1	297.0	140.6
28.0	55.7	118.0	91.0	208.0	117.2	298.0	140.7
29.0	56.6	119.0	91.1	209.0	117.3	299.0	140.9
30.0	57.5	120.0	91.2	210.0	117.4	300.0	141.0
31.0	58.3	121.0	96.9	211.0	117.5	301.0	141.1
32.0	59.2	122.0	99.1	212.0	117.6	302.0	141.3
33.0	59.9	123.0	100.6	213.0	117.7	303.0	141.4
34.0	60.7	124.0	101.8	214.0	117.8	304.0	141.5
35.0	61.4	125.0	102.7	215.0	117.9	305.0	141.7
36.0	62.2	126.0	103.6	216.0	118.0	306.0	141.8
37.0	62.9	127.0	104.3	217.0	118.1	307.0	142.0
38.0	63.6	128.0	105.0	218.0	118.2	308.0	142.1
39.0	64.3	129.0	105.6	219.0	118.3	309.0	142.2
40.0	65.0	130.0	106.1	220.0	118.4	310.0	142.4
41.0	65.6	131.0	106.5	221.0	118.5	311.0	142.5
42.0	66.3	132.0	106.9	222.0	118.6	312.0	142.6
43.0	66.9	133.0	107.2	223.0	118.8	313.0	142.8
44.0	67.5	134.0	107.5	224.0	118.9	314.0	142.9
45.0	68.1	135.0	107.8	225.0	119.0	315.0	143.1
46.0	68.7	136.0	108.1	226.0	119.1	316.0	143.2
47.0	69.3	137.0	108.3	227.0	119.2	317.0	143.3
48.0	69.8	138.0	108.5	228.0	119.3	318.0	143.5
49.0	70.5	139.0	108.7	229.0	119.4	319.0	143.6
50.0	71.1	140.0	108.9	230.0	119.5	320.0	143.8
51.0	71.8	141.0	109.1	231.0	119.6	321.0	143.9
52.0	72.4	142.0	109.3	232.0	119.7	322.0	144.1
53.0	73.0	143.0	109.4	233.0	119.8	323.0	144.2
54.0	73.6	144.0	109.6	234.0	120.0	324.0	144.4
55.0	74.2	145.0	109.8	235.0	120.1	325.0	144.5
56.0	74.7	146.0	109.9	236.0	120.2	326.0	144.6
57.0	75.2	147.0	110.1	237.0	120.3	327.0	144.8
58.0	75.7	148.0	110.2	238.0	120.4	328.0	144.9
59.0	76.2	149.0	110.3	239.0	120.5	329.0	145.1
60.0	76.6	150.0	110.4	240.0	120.6	330.0	145.2
61.0	77.0	151.0	110.6	241.0	126.6	331.0	145.4
62.0	77.4	152.0	110.7	242.0	128.4	332.0	145.5
63.0	77.7	153.0	110.9	243.0	129.5	333.0	145.6
64.0	78.1	154.0	111.0	244.0	130.4	334.0	145.7
65.0	78.5	155.0	111.1	245.0	131.1	335.0	145.9
66.0	78.9	156.0	111.3	246.0	131.7	336.0	146.0
67.0	79.3	157.0	111.4	247.0	132.1	337.0	146.1
68.0	79.7	158.0	111.5	248.0	132.4	338.0	146.3
69.0	80.1	159.0	111.6	249.0	132.8	339.0	146.5
70.0	80.4	160.0	111.8	250.0	133.1	340.0	146.6
71.0	80.8	161.0	111.9	251.0	133.3	341.0	146.8
72.0	81.1	162.0	112.0	252.0	133.4	342.0	146.9
73.0	81.4	163.0	112.1	253.0	133.7	343.0	147.0
74.0	81.7	164.0	112.2	254.0	133.9	344.0	147.2

75.0	82.0	165.0	112.4	255.0	134.1	345.0	147.3
76.0	82.2	166.0	112.5	256.0	134.3	346.0	147.4
77.0	82.5	167.0	112.6	257.0	134.5	347.0	147.6
78.0	82.8	168.0	112.7	258.0	134.6	348.0	147.7
79.0	83.1	169.0	112.8	259.0	134.8	349.0	147.9
80.0	83.4	170.0	112.9	260.0	135.0	350.0	148.0
81.0	83.6	171.0	113.1	261.0	135.2	351.0	148.1
82.0	83.9	172.0	113.2	262.0	135.3	352.0	148.3
83.0	84.1	173.0	113.3	263.0	135.5	353.0	148.4
84.0	84.4	174.0	113.4	264.0	135.7	354.0	148.6
85.0	84.6	175.0	113.5	265.0	135.8	355.0	148.7
86.0	84.9	176.0	113.7	266.0	136.0	356.0	148.9
87.0	85.1	177.0	113.8	267.0	136.2	357.0	149.0
88.0	85.4	178.0	113.9	268.0	136.3	358.0	149.2
89.0	85.6	179.0	114.0	269.0	136.4	359.0	149.3
90.0	85.9	180.0	114.1	270.0	136.6	360.0	149.4

Table A.14: 40 min F_{17} Trial 2: Collected Permeate Over Time

Time (min)	Permeate (g)	Time (min)	Permeate (g)	Time (min)	Permeate (g)	Time (min)	Permeate (g)
1.0	6.2	91.0	84.4	181.0	115.4	271.0	139.5
2.0	10.9	92.0	84.6	182.0	115.5	272.0	139.6
3.3	16.0	93.0	84.8	183.0	115.7	273.0	139.8
4.0	18.2	94.0	85.2	184.0	115.8	274.0	139.9
5.0	21.2	95.0	85.6	185.0	115.9	275.0	140.0
6.0	23.9	96.0	85.9	186.0	116.0	276.0	140.2
7.0	26.3	97.0	86.1	187.0	116.2	277.0	140.3
8.0	28.5	98.0	86.4	188.0	116.3	278.0	140.5
9.0	30.6	99.0	86.6	189.0	116.4	279.0	140.6
10.0	32.5	100.0	86.7	190.0	116.5	280.0	140.7
11.0	34.2	101.0	87.0	191.0	116.6	281.0	140.9
12.0	35.9	102.0	87.1	192.0	116.8	282.0	141.0
13.0	37.5	103.0	87.3	193.0	116.9	283.0	141.1
14.0	39.0	104.0	87.5	194.0	117.0	284.0	141.3
15.0	40.5	105.0	87.7	195.0	117.2	285.0	141.4
16.0	41.7	106.0	87.8	196.0	117.3	286.0	141.5
17.0	43.1	107.0	88.0	197.0	117.4	287.0	141.7
18.0	44.5	108.0	88.1	198.0	117.5	288.0	141.8
19.0	45.8	109.0	88.3	199.0	117.6	289.0	141.9
20.0	47.1	110.0	88.4	200.0	117.8	290.0	142.0
21.2	48.5	111.0	88.6	201.0	117.9	291.0	142.2
22.0	49.6	112.0	88.8	202.0	118.0	292.0	142.3
23.0	50.7	113.0	88.9	203.0	118.1	293.0	142.5
24.0	51.7	114.0	89.1	204.0	118.2	294.0	142.6
25.0	52.7	115.0	89.2	205.0	118.4	295.0	142.7
26.0	53.8	116.0	89.4	206.0	118.5	296.0	142.8
27.0	54.7	117.0	89.5	207.0	118.6	297.0	142.9
28.0	55.7	118.0	89.6	208.0	118.7	298.0	143.1
29.0	56.7	119.0	89.7	209.0	118.8	299.0	143.2
30.0	57.5	120.0	89.9	210.0	118.9	300.0	143.3
31.0	58.4	121.0	95.7	211.0	119.1	301.0	143.5
32.0	59.3	122.0	98.0	212.0	119.2	302.0	143.6
33.0	60.1	123.0	99.6	213.0	119.3	303.0	143.7

34.0	60.8	124.0	100.9	214.0	119.4	304.0	143.9
35.0	61.6	125.0	101.9	215.0	119.6	305.0	144.0
36.0	62.4	126.0	102.8	216.0	119.7	306.0	144.1
37.0	63.1	127.2	103.7	217.0	119.8	307.0	144.2
38.0	63.8	128.0	104.4	218.0	119.9	308.0	144.3
39.0	64.5	129.0	105.1	219.0	120.1	309.0	144.5
40.0	65.2	130.0	105.7	220.0	120.2	310.0	144.6
41.0	65.8	131.0	106.3	221.0	120.3	311.0	144.7
42.0	66.5	132.0	106.7	222.0	120.4	312.0	144.9
43.0	67.1	133.0	107.1	223.0	120.5	313.0	145.0
44.0	67.7	134.0	107.4	224.0	120.6	314.0	145.1
45.0	68.3	135.0	107.7	225.0	120.8	315.0	145.2
46.0	68.9	136.0	108.1	226.0	120.9	316.0	145.4
47.0	69.4	137.0	108.4	227.0	121.0	317.0	145.5
48.0	69.9	138.0	108.7	228.0	121.1	318.0	145.6
49.0	70.5	139.0	109.0	229.0	121.3	319.0	145.7
50.0	71.0	140.0	109.2	230.0	121.4	320.0	145.8
51.0	71.5	141.0	109.4	231.0	121.5	321.0	146.0
52.0	72.0	142.0	109.6	232.0	121.6	322.0	146.1
53.0	72.5	143.0	109.8	233.0	121.8	323.0	146.2
54.0	72.9	144.0	110.0	234.0	121.9	324.0	146.3
55.0	73.4	145.0	110.2	235.0	122.0	325.0	146.5
56.0	73.9	146.0	110.4	236.0	122.1	326.0	146.6
57.0	74.4	147.0	110.6	237.0	122.2	327.0	146.7
58.0	74.8	148.0	110.8	238.0	122.3	328.0	146.9
59.0	75.3	149.0	111.0	239.0	122.5	329.0	147.0
60.0	75.7	150.0	111.1	240.0	122.6	330.0	147.1
61.0	76.1	151.0	111.2	241.0	128.8	331.0	147.2
62.0	76.6	152.0	111.4	242.0	130.6	332.0	147.4
63.0	76.9	153.0	111.5	243.0	131.9	333.0	147.5
64.0	77.2	154.0	111.7	244.0	132.8	334.0	147.6
65.0	77.6	155.0	111.8	245.0	133.6	335.0	147.7
66.0	77.9	156.0	112.0	246.0	134.3	336.0	147.9
67.0	78.3	157.0	112.1	247.0	134.8	337.0	148.0
68.0	78.6	158.0	112.3	248.0	135.3	338.0	148.1
69.0	78.9	159.0	112.4	249.0	135.7	339.0	148.3
70.0	79.2	160.0	112.6	250.0	136.0	340.0	148.4
71.0	79.5	161.0	112.7	251.0	136.2	341.0	148.5
72.0	79.8	162.0	112.9	252.0	136.5	342.0	148.6
73.0	80.1	163.0	113.0	253.0	136.7	343.0	148.7
74.0	80.4	164.0	113.1	254.0	136.9	344.0	148.8
75.0	80.7	165.0	113.3	255.0	137.1	345.0	149.0
76.0	81.0	166.0	113.4	256.0	137.3	346.0	149.1
77.0	81.3	167.0	113.5	257.0	137.5	347.0	149.2
78.0	81.5	168.0	113.7	258.0	137.7	348.0	149.4
79.0	81.8	169.0	113.8	259.0	137.8	349.0	149.5
80.0	82.0	170.0	114.0	260.0	137.9	350.0	149.6
81.0	82.3	171.0	114.1	261.0	138.1	351.0	149.7
82.0	82.5	172.0	114.3	262.0	138.3	352.0	149.8
83.0	82.7	173.0	114.4	263.0	138.4	353.0	149.9
84.0	83.0	174.0	114.5	264.0	138.6	354.0	150.1
85.0	83.2	175.0	114.6	265.0	138.7	355.0	150.2
86.0	83.4	176.0	114.8	266.0	138.8	356.0	150.3
87.0	83.6	177.0	114.9	267.0	139.0	357.0	150.4

88.0	83.8	178.0	115.0	268.0	139.1	358.0	150.6
89.0	84.0	179.0	115.2	269.0	139.2	359.0	150.7
90.0	84.2	180.0	115.3	270.0	139.4	360.0	150.8

Table A.15: 40 min F_{17} Trial 3: Collected Permeate Over Time

Time (min)	Permeate (g)	Time (min)	Permeate (g)	Time (min)	Permeate (g)	Time (min)	Permeate (g)
1.0	6.7	91.0	84.8	181.0	114.8	271.0	141.1
2.0	11.9	92.0	85.0	182.0	114.9	272.0	141.3
3.2	16.7	93.0	85.2	183.0	115.0	273.0	141.4
4.0	19.6	94.0	85.4	184.0	115.1	274.0	141.6
5.0	22.6	95.0	85.6	185.0	115.3	275.0	141.7
6.0	25.2	96.0	85.7	186.0	115.4	276.0	141.9
7.0	27.6	97.0	85.9	187.0	115.5	277.0	142.1
8.0	29.7	98.0	86.1	188.0	115.7	278.0	142.3
9.0	31.7	99.0	86.3	189.0	115.8	279.0	142.5
10.0	33.4	100.0	86.5	190.0	115.9	280.0	142.7
11.0	35.1	101.0	86.6	191.0	116.1	281.0	142.9
12.0	36.7	102.0	86.8	192.0	116.2	282.0	143.0
13.0	38.1	103.0	87.0	193.0	116.4	283.0	143.2
14.0	39.5	104.0	87.2	194.0	116.5	284.0	143.4
15.0	40.8	105.0	87.4	195.0	116.6	285.0	143.6
16.0	41.9	106.0	87.6	196.0	116.7	286.0	143.8
17.0	43.2	107.0	87.7	197.0	116.9	287.0	144.0
18.0	44.3	108.0	87.9	198.0	117.0	288.0	144.1
19.0	45.5	109.0	88.1	199.0	117.2	289.0	144.3
20.0	46.7	110.0	88.2	200.0	117.4	290.0	144.5
21.0	47.9	111.0	88.3	201.0	117.5	291.0	144.7
22.0	49.1	112.0	88.5	202.0	117.7	292.0	144.9
23.0	50.2	113.0	88.6	203.0	117.8	293.0	145.1
24.0	51.3	114.0	88.8	204.0	118.0	294.0	145.3
25.0	52.3	115.0	88.9	205.0	118.1	295.0	145.4
26.0	53.3	116.0	89.1	206.0	118.2	296.0	145.6
27.3	54.5	117.0	89.2	207.0	118.4	297.0	145.8
28.0	55.2	118.0	89.4	208.0	118.6	298.0	146.0
29.0	56.2	119.0	89.5	209.0	118.8	299.0	146.1
30.0	57.1	120.0	89.7	210.0	118.9	300.0	146.3
31.0	58.0	121.0	96.3	211.0	119.0	301.0	146.4
32.0	59.0	122.0	98.7	212.0	119.2	302.0	146.6
33.0	60.0	123.0	100.3	213.0	119.5	303.0	146.9
34.0	60.9	124.0	101.6	214.0	119.7	304.0	147.0
35.0	61.7	125.0	102.6	215.0	119.9	305.0	147.2
36.0	62.6	126.0	103.5	216.0	120.1	306.0	147.4
37.3	63.5	127.0	104.3	217.0	120.3	307.0	147.6
38.0	64.0	128.0	105.0	218.0	120.5	308.0	147.7
39.0	64.8	129.0	105.4	219.0	120.6	309.0	147.9
40.0	65.5	130.0	105.9	220.0	120.7	310.0	148.1
41.0	66.2	131.0	106.3	221.0	120.9	311.0	148.3
42.0	66.9	132.0	106.6	222.0	121.1	312.0	148.5
43.0	67.6	133.0	106.9	223.0	121.2	313.0	148.7
44.0	68.3	134.0	107.2	224.0	121.3	314.0	148.8
45.0	68.8	135.0	107.5	225.0	121.5	315.0	149.0
46.0	69.4	136.0	107.7	226.0	121.6	316.0	149.2

47.0	70.0	137.0	108.0	227.0	121.8	317.0	149.4
48.0	70.6	138.0	108.2	228.0	121.9	318.0	149.6
49.0	71.1	139.0	108.3	229.0	122.1	319.0	149.7
50.0	71.7	140.0	108.6	230.0	122.2	320.0	149.9
51.0	72.2	141.0	108.8	231.0	122.3	321.0	150.1
52.0	72.8	142.0	108.9	232.0	122.4	322.0	150.2
53.0	73.2	143.0	109.1	233.0	122.6	323.0	150.4
54.0	73.6	144.0	109.3	234.0	122.7	324.0	150.6
55.0	74.0	145.0	109.5	235.0	122.8	325.0	150.8
56.0	74.5	146.0	109.7	236.0	123.0	326.0	151.0
57.0	74.9	147.0	109.9	237.0	123.1	327.0	151.1
58.0	75.3	148.0	110.1	238.0	123.2	328.0	151.4
59.0	75.9	149.0	110.3	239.0	123.4	329.0	151.5
60.0	76.3	150.0	110.5	240.0	123.5	330.0	151.6
61.0	76.7	151.0	110.7	241.0	129.1	331.0	151.8
62.0	77.0	152.0	110.8	242.0	130.7	332.0	152.0
63.0	77.3	153.0	110.9	243.0	131.9	333.0	152.2
64.0	77.7	154.0	111.1	244.0	132.9	334.0	152.3
65.0	78.0	155.0	111.3	245.0	133.7	335.0	152.5
66.0	78.4	156.0	111.4	246.0	134.4	336.0	152.6
67.0	78.7	157.0	111.6	247.0	135.0	337.0	152.8
68.0	79.0	158.0	111.7	248.0	135.4	338.0	153.0
69.0	79.3	159.0	111.9	249.0	135.9	339.0	153.1
70.0	79.7	160.0	112.0	250.0	136.3	340.0	153.3
71.0	79.9	161.0	112.1	251.0	136.6	341.0	153.5
72.0	80.2	162.0	112.3	252.0	136.9	342.0	153.7
73.0	80.5	163.0	112.5	253.0	137.2	343.0	153.9
74.0	80.8	164.0	112.6	254.0	137.5	344.0	154.0
75.0	81.0	165.0	112.7	255.0	137.7	345.0	154.2
76.0	81.3	166.0	112.8	256.0	138.0	346.0	154.4
77.0	81.5	167.0	113.0	257.0	138.2	347.0	154.6
78.0	81.8	168.0	113.1	258.0	138.4	348.0	154.7
79.0	82.1	169.0	113.2	259.0	138.6	349.0	154.9
80.0	82.3	170.0	113.4	260.0	138.8	350.0	155.1
81.0	82.5	171.0	113.5	261.0	139.1	351.0	155.3
82.0	82.8	172.0	113.6	262.0	139.3	352.0	155.4
83.0	83.1	173.0	113.7	263.0	139.5	353.0	155.6
84.0	83.4	174.0	113.9	264.0	139.7	354.0	155.7
85.0	83.6	175.0	114.0	265.0	139.9	355.0	155.9
86.0	83.8	176.0	114.1	266.0	140.1	356.0	156.1
87.0	84.0	177.0	114.2	267.0	140.3	357.0	156.2
88.0	84.2	178.0	114.3	268.0	140.5	358.0	156.4
89.0	84.4	179.0	114.5	269.0	140.7	359.0	156.6
90.0	84.6	180.0	114.6	270.0	140.9	360.0	156.8

A.3.6 Raw Ceramic Membrane Permeate Data for Figure 2.15

Table A.16: Untreated Control: Permeation Rate Over Time

Time (h)	Permeation Rate (mL/min)	Time (h)	Permeation Rate (mL/min)	Time (h)	Permeation Rate (mL/min)	Time (h)	Permeation Rate (mL/min)
1.0	215.0	64.5	110.0	134.4	63.0	323.2	46.0
2.0	215.0	65.5	109.0	136.4	63.0	326.9	46.0
3.0	210.0	66.5	108.0	137.4	63.0	329.7	45.0
4.0	209.0	67.5	106.0	139.4	63.0	333.0	45.0
6.2	197.0	68.5	106.0	140.4	63.0	346.4	45.0
7.3	190.0	69.5	105.0	155.1	62.0	349.6	44.0
21.0	155.0	70.5	104.0	157.1	63.0	354.5	43.0
22.0	143.0	71.5	104.0	159.4	62.0	355.9	43.0
23.0	139.0	72.5	102.0	161.4	62.0	374.1	42.0
24.0	132.0	73.5	100.0	164.1	62.0	395.5	42.0
25.0	132.0	74.5	100.0	179.1	62.0	419.5	41.0
26.6	130.0	88.3	98.0	181.4	61.0	425.2	42.0
27.6	125.0	89.3	97.0	182.7	60.0	430.2	42.0
28.6	122.0	89.3	60.0	184.4	60.0	442.7	42.0
29.6	120.0	90.2	62.0	186.4	59.0	449.2	41.0
30.6	119.0	91.2	61.0	188.4	59.0	452.1	42.0
31.6	118.0	92.2	61.0	205.7	56.0	466.8	42.0
32.4	118.0	93.2	63.0	227.2	54.0	470.7	42.0
45.0	112.0	107.1	64.0	251.0	52.0	474.2	42.0
46.0	112.0	108.1	64.0	256.0	51.0	477.4	42.0
47.0	112.0	109.6	64.0	260.5	50.0	491.2	42.0
48.0	111.0	111.1	63.0	275.1	49.0	494.4	42.0
49.0	111.0	112.2	63.0	278.0	48.0	500.1	42.0
50.0	111.0	113.2	63.0	282.0	48.0	515.1	40.0
51.0	111.0	115.5	63.0	285.4	48.0	520.4	37.0
52.0	111.0	117.4	63.0	298.2	48.0	524.4	36.0
53.0	110.0	131.1	64.0	302.0	47.0		
54.0	119.0	132.4	65.0	307.4	47.0		

Table A.17: Untreated Control: Collected Permeate Over Time (Integrated)

Time (h)	Permeate (L)	Time (h)	Permeate (L)	Time (h)	Permeate (L)	Time (h)	Permeate (L)
0.0	0.0	54.0	467.6	132.4	854.2	307.4	1434.1
1.0	12.6	64.5	539.6	134.4	861.9	323.2	1478.3
2.0	25.5	65.5	546.2	136.4	869.5	326.9	1488.4
3.0	38.3	66.5	552.7	137.4	873.3	329.7	1496.2
4.0	50.9	67.5	559.1	139.4	880.8	333.0	1504.9
6.2	77.9	68.5	565.5	140.4	884.6	346.4	1541.2
7.3	89.8	69.5	571.8	155.1	939.6	349.6	1549.6
21.0	232.2	70.5	578.1	157.1	947.1	354.5	1562.4
22.0	241.1	71.5	584.3	159.4	955.9	355.9	1566.1
23.0	249.6	72.5	590.5	161.4	963.3	374.1	1612.4
24.0	257.7	73.5	596.6	164.1	973.2	395.5	1666.4
25.0	265.6	74.5	602.6	179.1	1029.0	419.5	1726.2
26.6	278.0	88.3	684.8	181.4	1037.6	425.2	1740.5
27.6	285.7	89.3	690.6	182.7	1042.5	430.2	1753.1
28.6	293.1	89.3	690.6	184.4	1048.5	442.7	1784.6

29.6	300.3	90.2	694.0	186.4	1055.6	449.2	1800.8
30.6	307.5	91.2	697.7	188.4	1062.7	452.1	1807.8
31.6	314.6	92.2	701.3	205.7	1122.5	466.8	1845.0
32.4	320.6	93.2	705.0	227.2	1193.4	470.7	1854.9
45.0	407.4	107.1	757.8	251.0	1269.0	474.2	1863.5
46.0	414.1	108.1	761.6	256.0	1284.4	477.4	1871.7
47.0	420.8	109.6	767.4	260.5	1298.0	491.2	1906.3
48.0	427.5	111.1	773.1	275.1	1341.4	494.4	1914.5
49.0	434.2	112.2	777.5	278.0	1349.8	500.1	1928.8
50.0	440.8	113.2	781.3	282.0	1361.4	515.1	1965.7
51.0	447.5	115.5	789.8	285.4	1371.2	520.4	1978.0
52.0	454.1	117.4	797.0	298.2	1408.2	524.4	1986.8
53.0	460.8	131.1	849.1	302.0	1418.9		

Table A.18: Silanized Ceramic: Permeation Rate Over Time

Time (h)	Permeation Rate (mL/min)	Time (h)	Permeation Rate (mL/min)	Time (h)	Permeation Rate (mL/min)	Time (h)	Permeation Rate (mL/min)
0.0	113.0	104.8	89.0	202.6	81.0	349.3	81.0
1.4	96.0	105.8	89.0	203.6	81.0	352.0	76.0
2.4	95.0	106.8	89.0	205.6	81.0	369.7	79.0
3.4	92.0	107.8	89.0	206.9	81.0	372.5	75.0
4.4	91.0	108.8	89.0	208.6	81.0	374.7	78.0
5.4	90.0	109.8	89.0	209.8	81.0	378.0	76.0
6.4	90.0	110.8	89.0	224.2	82.0	379.4	76.0
20.1	91.0	111.8	88.0	234.0	82.0	382.1	77.0
21.1	91.0	112.8	87.0	248.9	86.0	395.7	78.0
22.1	91.0	113.8	86.0	260.6	88.0	404.3	74.0
23.1	91.0	114.8	87.0	273.0	86.0	417.9	75.0
24.1	91.0	128.2	87.0	274.0	82.0	429.8	74.0
25.1	91.0	129.2	87.0	275.0	81.0	441.0	72.0
26.1	91.0	129.9	87.0	276.0	81.0	443.0	72.0
27.1	91.0	131.4	87.0	277.0	82.0	446.3	73.0
29.3	91.0	132.6	86.0	278.0	82.0	449.0	70.0
30.4	91.0	133.4	86.0	279.0	82.0	451.0	70.0
43.6	92.0	134.4	87.0	280.0	82.0	452.0	70.0
44.6	93.0	137.3	87.0	281.0	82.0	465.0	70.0
45.6	93.0	138.3	86.0	281.9	82.0	468.0	70.0
46.6	93.0	152.0	88.0	295.7	82.0	470.0	68.0
47.6	93.0	154.2	85.0	296.7	82.0	472.0	68.0
49.7	93.0	155.3	85.0	298.4	82.0	475.0	68.0
50.6	92.0	156.0	84.0	300.7	82.0	489.3	68.0
51.6	92.0	157.7	84.0	303.7	82.0	491.3	68.0
52.6	92.0	159.5	84.0	306.7	80.0	493.0	68.0
69.0	92.0	161.6	83.0	307.6	80.0	495.0	68.0
69.8	92.0	176.3	83.0	320.3	78.0	497.0	67.0
70.8	92.0	177.3	84.0	322.3	79.0	499.0	67.0
71.8	92.0	178.3	83.0	324.3	80.0	513.0	66.0
72.8	92.0	179.3	78.0	325.0	80.0	515.0	69.0
73.8	92.0	180.1	79.0	327.0	79.0	517.0	69.0
74.8	92.0	182.6	81.0	329.3	78.0	519.0	69.0
75.8	92.0	185.4	80.0	330.8	78.0	520.3	69.0

92.8	91.0	200.3	81.0	345.1	82.0	522.3	69.0
103.8	90.0	201.6	81.0	346.8	82.0		

Table A.19: Silanized Ceramic: Collected Permeate Over Time (Integrated)

Time (h)	Permeate (L)	Time (h)	Permeate (L)	Time (h)	Permeate (L)	Time (h)	Permeate (L)
0.0	0.0	104.8	576.3	202.6	1072.3	349.3	1795.7
1.4	8.9	105.8	581.6	203.6	1077.1	352.0	1808.7
2.4	14.6	106.8	586.9	205.6	1086.8	369.7	1890.8
3.4	20.2	107.8	592.3	206.9	1093.4	372.5	1903.9
4.4	25.7	108.8	597.6	208.6	1101.4	374.7	1913.9
5.4	31.2	109.8	603.0	209.8	1107.1	378.0	1929.3
6.4	36.6	110.8	608.3	224.2	1177.6	379.4	1935.7
20.1	110.7	111.8	613.6	234.0	1226.0	382.1	1947.9
21.1	116.2	112.8	618.9	248.9	1301.2	395.7	2011.1
22.1	121.7	113.8	624.0	260.6	1362.0	404.3	2050.3
23.1	127.1	114.8	629.2	273.0	1426.9	417.9	2111.4
24.1	132.6	128.2	698.9	274.0	1431.9	429.8	2164.2
25.1	138.0	129.2	704.1	275.0	1436.8	441.0	2213.5
26.1	143.5	129.9	708.0	276.0	1441.7	443.0	2222.2
27.1	149.0	131.4	715.8	277.0	1446.6	446.3	2236.3
29.3	161.2	132.6	721.9	278.0	1451.5	449.0	2248.1
30.4	167.2	133.4	726.2	279.0	1456.4	451.0	2256.5
43.6	239.4	134.4	731.4	280.0	1461.3	452.0	2260.7
44.6	245.0	137.3	746.6	281.0	1466.2	465.0	2315.3
45.6	250.6	138.3	751.8	281.9	1470.8	468.0	2327.9
46.6	256.2	152.0	823.1	295.7	1538.4	470.0	2336.2
47.6	261.7	154.2	834.4	296.7	1543.3	472.0	2344.3
49.7	273.4	155.3	839.9	298.4	1551.9	475.0	2356.6
50.6	278.4	156.0	843.7	300.7	1563.0	489.3	2414.7
51.6	284.0	157.7	852.1	303.7	1577.8	491.3	2422.9
52.6	289.5	159.5	861.3	306.7	1592.4	493.0	2430.0
69.0	379.8	161.6	871.8	307.6	1596.7	495.0	2438.2
69.8	384.7	176.3	945.2	320.3	1656.8	497.0	2446.3
70.8	390.2	177.3	950.2	322.3	1666.2	499.0	2454.3
71.8	395.7	178.3	955.2	324.3	1675.7	513.0	2510.2
72.8	401.3	179.3	960.1	325.0	1679.3	515.0	2518.3
73.8	406.8	180.1	963.6	327.0	1688.9	517.0	2526.6
74.8	412.3	182.6	975.6	329.3	1699.5	519.0	2534.8
75.8	417.8	185.4	989.3	330.8	1706.5	520.3	2540.0
92.8	511.2	200.3	1060.9	345.1	1775.3	522.3	2548.6
103.8	570.9	201.6	1067.4	346.8	1783.5		

A.4 Untreated and F$_{17}$ Silanized RC55 Cellulose XPS Spectra

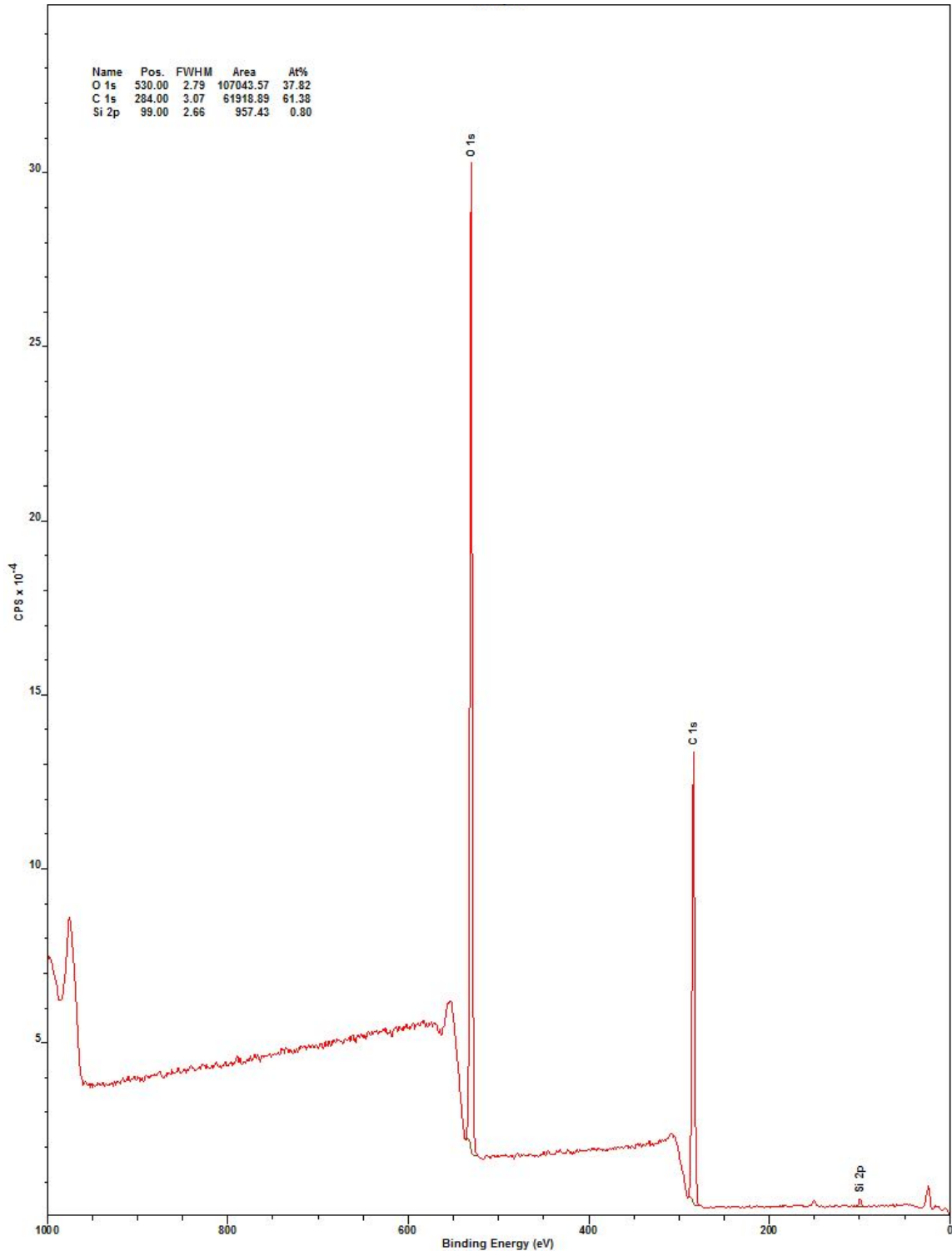| Name	Pos.	FWHM	Area	At%
O 1s	530.00	2.79	107043.57	37.82
C 1s	284.00	3.07	61918.89	61.38
Si 2p	99.00	2.66	957.43	0.80

Figure A.22: XPS survey scan on untreated RC55 membrane.
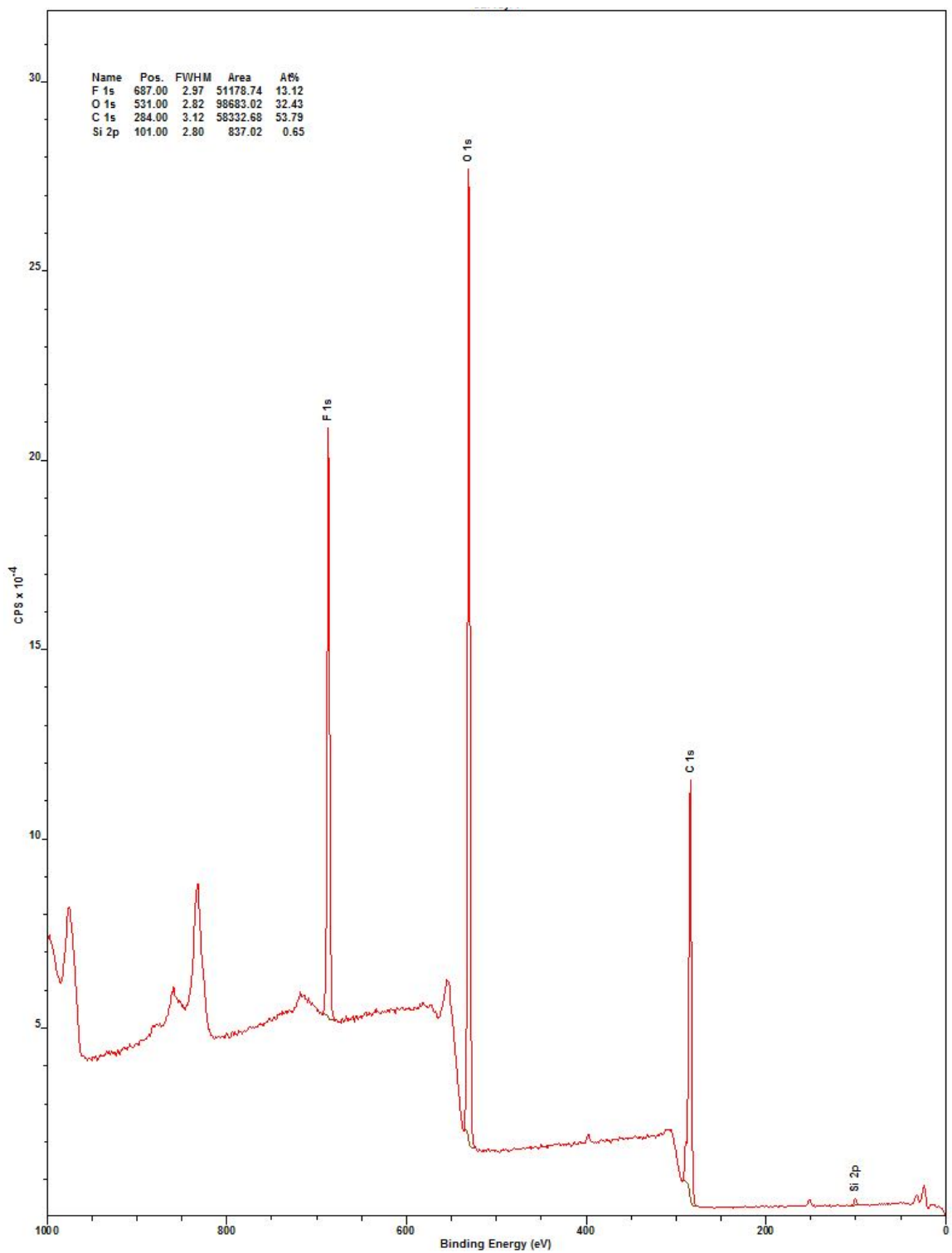
Figure A.23: XPS survey scan on 10 min F$_{17}$ RC55 membrane.
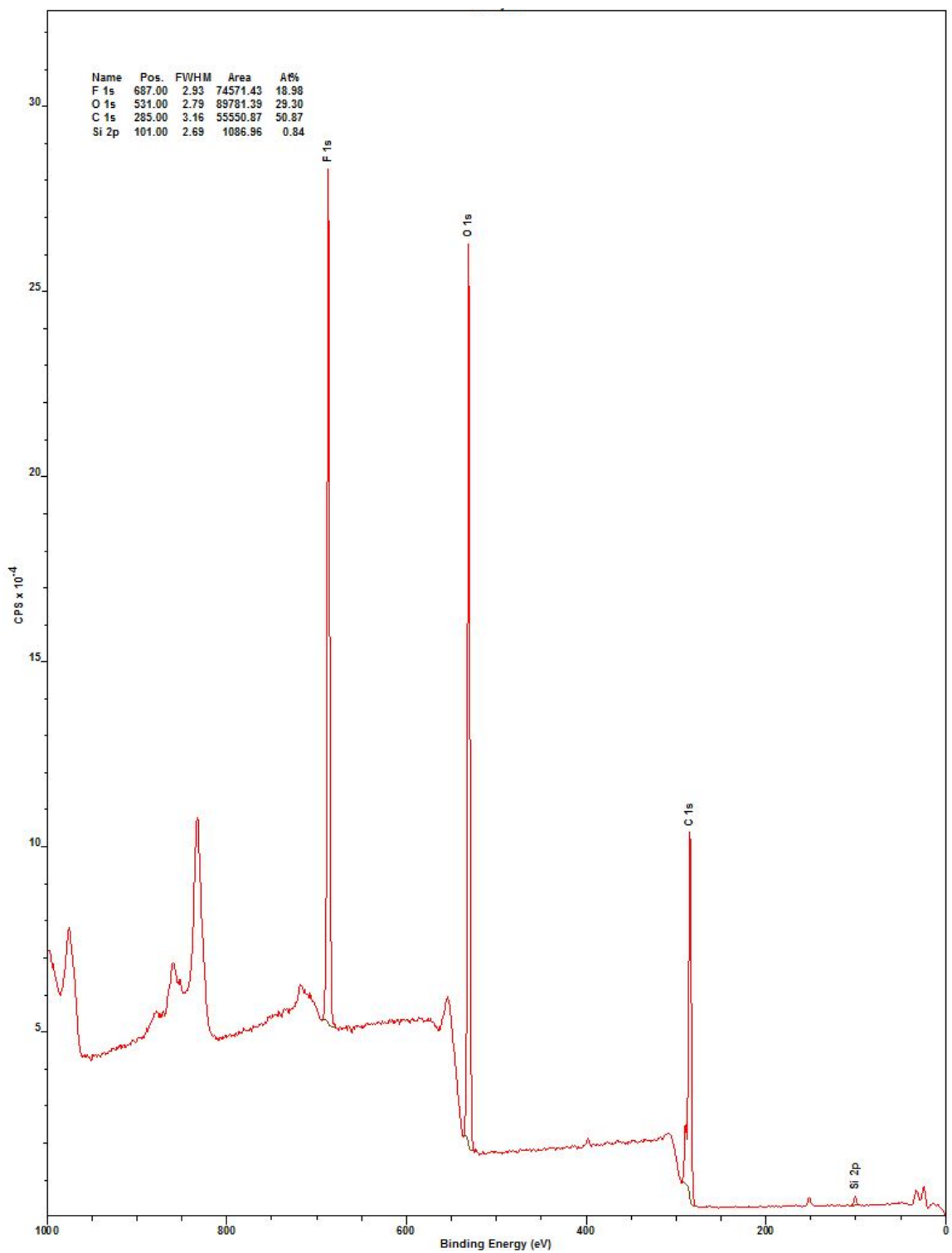
Figure A.24: XPS survey scan on 20 min F$_{17}$ RC55 membrane.

Appendix B

Chapter 3 Supplementary Information

B.1 Number Size Distribution of the SDS-stabilized Dodecane-in-DMF Emulsion

The number size distribution of the dispersed phase (i.e., dodecane) in the emulsion was determined using two techniques – optical microscopy image analysis for droplets above 1 μm in diameter and dynamic light scattering (DLS) for droplets below 1 μm. Figure B.1a shows a representative optical image for the 50:50 (vol:vol) sodium dodecyl sulfate (SDS)-stabilized dodecane-in-DMF emulsion (SDS forms non-polar in
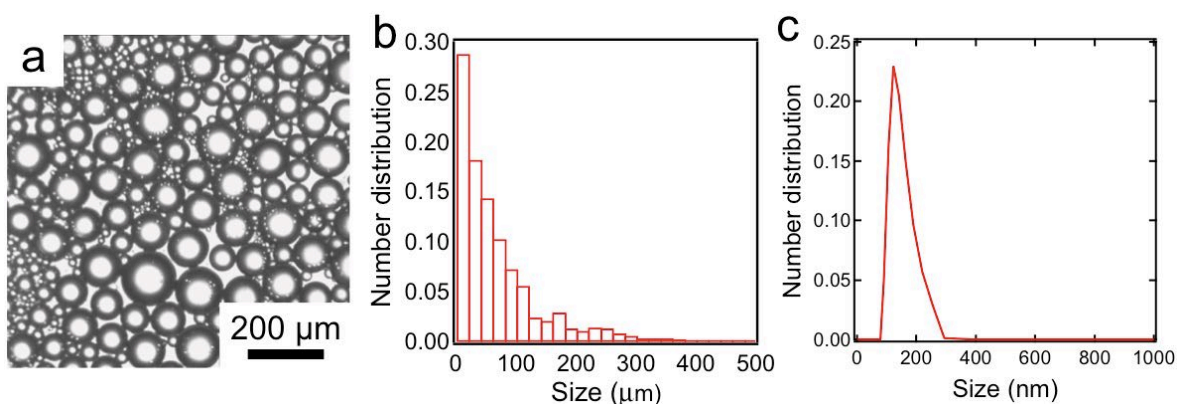

Figure B.1: (a) A representative optical microscopy image of a 50:50 (vol:vol) dodecane-in-DMF feed emulsion. (b) and (c) The number size distributions for the dodecane-in-DMF feed emulsion for droplets > 1 μm and < 1 μm, respectively.

polar emulsions). Twenty different images, with more than 50 droplets per image, were analyzed to minimize the error in the estimated number size distribution. Figure B.1b shows the number size distribution of the dodecane droplets determined using this image

217

analysis. The average size of the dispersed phase is between 1–20 μm. Figure B.1c shows the number size distribution of the dodecane droplets, determined using DLS. The size varies between 100 - 300 nm.

B.2 Refractive Index Measurement to Analyze Remaining Methanol in the Methyl Oleate Phase after Separations

The amount of methanol in the methyl oleate phase was determined by measuring its refractive index and comparing it with a calibration curve. The curve was developed by measuring refractive indices of methyl oleate and methanol mixtures, with varying methanol vol% (Figure B.2).
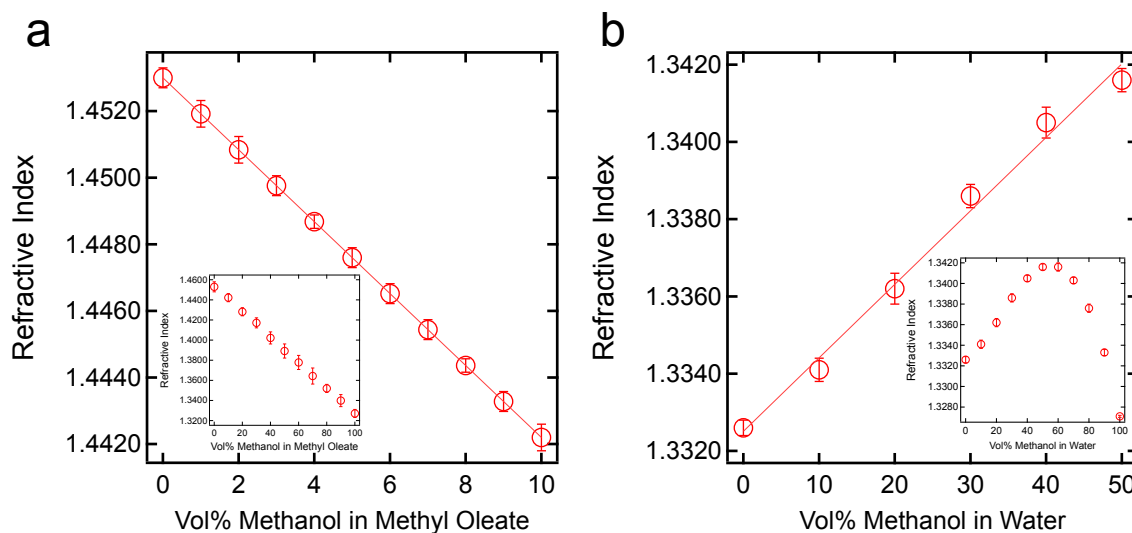

Figure B.2: (a) Refractive index data for methyl oleate as a function of methanol concentration (0 – 10 vol%). (b) Refractive index data for water as a function of methanol concentration (0 – 50 vol%). Insets show respective full-scale data (0 – 100 vol%). The non-linear portion is unutilized.

First, consider the methanol-depleted methyl oleate phase using a 90:10 feed:extractant volumetric flow ratio. The refractive index of the methanol-depleted methyl oleate phase is 1.4503 ± 0.0002. By comparing this with the calibration curve (Figure B.2a), it is evident that the methanol concentration in the methyl oleate phase

after extraction using the CLEANS methodology is ≈ 2.5 vol%. On the other hand, the refractive index of the methanol-depleted methyl oleate phase without emulsification is 1.4471 ± 0.0003, yielding a concentration of ≈ 5.5 vol%. This clearly indicates that the CLEANS methodology can more efficiently extract methanol from the methyl oleate phase.

The amount of methanol in the aqueous phase after extraction was also determined using a calibration curve, developed by measuring refractive indices of water with various methanol vol% (Figure B.2b). The refractive index of the methanol-enriched aqueous phase, after separation with 90:10 feed:extractant volumetric flow ratio using CLEANS methodology, is 1.3406 ± 0.0002, yielding a concentration of ≈ 41 vol%. These values matched well with our calculated mass balance. Refractive indices of the methyl oleate-rich and aqueous phases, after separations with various feed:extractant volumetric flow ratios, with and without the CLEANS methodology are listed in Table B.1.

Table B.1: Measured average refractive indices (five trials) for the methanol-depleted methyl oleate phases and the methanol-enriched aqueous phases after extractions, using various feed:extractant volumetric flow ratios.

Feed:Extractant flow ratio (vol:vol)	Refractive index			
	Methyl Oleate phase		Aqueous phase	
	Emulsified	Non-emulsified	Emulsified	Non-emulsified
90:10	1.4503	1.4471	1.3407	1.3388
80:20	1.4507	1.4478	1.3374	1.3358
70:30	1.4514	1.4490	1.3355	1.3347
60:40	1.4521	1.4508	1.3345	1.3343
50:50	1.4525	1.4515	1.3339	1.3336

B.3 Refractive Index Measurements to Analyze the Remaining Ethanol in the Heptane Phase after Separations

The remaining ethanol concentration in the heptane phase was determined by measuring the refractive index and comparing it to a calibration curve. The curve was developed by measuring refractive indices of ethanol-heptane mixtures with various ethanol concentrations. Because water is virtually insoluble in heptane, the refractive index of the ethanol-depleted heptane phase, obtained after the separation, could be directly compared with that of the ethanol-heptane mixture.
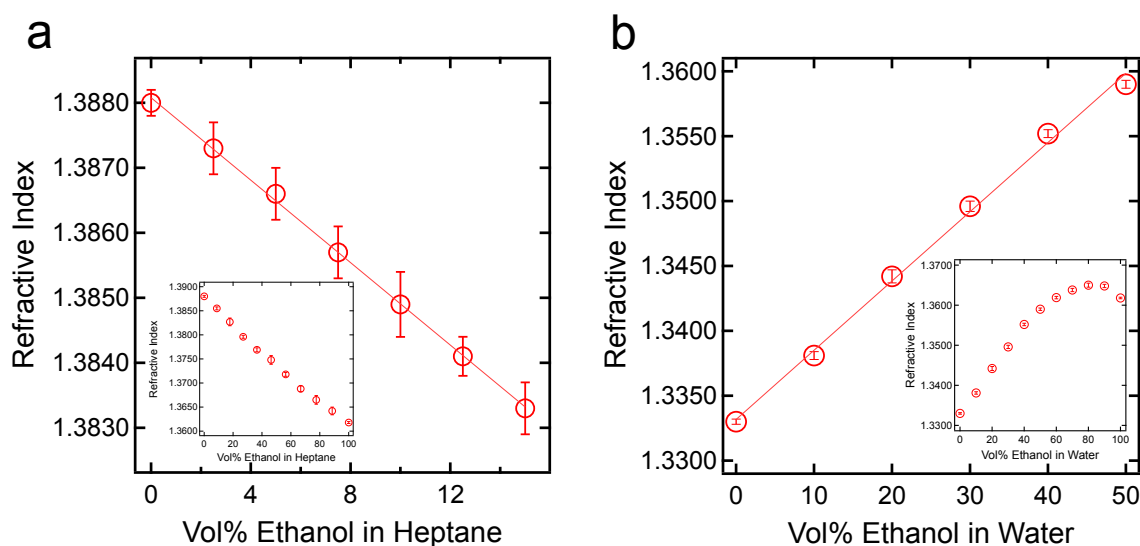

Figure B.3: (a) Refractive index data for heptane as a function of ethanol concentration (0 − 15 vol%). (b) Refractive index data for water as a function of ethanol concentration (0 − 50 vol%). Insets show the full-scale data (0 − 100 vol%). The non-linear portion is unutilized.

First, consider the ethanol-depleted heptane phase, obtained from the separation with a 50:50 feed:extractant volumetric flow ratio, using the CLEANS methodology. The refractive index of the ethanol-depleted heptane phase is 1.3879 ± 0.0001. By comparing this with the calibration curve (Figure B.3a), the ethanol concentration is ≈ 0.4 vol%. In contrast, the refractive index of the ethanol-depleted heptane phase without

emulsification is 1.3877 ± 0.0001 yielding a concentration of ≈ 1.0 vol% ethanol in heptane.

The amount of ethanol in the aqueous phase after separation was also determined using a calibration curve, developed by measuring refractive index of water with various ethanol concentrations (Figure B.3b). The refractive index of the ethanol-enriched aqueous phase, after separation with 50:50 feed:extractant volumetric flow ratio, using the CLEANS methodology is 1.3502 ± 0.0002. This value corresponds to a concentration of ≈ 32 vol% ethanol in the aqueous phase. These values matched well with our calculation, based on the overall mass balance for the system. Refractive indices of the ethanol-depleted heptane phases and the aqueous phases after separations are listed in Table B.2.

Table B.2: Measured average refractive indices (three trials) for the ethanol-depleted heptane phases and the ethanol-enriched aqueous phases after separations using various feed:extractant volumetric flow ratios.

Feed:Extractant flow ratio (vol:vol)	Refractive index			
	Heptane phase		Aqueous phase	
	Emulsified	Non-emulsified	Emulsified	Non-emulsified
97:3	1.3840	1.3835	1.3640	1.3641
96:4	1.3849	1.3844	1.3647	1.3647
95:5	1.3860	1.3854	1.3650	1.3650
94:6	1.3865	1.3858	1.3648	1.3647
92:8	1.3868	1.3862	1.3649	1.3648
91:9	1.3871	1.3868	1.3649	1.3649
90:10	1.3874	1.3871	1.3650	1.3650
80:20	1.3876	1.3873	1.3629	1.3628
70:30	1.3877	1.3875	1.3593	1.3590
60:40	1.3878	1.3876	1.3552	1.3550
50:50	1.3879	1.3877	1.3502	1.3497

B.4 UV-Vis Absorbance Measurements to Analyze the Concentration of Benzothiophene in the Dodecane Phase after Extraction

The concentration of benzothiophene in the dodecane phase after extraction was quantified by measuring its UV-Vis absorbance and comparing it to a calibration curve, developed by measuring the absorbance of dodecane with varying concentrations of benzothiophene. Figure B.4a shows the UV-Vis absorbance data of dodecane with various benzothiophene concentrations.
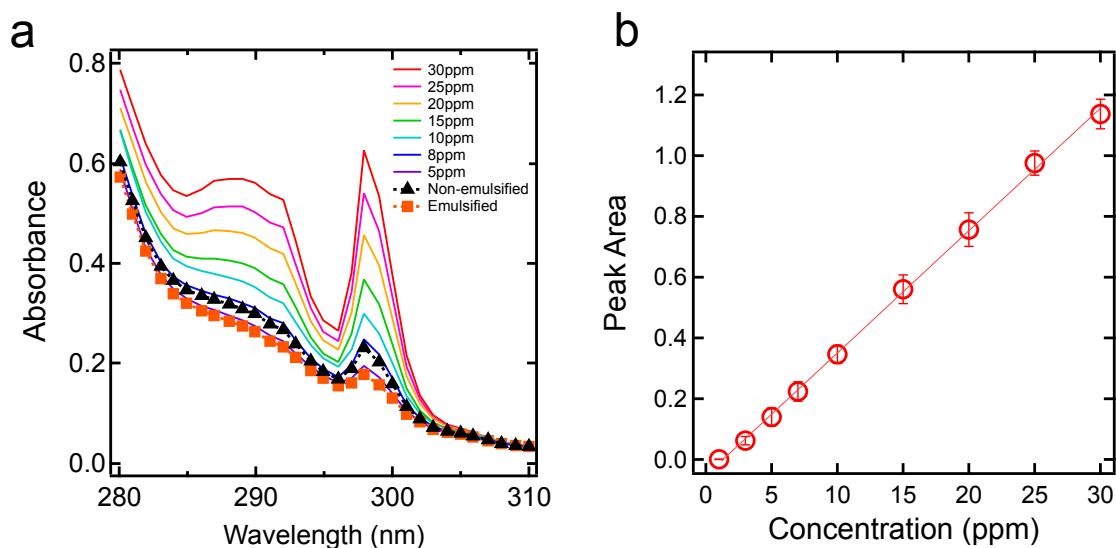

Figure B.4: (a) UV-Vis absorbance data for the benzothiophene-depleted dodecane phases obtained using the CLEANS methodology and without emulsification. Note that a 50:50 feed:extractant volumetric flow ratio is used. UV-Vis absorbance data for dodecane with varying benzothiophene concentrations are shown for comparison. (b) A calibration curve developed by calculating the area under the UV-Vis absorbance peak at 298 nm as a function of benzothiophene concentration.

Consider the benzothiophene-depleted dodecane, obtained from the separation with a 50:50 feed:extractant volumetric flow ratio, using the CLEANS methodology. The absorbance data for the benzothiophene-depleted dodecane is shown in Figure B.4a. By comparing the permeate spectrum with curves of known concentration, the concentration of benzothiophene in the dodecane phase is ≈ 5 ppm. In contrast, the absorbance data for

the dodecane phase after separation without emulsification indicates that the concentration of benzothiophene is ≈ 8 ppm.

For a more quantitative study, we developed a calibration curve by calculating the area under the UV-Vis absorbance curves. Figure B.4b shows the calculated area under the UV-Vis absorbance curves for dodecane as a function of benzothiophene concentration. The calculated area under the UV-Vis absorbance curve for the dodecane phase, after extraction with a 50:50 feed:extractant volumetric flow ratio using the CLEANS methodology, is 0.168. By comparing this with the calibration curve (Figure B.4b), the concentration of benzothiophene is estimated to be ≈ 5.4 ppm. Utilizing a similar estimation procedure, the area under the UV-Vis absorbance curve for extraction without emulsification, is 0.296, which is equivalent to a concentration of ≈ 8.6 ppm. The calculated values of area under the UV-Vis absorbance curves and corresponding benzothiophene concentrations are listed in Table B.3.

Table B.3: Average calculated area under the UV-Vis absorbance curves (three trials) for the benzothiophene-depleted dodecane phases obtained from continuous separations, with and without emulsification, using various feed:extractant volumetric flow ratios.

Feed:Extractant Flow Ratio (vol:vol)	Emulsified		Non-emulsified	
	Calculated Area under the UV-Vis Curve	Benzothiophene Concentration (ppm)	Calculated Area under the UV-Vis Curve	Benzothiophene Concentration (ppm)
90:10	0.767	20.4	0.827	21.9
80:20	0.575	15.6	0.647	17.4
70:30	0.336	9.6	0.388	10.9
60:40	0.264	7.8	0.336	9.6
50:50	0.168	5.4	0.296	8.6

B.5 Extraction of *tert*-Butyl Thiol from Oil

We also demonstrated the separation of *tert*-butyl thiol using the CLEANS methodology. Similar to the separation of benzothiophene described in Chapter 3, dodecane containing 50 ppm of *tert*-butyl thiol and DMF with dissolved SDS were continuously fed to the chamber, and emulsified *in-situ*. The *tert*-butyl thiol-enriched DMF permeated through the membrane at the bottom, while *tert*-butyl thiol-depleted dodecane passed through the HP/OL sidewall membrane. Gas Chromatography-Mass Spectroscopy (GC-MS) was used to determine the concentration of *tert*-butyl thiol in the dodecane phase after extraction. Small sample volumes (ranging from 1-10 μL) were injected into the GC-MS instrument, and the peak areas determined the *tert*-butyl thiol concentrations. Concentration values of *tert*-butyl thiol in the dodecane phases using various feed:extractant volumetric flow ratios are listed in Table B.4 and the extraction factors are shown in Figure B.5.

Table B.4: The average concentrations of *tert*-butyl thiol remaining (three trials) in the dodecane phases obtained from continuous separations, with and without emulsification, using various feed:extractant volumetric flow ratios.

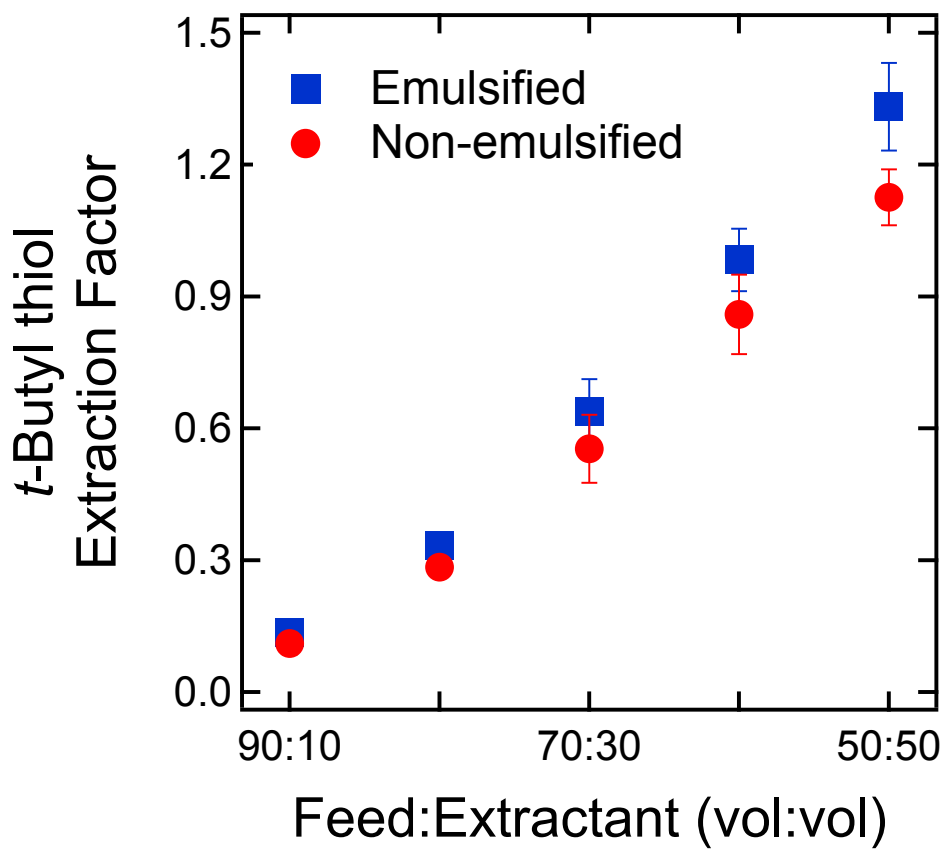| Feed:Extractant (vol:vol)	Concentration of *tert*-butyl thiol (ppm)	
	Emulsified	Non-emulsified
90:10	44.0	45.0
80:20	37.5	39.0
70:30	30.5	32.3
60:40	25.3	27.0
50:50	21.5	23.5

Figure B.5: The extraction factors for *tert*-butyl thiol removal from dodecane using DMF at various feed:extractant ratios, with and without surfactant.

Appendix C

Chapter 4 Supplementary Information

C.1 Anti-Fog Coating Water Capacity: Swelling Test

Approximately 1" x 3" polycarbonate slides, of known mass, were coated as described in Methods 4.2.3.1. The coated slide mass was measured and the slides were each immersed in 25 mL of deionized water for 7 days, with new water being exchanged daily. After swelling, surface water was absorbed off and the mass of the swollen coated slide was measured. The average mass swell ratio was 3.8 ± 0.3 (swollen coating mass/dry coating mass), showing that a significant amount of water can be taken into the coating while preventing fog formation. The percent swelling was also calculated as the mass of water absorbed divided by the original coating mass times 100.

Table C.1: Anti-fog coating on polycarbonate slide swelling tests

Sample #	Coating Mass (g)	Swollen Coating Mass (g)	Mass Swell Ratio	Average Mass Swell Ratio
1	0.0034	0.0137	4.029	3.8 ± 0.3
2	0.0030	0.0110	3.667	
3	0.0033	0.0116	3.515	Average % Swelling
4	0.0028	0.0115	4.107	280 ± 30%

C.2 Predicted Sliding Contact Angles

The predicted sliding angles were calculated using the Furmidge equation:

$$\frac{mg \sin(\alpha)}{w} = \gamma_{LV}(\cos \theta_R - \cos \theta_A) \qquad (C.1)$$

where *m* is the oil droplet mass, *g* is the gravitational constant, α is the sliding angle, *w* is the oil droplet width, γ_{LV} is surface tension, θ_R is the receding angle, and θ_A is the advancing angle. This equation showed that the experimental sliding angles are consistent with the measured advancing and receding angles found in Tables 4.3 and 4.4. All values are the average of at least 6 measurements (of angle and droplet width) and standard deviation denotes the error.

Appendix D

Chapter 5 Supplementary Information
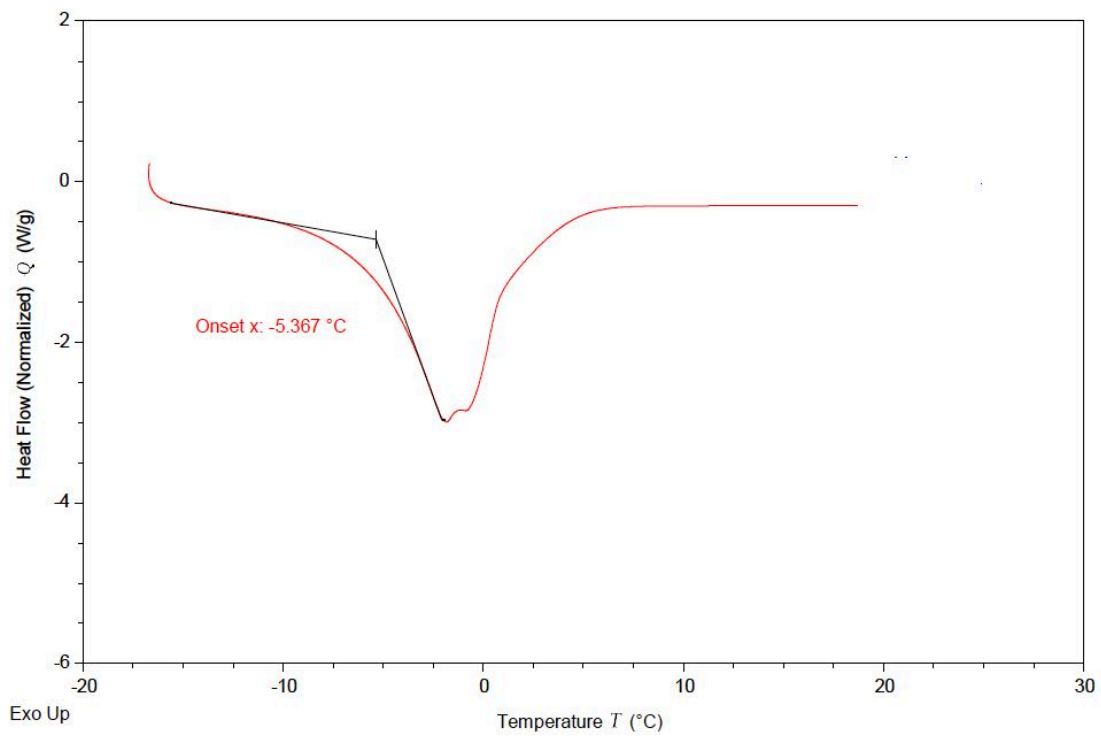
D.1 Kroger Apple Juice Melting Peak

Figure D.1: Differential scanning calorimetry with apple juice (Methods 5.2.6)
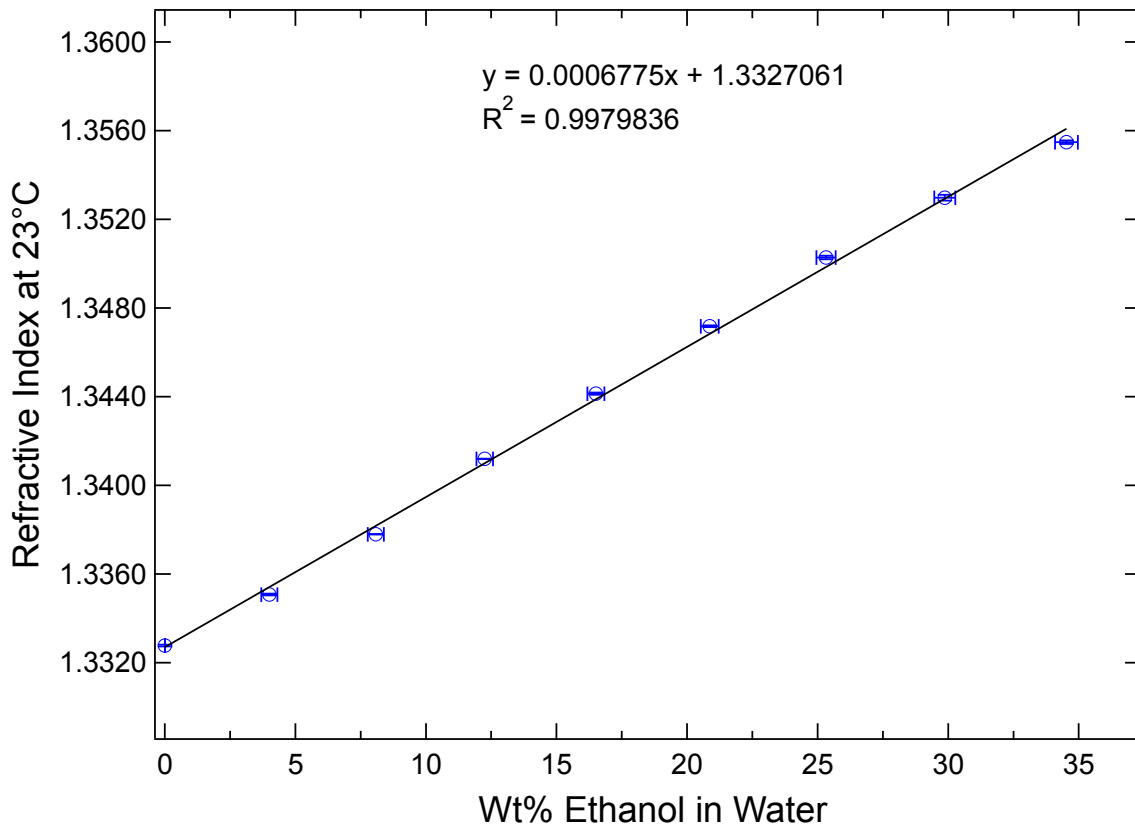
D.2 Ethanol in Water Calibration Curve

Figure D.2: Ethanol in water calibration curve. The refractive index is linear with respect to concentration to about 35 wt% ethanol. The refractive index of the permeate and retentate was used to quantify the freeze concentration performance.
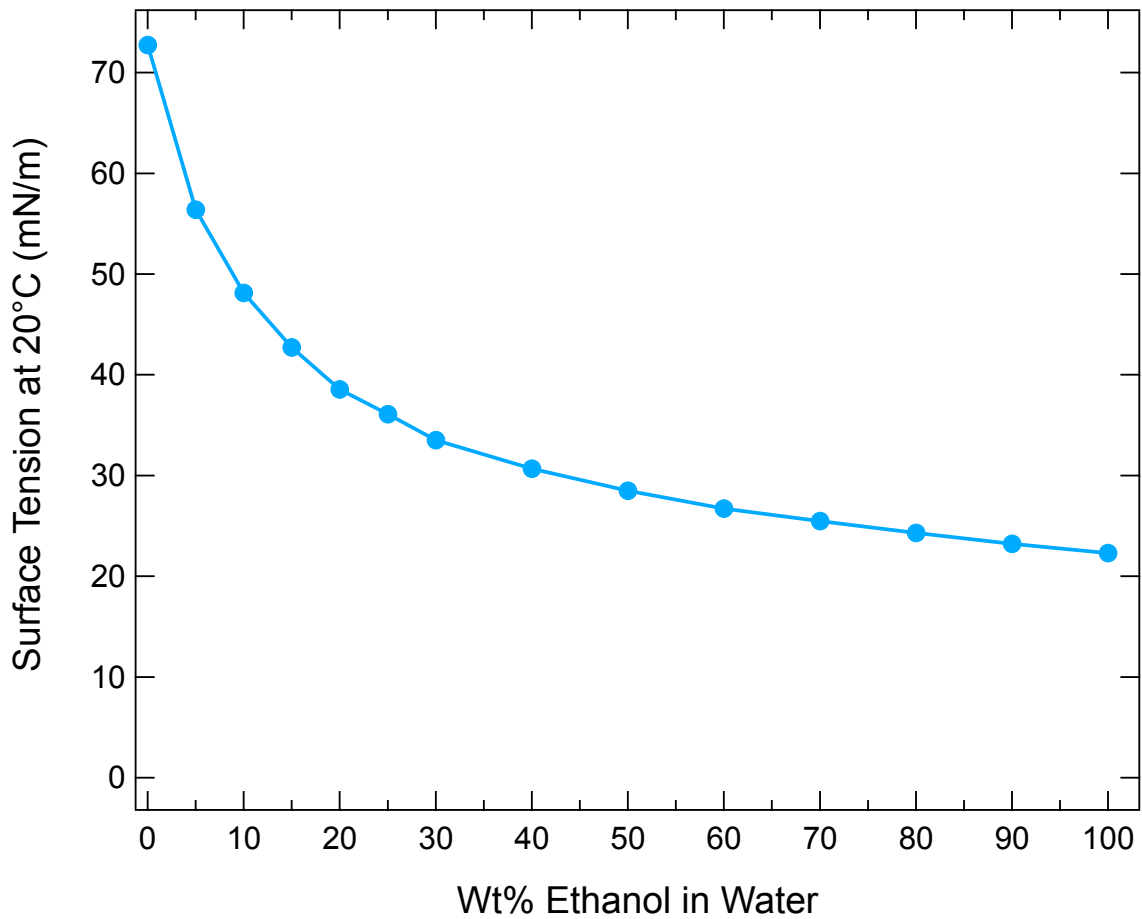
D.3 Ethanol Solution Surface Tension

Figure D.3: Effect of ethanol concentration on surface tension. The surface tension drops rapidly as the wt% of ethanol increases. Because of this, a PVDF membrane is required instead of the hydrophobic Whatman 114. Data acquired from: Vazquez, G.; Alvarez, E.; Navaza, J. M., Surface tension of alcohol water + water from 20 to 50°C. *J. Chem. Eng. Data* **1995,** *40* (3), 611-614.

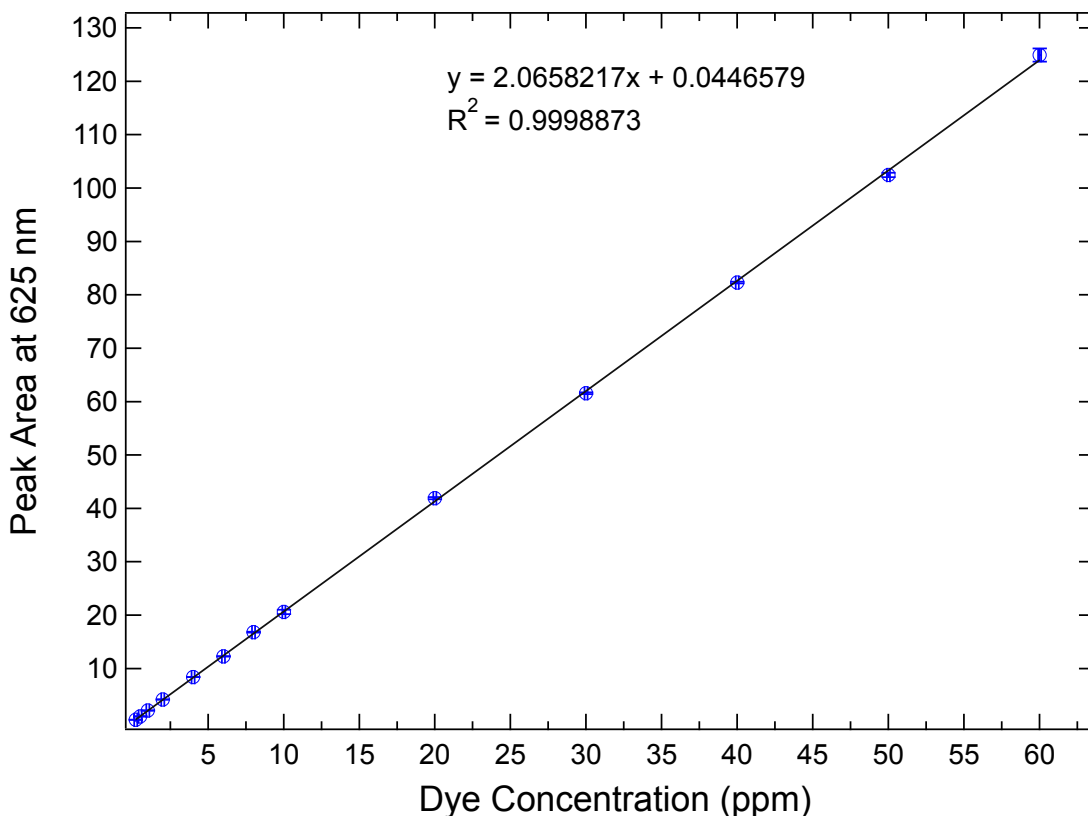## D.4 Fast Green FCF in Water Concentration

Figure D.4: Fast Green FCF in water calibration curve. The curve was developed through serial dilutions from 60 ppm to 0.2 ppm using 100 mL volumetric flasks.

Table D.1: Calculated 625 nm peak areas from UV-Vis spectroscopy

| Concentrate	Measurement #1	Measurement #2	Measurement #3
Peak Area Trial #1	72.00694	72.01994	72.19995
Peak Area Trial #2	69.87704	69.65284	69.69090
Peak Area Trial #3	67.11715	67.17803	67.22561
Purified Water	Measurement #1	Measurement #2	Measurement #3
Peak Area Trial #1	0.76893	0.77577	0.80832
Peak Area Trial #2	1.47636	1.47251	1.49849
Peak Area Trial #3	0.29846	0.32018	0.32864
Feed	Measurement #1	Measurement #2	Measurement #3
Peak Area	39.94114	39.76022	40.03435
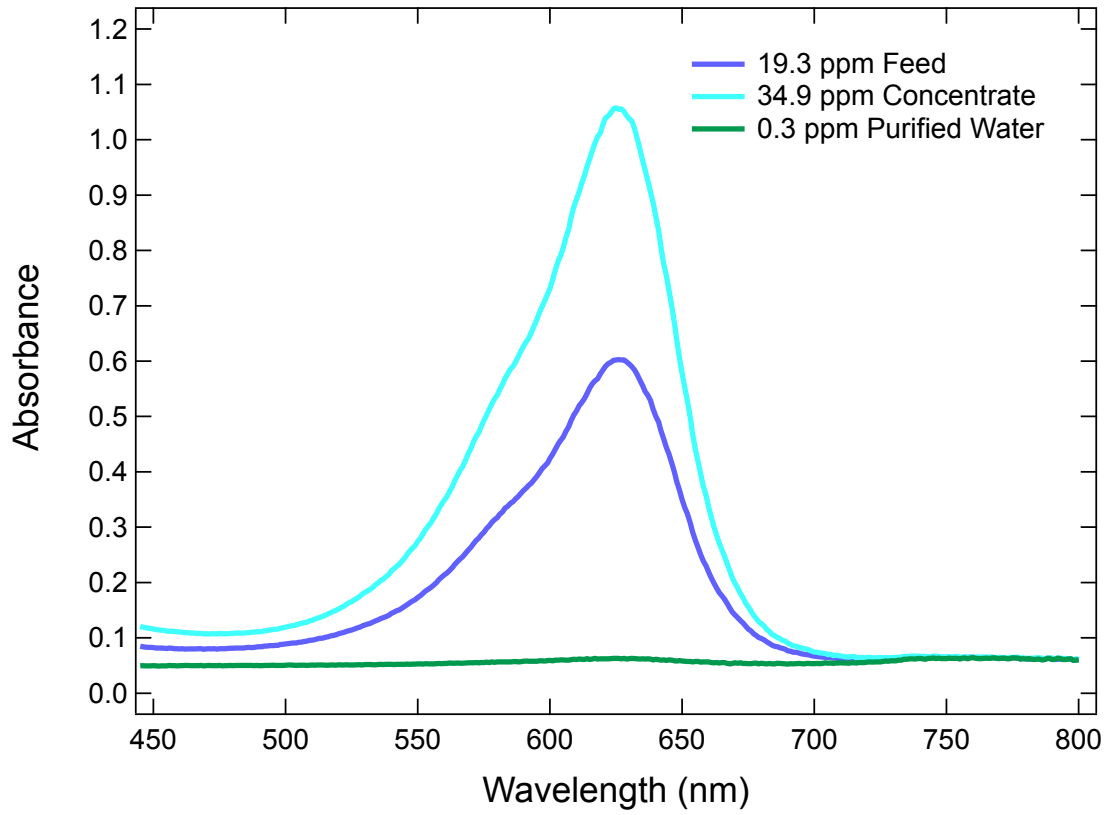
Figure D.5: UV-Vis spectra for Trial #1 of dye removal from water